

Mechanistic Characterization of Transaldolase from
Thermoplasma Acidophilum and Preliminary Analysis of the
QncN/L-M Protein System from *Streptomyces*
Melanovinaceus

Dissertation
for the award of the degree
„Doctor rerum naturalium“
of the Georg-August-Universität Göttingen

within the doctoral program Biomolecules: Structure-Function-Dynamics
of the Georg-August-University School of Science (GAUSS)

submitted by
Viktor Sautner
from Karaganda (Kazakhstan)

Göttingen 2016

Members of the Thesis Committee

Prof. Dr. Kai Tittmann (Referee)

Department of Molecular Enzymology
Georg-August-Universität Göttingen

Prof. Dr. Marina Rodnina (Referee)

Department of Physical Biochemistry
Max Planck Institute for Biophysical Chemistry Göttingen

Prof. Dr. Holger Stark

Structural Dynamics
Max Planck Institute for Biophysical Chemistry Göttingen

Further members of the Examination Board

Prof. Dr. Ralf Ficner

Department of Molecular Structural Biology
Georg-August-Universität Göttingen

Dr. Manfred Konrad

Department of Enzyme Biochemistry
Max Planck Institute for Biophysical Chemistry Göttingen

Dr. Fabian Commichau

Department of General Microbiology
Georg-August-Universität Göttingen

Date of the oral examination: 23.08.2016

Herewith I declare that I prepared this thesis „Mechanistic Characterization of Transaldolase from *Thermoplasma Acidophilum* and Preliminary Analysis of the QncN/L-M Protein System from *Streptomyces Melanovinaceus*“ independently and with no other sources and aids than quoted. This thesis (wholly or in part) has not been submitted elsewhere for any academic award or qualification.

Göttingen, 30.06.2016

Viktor Sautner

Contents

List of Tables	1
List of Schemes	2
List of Figures	3
Acknowledgements	6
Abbreviations	9
1 Materials and methods	14
1.1 Materials	14
1.2 Devices	19
1.3 Commodities	21
1.4 Utilized Primers	21
1.5 Media	22
1.6 Methods	25
1.6.1 Molecular Biology	25
1.6.1.1 Determination of DNA Concentration	25
1.6.1.2 Plasmid Transformation	25
1.6.1.3 Isolation of Plasmid DNA	25
1.6.1.4 DNA Sequencing	26
1.6.1.5 Polymerase Chain Reaction	26
1.6.1.6 DNA Fragment Separation via Agarose Gel Electrophoresis	26
1.6.1.7 General Cloning Procedure	27
1.6.1.8 Generation of the QncNL-pCDFDuet-1 Construct	27
1.6.1.9 Generation of the QncM-pET-SUMO Construct	28
1.6.1.10 Generation of the QncNL-pET-SUMO Construct	28
1.6.1.11 Cultivation of <i>Streptomyces melanovinaceus</i>	29
1.6.1.12 Isolation of Genomic DNA from <i>St. melanovinaceus</i>	29
1.6.1.13 Sequencing of Genomic DNA from <i>St. melanovinaceus</i>	29
1.6.1.14 Storage of Recombinant <i>E. coli</i> Cells	29
1.6.1.15 Storage of <i>St. melanovinaceus</i> as a Glycerol Stock	30

1.6.1.16	Generation of the <i>SmeE3</i> -pJET1.2 Construct	30
1.6.1.17	Generation of the <i>SmeQncNML</i> -pET28a Construct	31
1.6.2	Protein Preparation	31
1.6.2.1	Sodium Dodecyl Sulfate – Polyacrylamide Gel Electrophoresis (SDS-PAGE)	31
1.6.2.2	Determination of Protein Concentration	32
1.6.2.3	General Expression Test	33
1.6.2.4	Recombinant Expression of the His ₆ -QncN/L Component . . .	33
1.6.2.5	Purification of the His ₆ -QncN/L Component	34
1.6.2.6	Recombinant Expression of the His ₆ -SUMO-QncM Component	34
1.6.2.7	Purification of the holoQncM Component	35
1.6.2.8	Recombinant Expression of the His ₆ - <i>SliE3</i> Component	36
1.6.2.9	Purification of the <i>SliE3</i> Component	37
1.6.2.10	Recombinant Expression of the <i>TacTAL</i> Wild Type Protein and Variants	38
1.6.2.11	Purification of the <i>TacTAL</i> Wild Type Protein and Variants . .	38
1.6.3	X-Ray Crystallography	40
1.6.3.1	Finding of Crystallization Conditions for holoQncM- and <i>SliE3</i> Components	40
1.6.3.2	Crystallization of <i>TacTAL</i> Wild Type Protein and Variants . . .	40
1.6.3.3	X-ray Data Collection and Processing	41
1.6.3.4	Initial Structure Determination	41
1.6.3.5	Model Building and Refinement	42
1.6.4	UV-Vis Spectroscopy	42
1.6.4.1	Concentration Measurement of NADH, FAD and Lipoamide .	42
1.6.4.2	Steady-State Measurements of <i>TacTAL</i> Wild Type Protein and Variants	42
1.6.4.3	pH-Dependency of Enzymatic Activity of <i>TacTAL</i> Variants . .	44
1.6.4.4	Stopped-Flow Measurements of <i>TacTAL</i> Wild Type Protein and Variants	45
1.6.4.5	Activity Assay for QncN/L Component	46
1.6.4.6	Steady-State Measurements of the <i>SliE3</i> Component	47

1.6.4.7	Stopped-Flow Measurements of the <i>SlIE3</i> Component	48
1.6.5	Analytical Methods	48
1.6.5.1	Size Exclusion Chromatography Coupled Multiangle Light Scattering (SEC-MALS)	48
1.6.5.2	MALDI-TOF Mass Spectrometry	49
1.6.5.3	Liquid Chromatography Mass Spectrometry	49
1.6.5.4	ThermoFluor Assay	50
2	Mechanistic Characterization of Transaldolase from <i>Thermoplasma Acidophilum</i>	51
2.1	Introduction	51
2.1.1	<i>Thermoplasma Acidophilum</i>	51
2.1.2	Pentose Phosphate Pathway	52
2.1.3	Transaldolase	53
2.1.4	Crystal Structure of <i>TacTAL</i>	54
2.1.5	Active Site and the Reaction Mechanism of <i>TacTAL</i>	58
2.1.6	Motivation	63
2.2	Results	65
2.2.1	Crystallographic Studies on Enzyme Bound Intermediates	65
2.2.2	Interactions of the Intermediate's C1OH-Group with the Active Site of <i>TacTAL</i>	74
2.2.2.1	Perturbation of the Interaction between the Intermediate's C1OH-Group and the Active Site of <i>TacTAL</i> impairs the donor half-reaction	75
2.2.2.2	An Additional Water Molecule is Present in the Active Sites of <i>TacTAL</i> _{wt} and <i>TacTAL</i> _{N108A/S130A} Co-Crystallized with A5P and F6P, Respectively	78
2.2.3	Analysis of <i>TacTAL</i> Variants with Enhanced Aldolase Activity	82
2.2.3.1	Introduction of a Phe/Tyr-Mutation and Simultaneous Removal of the General Acid-Base Catalyst Glu ⁶⁰ in <i>TacTAL</i> 's Active Site Results in a Highly Efficient Aldolase	83
2.2.3.2	The Active Site of <i>TacTAL</i> _{FSA-mimic} Variant Shows a Different pK _a Behavior Compared to Other Variants with Enhanced Aldolase Activity	86

2.2.3.3	Co-Existence of Two Potential Acid-Base Catalysts (Glu ⁶⁰ and Tyr ¹³²) in the Active Site Perturbs the Donor Half-Reaction of <i>TacTAL</i>	88
2.2.3.4	Relative Orientation of the Catalytic Tyrosine is Geometrically Favorable for a Direct Protonation of the Central Intermediate	91
2.2.4	Studies on „Open“/„Closed“ Conformations of <i>TacTAL</i>	96
2.3	Discussion	106
2.4	Outlook	123
2.5	Summary	124
3	Preliminary Analysis of the QncN/L-M Protein System from <i>Streptomyces Melanovinaceus</i>	126
3.1	Introduction	126
3.1.1	Quinocarcin	126
3.1.2	The Role of the QncN/L-M Protein System in the Biosynthesis of Quinocarcin	127
3.1.3	Motivation	131
3.2	Results	132
3.2.1	Recombinant Expression and Purification of the QncN/L Component	132
3.2.2	Recombinant Expression and Purification of the holoQncM Component	134
3.2.3	Crystal Structure of the holoQncM Component	135
3.2.4	Purification of the <i>SliE3</i> Component	136
3.2.5	Steady-State Analysis of the <i>SliE3</i> Component	137
3.2.6	Stopped-Flow Measurements of the <i>SliE3</i> Component	139
3.2.7	Crystal Structure of the <i>SliE3</i> Component	140
3.2.8	Sequence of the E3 Component from <i>Streptomyces Melanovinaceus</i>	141
3.3	Discussion	142
	Appendix	146
	A Tables	146
	B Schemes	153
	C Figures	154

References	160
Curriculum Vitae	183

List of Tables

1.6.1 Elution buffer gradient for the purification of <i>Tac</i> TAL using TMAE anion-exchange chromatography	39
2.2.1 Overview of microscopic kinetic constants for the donor half-reaction of <i>Tac</i> TAL _{wt} and variants	77
2.2.2 Overview of macroscopic kinetic constants for aldolase activity of <i>Ec</i> FSA _{wt} , <i>Tac</i> TAL _{wt} and <i>Tac</i> TAL variants	84
2.2.3 Overview of macroscopic kinetic constants for transaldolase activity of <i>Tac</i> TAL _{wt} and variants (enhanced aldolase activity)	85
2.2.4 Overview of the p <i>K</i> _a values for the enzyme-substrate complex of <i>Tac</i> TAL _{wt} and variants (enhanced aldolase activity)	87

List of Schemes

1.1	Minimal reaction sequence of transaldolase/aldolase activity assay	43
1.2	Minimal reaction sequence of the E3 component activity assay	47
2.1	The pentose phosphate pathway (PPP)	53
2.2	Transaldolase reaction in physiological context	54
2.3	Proposed reaction mechanism of transaldolase/aldolase	59
2.4	Coordination of the F6P-SCHIFF base intermediate in the active site of <i>Tac</i> TAL	62
2.5	Structural formula of S6P, F6P and M1P	68
2.6	Structural formula of A5P and F6P	74
2.7	Minimal reaction sequence of transaldolase single-turnover	76
2.8	Minimal reaction sequence of aldolase reaction catalyzed by transaldolase	89
2.9	Proposed mechanism for the catalysis of the FSA reaction illustrated on <i>Tac</i> TAL _{E60Q/F132Y} variant. A tyrosine residue is the general acid-base catalyst.	121
2.10	Proposed mechanism for the catalysis of the <i>Tac</i> TAL reaction. A glutamate residue is the general acid-base catalyst.	122
3.1	Structural formula of quinocarcin	126
3.2	Proposed catalytic cycle of the QncN/L-QncM reaction	129
3.3	Proposed catalytic cycle of the E3 reaction	130

List of Figures

2.1.1	A monomer of <i>TacTAL</i>	55
2.1.2	Inter-subunit helix swapping between two neighboring subunits of <i>TacTAL</i>	56
2.1.3	Crystal structures of <i>TacTAL</i> and <i>EcFSA</i>	57
2.1.4	<i>TacTAL</i> monomer in its „open“ and „closed“ states	58
2.1.5	Catalytic water in the active site of <i>TacTAL</i>	60
2.1.6	„Up“ and „down“ conformations of the C1 hydroxy group of the F6P-SCHIFF base intermediate in the active site of <i>TacTAL</i> _{wt} co-crystallized with F6P	63
2.2.7	Active site of <i>TacTAL</i> _{wt} co-crystallized with F6P	66
2.2.8	Active site of <i>TacTAL</i> _{E60Q} co-crystallized with F6P	67
2.2.9	Active site of <i>TacTAL</i> _{wt} co-crystallized with M1P	69
2.2.10	Active site of <i>TacTAL</i> _{K86Q} co-crystallized with F6P	72
2.2.11	Ideal BÜRGI-DUNITZ angle compared to the non-covalently bound F6P in <i>TacTAL</i> and <i>FtuTAL</i>	73
2.2.12	Pre-steady-state analysis of the donor half-reaction of <i>TacTAL</i> _{wt} and variants	77
2.2.13	Active sites of <i>TacTAL</i> _{wt} and <i>TacTAL</i> _{N108A/S130A} co-crystallized with F6P and/or A5P	79
2.2.14	Superposition of active sites of <i>TacTAL</i> _{wt} and <i>TacTAL</i> _{N108A/S130A} co-crystallized with F6P and/or A5P	80
2.2.15	Different conformations of Ser ⁵⁸ in the structure of <i>TacTAL</i> _{wt} co-crystallized with F6P	81
2.2.16	Superposition of the active sites of <i>TacTAL</i> _{wt} and <i>EcFSA</i>	82
2.2.17	Dependency of the aldolase activity of <i>TacTAL</i> variants on F6P concentration	84
2.2.18	pH-dependency of aldolase activity of <i>TacTAL</i> variants (enhanced aldolase activity)	87
2.2.19	Representative stopped-flow progress curves of <i>TacTAL</i> _{wt} and variants (enhanced aldolase activity)	90
2.2.20	Active site of <i>TacTAL</i> _{E60Q/F132Y} co-crystallized with F6P	92
2.2.21	DHA-SCHIFF base intermediate in the active site of <i>TacTAL</i> _{E60Q/F132Y}	93
2.2.22	Superposition of the active sites of variants with enhanced aldolase activity co-crystallized with F6P and <i>EcFSA</i>	94
2.2.23	Active site of <i>TacTAL</i> _{FSA-mimic} co-crystallized with F6P	95

2.2.24	Superposition of the active sites of <i>TacTAL</i> _{FSA-mimic} and <i>TacTAL</i> _{E60Q/F132Y} co-crystallized with F6P	95
2.2.25	Superposition of the active sites of <i>TacTAL</i> _{E60Q/F132Y} co-crystallized with F6P in their „open“ and „closed“ states	96
2.2.26	„Open“ and „closed“ conformations of functional subunits in <i>TacTAL</i> _{E60Q/F132Y}	97
2.2.27	Relative orientation of Asp ²¹¹ and Thr ³⁰ to each other in the „open“ and „closed“ conformation	98
2.2.28	Introduction of an intersubunit disulfide bridge in <i>TacTAL</i>	99
2.2.29	Comparison of the „open“/„closed“ conformations observed in resting state wild type structure with the resting state of <i>TacTAL</i> _{T30C/D211C}	100
2.2.30	Active site of <i>TacTAL</i> _{T30C/D211C} co-crystallized with F6P	101
2.2.31	Active site of <i>TacTAL</i> _{T30C/D211C} soaked simultaneously with F6P and DTT . . .	102
2.2.32	Active site of <i>TacTAL</i> _{T30C/D211C} soaked with F6P	103
2.2.33	Dependency of the transaldolase activity of <i>TacTAL</i> _{T30C/D211C} on F6P concentration	104
2.2.34	Pre-steady-state analysis of the donor half-reaction of <i>TacTAL</i> _{T30C/D211C} in its reduced and oxidized forms	105
2.3.35	Superposition of „open“/„closed“ conformations of <i>TacTAL</i> _{wt} and <i>TacTAL</i> _{T30C/D211C}	108
2.3.36	Comparison of the active sites of <i>TacTAL</i> _{wt} and <i>TacTAL</i> _{E60Q/F132Y} with FBPA .	114
2.3.37	Glycerol and acetate molecules bound between two opposite active sites of the homodecamer	121
3.2.1	Expression of the QncN/L-M components from the <i>SmeQncNML</i> -pET28a construct	132
3.2.2	Expression and purification of the QncN/L component from the QncNL-pET-SUMO construct	133
3.2.3	F6P-dependend reduction of NAD ⁺ in a spectrophotometric assay	134
3.2.4	Normalized melting curves of the holoQncM protein in presence of SYPRO [®] Orange	134
3.2.5	Crystal structure of the holoQncM protein	136
3.2.6	Molar extinction coefficient of the <i>SliE3</i> bound FAD	137
3.2.7	Steady-state analysis of <i>SliE3</i>	138
3.2.8	Double reciprocal plot for the lipamide conversion by <i>SliE3</i>	139
3.2.9	Stopped-flow spectra of the <i>SliE3</i> component	139
3.2.10	Crystal structure of the <i>SliE3</i> protein	141

3.2.11	The coding sequence for the E3 component from <i>Streptomyces melanovinaceus</i>	142
3.3.12	The Trp ³¹ -His ³⁶ dyad in holoQncM structure	143
3.3.13	Sequence alignment of the E3 components from <i>Streptomyces melanovinaceus</i> and <i>Streptomyces lividans</i>	144
3.3.14	The active site of the <i>SliE3</i> component	145

Acknowledgements

This Doctorate would not have been possible without my supervisor PROF. DR. KAI TITTMANN, who supported me during this project. His ideas and inspiring discussions with him have been very helpful for developing the present work.

I would like to thank my co-supervisor PROF. DR. MARINA RODNINA for accepting responsibility of being the second referee and being member of my thesis committee.

I would like to thank PROF. DR. HOLGER STARK for the co-supervision of this thesis and for taking part in the thesis committee and meetings. I am thankful to him for the ability to use facilities of his department.

My appreciation is extended to PROF. DR. RALF FICNER for being a member of the extended thesis committee and for the ability to use facilities and devices of his department.

Furthermore, I am thankful to DR. MANFRED KONRAD and DR. FABIAN COMMICHAU for being members of the extended thesis committee.

I am truly thankful to DR. DANILO MEYER and DR. KATHRIN SCHRÖDER-TITTMANN for the start-up aid during the initial phase of the project.

DR. FLORIAN BRODHUN I acknowledge for the discussions and help in the lab.

PROF. DR. IVO FEUSSNER I acknowledge for the ability to use facilities and devices of his department.

I would like to thank DR. CORNELIA HERRFURTH for performing mass spectrometric product analysis.

I am grateful to MALTE BÜRSING and GERHARD MADER for the technical support. Furthermore, I would like to thank CHRISTOPH MADER for the IT-support.

I am deeply grateful to DR. PIOTR NEUMANN for contributing his expertise in field of X-ray crystallography. His support, suggestions and comments were essential for my investigations within the present work and for my understanding of the field in general.

In addition I would like to thank MICHAEL FRANKE for performing the crystallization screens and DANIEL WEINRICH for technical support.

Acknowledgement is also extended to PROF. DR. M. A. MARAHIEL from Philipps-University (Marburg) for providing the Sfp-pQE60 plasmid.

I thank Agricultural Research Service of United States Department of Agriculture for the providing of the *Streptomyces melanovinaceus* strain.

Moreover, I am grateful to DR. ANJA POEHLEIN for the sequencing of the genomic DNA of *Streptomyces melanovinaceus*.

I would like to thank DR. GUIDO KRIETE for making the settling in the new labs in the Schwann-Schleiden-Forschungszentrum easier.

A special thank is also extended to DR. OLIVER VALERIUS and his co-workers for performing mass spectrometric analysis to confirm the identity and the correct post-translational modification of the proteins purified during this work.

Besides, it is a great pleasure to thank LISA-MARIE FUNK, scientific assistant and friend in the lab and the students I supervised during the project ARNE GLÜER, MASCHA MIRIAM FRIEDRICH, TATJANA LIETZOW for realizing certain experiments of the study.

I am honestly grateful to my colleagues FABIAN RABE VON PAPPENHEIM, SÖREN RINDFLEISCH, DR. ANJA LEHWESS-LITZMANN and FABIENNE LIBUDA for proofreading this manuscript. Thank you for nice discussions, comments and helpful feedback.

I would like to thank JOHANNES ARENS and MARCEL TAUCHERT, doctoral students in the Department of Molecular Structural Biology, for their help by performing of the SEC-MALS and ThermoFluor experiments.

I would like to thank DR. ASHWIN CHARI and DR. DAVID HASELBACH from the Department of Structural Dynamics (MPI) for helpful discussions about the crystallographic studies and purification of large protein complexes.

I would like to thank all former and present members of the department of Molecular Enzymology for their help in the lab and great working atmosphere.

I am indebted to Göttingen Graduate School for Neuroscience, Biophysics and Molecular Bioscience (GGNB) office for the organization of the graduate school and for the assistance through the administrative work that I went through.

Finally, a special recognition goes out to my family and friends, for their support, encouragement and patience during my studies. I am especially grateful to my girlfriend Raphaela for being there for me!

Abbreviations

6PGL	6-phosphoglucono- δ -lactone
6PGLase	6-phosphoglucono- δ -lactonase
6PG	6-phosphogluconate
6PGDH	6-phosphogluconate dehydrogenase
A5P	Arabinose 5-phosphate
<i>A. thaliana</i>	<i>Arabidopsis thaliana</i>
aa	Amino acid
ACP	Acyl carrier protein
ACT	Acetate
<i>Ae. hydrophila</i>	<i>Aeromonas hydrophila</i>
Ala	Alanine
AMP	Adenosine monophosphate
Arg	Arginine
Asn	Asparagine
Asp	Aspartic acid
ATP	Adenosine triphosphate
BisTris	Bis-(2-hydroxy-ethyl)-amino-tris(hydroxymethyl)-methane
<i>Bs</i>	<i>Bacillus subtilis</i> (<i>B. subtilis</i>)
BSA	Bovine serum albumin
<i>C. thermophilum</i>	<i>Chaetomium thermophilum</i>
CC	Correlation coefficient
CD	Circular dichroism
<i>Ci. amalonaticus</i>	<i>Citrobacter amalonaticus</i>
<i>Cl. beijerinckii</i>	<i>Clostridium beijerinckii</i>
CoA	Coenzyme A
CV	Column volume
Cys	Cysteine
<i>D. melanogaster</i>	<i>Drosophila melanogaster</i>
DESY	Deutsches Elektronen-Synchrotron
DHA	Dihydroxyacetone

DHAP	Dihydroxyacetone phosphate
DHB	Dihydroxybenzoic acid
DMSO	Dimethyl sulfoxide
DNA	Deoxyribonucleic acid
DTT	Dithiothreitol
E1	Pyruvate dehydrogenase
E2	Dihydrolipoyl transacetylase
E3	Dihydrolipoamide dehydrogenase
E4P	Erythrose 4-phosphate
<i>E. coli</i>	<i>Escherichia coli</i> (<i>Ec</i>)
EC	Enzyme commission
EDTA	Ethylenediaminetetraacetic acid
ESRF	European Synchrotron Radiation Facility
eq.	Equation
F6P	Fructose 6-phosphate
FAD	Flavin adenine dinucleotide
FBP	Fructose 1,6-bis(phosphate)
FBPA	Fructose-1,6-bis(phosphate) aldolase
FMN	Flavin mononucleotide
FSA	Fructose 6-phosphate aldolase
<i>Ftu</i>	<i>Francisella tularensis</i> (<i>F. tularensis</i>)
G3P	Glycerol 3-phosphate
G6P	Glucose 6-phosphate
G6PDH	Glucose-6-phosphate dehydrogenase
GA3P	Glyceraldehyde 3-phosphate
GDH	α -Glycerophosphate dehydrogenase from rabbit muscle
Gln	Glutamine
Glu	Glutamic acid
Gly	Glycine
GOL	Glycerol
HEPES	2-[4-(2-Hydroxyethyl)piperazin-1-yl]ethanesulfonic acid
His	Histidine

His₆-tag	Hexa-histidine tag
HPLC	High-pressure liquid chromatography
Ile	Isoleucine
IPTG	Isopropyl β -D-thiogalactopyranoside
<i>L. monocytogenes</i>	<i>Listeria monocytogenes</i>
LB	Lysogeny broth
LC	Liquid Chromatography
Leu	Leucine
Lys	Lysine
MIP	Mannitol 1-phosphate
MALDI	Matrix-assisted laser desorption/ionization
MALS	Multiangle light scattering
MBP	Mannitol-1,6-bis(phosphate)
MCS	Multiple cloning site
MES	2-(<i>N</i> -morpholino)ethanesulfonic acid
Met	Methionine
MOPS	3-(<i>N</i> -morpholino)propanesulfonic acid
MRW	Mean residue weight
MS	Mass Spectrometry
MW	Molecular weight
MWCO	Molecular weight cut-off
<i>M. tuberculosis</i>	<i>Mycobacterium tuberculosis</i>
NAD⁺	Nicotinamide adenine dinucleotide (oxidized form)
NADH	Nicotinamide adenine dinucleotide (reduced form)
NADP⁺	Nicotinamide adenine dinucleotide phosphate (oxidized form)
NADPH	Nicotinamide adenine dinucleotide phosphate (reduced form)
nd	Not detectable
ND	Not determined
Ni²⁺-NTA	Ni ²⁺ nitrilotriacetic acid
NMR	Nuclear magnetic resonance
NRPS	Nonribosomal peptide synthetases
OD	Optical density

PAGE	Polyacrylamide gel electrophoresis
PCP	Peptidyl carrier protein
PCR	Polymerase chain reaction
PDB	Protein data bank
PDH	pyruvate dehydrogenase
PDHc	pyruvate dehydrogenase complex
PEG	Polyethylene glycol
PEGmme	Polyethylene glycol monomethyl ether
PIPES	1,4-Piperazinediethanesulfonic acid
PPP	Pentose phosphate pathway
Phe	Phenylalanine
PMSF	Phenylmethanesulfonylfluoride
PNS	Phosphopantetheine
Pro	Proline
psi	Pound-force per square inch
R5P	Ribose 5-phosphate
R5PI	Ribose-5-phosphate isomerase
RBS	Ribosomal binding site
rmsd	Root-mean-square deviation
RNA	Ribonucleic acid
rpm	Revolutions per minute
RT	Room temperature
Ru5P	Ribulose 5-phosphate
Ru5PE	Ribulose-5-phosphate-3-epimerase
<i>S. cerevisiae</i>	<i>Saccharomyces cerevisiae</i> (<i>Sc</i>)
S6P	Sorbitol 6-phosphate
S7P	Sedoheptulose 7-phosphate
<i>Sa. typhi</i>	<i>Salmonella typhi</i>
<i>Sh. sonnei</i>	<i>Shigella sonnei</i>
SDS	Sodium dodecyl sulfate
SEC	Size Exclusion Chromatography
Ser	Serine

<i>Sme</i>	<i>Streptomyces melanovinaceus</i>
<i>Sli</i>	<i>Streptomyces lividans</i>
<i>St.</i>	<i>Streptomyces</i>
<i>Str.</i>	<i>Streptococcus</i>
SOC	Super optimal broth with catabolite repression
<i>Tac</i>	<i>Thermoplasma acidophilum</i> (<i>T. acidophilum</i>)
TAE	Tris-Acetate-EDTA-Buffer
TAL	Transaldolase
TCS	Thrombin cleavage site
TEMED	N,N,N',N'-Tetramethylethylenediamine
ThDP	Thiamine diphosphate
Thr	Threonine
TIM	Triosephosphate isomerase
TK	Transketolase
TLS	Translation/libration/screw
TMAE	Trimethylaminoethyl
TOF	Time-of-flight
Tris	Tris-(hydroxymethyl)-aminomethan
Trp	Tryptophan
TSB	Tryptic soy broth
Tyr	Tyrosine
UV	Ultraviolet fraction of electromagnetic radiation
UV-Vis	Ultraviolet and visible fraction of electromagnetic radiation
v/v	Volume/volume
Val	Valine
w/v	Mass/volume
wt	Wild type
X5P	Xylulose 5-phosphate
XDS	X-ray Detector Software

1 Materials and methods

1.1 Materials

Chemicals

Product

Acetic acid	Carl Roth GmbH & Co. KG (Karlsruhe, Germany)
Acetonitrile	Fisher Scientific (Leicestershire, UK)
Acrylamide	Carl Roth GmbH & Co. KG (Karlsruhe, Germany)
Agar	AppliChem GmbH (Darmstadt, Germany)
Agarose	AppliChem GmbH (Darmstadt, Germany)
Ammonium acetate	Sigma-Aldrich (Munich, Germany)
Ammonium chloride	Carl Roth GmbH & Co. KG (Karlsruhe, Germany)
Ammonium hydrogen carbonate	Carl Roth GmbH & Co. KG (Karlsruhe, Germany)
Ammonium sulfate	AppliChem GmbH (Darmstadt, Germany)
Antifoam 204	Sigma-Aldrich (Munich, Germany)
D-Arabinose 5-phosphate, disodium salt trihydrate	Sigma-Aldrich (Munich, Germany)
Barium chloride, dihydrate	Carl Roth GmbH & Co. KG (Karlsruhe, Germany)
Beef extract powder	Sigma-Aldrich (Munich, Germany)
Bis-(2-hydroxy-ethyl)-amino-tris(hydroxymethyl)-methane (BisTris)	AppliChem GmbH (Darmstadt, Germany)
Bromphenol blue, sodium salt	AppliChem GmbH (Darmstadt, Germany)
Bovine serum albumin (BSA)	AppliChem GmbH (Darmstadt, Germany)
Calcium chloride, hexahydrate	Carl Roth GmbH & Co. KG (Karlsruhe, Germany)
Carbenicillin, disodium salt	AppliChem GmbH (Darmstadt, Germany)
Coomassie Brilliant Blue G250	AppliChem GmbH (Darmstadt, Germany)
Cover plates, 18 mm (siliconized)	Jena Bioscience GmbH, (Jena, Germany)
Cryoloops (0.05 - 0.5 mm)	Hampton Research Corp, (CA, USA)
Crystallization plates, greased	Hampton Research Corp, (CA, USA)
Dihydroxybenzoic acid (DHB)	Bruker Daltonics (Bremen, Germany)
Dimethylsulfoxide (DMSO)	Sigma-Aldrich (Munich, Germany)
Dithiothreitol (DTT)	AppliChem GmbH (Darmstadt, Germany)
Ethanol (denatured)	Frau Magerkuth Apotheke (Karlsruhe, Germany)
Ethanol (purest)	Nordhäuser Spirituosen GmbH (Nordhausen, Germany)
Ethidium bromide	Carl Roth GmbH & Co. KG (Karlsruhe, Germany)
Ethylenediaminetetraacetic acid (EDTA)	AppliChem GmbH (Darmstadt, Germany)
Flavin adenine dinucleotide disodium salt di-hydrate (FAD)	AppliChem GmbH (Darmstadt, Germany)
Flavin mononucleotide monosodium salt di-hydrate (FMN)	AppliChem GmbH (Darmstadt, Germany)
Formamide	Sigma-Aldrich (Munich, Germany)
Formic acid	Sigma-Aldrich (Munich, Germany)
D-Fructose 6-phosphate, disodium salt hydrate	Sigma-Aldrich (Munich, Germany)
D-Glucose	Carl Roth GmbH & Co. KG (Karlsruhe, Germany)

Supplier

Glycerol (87 %)	AppliChem GmbH (Darmstadt, Germany)
Glycerol (anhydrous)	AppliChem GmbH (Darmstadt, Germany)
Glycine	Carl Roth GmbH & Co. KG (Karlsruhe, Germany)
Glycylglycine	AppliChem GmbH (Darmstadt, Germany)
Guanidinium chloride	AppliChem GmbH (Darmstadt, Germany)
2-[4-(2-hydroxyethyl)piperazin-1-yl]ethanesulfonic acid (HEPES)	AppliChem GmbH (Darmstadt, Germany)
Hydrochloric acid (37 %)	Th.Geyer GmbH & CoKG (Renningen, Germany)
Imidazole	AppliChem GmbH (Darmstadt, Germany)
Isopropyl β -D-thiogalactopyrano- side (IPTG)	Carl Roth GmbH & Co. KG (Karlsruhe, Germany)
Kanamycin sulfate	AppliChem GmbH (Darmstadt, Germany)
D-Lactose 1-hydrate	AppliChem GmbH (Darmstadt, Germany)
(+/-)- α -Lipoic acid	Sigma-Aldrich (Munich, Germany)
(+/-)- α -Lipoamide	Sigma-Aldrich (Munich, Germany)
Magnesium chloride, hexahydrate	Carl Roth GmbH & Co. KG (Karlsruhe, Germany)
Magnesium sulfate, hydrate	Carl Roth GmbH & Co. KG (Karlsruhe, Germany)
D-Mannitol 1-phosphate lithium salt	Carl Roth GmbH & Sigma-Aldrich (Munich, Germany)
2-(N-morpholino)ethanesulfonic acid (MES)	AppliChem GmbH (Darmstadt, Germany)
3-(N-morpholino)propanesulfonic acid (MOPS)	AppliChem GmbH (Darmstadt, Germany)
β -Mercaptoethanol	Carl Roth GmbH & Co. KG (Karlsruhe, Germany)
Manganese(II) chloride, tetrahydrate	AppliChem GmbH (Darmstadt, Germany)
Methanol	Carl Roth GmbH & Co. KG (Karlsruhe, Germany)
Nicotinamide adenine dinucleotide (NADH)	AppliChem GmbH (Darmstadt, Germany)
Oatmeal agar	Sigma-Aldrich (Munich, Germany)
1,4-Piperazinediethanesulfonic acid (PIPES)	AppliChem GmbH (Darmstadt, Germany)
D-Pantothenic acid calcium salt	AppliChem GmbH (Darmstadt, Germany)
Phenylmethanesulfonyl fluoride (PMSF)	AppliChem GmbH (Darmstadt, Germany)
Phosphoric acid (85 %)	Carl Roth GmbH & Co. KG (Karlsruhe, Germany)
Polyethylene glycol (PEG) 200	AppliChem GmbH (Darmstadt, Germany)
Polyethylene glycol (PEG) 400	Sigma-Aldrich (Munich, Germany)
Polyethylene glycol (PEG) 3350	Hampton Research Corp, (CA, USA)
Polyethylene glycol (PEG) 6000	Carl Roth GmbH & Co. KG (Karlsruhe, Germany)
Polyethylene glycol (PEG) 8000	Sigma-Aldrich (Munich, Germany)
Polyethylene glycol monomethyl ether (PEGmme) 2000	Fluka Chemie AG (Buchs, Switzerland)
di-Potassium hydrogen phosphate anhydrous p.A	AppliChem GmbH (Darmstadt, Germany)
Potassium di-hydrogen phosphate anhydrous	AppliChem GmbH (Darmstadt, Germany)
Potassium hydroxide	AppliChem GmbH (Darmstadt, Germany)
(-)-Riboflavin	Sigma-Aldrich (Munich, Germany)

D-Ribose 5-phosphate, disodium salt dihydrate	Sigma-Aldrich (Munich, Germany)
SYPRO® Orange protein stain	BioRad Laboratories GmbH (Munich, Germany)
Sodium chloride	AppliChem GmbH (Darmstadt, Germany)
Sodium dodecyl sulfate (SDS)	AppliChem GmbH (Darmstadt, Germany)
di-Sodium hydrogen phosphate anhydrous	AppliChem GmbH (Darmstadt, Germany)
Sodium hydroxide	AppliChem GmbH (Darmstadt, Germany)
Sodium sulfate anhydrous	AppliChem GmbH (Darmstadt, Germany)
Starch, soluble	Sigma-Aldrich (Munich, Germany)
Streptomycin sulfate	AppliChem GmbH (Darmstadt, Germany)
N,N,N',N'-	Carl Roth GmbH & Co. KG (Karlsruhe, Germany)
Tetramethylethylenediamine (TEMED)	
Thiamine hydrochloride	AppliChem GmbH (Darmstadt, Germany)
Thiamine diphosphate	Sigma-Aldrich (Munich, Germany)
2-Amino-2-hydroxymethyl-propane-1,3-diol (Tris)	AppliChem GmbH (Darmstadt, Germany)
Tryptic soy broth	Sigma-Aldrich (Munich, Germany)
Tryptone	AppliChem GmbH (Darmstadt, Germany)
Yeast extract	AppliChem GmbH (Darmstadt, Germany)
Yeast extract for high-density fermentation	Ohly GmbH (Hamburg, Germany)

Enzymes

Product

α -Glycerophosphate Dehydrogenase
 Triosephosphate Isomerase from rabbit muscle (Type III, ammonium sulfate suspension)

DNase I

FastAP (Thermosensitive Alkaline Phosphatase)

Lysozyme

Phusion® High Fidelity

DNA polymerase

Restriction endonucleases

SUMO-protease

T4-DNA-Ligase

Taq DNA polymerase

Thrombin from bovine plasma

Sequencing Grade Modified Trypsin, porcine

Supplier

Sigma-Aldrich (Munich, Germany)

AppliChem GmbH (Darmstadt, Germany)

Thermo Fisher Scientific (Braunschweig, Germany)

AppliChem GmbH (Darmstadt, Germany)

Thermo Fisher Scientific (Braunschweig, Germany)

Thermo Fisher Scientific (Braunschweig, Germany)

provided by DR. STEFAN LÜDTKE

Thermo Fisher Scientific (Braunschweig, Germany)

Thermo Fisher Scientific (Braunschweig, Germany)

Sigma-Aldrich (Munich, Germany)

Promega Corporation (Mannheim, Germany)

Bacterial strains

<i>Product</i>	<i>Supplier</i>
<i>E. coli</i> -BL21 (DE3)	Invitrogen™, (Karlsruhe, Germany)
<i>E. coli</i> -BL21 Star™ (DE3)	Invitrogen™, (Karlsruhe, Germany)
<i>E. coli</i> -DH5α	Invitrogen™, (Karlsruhe, Germany)
<i>E. coli</i> -Rosetta (DE3)	Invitrogen™, (Karlsruhe, Germany)
<i>E. coli</i> -Rosetta 2 (DE3)	Invitrogen™, (Karlsruhe, Germany)
<i>E. coli</i> -SoluBL21 (DE3)	Invitrogen™, (Karlsruhe, Germany)
<i>E. coli</i> -Top10	Invitrogen™, (Karlsruhe, Germany)
<i>E. coli</i> -XL1-Blue	Stratagene, (Heidelberg, Germany)
<i>St. melanovinaceus</i>	United States Department of Agriculture/ Agricultural Research Service, (Peoria, USA)

Vectors

<i>Product</i>	<i>Supplier</i>
pCDFDuet-1	Novagen (Schwalbach/Ts., Germany)
pET28a	Novagen (Schwalbach/Ts., Germany)
pET-SUMO	Invitrogen™, (Karlsruhe, Germany)
pJET1.2	Fisher Scientific GmbH, (Schwerte, Germany)
pMA-T	GeneArt™ (Regensburg, Germany)
pMA-RQ	GeneArt™ (Regensburg, Germany)
pMK-RQ	GeneArt™ (Regensburg, Germany)
pQE-60	QIAGEN (Hilden, Germany)

Commercially synthesized plasmids

<i>Name</i>	<i>Vector</i>	<i>Insert</i>
QncN-pET28a	pET28a	QncN
QncM-pET28a	pET28a	QncM
pMA-RQ-QncL	pMA-RQ	QncL
<i>SliE3</i> -pET28a	pET28a	<i>SliE3</i>

Generated plasmids

<i>Name</i>	<i>Vector</i>	<i>Insert</i>
QncM-pET-SUMO	pET-SUMO	QncM
QncNL-pET-SUMO	pET-SUMO	QncN/QncL
<i>SmeE3</i> -pJET1.2	pJET1.2	<i>SmeE3</i>
<i>SmeQncNML</i> -pJET1.2	pJET1.2	QncN/QncM/QncL
<i>SmeQncNML</i> -pET28a	pET28a	QncN/QncM/QncL
QncNL-pCDFDuet-1	pCDFDuet-1	<i>MCSI</i> : His ₆ -tag-TCS-QncN <i>MCSII</i> : QncL

Kit systems and solutions

<i>Product</i>	<i>Supplier</i>
Champion™ pET-SUMO Protein Expression System	Invitrogen™, (Karlsruhe, Germany)
CloneJet PCR cloning Kit	Thermo Fisher Scientific (Braunschweig, Germany)
GC-buffer	Thermo Fisher Scientific (Braunschweig, Germany)
HF-buffer	Thermo Fisher Scientific (Braunschweig, Germany)
MasterPure™ Gram positive DNA Purification Kit	Epicentre (Madison, USA)
dNTP mix (10 mM)	Thermo Fisher Scientific (Braunschweig, Germany)
NucleoSpin™ Plasmid Kit	Macherey Nagel (Düren, Germany)
NucleoSpin™ Gel and PCR Clean-Up Kit	Macherey Nagel (Düren, Germany)
BRADFORD reagent, 5x concentrate	SERVA Electrophoresis GmbH (Heidelberg, Germany)

DNA and protein standards

<i>Product</i>	<i>Supplier</i>
Gel filtration standard	BioRad Laboratories GmbH (Munich, Germany)
Gene Ruler™ 1kb DNA-Ladder	Thermo Fisher Scientific (Braunschweig, Germany)
PageRuler Unstained Protein Ladder	Thermo Fisher Scientific (Braunschweig, Germany)
Peptide Calibration Standard II	Bruker Daltonics (Bremen, Germany)
Prestained Protein Molecular Weight Marker	Thermo Fisher Scientific (Braunschweig, Germany)
Unstained Protein Molecular Weight Marker	Thermo Fisher Scientific (Braunschweig, Germany)

Crystallization screens

<i>Product</i>	<i>Supplier</i>
Additive Screen™	Hampton Research Corp, (CA, USA)
JBScreen Classic 1 – 10	Jena Bioscience GmbH, (Jena, Germany)
JBScreen Nuc-Pro HTS	Jena Bioscience GmbH, (Jena, Germany)
JCSG- <i>plus</i> ™	Molecular Dimensions Limited (Suffolk, United Kingdom)
MIDAS™	Molecular Dimensions Limited (Suffolk, United Kingdom)
Morpheus™	Molecular Dimensions Limited (Suffolk, United Kingdom)
Natrix HT™	Hampton Research Corp, (CA, USA)
ProPlex™ HT-96	Molecular Dimensions Limited (Suffolk, United Kingdom)
The AmSO ₄ Suite	QIAGEN (Hilden, Germany)
The PGA Screen™	Molecular Dimensions Limited (Suffolk, United Kingdom)

1.2 Devices

Cell cultivation

<i>Product</i>	<i>Supplier</i>
Biofermenter, Biostat C	Sartorius AG (Göttingen, Germany)
Incubation shaker, Unitron	Infors AG (Bottmingen, Switzerland)
Laminar flow Prettl®-Telstar Bio-II-A	Telstar (Terrassa, Spain)

Cell disruption

<i>Product</i>	<i>Supplier</i>
Microfluidizer, M-110S	Microfluidics (Newton, MA, USA)
Mortar Grinder RM 200	Retsch GmbH (Haan, Germany)
Sonoplus GM 70	Bandelin GmbH & Co. KG (Berlin, Germany)

Centrifuges and rotors

<i>Product</i>	<i>Supplier</i>
Avanti™ HP-30I	Beckmann Coulter GmbH (Krefeld, Germany)
Rotor JA-10	Beckmann Coulter GmbH (Krefeld, Germany)
Rotor JA-30.50 Ti	Beckmann Coulter GmbH (Krefeld, Germany)
Avanti™ J-20XPI	Beckmann Coulter GmbH (Krefeld, Germany)
Rotor JLA-8.1000	Beckmann Coulter GmbH (Krefeld, Germany)
Centrifuge tubes	Beckmann Coulter GmbH (Krefeld, Germany)
Eppendorf 5810R	Eppendorf AG (Wesseling-Berzdorf, Germany)
Rotor A-4-81	Eppendorf AG (Wesseling-Berzdorf, Germany)
Mikro 200	Hettich GmbH & Co. KG (Tuttlingen, Germany)
Rotor 2424 B	Hettich GmbH & Co. KG (Tuttlingen, Germany)
Optima™ L-90K Ultracentrifuge	Beckman Coulter GmbH (Krefeld, Germany)
Rotor SW40 Ti	Beckman Coulter GmbH (Krefeld, Germany)
Rotor SW60 class GH	Beckman Coulter GmbH (Krefeld, Germany)
Universal 320R	Hettich GmbH & Co. KG (Tuttlingen, Germany)
Rotor 1420 A/B	Hettich GmbH & Co. KG (Tuttlingen, Germany)
Rotor 1617 A	Hettich GmbH & Co. KG (Tuttlingen, Germany)
Rotor 1620 A	Hettich GmbH & Co. KG (Tuttlingen, Germany)

Liquid chromatography

<i>Product</i>	<i>Supplier</i>
ÄKTAprime plus	GE Healthcare Europe (Munich, Germany)
ÄKTApurifier	GE Healthcare Europe (Munich, Germany)
Fractogel [®] EMD TMAE 650 (S)	Merck KGaA (Darmstadt, Germany)
HiPrep [™] 26/10 desalting	GE Healthcare Europe (Munich, Germany)
HisPrep [™] FF 5 mL	GE Healthcare Europe (Munich, Germany)
Superdex [™] 75 HiLoad [™] 16/60 prep grade	GE Healthcare Europe (Munich, Germany)
Superdex [™] 75 10/300 GL	GE Healthcare Europe (Munich, Germany)
Superdex [™] 200 HiLoad [™] 16/60 prep grade	GE Healthcare Europe (Munich, Germany)
Superdex [™] 200 10/300 GL	GE Healthcare Europe (Munich, Germany)
Superloop (50 mL, 150 mL)	GE Healthcare Europe (Munich, Germany)

UV-Vis-Spectroscopy

<i>Product</i>	<i>Supplier</i>
Chirascan plus CD Spectrometer	Applied Photophysics Ltd., UK
NanoDrop 2000	Thermo Scientific, USA
Stopped-flow system SX.20	Applied Photophysics Ltd., UK
UV-Vis spectrometer, V-650	Jasco GmbH, (Groß-Umstade, Germany)
UV-Vis spectrometer, V-630	Jasco GmbH, (Groß-Umstade, Germany)
Precision cuvettes, suprasil	Hellma GmbH & Co.KG (Mühlheim, Germany)

X-ray

<i>Product</i>	<i>Supplier</i>
X-ray MicroMax [™] -007 rotating-anode generator,	Rigaku Corp., (MI, USA)
X-stream [™] 2000 Cryogenic Crystal Cooler	
Mar 345dtb image plate	

Miscellaneous

<i>Product</i>	<i>Supplier</i>
Arium [®] pro VF	Sartorius AG (Göttingen, Germany)
C1000 thermal cycler	BioRad Laboratories GmbH (Munich, Germany)
CFX96 [™] Optical Reaction Module	BioRad Laboratories GmbH (Munich, Germany)
Thermocycler TProfessional	Biometra (Göttingen, Germany)
miniDAWN TREOS [™] Light Scattering Instrument	Wyatt Technology Corporation (Santa Barbara, USA)
MTP target frame III	Bruker Daltonics (Bremen, Germany)
Optilab T-rEX Refractive Index Detector	Wyatt Technology Corporation (Santa Barbara, USA)
pH-electrode Minitrode	Hamilton Bonaduz AG (Bonaduz, Switzerland)
pH-electrode InLab [®] Easy DIN	Mettler-Toledo GmbH (Giessen, Germany)
REFLEX [™] III MALDI-TOF mass spectrometer	Bruker Daltonics (Bremen, Germany)

1.3 Commodities

<i>Product</i>	<i>Supplier</i>
Spin-X [®] UF concentrator 6, 20 mL (5 – 100 kDa MWCO)	Corning GmbH (Kaiserslautern, Germany)
ZelluTrans/Roth [®] dialysis membrane (3.5 kDa MWCO)	Carl Roth GmbH & Co. KG (Karlsruhe, Germany)
ZipTip _{C18} [™] pipette tips	Merck KGaA (Darmstadt, Germany)

1.4 Utilized Primers

All primers were purchased from Sigma-Aldrich (Munich, Germany). Restriction sites, as well as mutated bases are highlighted in red.

Mutagenesis primers

<i>Name</i>	<i>Sequence</i>
<i>Tac</i> TAL _{E60Q} sense	5' -GGTCCGTAAGCGTTCAGGTGGTTTCAACAAAGTACG-3'
<i>Tac</i> TAL _{E60Q} antisense	5' -CGTACTTTGTTGAAACCACCTGAACGCTTACCGGACC-3'
<i>Tac</i> TAL _{F132Y} sense	5' -CCTACGTATCACCATATGTTGGAAGACTTGACG-3'
<i>Tac</i> TAL _{F132Y} antisense	5' -CGTCAAGTCTTCCAACATATGGTGATACGTAGG-3'
<i>Tac</i> TAL _{S130A} sense	5' -GCGTAACCACGGCTCCAACGCTC-3'
<i>Tac</i> TAL _{S130A} antisense	5' -GAGCGTTGGA GCCGTGGTTACGC-3'
<i>Tac</i> TAL _{N108A} sense	5' -CAGAGCACATAAATACAGCCTGTACTCTTG-3'
<i>Tac</i> TAL _{N108A} antisense	5' -CAAGAGTACAGGCTGTATTTATGTGCTCTG-3'
<i>Tac</i> TAL _{N108L} sense	5' -GCACATAAATACACTGTGTACTCTTGTTCATCC-3'
<i>Tac</i> TAL _{N108L} antisense	5' -GGATTGAAAACAAGAGTACACAGTGTATTTATGTGC-3'
<i>Tac</i> TAL _{D211C} sense	5' -GCAAAATTCCTGGAA TGCTGGAAAAAGTTTCTCC-3'
<i>Tac</i> TAL _{D211C} antisense	5' -GGAGAAACTTTTTCCAGCATTCCAGGAATTTTGC-3'
<i>Tac</i> TAL _{T30C} sense	5' -CGTAACCACGAATCCATGCCTCATATCCAAAGAGG-3'
<i>Tac</i> TAL _{T30C} antisense	5' -CCTCTTTGGATATGAGGCATGGATTTCGTGGTTACG-3'
<i>Tac</i> TAL _{K86Q} sense	5' -GGAGACAATGCTGTTGTACAGATACCGATGACTGAGG-3'
<i>Tac</i> TAL _{K86Q} antisense	5' -CCTCAGTCATCGGTATCTGTACAACAGCATTGTCTCC-3'
<i>Tac</i> TAL _{S130A/F132Y} sense	5' -GTAACCTACGTAGCACCATATGTTGG-3'
<i>Tac</i> TAL _{S130A/F132Y} antisense	5' -CCAACATATGGTGTCTACGTAGGTTAC-3'
<i>QncNpDuetNdeI</i> sense	5' -CCGCGCGGCAGCCACATGGCAGCACC-3'
<i>QncNpDuetNdeI</i> antisense	5' -GGTGCTGCCATGTGGCTGCCGCGGG-3'

Cloning primers

<i>Name</i>	<i>Sequence</i>
<i>T5 terminator forward</i>	5' -GTTCTGAGGTCATTACTGG-3'
<i>T5 terminator reverse</i>	5' -CCAGTAATGACCTCAGAAC-3'
<i>SumoQncM forward</i>	5' -ATGACCACCGTTGAAAATCTGG-3'
<i>SumoQncM reverse</i>	5' -GCTATTCAGACCTTTTGC-3'
<i>pJETQncNML forward</i>	5' -GTGGCAGCACCGACCCACGGACC-3'

<i>pJETQncNML reverse</i>	5' -TCAGCTGTCGAGGAGACGGGCGAGTGACTCC-3'
<i>pET28aQncNML forward</i>	5' - [Phos]GCAGCACCCACCCACGGACCGACAGC-3'
<i>pET28aQncNML reverse</i>	5' - [Phos]CATGGTATATCTCCTTCTTAAAGTTAAACAAAATTATTTTC-3'
<i>pJETSmeE3 forward</i>	5' -ATGCATGGAGGACGTGACGTGGCGAACGACG-3'
<i>pJETSmeE3 reverse</i>	5' -TCAGTCGTGGGAGTGCAGAGGCTTGC-3'
<i>pET28aSmeE3 forward</i>	5' -GGCCATGCCATATGCATGGAGGACGTGACGTGGCGAACGACG-3'
<i>pET28aE3 reverse</i>	5' -CCGGTACGCTCGAGTCAGTCGTGGGAGTGCAGAGGCTTGC-3'

Sequencing primers

Name	Sequence
<i>T5 promotor</i>	5' -CCCGAAAAGTGCCACCTG-3'
<i>T7 promotor</i>	5' -TAATACGACTCACTATAGGG-3'
<i>T7 terminator</i>	5' -AGCTAGTTATTGCTCAGCGG-3'
<i>ACYCDuetUP1</i>	5' -GGATCTCGACGCTCTCCCT-3'
<i>DuetUP2</i>	5' -TTGTACACGGCCGCATAATC-3'
<i>DuetDOWN1</i>	5' -GATTATGCGGCCGTGTACAA-3'
<i>SUMO forward</i>	5' -AGATTCTTGTACGACGGTATTAG-3'
<i>pJET1.2 forward, 23-mer</i>	5' -CGACTCACTATAGGGAGAGCGGC-3'
<i>pJET1.2 reverse, 24-mer</i>	5' -AAGAACATCGATTTTCCATGGCAG-3'
<i>QncNL1</i>	5' -GGTGCTAAACAGGTCCAGCAGTGC-3'
<i>QncNL2</i>	5' -GCACGTGCCTTTGGTATTCC-3'
<i>QncNL3</i>	5' -GGTGGGCACATATTCATCC-3'
<i>QncNML1</i>	5' -GGTGTCTCCGAGGTTGC-3'
<i>QncNML2</i>	5' -GCAGCGCGACCACATTGCCGAGC-3'
<i>QncNML3</i>	5' -GCTCGTGATCCAGTTCAATACC-3'
<i>QncNML4</i>	5' -CGTGATCGCCGAGATCATGTTTCG-3'
<i>QncNML5</i>	5' -CGAAAAACAGTGGGAAGCTCTCG-3'

1.5 Media

LB medium (BERTANI, 1951)

Compound	Concentration
Yeast extract	0.5 % (w/v)
Tryptone	1 % (w/v)
NaCl	0.5 % (w/v)

LB-agar plates

Compound	Concentration
Yeast extract	0.5 % (w/v)
Tryptone	1 % (w/v)
NaCl	0.5 % (w/v)
Agar	2 % (w/v)

Oatmeal-agar plates

<i>Compound</i>	<i>Concentration</i>
Oatmeal agar	7.25 % (w/v)

High-density fermentation medium

<i>Compound</i>	<i>Concentration</i>
Yeast extract	5 % (w/v)
NH ₄ Cl	0.05 % (w/v)
Antifoam	1 mL for 6 L medium
Glucose	0.5 % (w/v)
MgSO ₄	2.75 mM
K ₂ HPO ₄	63.15 mM
Kanamycin sulfate	50 µg/mL
Carbenicillin	100 µg/mL

Feeding solution

<i>Compound</i>	<i>Concentration</i>
Yeast extract	30 % (w/v)
Glycerol	25 % (v/v)

ZYM5052 auto-induction medium (STUDIER, 2005)**ZY**

<i>Compound</i>	<i>Concentration</i>
Yeast extract	0.5 % (w/v)
Tryptone	1 % (w/v)

25xM

<i>Compound</i>	<i>Concentration</i>
Na ₂ HPO ₄	25 mM
KH ₂ PO ₄	25 mM
NH ₄ Cl	50 mM
Na ₂ SO ₄	5 mM

50x5052

<i>Compound</i>	<i>Concentration</i>
Glycerol	25 % (w/v)
D-Glucose	2.5 % (w/v)
D-Lactose	10 % (w/v)

The pH of 25xM was adjusted with KOH to 7.0. 8 mL 50x5052, 16 mL 25xM and 2 mM MgSO₄ were added to 400 mL ZY after treatment by autoclave (20 min, 121 °C).

M9 minimal medium (STUDIER, 2005)**10x M9 salt solution**

<i>Compound</i>	<i>Concentration</i>
Na ₂ HPO ₄	478 mM
KH ₂ PO ₄	220 mM
NaCl	86 mM
NH ₄ Cl	187 mM

1000x trace element solution (in 60 mM HCl)

<i>Compound</i>	<i>Concentration</i>
FeCl ₃	50 mM
CaCl ₂	20 mM
MnCl ₂ , ZnSO ₄	10 mM each
CoCl ₂ , CuCl ₂ , NiCl ₂	2 mM each
Na ₂ MoO ₄ , Na ₂ SeO ₃ , H ₃ BO ₃	2 mM each

The pH of the 10x M9 salt solution was adjusted with KOH to 7.0. 50 mL of the M9 salt solution, 500 µL of the 100 mM CaCl₂ stock solution, 500 µL of the 1 M MgSO₄ stock solution, 100 µL of the 1000x trace element solution and 3 mL of the 50 % (v/v) glycerol solution were added to 446 mL water after treatment by autoclave (20 min, 121 °C).

Seed medium for *Streptomyces* cultivation

<i>Compound</i>	<i>Concentration</i>
Soluble starch	2.4 % (w/v)
Yeast extract	0.5 % (w/v)
Tryptone	0.5 % (w/v)
Beef extract	0.3 % (w/v)

100x Salt solution

<i>Compound</i>	<i>Concentration</i>
K ₂ HPO ₄	230 mM
KH ₂ PO ₄	220 mM

The pH of the seed medium and salt solution was adjusted to 7.0. The seed medium was supplemented with 1.0 % (w/v) glucose, 1x salt solution and 0.2 g/L MgSO₄ after treatment by autoclave (45 min, 121 °C).

TSB/glycine-medium

<i>Compound</i>	<i>Concentration</i>
Tryptic soy broth	3 % (w/v)
Glycine	0.5 % (w/v)

The pH of the medium was adjusted to 7.0. The medium was supplemented with 5.0 % (w/v) glucose after treatment by autoclave (45 min, 121 °C).

1.6 Methods

1.6.1 Molecular Biology

1.6.1.1 Determination of DNA Concentration

The DNA concentration was measured using a NanoDrop 2000 device. The absorbance (A_{260}) of the DNA solution was measured at 260 nm (path length $d = 1$ cm). The DNA concentration (c) was calculated according to the BEER-LAMBERT equation (eq. 1.6.1) using an extinction coefficient of $\varepsilon = 20$ (mL/ng · cm⁻¹) according to the manufacturer's manual (Thermo Scientific, USA).

$$A_{260} = c \cdot \varepsilon \cdot d \quad (1.6.1)$$

1.6.1.2 Plasmid Transformation

Plasmid DNA was transferred into different chemical competent *E. coli*-strains for the purpose of plasmid proliferation (DH5 α , XL1-Blue and Top10) or for the recombinant protein expression (BL21 (DE3), BL21 StarTM (DE3), SoluBL21 (DE3), Rosetta (DE3) and Rosetta 2 (DE3)). The chemical competent cells were prepared according to INOUE *et al.* (1990) or acquired by purchase (for details see page 17).

For the plasmid transformation, 1 μ L of DNA solution (5 ng/ μ L) was added to 50 μ L of respective chemical competent cells. The cells were incubated on ice for 30 min. After heat shock (30 s, 42 °C) and further incubation on ice for 5 min, the cells were supplied with 1 mL SOC-medium. The cells were grown for 1 h at 37 °C.

The selection of transformants, containing plasmid DNA of interest, took place on LB-agar plates (section 1.5) supplemented with appropriate antibiotic (100 μ g/mL carbenicillin, 50 μ g/mL kanamycin or 50 μ g/mL streptomycin).

1.6.1.3 Isolation of Plasmid DNA

In order to isolate plasmid DNA, 10 mL of LB medium culture ($OD_{600} = 2.5 - 3.5$) of transformed *E. coli* cells were pelleted by centrifugation (8 °C, 3220 x g, 10 min). The cell pellet was used

for plasmid isolation using NucleoSpin™ Plasmid Kit according to the manufacturer's manual (Macherey Nagel, Germany).

1.6.1.4 DNA Sequencing

The sequence of the generated gene constructs was determined by a company (Seqlab [Göttingen, Germany] or GATC Biotech AG [Constance, Germany]) and checked for correctness. The primers utilized for the sequencing reaction are listed on page 22.

1.6.1.5 Polymerase Chain Reaction

Polymerase chain reaction (PCR, (MULLIS *et al.*, 1986)) was used to amplify specific DNA fragments for cloning procedure, as well as for the introduction of desired mutations into the insert sequence. Phusion® DNA-polymerase was used in the standard approach according to the supplier's instructions (MBI Fermentas, Germany).

The designed protein variants were generated using the QuikChange site-directed mutagenesis protocol (Stratagene, La Jolla, USA) adapted for Phusion® DNA-polymerase.

The methylated template DNA was digested using *DpnI* restriction endonuclease according to the manufacturer's manual (MBI Fermentas, Germany).

DNA fragments amplified in the polymerase chain reaction were purified using the NucleoSpin™ Gel and PCR Clean-Up Kit according to the manufacturer's manual (Macherey Nagel, Germany).

1.6.1.6 DNA Fragment Separation via Agarose Gel Electrophoresis

In order to separate DNA fragments by their sequence length, agarose gel electrophoresis was used for analytical or preparative purposes. The DNA solution was mixed with 6x DNA gel loading dye (Thermo Scientific™, Germany) in a 1:5 volume ratio and loaded onto a 1% agarose/TAE gel. The electrophoresis was performed at constant voltage of 100 V in TAE-buffer (40 mM Tris/HCl, 20 mM acetic acid, 1 mM EDTA, pH 7.0). The gel was stained for 30 min in an ethidium bromide bath (2 µg/mL). The DNA detection was carried out by exposure of the ethidium bromide stained gel to UV light. The size of distinct DNA-fragments was determined using Gene Ruler™ 1kb DNA-Ladder as a size standard. In the preparative approach, the DNA fragment of expected size

was extracted from the agarose slice using NucleoSpin[™] Gel and PCR Clean-Up Kit according to the provided manual (Macherey Nagel, Germany).

1.6.1.7 General Cloning Procedure

In order to insert a desired sequence into the multiple cloning site (MCS) of the appropriate vector (e.g. pET28a or pCDFDuet-1), sticky-end cloning was used as standard approach. The coding sequence containing plasmid or PCR amplification and the target vector were digested using appropriate restriction endonucleases (*NcoI* and *HindIII* or *NdeI* and *XhoI*) according to the supplier's instructions (MBI Fermentas, Germany).

The linearized target vector was dephosphorylated using thermosensitive alkaline phosphatase (FastAP) following the manufacturer's protocol (MBI Fermentas, Germany). The DNA fragments were isolated and purified as described in section 1.6.1.6.

The sequence to be inserted was ligated into the linearized dephosphorylated target vector using T4-DNA-ligase corresponding to the product information (MBI Fermentas, Germany).

The resulting plasmid containing the desired sequence in the MCS was transferred into a chemical competent *E. coli* strain as described in section 1.6.1.2. The plasmid DNA was isolated according to section 1.6.1.3 and the insert of the isolated construct was verified by sequencing (section 1.6.1.4).

1.6.1.8 Generation of the QncNL-pCDFDuet-1 Construct

In order to recombinantly co-express the QncN- and QncL-subunits, the coding sequences of the respective proteins were cloned into the MCSI and MCSII of pCDFDuet-1 vector, respectively. The codon optimized (*E. coli*) sequence of the QncN-subunit was synthesized by GeneArt[™] (Regensburg, Germany). The gene was supplied as an *NdeI/HindIII*-insert in the pET28a vector (QncN-pET28a). The sequence, containing a His₆-tag, thrombin cleavage site (TCS), *NdeI* restriction site and the QncN gene was cloned as an *NcoI/HindIII*-insert from the QncN-pET28a plasmid into the MCSI of the pCDFDuet-1 vector. The sequence of the *NdeI* restriction site (*CATATG*) was mutated to *CACATG*.

The codon optimized (*E. coli*) sequence of the QncL gene was supplied by GeneArt[™] (Regensburg, Germany) as an *SfeI/SfeI*-insert in pMA-RQ vector (pMA-RQ-QncL). The QncL gene was

cloned into the MCSII of pCDFDuet-1 vector using the *NdeI/XhoI* restriction sites. The resulting QncNL-pCDFDuet-1 plasmid containing the coding sequence of an N-terminal His₆-tag, thrombin cleavage site (TCS) and the QncN gene in the MCSI and the coding sequence of the QncL-subunit as an *NdeI/XhoI* insert in the MCSII of the pCDFDuet-1 vector was transferred into the chemical competent *E. coli* XL1-blue strain. The inserts of the QncNL-pCDFDuet-1 construct were verified by sequencing using the *ACYCDuetUP1*, *DuetDOWN1*, *DuetUP2*, *QncNL1-3* and *T7 terminator* sequencing primers (see page 22).

1.6.1.9 Generation of the QncM-pET-SUMO Construct

The codon optimized (*E. coli*) sequence of the QncM component was synthesized by GeneArt[™] (Regensburg, Germany). The QncM gene was supplied as *NdeI/XhoI*-insert in the pET28a vector (QncM-pET28a). The insert was amplified using *Taq* DNA polymerase in a PCR approach (section 1.6.1.5) according to the manufacturer's manual (MBI Fermentas, Germany). The amplified DNA fragment was cloned into the pET-SUMO vector (Champion[™] pET-SUMO Protein Expression System) using TA-Cloning[®] according to the manufacturer's manual (Invitrogen[™], Germany).

The resulting QncM-pET-SUMO plasmid containing the coding sequence of an N-terminal His₆-tag, SUMO fusion protein and the QncM component was transferred into the chemical competent *E. coli* XL1-blue strain. The plasmid DNA was isolated as described in section 1.6.1.3. The sequence of the gene of interest was verified by sequencing using the *T7 terminator* sequencing primer (see page 22).

1.6.1.10 Generation of the QncNL-pET-SUMO Construct

A DNA fragment from the QncNL-pCDFDuet-1 construct, containing the coding sequences of QncN- and QncL-subunits was amplified using *Taq* DNA polymerase in a PCR approach (section 1.6.1.5) according to the manufacturer's manual (MBI Fermentas, Germany). The amplified DNA fragment was cloned into the pET-SUMO vector (Champion[™] pET-SUMO Protein Expression System) using TA-Cloning[®] according to the manufacturer's manual (Invitrogen[™], Germany).

The resulting QncNL-pET-SUMO plasmid contains the coding sequence of an N-terminal His₆-tag, SUMO fusion protein and the QncN-subunit, as well as the coding sequence for the QncL-subunit

and an additional T7-promotor and ribosomal binding site (RBS) originating from the pCDFDuet-1 vector. The construct was transferred into the chemical competent *E. coli* XL1-blue strain. The plasmid DNA was isolated as described in section 1.6.1.3. The sequences of the genes of interest were verified by sequencing using the *SUMO forward*, *DuetDOWN1*, *DuetUP2*, *QncNLI-3* and *T7 terminator* sequencing primers (see page 22). A schematic overview of the cloning strategy for generation of the QncNL-pET-SUMO construct is shown in the appendix part (Scheme B.1).

1.6.1.11 Cultivation of *Streptomyces melanovinaceus*

The *Streptomyces melanovinaceus* (*St. melanovinaceus*, *Sme*) strain (NRRL 12388) was kindly provided by the Agricultural Research Service of United States Department of Agriculture. The strain was cultivated according to TOMITA *et al.* (1983), NIKODINOVIC *et al.* (2003) and SHEPHERD *et al.* (2010) in 20 mL seed medium (section 1.5) for 24 h at 28 °C under constant shaking (200 rpm). This pre-culture was used to inoculate 20 mL TSB/glycine-medium in a 100 mL culture flask. The TSB/glycine-culture was grown for 72 h at 28 °C under constant shaking (200 rpm).

1.6.1.12 Isolation of Genomic DNA from *St. melanovinaceus*

In order to isolate *St. melanovinaceus* genomic DNA, 1 mL of the TSB/glycine culture was centrifuged (30 min, 8 °C, 21382 x g). The mycelium pellet was subjected for the isolation of the genomic DNA using MasterPure™ Gram positive DNA Purification Kit according to the manufacturer's manual (Epicentre, USA).

1.6.1.13 Sequencing of Genomic DNA from *St. melanovinaceus*

A part of genomic DNA from *St. melanovinaceus* was sequenced by DR. ANJA POEHLEIN (Georg-August University of Göttingen, Department of Genomic and Applied Microbiology). The draft sequence was automatically annotated by the Integrated Microbial Genomes Database (<https://img.jgi.doe.gov/>, MARKOWITZ *et al.* (2012)).

1.6.1.14 Storage of Recombinant *E. coli* Cells

For the long-term storage, *E. coli* cells were prepared as a glycerol stock solution. 0.5 mL of an LB medium cell culture (OD₆₀₀ = 0.6 – 0.8) were mixed with 0.5 mL glycerol stock solution

(65 % (v/v) glycerol, 1 mM MgSO₄, 25 mM Tris/HCl, pH 8.0), flash frozen in liquid nitrogen and stored at -80 °C.

1.6.1.15 Storage of *St. melanovinaceus* as a Glycerol Stock

The *St. melanovinaceus* mycelium was stored as a glycerol stock. 0.5 mL of the *St. melanovinaceus* culture (seed medium culture or TSB/glycine culture, section 1.6.1.11) were mixed with 0.5 mL glycerol solution (final concentration: 25 % (v/v)), flash frozen in liquid nitrogen and stored at -80 °C.

For long-term storage, a glycerol stock of a *St. melanovinaceus* spore suspension was prepared. 200 µL of the seed medium culture (section 1.6.1.11) were transferred to an oatmeal-agar plate and incubated for a week at 28 °C. The sporulated culture was used to prepare glycerol stocks according to SHEPHERD *et al.* (2010). The spores of a freshly sporulated oatmeal-agar plate were re-suspended in 3 mL sterile water. The *St. melanovinaceus* spores containing suspension was diluted in 35 mL sterile water and vigorously mixed using a vortex mixer. The suspension was filtered using a sterile cotton filter. The filtrate was discarded and the remaining spores were collected in 10 mL sterile water and pelleted via centrifugation (10 min, 8 °C, 2000 x g). The pellet was re-suspended in 1 mL sterile water. The *St. melanovinaceus* spores suspension was mixed with glycerol solution (50 % (v/v)) in a 1:1 volume ratio, flash frozen in liquid nitrogen and stored at -80 °C.

1.6.1.16 Generation of the *SmeE3*-pJET1.2 Construct

The native coding sequence of the E3 component from *St. melanovinaceus* (*SmeE3*) was amplified from the isolated *St. melanovinaceus* genome in a PCR approach using *pJETSmE3 forward* and *reverse* primers (see page: 21). The amplified PCR product was isolated according to section 1.6.1.6. The purified DNA fragment was cloned into the pJET1.2 vector (CloneJet PCR cloning Kit) using blunt-end cloning according to the manufacturer's manual (MBI Fermentas, Germany).

The resulting *SmeE3*-pJET1.2 plasmid, containing the coding sequence of the *SmeE3* gene was transferred into the chemical competent *E. coli* DH5α strain. The plasmid DNA was isolated as described in section 1.6.1.3. The sequence of the gene of interest was verified by sequencing using the *pJET1.2 forward*, 23-mer and *pJET1.2 reverse*, 24-mer sequencing primers (see page 22).

1.6.1.17 Generation of the *SmeQncNML*-pET28a Construct

In order to generate a DNA construct for a more natural expression of the QncN/L component, the original gene sequences for QncN/QncL-subunits and the QncM protein were cloned into the pET28a vector. The coding cassette, containing the gene sequences for all three proteins, was amplified from the *St. melanovinaceus* genomic DNA using the PCR technique (primers: *pJETQncNML forward* and *pJETQncNML reverse*). The PCR product was isolated according to section 1.6.1.6. The purified DNA fragment was cloned into the pJET1.2 vector (CloneJet PCR cloning Kit) using blunt-end cloning according to the manufacturer's manual (MBI Fermentas, Germany).

The resulting *SmeQncNML*-pJET1.2 plasmid, containing the coding cassette for the QncN, QncL and QncM proteins was transferred into the chemical competent *E. coli* XL1-blue strain. The plasmid was isolated as described in section 1.6.1.3. The QncNML-cassette was cloned from the resulting *SmeQncNML*-pJET1.2 plasmid into the pET28a vector according to section 1.6.1.7 using *NcoI* and *XhoI* restriction endonucleases.

The resulting construct contains a DNA sequence originating from the pJET1.2 plasmid between the *NcoI* restriction site and the start codon of QncN from *SmeQncNML* coding cassette. In order to remove this additional sequence, a PCR amplification was applied using *pET28aQncNML forward* and *pET28aQncNML reverse* primers. The resulting PCR product was ligated using T4-DNA-ligase according to the product information (MBI Fermentas, Germany).

The *SmeQncNML*-pET28a construct, containing the coding cassette for QncN/QncL-subunits and the QncM protein was transferred into the chemical competent *E. coli* XL1-blue strain. The plasmid DNA was isolated as described in section 1.6.1.3. The sequences of the genes of interest were verified by sequencing using the *QncNML1-5*, as well as *T7 terminator/promotor* sequencing primers (see page 22).

1.6.2 Protein Preparation

1.6.2.1 Sodium Dodecyl Sulfate – Polyacrylamide Gel Electrophoresis (SDS-PAGE)

In order to monitor the purification process of the respective proteins and to evaluate the homogeneity of a protein sample, sodium dodecyl sulfate – polyacrylamide gel electrophoresis (SDS-PAGE)

was applied (LAEMMLI, 1970). This method allows to separate denatured proteins by molecular weight. In order to visualize the separated proteins, the polyacrylamide gel was stained with Coomassie Brilliant Blue G250 after the electrophoresis. The molecular weight of the proteins assigned to the distinct bands detected on the gel was estimated using molecular weight size markers listed on page 18.

1.6.2.2 Determination of Protein Concentration

The protein concentration was determined according to the method published by BRADFORD (1976) using a commercially available BRADFORD reagent according to the manufacturer's manual (SERVA Electrophoresis GmbH, Germany). The reagent was calibrated using different bovine serum albumin solutions of known concentration (0.1 – 0.9 mg/mL).

In addition to the BRADFORD measurements, the concentration of the active sites of the E3 component from *St. lividans* (*SliE3*), containing enzyme bound FAD, was determined optically, using the intrinsic absorption signal of the cofactor at 458 nm.

The molar extinction coefficient (ϵ_{458}) of enzyme bound FAD in *SliE3* was determined according to the method published by HOPKINS AND WILLIAMS (1995). The absorbance of *SliE3* containing solutions (0.5 – 15.0 mg/mL *SliE3*, 10 mM $\text{KH}_2\text{PO}_4/\text{K}_2\text{HPO}_4$, 0.3 mM EDTA, pH 7.6) was measured at 458 nm, as well as in presence of 4.5 mM guanidinium chloride (incubated for 1 h at RT) at 450 nm in a 1 mL quartz cuvette with a path length of 1 cm. The concentration of FAD was optically determined at 450 nm using the molar extinction coefficient of free FAD ($\epsilon_{450} = 11800 \text{ M}^{-1} \text{ cm}^{-1}$ (HOPKINS AND WILLIAMS, 1995)) in guanidinium chloride containing buffer according to the BEER-LAMBERT equation (eq. 1.6.1).

The determined concentration of free FAD in guanidinium chloride containing buffer was plotted against the measured absorption of the enzyme bound FAD at 458 nm. The slope of the applied linear regression corresponds to the molar extinction coefficient (ϵ_{458}) of enzyme bound FAD in *SliE3* at 458 nm according to the BEER-LAMBERT equation (eq. 1.6.1).

The protein concentration of *TacTAL* was determined by measuring the intrinsic absorption signal of aromatic amino acid residues (especially Tyr and Trp) and cystines at 280 nm. The concentration of *TacTAL* (wild type and variants) was measured in a NanoDrop 2000 device. The molar extinction coefficients (ϵ_{280}) were calculated using the ProtParam online-tool (<http://web.expasy.org/protparam/>,

GASTEIGER *et al.* (2005)) according to EDELHOCH (1967), GILL AND VON HIPPEL (1989) and PACE *et al.* (1995). An overview of calculated molar extinction coefficients is shown in the appendix part (Table A.1).

1.6.2.3 General Expression Test

In order to determine the cultivation conditions for the optimal recombinant expression of particular proteins, a preliminary expression test was performed. As standard approach, different *E. coli*-strains (BL21 (DE3), BL21 StarTM (DE3), SoluBL21 (DE3), Rosetta (DE3) and Rosetta 2 (DE3)) were used for the recombinant expression. The cells were grown in three different media (LB medium, ZYM5052 autoinduction medium or M9 minimal medium). Optionally, the recombinant expression was performed at different temperatures (16 °C or 37 °C). Additionally, different concentrations of IPTG (0.05 mM, 0.1 mM, 0.2 mM or 1 mM) were used for the induction.

Expression of the protein of interest was verified via SDS-PAGE. The cells were harvested via centrifugation (30 min, 8 °C, 5749 x g). In order to analyze the solubility of the recombinantly expressed protein, 1 g of cell pellet was re-suspended in 70 mL of appropriate lysis buffer supplemented with 500 µM PMSF. The cell disruption was achieved via sonication. After centrifugation (30 min, 8 °C, 75000 x g), the soluble and insoluble fractions were analyzed via SDS-PAGE.

1.6.2.4 Recombinant Expression of the His₆-QncN/L Component

For recombinant, heterologous co-expression of QncN- and QncL-subunits, the QncNL-pCDFDuet-1 plasmid (section 1.6.1.8) was transferred into the BL21 StarTM (DE3) *E. coli* strain. The transformants were used to inoculate 200 mL of LB medium supplemented with 50 µg/mL streptomycin sulfate. This pre-culture was incubated overnight at 30 °C under constant shaking (200 rpm) in a 1 L baffled flask. The pre-culture was used for the inoculation (final OD₆₀₀ = 0.1) of 400 mL main-culture (ZYM5052 autoinduction medium supplemented with 1 mM (+/-)- α -lipoic acid, 1.5 mM thiamine hydrochloride, 250 µM D-pantothenic acid calcium salt and 50 µg/mL streptomycin sulfate). The main-culture was incubated at 30 °C under constant shaking (220 rpm) in a 2 L baffled flask. After an OD₆₀₀ of 0.4 – 0.5 was reached, the main-culture was cooled to 16 °C and incubated for 24 h under constant shaking (220 rpm).

The recombinant expression of QncN- and QncL-subunits was verified via SDS-PAGE (section 1.6.2.1). The cells were harvested via centrifugation (30 min, 8 °C, 5749 x g). The flash frozen cell pellets were stored at -20 °C.

1.6.2.5 Purification of the His₆-QncN/L Component

The purification of QncN/L component was performed based on a previously published protocol (PENG *et al.*, 2012). For the cell disruption, 10 – 15 g of cells were re-suspended on ice in 20 – 30 mL loading buffer (50 mM MOPS, 20 mM imidazole, 300 mM NaCl, 400 µM ThDP, 2.5 mM MgCl₂, 10 % (v/v) glycerol, pH 7.8) supplemented with 500 µM PMSF. After addition of a tip of a spatula of lysozyme, the cell suspension was stirred for 30 min at 8 °C. In order to digest DNA molecules, DNase I was added to a concentration of 5 µg/mL. After further incubation for 1 h at 8 °C under constant stirring, the cell disruption was completed by 3 – 4 passages through the microfluidizer device (80 psi). The cell debris were removed via centrifugation (30 min, 8 °C, 75000 x g).

The soluble fraction was applied onto a 5 mL HisPrepTM fast flow column, equilibrated with loading buffer. In order to remove unspecifically bound proteins, the column was washed with washing buffer (50 mM MOPS, 50 mM imidazole, 300 mM NaCl, 400 µM ThDP, 2.5 mM MgCl₂, 10 % (v/v) glycerol, pH 7.8) until the flow-through did not contain any detectable amounts of protein. QncN/L component was eluted with the elution buffer (50 mM MOPS, 300 mM imidazole, 300 mM NaCl, 400 µM ThDP, 2.5 mM MgCl₂, 10 % (v/v) glycerol, pH 7.8).

The concentration of QncN/L component was adjusted to a concentration of 5 – 10 mg/mL (BRADFORD reagent, section 1.6.2.2) using a centrifugal concentrator (20 mL, 100 kDa MWCO, 4 °C, 3220 x g).

The protein was dialyzed overnight at 8 °C against storage buffer (50 mM MOPS, 50 mM NaCl, 400 µM ThDP, 2.5 mM MgCl₂, 10 % (v/v) glycerol, pH 7.8) in a 1:2000 ratio. The purity of the isolated protein was assessed by SDS-PAGE. The protein was stored on ice for a couple of days.

1.6.2.6 Recombinant Expression of the His₆-SUMO-QncM Component

In order to recombinantly express the QncM SUMO-fusion protein in its physiological active holo-form, the Sfp-pQE60 plasmid (kindly provided by PROF. DR. M. A. MARAHIEL [Philipps-University, Marburg]) was co-transferred into the QncM-pET-SUMO plasmid containing BL21 StarTM (DE3) *E. coli* strain. The Sfp-pQE60 plasmid contains the coding sequence for the phosphopantetheinyl

transferase from *Bacillus subtilis* (*BsSfp*). *BsSfp* catalyzes the transfer of the phosphopantetheinyl moiety from CoA to the conserved Ser-residue of ACP homologs (MARAHIEL *et al.*, 1997; MOFID *et al.*, 1999; PENG *et al.*, 2012; QUADRI *et al.*, 1998).

The transformants were used to inoculate 200 mL of LB medium supplemented with 50 µg/mL kanamycin sulfate and 50 µg/mL carbenicillin. This pre-culture was incubated overnight at 30 °C under constant shaking (200 rpm) in a 1 L baffled flask.

The pre-culture was used for the inoculation (final OD₆₀₀ = 0.1) of 6 L high-density fermentation medium supplemented with 50 µg/mL kanamycin sulfate and 50 µg/mL carbenicillin. The fermentation was performed in a 10 L fermenter, while stirring (200 – 1500 rpm). The cells were grown at 37 °C. The glycerol feeding was started after the glucose in the medium was consumed. When an OD₆₀₀ of 24 was reached, the culture was cooled to 18 °C before it was supplemented with 50 µM IPTG (expression start), 1 mM D-pantothenic acid calcium salt and additional 50 µg/mL carbenicillin.

The fermentation occurred at constant O₂-concentration of 25 % (airflow 5 L/min) and pH 7.0 (automated adjustment with 10 % NaOH or 10 % H₃PO₄). After 22 h (OD₆₀₀ of 100), the cells were harvested via centrifugation (30 min, 8 °C, 5749 x g). The cell pellet (1.4 kg) was stored at -80 °C. The expression of SUMO-QncM was verified via SDS-PAGE.

1.6.2.7 Purification of the holoQncM Component

The His₆-tagged SUMO-QncM fusion-protein was purified using Ni²⁺-NTA affinity chromatography. 50 g of cells from high-density fermentation were re-suspended in 100 mL loading buffer (50 mM MOPS, 40 mM imidazole, 300 mM NaCl, 1 mM DTT, 10 % (v/v) glycerol, pH 7.6) supplemented with 500 µM PMSF. After addition of a tip of a spatula of lysozyme, the cell suspension was stirred for 30 min at 8 °C. In order to digest DNA molecules, DNase I was added to a final concentration of 5 µg/mL together with 5 mM MgCl₂. After further incubation for 1 h at 8 °C under constant stirring, the cell disruption was completed by 3 – 4 passages through the microfluidizer device (80 psi). The cell debris were removed via centrifugation (30 min, 8 °C, 75000 x g).

The soluble fraction was applied onto 3x5 mL HisPrep[™] fast flow columns, previously equilibrated with loading buffer. In order to remove unspecifically bound proteins, the columns were washed with the loading buffer until the flow-through did not contain any detectable amounts of

protein. The His₆-tagged SUMO-QncM protein was eluted with the elution buffer (50 mM MOPS, 250 mM imidazole, 300 mM NaCl, 1 mM DTT, 10 % (v/v) glycerol, pH 7.4).

The fractions containing the His₆-tagged SUMO-QncM protein were pooled and the elution buffer was exchanged by loading buffer using a HiPrepTM 26/10 desalting column. The desalted protein was supplemented with 80 nM SUMO-protease, in order to cleave the N-terminal fused His₆-tagged SUMO-protein. The SUMO-protease cleavage was performed overnight at 8 °C.

After SUMO-protease cleavage, the protein solution was applied onto 3x5 mL HisPrepTM fast flow columns, equilibrated with the loading buffer, in order to remove cleaved His₆-tagged SUMO-protein. The flow-through, containing untagged holoQncM protein, was collected.

The protein concentration was adjusted to 40 mg/mL using a centrifugal concentrator (20 mL, 5 kDa MWCO, 4 °C, 3220 x g). The flash frozen protein solution can be stored at -80 °C for several month.

Before usage, the protein was applied onto a SuperdexTM 75 HiLoadTM 16/60 prep grade column, equilibrated with the storage buffer (100 mM imidazole, 100 mM NaCl, 10 % (v/v) glycerol, pH 7.4) supplemented with 1 mM DTT. The purity of the isolated protein was assessed by SDS-PAGE.

1.6.2.8 Recombinant Expression of the His₆-*SliE3* Component

The codon optimized (*E. coli*) sequence of *SliE3* was synthesized by GeneArtTM (Regensburg, Germany). The *SliE3* gene was supplied as an *NdeI/XhoI*-insert in pET28a vector (*SliE3*-pET28a). The *SliE3*-pET28a plasmid was transferred into BL21 StarTM (DE3) *E. coli* strain. The transformants were used to inoculate 200 mL of LB medium supplemented with 50 µg/mL kanamycin sulfate. This pre-culture was incubated overnight at 30 °C under constant shaking (200 rpm) in a 1 L baffled flask. The pre-culture was used for the inoculation (final OD₆₀₀ = 0.1) of 400 mL main-culture (ZYM5052 autoinduction medium supplemented with 0.5 g/L riboflavin, 75 µg/mL FMN and 50 µg/mL kanamycin sulfate). The main-culture was incubated at 30 °C under constant shaking (200 rpm) in a 2 L baffled flask. After an OD₆₀₀ of 0.4 – 0.5 was reached, the main-culture was cooled to 16 °C and incubated for 24 h under constant shaking (200 rpm).

The expression of *SliE3* was verified via SDS-PAGE. The cells were harvested via centrifugation (30 min, 8 °C, 5749 x g). The flash frozen cell pellets were stored at -20 °C.

1.6.2.9 Purification of the *SliE3* Component

Since the recombinantly expressed *SliE3* protein contains an N-terminal His₆-tag linked by the thrombin cleavage site (TCS), the purification of *SliE3* component was performed using Ni²⁺-NTA affinity chromatography. 10 g of cells were re-suspended on ice in 40 mL loading buffer (50 mM KH₂PO₄/K₂HPO₄, 50 mM imidazole, 300 mM NaCl, pH 7.6) supplemented with 500 μM PMSF and 250 μM FAD. After addition of a tip of a spatula of lysozyme, the cell suspension was stirred for 30 min at 8 °C. In order to digest DNA molecules, DNase I was added to a concentration of 5 μg/mL together with 1 mM MgCl₂. After further incubation for 1 h at 8 °C under constant stirring, the cell disruption was completed by 3 – 4 passages through the microfluidizer device (80 psi). The cell debris were removed via centrifugation (30 min, 8 °C, 75000 x g).

The soluble fraction was applied onto 2x5 mL HisPrep[™] fast flow columns, previously equilibrated with the loading buffer. In order to remove unspecifically bound proteins the columns were washed with the loading buffer until the flow-through did not contain any detectable amounts of protein. The *SliE3* protein was eluted with the elution buffer (50 mM KH₂PO₄/K₂HPO₄, 250 mM imidazole, 300 mM NaCl, pH 7.6).

The *SliE3* containing fractions were pooled and the elution buffer was exchanged by loading buffer using a HiPrep[™] 26/10 desalting column. The desalted protein was supplemented with a tip of a spatula of thrombin from bovine plasma and 250 μM FAD, in order to cleave the N-terminal His₆-tag. The thrombin cleavage was performed overnight at 8 °C.

After thrombin cleavage, the protein solution was applied onto 2x5 mL HisPrep[™] fast flow columns, equilibrated with the loading buffer, in order to separate the cleaved fragments and to remove uncleaved His₆-tagged *SliE3*. The flow-through was collected and its volume was reduced to 1 mL using a centrifugal concentrator (20 mL, 50 kDa MWCO, 4 °C, 3220 x g).

The concentrated protein was applied onto a Superdex[™] 200 HiLoad[™] 16/60 prep grade column, equilibrated with the storage buffer (50 mM KH₂PO₄/K₂HPO₄, 150 mM NaCl, pH 7.6), to remove the free FAD and the remaining thrombin from bovine plasma.

Finally, the concentration of the *SliE3* component was adjusted to approximately 60 mg/mL (BRADFORD reagent, section 1.6.2.2) using a centrifugal concentrator (20 mL, 50 kDa MWCO, 4 °C, 3220 x g). The amino acid sequence of the resulting protein is identical with the native sequence of untagged protein, except the three additional amino acid residues (Gly-Ser-His) remaining on

the N-terminal part after thrombin cleavage. The purity of the isolated protein was assessed by SDS-PAGE.

1.6.2.10 Recombinant Expression of the *TacTAL* Wild Type Protein and Variants

The pET28a-construct containing the coding sequence for transaldolase from *Thermoplasma acidophilum*, as well as for the N- and C-terminal subunits of transketolase (TKI/TKII) inserted between *NdeI* and *HindIII* restriction sites of MCS (*TacTAL*-pET28a), was used as described by LEHWESS-LITZMANN (2011).

The *TacTAL*-pET28a plasmid was transferred into the BL21 StarTM (DE3) *E. coli* strain. The transformants were used to inoculate 200 mL of LB medium supplemented with 50 µg/mL kanamycin sulfate. This pre-culture was incubated overnight at 30 °C under constant shaking (200 rpm) in a 1 L baffled flask. The pre-culture was used for the inoculation (final OD₆₀₀ = 0.1) of 500 mL main-culture (LB-medium supplemented with 50 µg/mL kanamycin sulfate). The main-culture was incubated at 37 °C under constant shaking (200 rpm) in a 2 L baffled flask. After an OD₆₀₀ of 0.6 – 0.8 was reached, the recombinant expression of *TacTAL* was induced by addition of 200 µM of IPTG.

The expression of *TacTAL* was verified via SDS-PAGE. The cells were harvested via centrifugation (30 min, 8 °C, 5749 x g). The flash frozen cell pellets were stored at -20 °C.

1.6.2.11 Purification of the *TacTAL* Wild Type Protein and Variants

The purification of *TacTAL* wild type protein and variants was performed based on a previously published protocol (LEHWESS-LITZMANN *et al.*, 2011a). For cell disruption, 20 g of cells were re-suspended in 40 – 60 mL of lysis buffer (100 mM Tris/HCl, pH 7.5) supplemented with 500 µM PMSF and 1 mM EDTA. After addition of a tip of a spatula of lysozyme, the cell suspension was stirred for 15 min at RT. In order to digest DNA molecules, DNase I was added to a concentration of 5 µg/mL together with 5 mM MgCl₂. After further incubation for 45 min at RT under constant stirring, the cell disruption was completed by 3 – 4 passages through the microfluidizer device (80 psi). The cell debris were removed via centrifugation (30 min, 8 °C, 75000 x g).

The soluble fraction was subjected to fractional ammonium sulfate precipitation at 8 °C. Firstly, the soluble fraction was treated with 25 % of saturation (NH₄)₂SO₄ and incubated for 30 min,

under constant stirring. After centrifugation (20 min, 8 °C, 75000 x g), the pellet, containing *E. coli* proteins, was discarded. The supernatant was subjected to a second precipitation procedure using 50 % of saturation (NH₄)₂SO₄. After another centrifugation step, the supernatant was used for the last precipitation step (80 % of saturation (NH₄)₂SO₄), in order to salt out the *Tac*TAL protein. After centrifugation, the supernatant was discarded. The pellet, containing *Tac*TAL, was dissolved in a small volume of the loading buffer (20 mM Tris/HCl, pH 7.5). The protein solution was dialyzed against 1 L loading buffer overnight at 8 °C.

Since *Tac*TAL is a thermophilic protein, most of the remaining *E. coli* proteins can be removed via heat precipitation. For this purpose, the concentration of the dialyzed protein solution was adjusted to 10 mg/mL. The solution was heated for 30 – 45 min at 60 °C, under constant shaking (500 rpm). The denatured *E. coli* proteins were removed via centrifugation (30 min, 8 °C, 75000 x g).

In order to purify *Tac*TAL to homogeneity, anion-exchange chromatography was used. The supernatant from the heat precipitation was applied onto a 50 mL TMAE-column, equilibrated with the loading buffer. To remove unspecifically bound proteins the column was washed with 19 % of the elution buffer (20 mM Tris/HCl, 1 M NaCl, pH 7.5) until the flow-through did not contain any detectable amounts of protein. Finally, a custom elution buffer gradient (Table 1.6.1) was applied. The *Tac*TAL elutes between 22 % and 30 % of the elution buffer (220-300 mM NaCl).

Table 1.6.1: Elution buffer gradient for the purification of *Tac*TAL using TMAE anion-exchange chromatography. The *Tac*TAL elutes between 22 % and 30 % of the elution buffer.

Elution buffer (%)	Volume (xCV)
19	3
22	2
22-30	1
30	1
100	2

In case of the *Tac*TAL disulfide variant (*Tac*TAL_{T30C/D211C}), a final gel filtration step was performed, in order to ensure the homopentamer formation. The *Tac*TAL containing fractions from the previous step were pooled and the volume was reduced to 1 mL using a centrifugal concentrator (20 mL, 50 kDa MWCO, 12 °C, 3220 x g). The solution was applied onto a SuperdexTM 200 HiLoadTM 16/60 prep grade column, equilibrated with the gel filtration buffer (20 mM Tris, 150 mM NaCl, pH 7.5). The gel filtration step was performed at 8 °C.

The buffer was exchanged by the storage buffer (20 mM GlyGly, pH 7.5) and the concentration of the *Tac*TAL protein was adjusted to approximately 50 mg/mL using a centrifugal concentrator (20 mL, 50 kDa MWCO, 12 °C, 3220 x g). The protein can be stored at 8 °C for a couple of weeks.

1.6.3 X-Ray Crystallography

1.6.3.1 Finding of Crystallization Conditions for holoQncM- and *Sl*E3 Components

In order to find the conditions for crystallization of the holoQncM and *Sl*E3 proteins, an automated crystallization screen was performed. The screen was carried out by MICHAEL FRANKE in the department of Molecular Structural Biology (Institute for Microbiology and Genetics, Georg-August-University Göttingen). The crystallization screen was applied at 4 °C using the solutions listed on page 18.

The screen conditions, which resulted in crystallization of the respective protein, were reproduced manually using the hanging-drop vapor diffusion approach. The diffraction ability and the quality of the crystals were tested in-house (CuK α radiation, wavelength 1.5418 Å) using the devices provided by the department of Molecular Structural Biology (listed on page 20).

Furthermore, an additive screen was performed for the holoQncM protein according to the manufacturer's manual (Hampton Research Corp, USA), in order to improve the crystallization conditions from the initial crystallization screen.

The resulting crystallization conditions for the holoQncM- and *Sl*E3 components are discussed in the results part (sections 3.2.3 and 3.2.7).

1.6.3.2 Crystallization of *Tac*TAL Wild Type Protein and Variants

The crystallization of the *Tac*TAL wild type protein and variants was performed as published before (LEHWESS-LITZMANN *et al.*, 2011a,b) using the hanging-drop vapor diffusion method. 3 μ L of protein solution (16 mg/mL *Tac*TAL in 14 mM GlyGly and 6 mM Tris-HCl, pH 7.5) were mixed at RT with 3 μ L of the reservoir solution (188 mM ammonium acetate, pH 4.4, 10 % (w/v) PEG 6000 and 25 % (v/v) glycerol). For the intermediate studies, the protein solution was supplemented with either 34 mM F6P, 24 mM A5P or 34 mM M1P before mixing with the reservoir solution. The crystallization mix was equilibrated against 250 μ L of the reservoir solution.

Under these conditions *TacTAL* can crystallize in two different space groups either $C222_1$ or $P2_1$ (LEHWESS-LITZMANN *et al.*, 2011a). In order to obtain the preferred space group $C222_1$, the crystallization solution was microseeded with previously obtained *TacTAL*-crystals of the aforementioned space group and incubated for 10 min at 30 °C. The protein crystals were grown for 7 – 14 days at 20 °C.

*TacTAL*_{T30C/D211C} was co-crystallized with 34 mM F6P and/or 1 mM DTT (before mixing with the reservoir solution). Additionally to the co-crystallization approach, resting state crystals were soaked with 100 mM F6P and/or 50 mM DTT solved in the reservoir solution. The soaking procedure was performed at 20 °C for 2 or 10 min.

1.6.3.3 X-ray Data Collection and Processing

The diffraction data collection of single protein crystals was performed under cryogenic conditions (100 K) using synchrotron radiation (ESRF, beamline ID23-1 [Grenoble, France]; DESY, beamline P13 [Hamburg, Germany]). Diffraction images were indexed, integrated and scaled using the XDS package (KABSCH, 2010).

1.6.3.4 Initial Structure Determination

Since the crystallization of *TacTAL* results in nearly isomorphous protein crystals, with a maximal deviation of the cell constants lower than 3 %, the previously published structures (PDB entries: 3S0C and 3S1V (LEHWESS-LITZMANN *et al.*, 2011a,b)) were used as the initial models for the rigid-body refinement.

As no published structural information about the *SliE3* and holoQncM proteins are available, the molecular replacement approach was used for the initial phase determination for *SliE3* diffraction data. This was performed using Phaser crystallographic software (McCoy *et al.*, 2007). The search model was generated from the previously published structure of dihydrolipoamide dehydrogenase of glycine decarboxylase from *Pisum sativum* (40 % sequence identity, PDB entry 1DXL (FAURE *et al.*, 2000)) using the phenix.sculptor software (BUNKÓCZI AND READ, 2011).

For the holoQncM protein, there are no published structures available, which would be suitable for the molecular replacement approach (sequence identity > 30 %). The initial phase determination was performed by DR. PIOTR NEUMANN (Department of Molecular Structural Biology, Institute

for Microbiology and Genetics, Georg-August-University Göttingen) using the ARCIMBOLDO_₋LITE-software (SAMMITO *et al.*, 2015).

The resulting structure models were completed manually using the Coot-software (EMSLEY *et al.*, 2010; EMSLEY AND COWTAN, 2004).

1.6.3.5 Model Building and Refinement

All structure models were manually improved and refined against the diffraction data in an iterative manner using the Coot-software (EMSLEY *et al.*, 2010; EMSLEY AND COWTAN, 2004) and phenix.refine crystallographic package (ADAMS *et al.*, 2010). The last few refinement cycles were performed using TLS parameterization. The TLS-grouping was chosen automatically by phenix.refine crystallographic package (ADAMS *et al.*, 2010). The geometry of the final model was validated using the MolProbity server (CHEN *et al.*, 2010). The structure representation was performed with PyMOL Molecular Graphics System (Schrödinger, LLC).

1.6.4 UV-Vis Spectroscopy

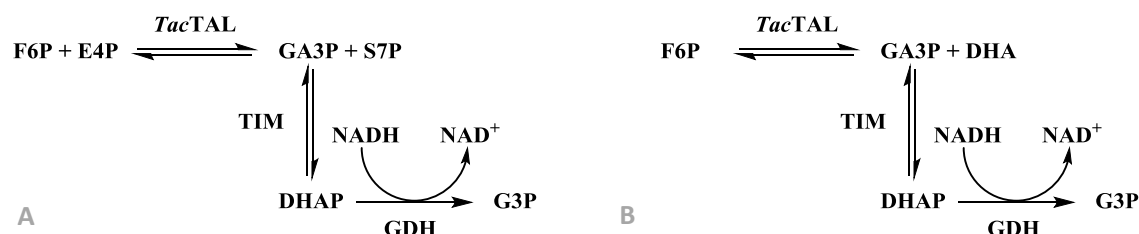
1.6.4.1 Concentration Measurement of NADH, FAD and Lipoamide

The concentrations of lipoamide, NADH and FAD in solution were determined optically. The absorbance was measured at 333 nm (lipoamide), 340 nm (NADH) and 450 nm (FAD) in a 1 mL quartz cuvette with a path length of 1 cm. The concentration was calculated according to the BEER-LAMBERT equation (eq. 1.6.1) using published molar extinction coefficients (NADH: $\epsilon_{340\text{nm}} = 6220\text{M}^{-1}\text{cm}^{-1}$ (HAID *et al.*, 1975), FAD: $\epsilon_{450\text{nm}} = 11300\text{M}^{-1}\text{cm}^{-1}$ (KOZIOL, 1971), lipoamide: $\epsilon_{340\text{nm}} = 150\text{M}^{-1}\text{cm}^{-1}$ (REED *et al.*, 1958)).

1.6.4.2 Steady-State Measurements of TacTAL Wild Type Protein and Variants

The steady-state kinetics of TacTAL wild type protein and variants were measured in a coupled spectrophotometric assay to detect the formation of the first product glyceraldehyde 3-phosphate (GA3P). The auxiliary enzymes used for the assay are triosephosphate isomerase (TIM) and α -glycerophosphate dehydrogenase (GDH) (TSOLAS AND JORIS, 1975). The formed GA3P as result of cleavage of fructose 6-phosphate (F6P) by TacTAL is converted to dihydroxyacetone phos-

phate (DHAP) by TIM, followed by reduction to glycerol 3-phosphate (G3P) and simultaneous oxidation of NADH to NAD⁺ by GDH (scheme 1.1 A). The oxidation of NADH was monitored spectrophotometrically in an UV-Vis spectrometer (V-650, Jasco GmbH) at 340 nm and 30 °C.



Scheme 1.1: Minimal reaction sequence of transaldolase/aldolase activity assay coupled to NADH oxidation. The cleavage of F6P by *TacTAL* results in the formation of GA3P. The auxiliary enzyme TIM, converts GA3P to DHAP. Subsequently GDH reduces DHAP to G3P. The simultaneous oxidation of NADH monitors the activity (depletion of absorbance at 340 nm). **A:** In presence of E4P, the transaldolase reaction takes place (reversible transfer of a DHA-unit from F6P to E4P). **B:** The aldolase side-reaction results in the aldolytic cleavage of F6P to DHA and GA3P.

The reaction mixture (200 μ L) contained 3 – 4 U/mL TIM/GDH [8 mM (NH₄)₂SO₄], 0.22 mM NADH, 2 mM E4P, and varying concentrations of F6P (0.1 – 100 mM) in 20 mM GlyGly (pH 7.5). The reaction was started by the addition of the enzyme to the reaction mixture (final concentrations: 0.015 – 1.0 mg/mL).

The transaldolase activity of the disulfide variant (*TacTAL*_{T30C/D211C}) was additionally measured under reducing conditions. The enzyme solution (1 mg/mL) was supplemented with 20 mM DTT and incubated for 10 min. The transaldolase reaction was started by addition of reduced enzyme to the DTT free reaction mixture (final concentrations: 0.05 mg/mL *TacTAL*_{T30C/D211C}, 1 mM DTT). Sets of triplicates were measured for each F6P concentration. The reduced enzyme was freshly prepared for each $v/[S]$ -characteristic data set immediately before measurement, in order to avoid the loss of activity of the variant during the experiment.

The aldolase activity of *TacTAL* wild type protein and variants with enhanced aldolase activity was measured in absence of E4P using the same coupled spectrophotometric assay as described above (scheme 1.1 B).

The measured initial rates were plotted against substrate concentration ($[S]$). The macroscopic kinetic constants (V_{\max} and K_M^{app}) were determined by fitting of the data according to the MICHAELIS-MENTEN-equation (eq. 1.6.2) (MICHAELIS AND MENTEN, 1913). The specific activity (A_{spec}) as well as

the turnover number per active site (k_{cat}) were calculated from the determined V_{max} considering the respective enzyme concentration.

$$v = \frac{V_{max} \cdot [S]}{K_M + [S]} \quad \begin{array}{l} V_{max} = \text{maximal activity} \\ \text{at substrate saturation} \\ K_M = \text{Michaelis constant} \end{array} \quad (1.6.2)$$

1.6.4.3 pH-Dependency of Enzymatic Activity of TacTAL Variants

For the variants showing enhanced aldolase activity (*TacTAL*_{F132Y}, *TacTAL*_{E60Q/F132Y} and *TacTAL*_{FSA-mimic}), pH-dependency of the enzymatic activity was measured under steady-state conditions at 30 °C. The activity measurements were performed at constant ionic strength using a three-component buffer system (50 mM acetic acid, 50 mM MES and 100 mM Tris (ELLIS AND MORRISON, 1982)), which keeps the ionic strength constant (0.1 M) at different pH (4.5 – 9.5).

The reaction mixture (200 μ L) contained 3 – 4 U/mL TIM/GDH [8 mM (NH₄)₂SO₄], 0.22 mM NADH, 50 mM F6P in three-component buffer of different pH (5.6 – 9.2). The reaction was started by addition of the enzyme to the reaction mixture (final concentrations: 0.025 – 0.125 mg/mL).

The pH-value of the reaction mixture was measured immediately after the experiment. The measured aldolase activity (V_{app}) was plotted versus the respective pH-value. The pK_a values of the enzyme-substrate complex (pK_{ES1} and pK_{ES2}) as well as the aldolase activity at the pH-optimum (V_{max}) were determined by fitting the data according to equation 1.6.3 for bell-shaped plots or equation 1.6.4 for sigmoidal plots.

$$V_{app} = \frac{V_{max}}{1 + 10^{(pK_{ES1}-pH)} + 10^{(pH-pK_{ES2})}} + V_0 \quad \begin{array}{l} V_{app} = \text{measured activity} \\ V_{max} = \text{activity at pH-optimum} \end{array} \quad (1.6.3)$$

$$V_{app} = \frac{V_{max}}{1 + 10^{(pK_{ES1}-pH)}} + V_0 \quad \begin{array}{l} V_0 = \text{offset} \end{array} \quad (1.6.4)$$

The pH-stability of the variants was tested by measurements of far-UV-CD-spectra of the protein after incubation (5 min) in 10 mM KH₂PO₄/K₂HPO₄ of respective pH. A far-UV-CD spectrum of a protein gives a characteristic signature for secondary structures (e.g. α -helices and β -sheets) and can be used to distinguish between folded and denatured protein (KELLY *et al.*, 2005).

The CD-spectra were recorded in a wavelength range of 180 – 260 nm (step: 1 nm, time per point: 5 s) using a 300 μ L quartz cuvette with a path length of 0.1 cm. The enzyme concentration was 92.5 μ g/mL. The measurement was performed at 30 °C.

The CD-spectra were corrected for buffer (10 mM $\text{KH}_2\text{PO}_4/\text{K}_2\text{HPO}_4$, pH 7.8). The data were normalized by scaling to peptide-bound concentration according to equation 1.6.5 (KELLY *et al.*, 2005).

$$[\Theta]_{\text{MRW}} = \frac{\Theta \cdot \text{MRW}}{10 \cdot c \cdot d} \text{ (deg} \cdot \text{cm}^2 \cdot \text{dmol}^{-1}\text{)}$$

Θ = molar ellipticity (mdeg)
 MRW = mean residue weight (Da) (1.6.5)
 c = protein concentration (mg/mL)
 d = optical path length (cm)

Tris was described as an inhibitor of the fructose 6-phosphate aldolase from *E. coli* (*EcFSA*) (SCHÜRSMANN AND SPRENGER, 2001). Because the three-component buffer contains 100 mM Tris, its inhibition ability was tested for *TacTAL*_{E60Q/F132Y} under the steady-state conditions. The steady-state activity was measured as described above (section 1.6.4.2) in 20 mM Tris (pH 7.5) as buffer substance and compared with the activity in 20 mM GlyGly. The tested F6P concentration was 50 mM.

1.6.4.4 Stopped-Flow Measurements of *TacTAL* Wild Type Protein and Variants

In order to analyze the kinetic properties of the donor half-reaction (cleavage of F6P), a rapid mixing method (dead time of approx. 1.5 ms) was performed using a stopped-flow device. The reaction was monitored using a coupled spectrophotometric assay as described above (section 1.6.4.2). The solution, containing *TacTAL* (0.44 mg/mL), TIM/GDH (200 U/mL) and NADH (0.44 mM) in 20 mM GlyGly (pH 7.5) was rapidly mixed with the substrate solution (0.1 – 100 mM F6P in 20 mM GlyGly, pH 7.5). The measurements were performed at 30 °C. The mixing ratio was 1:1.

The idea of the experiment is comparable to the classic kinetics of the chymotrypsin-catalyzed conversion of *p*-nitrophenyl ester substrates (HARTLEY AND KILBY, 1952, 1954). The apparent rate constants (k_{obs}) were determined by fitting of progress curves according to either single- or double-exponential equations combined with a linear term (equation 1.6.6 or 1.6.7, respectively) as previously described (LEHWESS-LITZMANN, 2011).

$$A_{340}(t) = a_1 \cdot e^{-k_1^{\text{obs}} \cdot t} - v \cdot t + y_0 \quad k_1^{\text{obs}}, k_2^{\text{obs}} = \text{first order rate constants} \quad (1.6.6)$$

$$A_{340}(t) = a_1 \cdot e^{-k_1^{\text{obs}} \cdot t} + a_2 \cdot e^{-k_2^{\text{obs}} \cdot t} - v \cdot t + y_0 \quad a_1, a_2 = \text{amplitudes} \quad (1.6.6)$$

$$v = \text{aldolase steady-state activity} \quad (1.6.7)$$

$$y_0 = \text{offset}$$

The measured apparent rate constants (k_{obs}) were plotted versus respective substrate concentrations ([S]). The data was fitted according either to the equation 1.6.8 for data showing an optimum or to the equation 1.6.9 for data with a saturation.

$$k_{\text{obs}} = \frac{k_{\text{obs}}^{\text{max}}}{1 + \frac{K_S^{\text{app}}}{[S]} + \frac{[S]}{K_I}} \quad k_{\text{obs}}^{\text{max}} = \text{first order rate constant} \quad (1.6.8)$$

$$\text{at substrate saturation}$$

$$k_{\text{obs}} = \frac{k_{\text{obs}}^{\text{max}} \cdot [S]}{K_S^{\text{app}} + [S]} \quad K_S^{\text{app}} = \text{equilibrium constant of the fast} \quad (1.6.9)$$

$$\text{substrate binding pre-equilibrium}$$

$K_I = \text{inhibition equilibrium constant of the putative substrate inhibition}$

1.6.4.5 Activity Assay for QncN/L Component

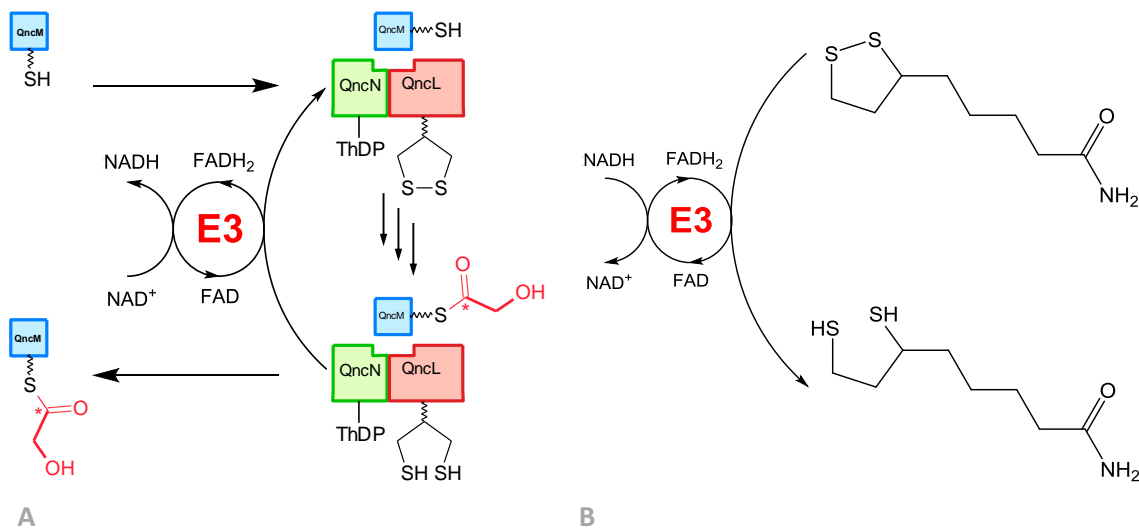
The activity of the QncN/L component was measured in a spectrophotometric assay using F6P as donor-substrate. The QncN/L component transfers the C2-unit from F6P to the phosphopantetheine moiety of the holoQncM component. The transfer reaction results in the reduction of the lipoyl moiety of the enzyme. The catalytic cycle of the QncN/L component is completed by the reoxidation of the dihydrolipoyl moiety by the E3 component (PENG *et al.*, 2012). This reaction is coupled to NAD⁺ reduction (scheme 1.2 A). The concomitant NADH formation can be monitored by measuring the absorbance at 340 nm. The activity of the QncN/L component was determined by the linear fit of the initial phase of the progress curve.

The reaction mixture (200 μL) contained 1 mM NAD⁺, 30 mM F6P, 2.5 μM *SliE3*, 3 mg/mL holo-QncM, 400 μM ThDP and 2.5 mM MgCl₂ in 50 mM MOPS supplemented with 10 % (v/v) glycerol (pH 7.5). The reaction was started by the addition of the enzyme to the reaction mixture (final concentration: 0.5 mg/mL). The activity measurements were performed at 20 °C.

The apparent specific activity (A_{spec}) as well as the apparent turnover number per active site (k_{cat}) were calculated from the initial reaction rate at saturated F6P-concentration (30 mM) taking the enzyme concentration into account.

1.6.4.6 Steady-State Measurements of the *SliE3* Component

The activity of the *SliE3* component was analyzed by measurement of lipamide reduction by *SliE3* enzyme using NADH as reducing equivalent. This reaction corresponds to the reverse reaction of the *SliE3* component in physiological context (scheme 1.2 A) using lipamide acting as an artificial substrate (scheme 1.2 B). In this assay, the E3 component reduces the lipamide to dihydrolipamide using NADH. The NADH consumption was used to monitor the progress of the reaction by absorbance depletion at 340 nm. The NAD^+ resulting from the reaction acts as an activator of some orthologous E3 enzymes (ARGYROU AND BLANCHARD, 2001). In order to avoid the perturbation of the initial phase of the reaction by the product activation effect of the concomitant NAD^+ formation, NAD^+ was added to the reaction mixture in a concentration resulting in constitutively activated E3 component according to ARGYROU AND BLANCHARD (2001).



Scheme 1.2: Minimal reaction sequence of the E3 component activity assay. **A:** Reaction in physiological context. The E3 component fulfills the catalytic cycle of the QncN/L component by the reoxidation of the dihydrolipoyl moiety using NAD^+ (PENG *et al.*, 2012). **B:** Reaction used in the activity assay. E3 component reduces the lipamide using NADH (ARGYROU AND BLANCHARD, 2001).

The reaction mixture (1 mL) contained 0.2 mM NADH, 50 μM NAD^+ , and varying concentrations of lipamide (0.1 – 3.0 mM) [5.25 % Ethanol] in 45 mM $\text{KH}_2\text{PO}_4/\text{K}_2\text{HPO}_4$ (pH 7.6) supplemented

with 135 mM NaCl. The reaction was started by the addition of the enzyme to the reaction mixture (final concentration: 10 nM, determined using *SliE3*-bound FAD extinction coefficient, section 1.6.2.2). The activity measurements were performed at 20 °C.

The measured initial rates were plotted against the lipoamide concentration. The macroscopic kinetic constants (V_{\max} and K_M^{app}) were determined by fitting of the data according to the MICHAELIS-MENTEN-equation (eq. 1.6.2) (MICHAELIS AND MENTEN, 1913). The specific activity (A_{spec}) as well as the turnover number per active site (k_{cat}) were calculated from the determined V_{\max} considering the enzyme concentration.

1.6.4.7 Stopped-Flow Measurements of the *SliE3* Component

The intermediates of the reduction of the E3-bound FAD by NADH can be studied via fast-kinetics stopped-flow absorbance spectroscopy measurements (ARGYROU *et al.*, 2002). For this purpose, the *SliE3* solution was rapidly mixed (dead time of approx. 1.5 ms) in a stopped-flow device with an NADH solution at 4 °C. The mixing ratio was 1:1 giving either 10x excess or equimolar concentration of NADH compared to the final *SliE3*-concentration (20 μM) in 50 mM imidazole supplemented with 150 mM NaCl (pH 7.6). The spectra of E3-bound FAD were recorded using a photo-diode array. For single wavelength measurements, a photomultiplier was used.

1.6.5 Analytical Methods

1.6.5.1 Size Exclusion Chromatography Coupled Multiangle Light Scattering (SEC-MALS)

In order to analyze the oligomerization state of the holoQncM component in solution, size exclusion chromatography coupled multiangle light scattering (SEC-MALS) was performed. 500 μL holoQncM sample (0.2 mg/mL) was applied onto a SuperdexTM 75 10/300 GL, equilibrated with the storage buffer (100 mM imidazole, 100 mM NaCl, 10 % (v/v) glycerol, pH 7.4). The eluted solution (flow rate 0.3 mL/min) was subsequently analyzed using the miniDAWN TREOSTM light scattering instrument in combination with an Optilab T-rEX refractive index detector. The SEC-MALS experiment was performed at RT.

1.6.5.2 MALDI-TOF Mass Spectrometry

The QncM component was co-expressed with phosphopantetheinyl transferase from *Bacillus subtilis* (*BsSfp*) in order to obtain the protein in its physiological relevant holo-form. The phosphopantetheinyl transferase *BsSfp* catalyzes the phosphopantetheinylation of Ser³³ of the QncM component *in vivo*. The presence of this post-translational modification after the protein purification was verified using MALDI-TOF mass spectrometry.

In order to obtain peptide fragments in a molecular weight region sufficient for the MALDI-TOF experiment, the holoQncM protein was digested using modified porcine trypsin. This sequencing grade trypsin is modified by reductive methylation of lysine residues to avoid autolytic digestion (KEIL-DLOUHÁ *et al.*, 1971; RICE *et al.*, 1977). 15 µL of sample, containing 170 µM holoQncM in 50 mM MOPS (pH 7.8), 50 mM NaCl and 1 % (v/v) glycerol were supplemented with 25 µL of NH₄HCO₃ solution (25 mM) and mixed with 10 µL of trypsin solution (100 µg/mL, prepared according to manufacturer's manual [Promega Corporation, Germany]). The tryptic digestion was conducted by incubation of the mixture at 37 °C for 3.5 h. An overview of the expected holoQncM fragments after tryptic cleavage is shown in the appendix part (Table A.2).

The digested sample was mixed with formic acid (85 % (v/v)) in a 1:1 volume ratio. The sample was prepared using ZipTip_{C18}TM pipette tip. The ZipTip_{C18}TM pipette tip was prepared according to manufacturer's manual (Merck KGaA, Germany) using 70 % (v/v) acetonitrile supplemented with 0.3 % (v/v) formic acid as wetting and elution solution and 1 % (v/v) formic acid as equilibration and washing solution.

The purified sample was mixed with DHB in a 1:1 volume ratio and transferred to a MALDI-TOF-MS carrier.

The measurements were performed in the department of Molecular Microbiology and Genetics (Institute for Microbiology and Genetics, Georg-August-University Göttingen) with DR. OLIVER VALERIUS.

1.6.5.3 Liquid Chromatography Mass Spectrometry

The isolated proteins (QncN/L and E3 components) were verified using liquid chromatography mass spectrometry (LC-MS) in the department of Molecular Microbiology and Genetics (Institute

for Microbiology and Genetics, Georg-August-University Göttingen). The sample preparation was performed by members of DR. OLIVER VALERIUS' research group (same department) according to a published protocol (SHEVCHENKO *et al.*, 1996). The LC-MS measurements and the data analysis were carried out by DR. OLIVER VALERIUS in a similar way as described in KOCH *et al.* (2016). The data were searched against an *E. coli* FASTA-database expanded for the *St. melanovinaceus* amino acid sequences of interest. The search was performed using the Proteome Discoverer software and the SequestHT search engine. For the QncL component, lipoylation of lysines was set as variable modification.

1.6.5.4 ThermoFluor Assay

In order to optimize the buffer conditions for the holoQncM component, the ThermoFluor assay was applied. This method allows to analyze the thermostability of proteins under different buffer conditions. Six buffer substances and a pH-range of 4.6 – 9.4 were screened (for details, see Table A.9 in the appendix part). The reaction mixture contained 100 mM of the respective buffer substance, 5x concentrated SYPRO[®] Orange protein stain, 10 μ M holoQncM and 10 % (v/v) glycerol. SYPRO[®] Orange gives a fluorescence signal by interacting with hydrophobic patches of the protein. Assuming a direct linear correlation between the thermal denaturation of the protein and the exposure of the hydrophobic protein regions to the stain-containing environment, the melting curve can be recorded by measuring the SYPRO[®] Orange fluorescence signal.

The ThermoFluor measurements were performed in the department of Molecular Structural Biology (Institute for Microbiology and Genetics, Georg-August-University Göttingen). The temperature range was 20 – 95 °C. The temperature increment (1 K/30 s) was performed using a C1000 thermal cycler. The thermal protein unfolding was monitored using a CFX96[™] Optical Reaction Module (excitation: 515 – 535 nm, detection: 560 – 580 nm).

2 Mechanistic Characterization of Transaldolase from *Thermoplasma Acidophilum*

2.1 Introduction

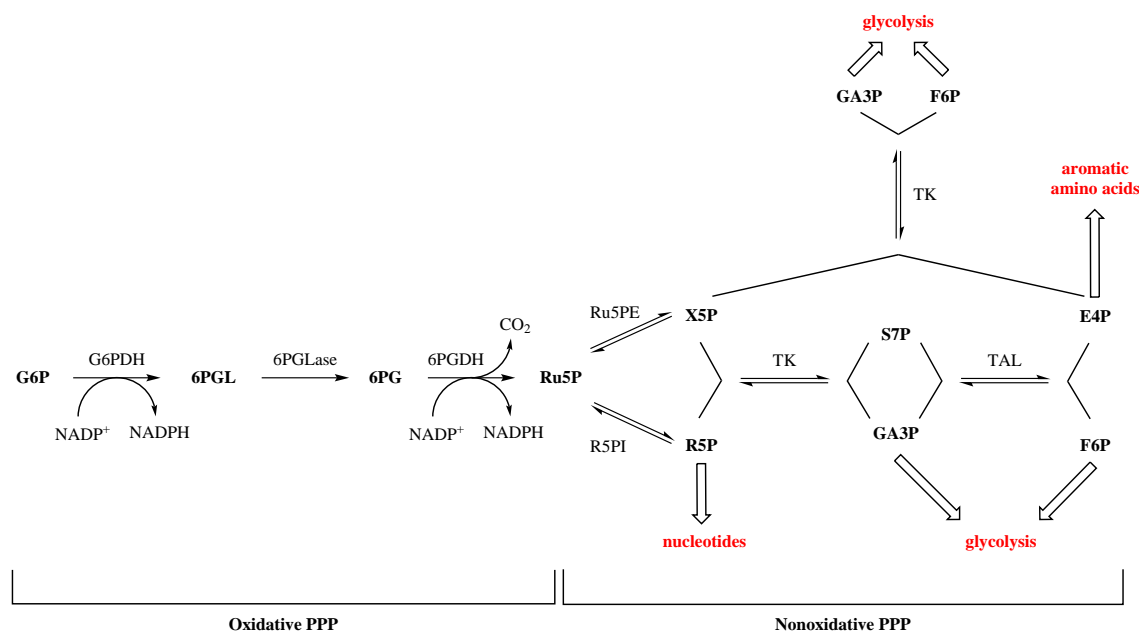
2.1.1 *Thermoplasma Acidophilum*

Thermoplasma acidophilum was first isolated and described by DARLAND *et al.* (1970). Initially, the organism was annotated as *mycoplasma* because of the lack of a cell wall. They isolated the organism from samples from self-heating coal refuse piles. In spite of its anthropogenic origin, it was the only known habitat of *Thermoplasma acidophilum* for nearly two decades. SEGERER *et al.* (1988) could isolate the organism from natural hot acidic solfatara fields and suggested this kind of biotopes as its natural habitat. *Thermoplasma acidophilum* culture grows optimally at a temperature of ~59 °C under acidic conditions (pH 1 – 2). This thermophilic and acidophilic properties are name giving for the prokaryote. According to the suggestion that the stability of the cells under extreme conditions is caused by the nature of the cell membrane (BROCK, 1967), the cell membrane of *Thermoplasma acidophilum* was analyzed in further studies. Analysis of the cell membrane behavior of the cultivated *Thermoplasma acidophilum* strain showed that the membrane is stable at acidic conditions, but the change of the pH to values > 8 induces cell lysis (BELLY AND BROCK, 1972). Although the acidic conditions are necessary for the organism to survive, the intracellular pH is nearly neutral (HSUNG AND HAUG, 1975). Further analysis of the membrane composition showed that the membrane of *Thermoplasma acidophilum* does not contain ester-bound fatty acids, which are usual for bacterial membranes (LANGWORTHY *et al.*, 1972), but long-chain isoprenols linked as diglycerol tetraethers (LANGWORTHY, 1977; LANGWORTHY *et al.*, 1972). These ether lipids were suggested to form monolayers, which is in contrast to the bilayer of the bacterial membrane. Today this kind of membrane is known in a number of prokaryotes, which belong to the kingdom of archaea. *Thermoplasma acidophilum* belongs to this kingdom as well, but was first annotated as *mycoplasma* because the archaea were not yet classified at the time of its discovery. This classification was done later on, based on the phylogenetic analysis of ribosomal RNA sequences (WOESE AND FOX, 1977). Finally, the complete genome sequence of *Thermoplasma acidophilum* was published by RUEPP *et al.* (2000) giving new opportunities for further studies.

2.1.2 Pentose Phosphate Pathway

Beside the unique membrane composition of archaea, these organisms exhibit differences in the metabolic pathways compared to the other kingdoms of life, as it is the case for the pentose phosphate pathway (PPP). Bacterial and eukaryotic cells use the pentose phosphate pathway to generate reducing equivalents in form of NADPH and sugar phosphates of different carbon chain lengths. The sugar phosphates are important precursors for biosynthesis of aromatic amino acids and nucleotides, while NADPH is used for the redox reactions in anabolic processes such as the biosynthesis of fatty acids. The pentose phosphate pathway can be subdivided in two parts: the oxidative and the nonoxidative branch. The oxidative branch converts glucose 6-phosphate (G6P) to ribulose 5-phosphate (Ru5P) and results in the reduction of two NADP⁺ molecules to NADPH per one G6P molecule. The nonoxidative branch, containing the enzymes ribulose-5-phosphate-3-epimerase (Ru5PE), ribose-5-phosphate isomerase (R5PI), transketolase (TK) and transaldolase (TAL), generates the sugar phosphate precursors. The nonoxidative PPP connects different metabolic pathways (glycolysis, biosynthesis of aromatic amino acids, biosynthesis of nucleotides and oxidative PPP) in a reversible manner (scheme 2.1).

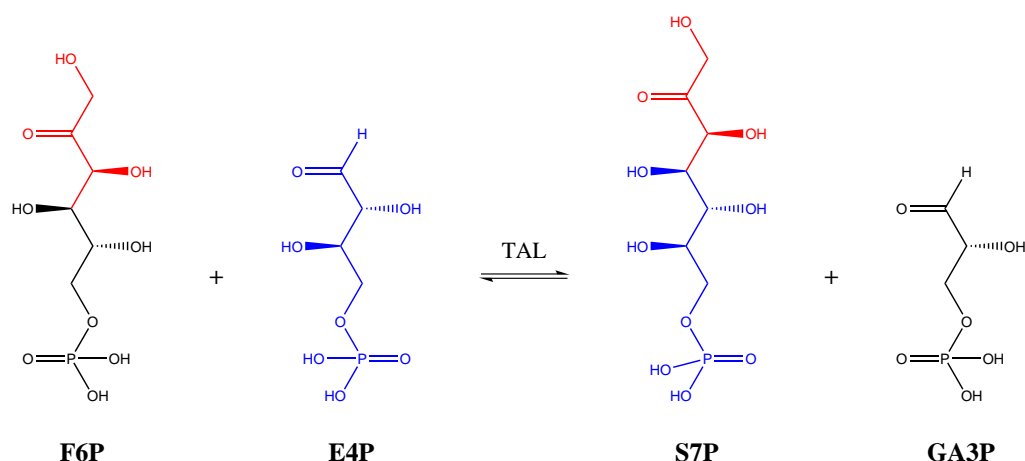
Phylogenetic analysis of the archeal genome sequences showed that archaea do not have the complete set of genes for the enzymes of the pentose phosphate pathway (SODERBERG, 2005). All genomes analyzed in this study (13 genomes) are lacking the gene orthologs for the enzymes of the oxidative PPP except the genome of *Halobacterium* in which an ortholog for the 6-phosphogluconate dehydrogenase could be annotated. Moreover, only three of the analyzed genomes, such as the genome of *Thermoplasma acidophilum*, contain the complete set of genes for the nonoxidative PPP. Other analyzed organisms are lacking at least the gene ortholog for transaldolase. In this context, alternative pathways were suggested for archeal organisms, compensating for the missing pentose phosphate pathway enzymes (AONO *et al.*, 2015; ORITA *et al.*, 2006; SODERBERG, 2005)



Scheme 2.1: The pentose phosphate pathway (PPP). G6P: glucose 6-phosphate; G6PDH: glucose-6-phosphate dehydrogenase; 6PGL: 6-phosphoglucono- δ -lactone; 6PGLase: 6-phosphoglucono- δ -lactonase; 6PG: 6-phosphogluconate; 6PGDH: 6-phosphogluconate dehydrogenase; Ru5P: ribulose 5-phosphate; Ru5PE: ribulose 5-phosphate-3-epimerase; R5PI: ribose-5-phosphate isomerase; R5P: ribose 5-phosphate; X5P: xylulose 5-phosphate; TK: transketolase; S7P: sedoheptulose 7-phosphate; GA3P: glyceraldehyde 3-phosphate; TAL: transaldolase; E4P: erythrose 4-phosphate; F6P: fructose 6-phosphate. Adapted from (SODERBERG, 2005).

2.1.3 Transaldolase

Since the transaldolase activity was observed for the first time in preparations from liver and yeast (HORECKER AND SMYRNIOTIS, 1955, 1953), transaldolases were found in most other eukaryotes, prokaryotes and some archaea. Transaldolases catalyze the reversible transfer of dihydroxyacetone units from ketose phosphates (donor substrate) to the C1 position of the aldose phosphates (acceptor substrate). According to their mechanism of action, transaldolases are related to the aldolases and are a part of the nonoxidative pentose phosphate pathway, where they catalyze the reversible conversion of F6P and E4P into S7P and GA3P (scheme 2.2, HORECKER AND SMYRNIOTIS (1953)). Depending on the catalytic mechanism, aldolases are classified into two classes. Class I aldolases use a lysine residue in the active site, which forms a reactive SCHIFF-base intermediate with the substrate (GEFFLAUT *et al.*, 1995; HORECKER *et al.*, 1972) and class II aldolases, which contain a bivalent cation in the active site for catalytic purposes (MORSE AND HORECKER, 1968). Transaldolases mechanistically belong to the class I aldolases.



Scheme 2.2: Transaldolase reaction in physiological context. Transaldolase (TAL) catalyzes the reversible transfer of a dihydroxyacetone unit from ketose phosphates (fructose 6-phosphate [F6P] or sedoheptulose 7-phosphate [S7P]) to the C1 position of the aldose phosphates (erythrose 4-phosphate [E4P] or glyceraldehyde 3-phosphate [GA3P]).

SAMLAND AND SPRENGER (2009) subdivided the transaldolase family into five subfamilies based on phylogenetic analysis of 46 coding sequences for transaldolases and related proteins from different origins. The "classical" transaldolases belong to the subfamily I. The polypeptide chains of these enzymes contain 310 – 350 amino acid residues. Nonactive isoforms of transaldolase in plants belong to the subfamily II. The transaldolases of the third subfamily have longer polypeptide chains (~380 aa). Transaldolase from *Thermoplasma acidophilum* (*TacTAL*) belongs to the fourth subfamily, whose subunits contains about 220 amino acid residues (223 aa in *TacTAL*). Enzymes of the fifth subfamily have similar polypeptide chain length as these of the subfamily IV, but catalyze an aldolase reaction (reversible aldolytic cleavage of sugar phosphate) instead of the transaldolase reaction. Fructose 6-phosphate aldolase from *Escherichia coli* (*EcFSA*) belongs to this type of enzymes (SCHÜRMMANN AND SPRENGER, 2001).

2.1.4 Crystal Structure of *TacTAL*

According to analytical ultracentrifugation experiments, *TacTAL* forms homopentamers and homodecamers (dimer of homopentamers) in solution (LEHWESS-LITZMANN, 2011). The equilibrium constant for the pentamer/decamer equilibrium was determined as $K_D = 0.44 \mu\text{M}$. Under the used conditions, *TacTAL* crystallized in two different space groups: $C222_1$ and $P2_1$ (LEHWESS-LITZMANN *et al.*, 2011a). The asymmetric unit of the structure in the $C222_1$ space group is a homopentamer, while a homodecamer is the asymmetric unit of the structure in the $P2_1$ space group. This ho-

modecamer can be reconstructed from the homopentamer in $C222_1$ when applying the symmetry operations of the space group.

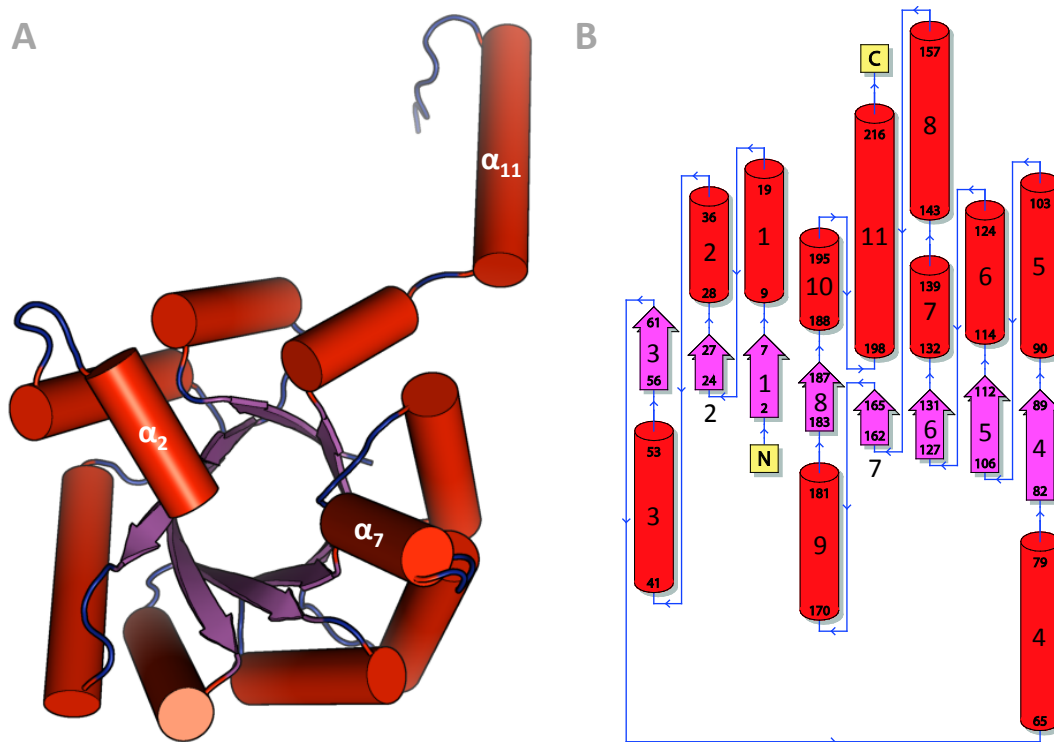


Figure 2.1.1: The monomer of *TacTAL*. Red: α -helices; purple: β -strands; blue: loops. **A:** Structure of a monomer of *TacTAL* **B:** Topology of a monomer of *TacTAL* (DE BEER *et al.*, 2014; HUTCHINSON AND THORNTON, 1990; LASKOWSKI, 2009). PDB entry: 3S1V (LEHWESS-LITZMANN *et al.*, 2011b).

A monomer of *TacTAL* exhibits a TIM-barrel fold (figure 2.1.1). The basic topology of this fold is a $(\beta/\alpha)_8$ -barrel structure, consisting of a β -barrel of eight parallel β -strands surrounded by eight α -helices (LEHWESS-LITZMANN *et al.*, 2011b). These secondary structure elements are ordered in an alternating sequence connected via short loops. In a monomer of *TacTAL*, two additional helices (α_2 and α_7) are inserted in this basic fold, flanking the C-terminal end of the β -barrel. Additionally, a C-terminal α -helix (α_{11}) from the neighboring monomer covers the C-terminal end of the β -barrel (figure 2.1.2). This helix interacts with the helix α_2 . In classical transaldolases, which usually form homodimers (SAMLAND AND SPRENGER, 2009), a corresponding C-terminal α -helix is present too, but it covers the β -barrel of the own monomer. In both cases, the resulting folding unit has a similar overall topology but in case of *TacTAL*, this unit is composed from different monomers. This inter-subunit helix swapping is assumed to contribute to the pentamer formation as it was described for the *EcFSA* (SAMLAND *et al.*, 2012; THORELL *et al.*, 2002).

The C-terminal α -helix residues Thr²⁰¹ and Asp²¹¹ perform hydrogen bonds with the side chains of Gln¹¹⁷ and Thr³⁰ of the neighboring subunit, respectively. Additionally, the side chain of Thr²⁰¹ can interact with the backbone carbonyl of Ile¹¹¹. The residues Phe²⁰⁸ and Trp²¹² perform hydrophobic interactions with Pro²⁹ and Tyr⁴², respectively. The side chain of Tyr⁴² coordinates the backbone nitrogen of the Ile²²² residue. Finally, the C-terminal carboxyl group forms a salt bridge with Arg⁴⁷. Beside the interaction of the C-terminal helix with the neighboring subunit, the barrel structures of the monomers interact with each other as well. The side chain of Asp²³ interacts with the Lys¹²³ residue, which in turn coordinates the backbone carbonyl of Met¹. The backbone carbonyl of Ala¹⁸² residue is coordinated by the side chain of Tyr¹⁵⁷. In addition, the hydrophobic interactions stabilize the pentamer formation, since the interaction surface between the monomers is faced with hydrophobic residues.

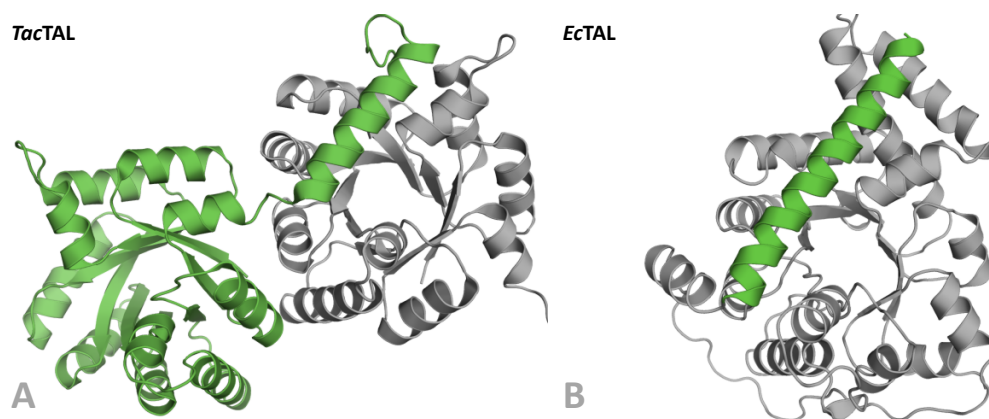


Figure 2.1.2: Inter-subunit helix swapping between two neighboring subunits of *TacTAL*. **A:** The C-terminal α -helix of the subunit A (green) covers the β -barrel of the neighboring subunit E (gray). PDB entry: 3S1V (LEHWESS-LITZMANN *et al.*, 2011b). **B:** A subunit of *EcTAL*. The C-terminal α -helix (green) and the β/α -barrel belong to the same polypeptide chain. PDB entry: 1ONR (JIA *et al.*, 1996).

Two pentamers of *TacTAL* form a homodecamer. In this homodecamer, the C-terminal ends of the β -barrels of one pentamer are face-to-face oriented to the C-terminal ends of the β -barrels of the opposite pentamer (LEHWESS-LITZMANN *et al.*, 2011b). A pentamer in this decameric structure is rotated around the noncrystallographic five-fold symmetry axis by 18° relative to the other pentamer (figure 2.1.3). The active site entrances of the opposite subunits of the homopentamer are oriented towards each other. Similar quaternary structure was described for the related *EcFSA* (THORELL *et al.*, 2002).

Fructose 6-phosphate aldolase from *Escherichia coli* (*EcFSA*) is a class I aldolase, which was first described by SCHÜRMAN AND SPRENGER (2001). *EcFSA* exhibits a similar overall structure

(Z-score=30, rmsd=1.5; on basis of the C_{α} positions in a monomer) and shows 31.1 % identity and 60.9 % similarity to *Tac*TAL based on structure-assisted alignment (DI TOMMASO *et al.*, 2011; HOLM AND ROSENSTRÖM, 2010). Surprisingly, this novel enzyme does not show transaldolase activity, but fructose 6-phosphate aldolase activity. *Ec*FSA does not transfer three-carbon units from donor substrates to acceptor substrates, but catalyzes the reversible cleavage of the ketose-phosphate substrate.

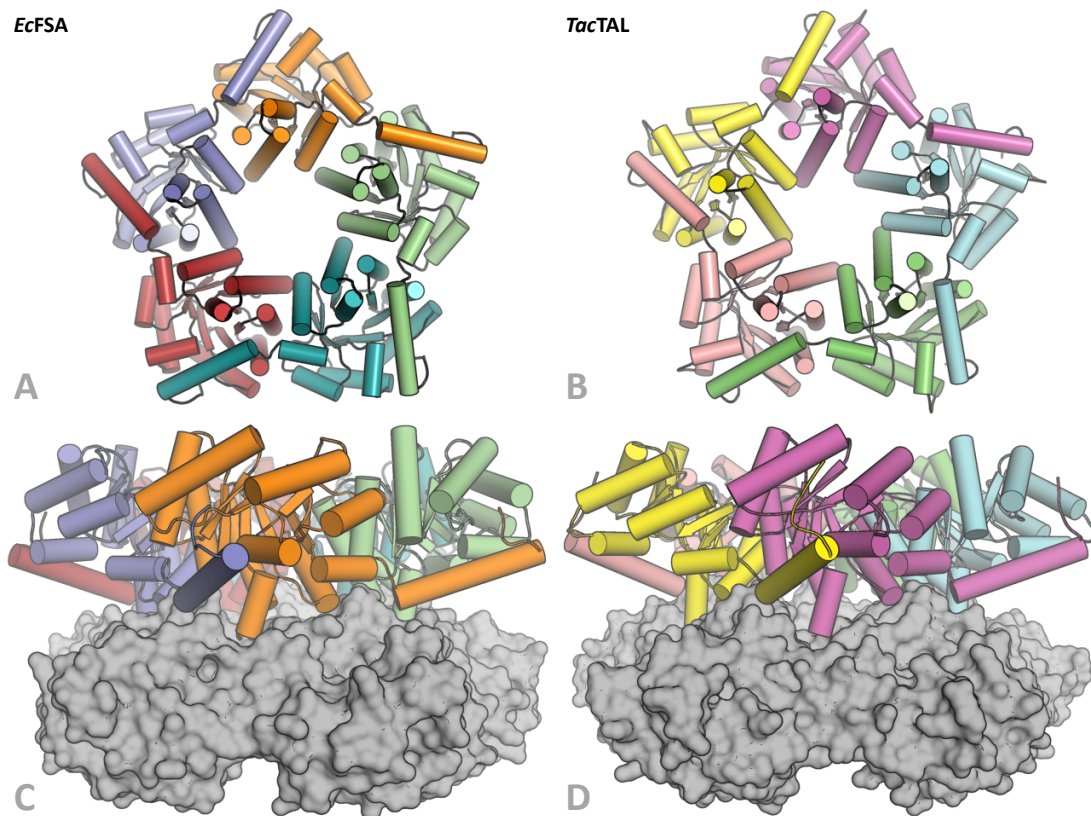


Figure 2.1.3: Crystal structures of *Tac*TAL and *Ec*FSA. **A:** Front view of the homopentamer of *Ec*FSA as secondary structure. PDB entry: 1L6W (THORELL *et al.*, 2002). **B:** Front view of the homopentamer of *Tac*TAL as secondary structure. PDB entry: 3S1V (LEHWESS-LITZMANN *et al.*, 2011b). **C:** Side view of the homodecamer of *Ec*FSA. The homopentamers are represented as secondary structure or surface. PDB entry: 1L6W (THORELL *et al.*, 2002). **D:** Side view of the homodecamer of *Tac*TAL. The homopentamers are represented as secondary structure or surface.

The subunits of *Tac*TAL crystallized in resting state adopt two different conformational states („open“ and „closed“) (LEHWESS-LITZMANN, 2011). In the „closed“ state, the flexible N-terminal part (6 – 55 aa) interacts with the C-terminal α -helix of the neighboring subunit (figure 2.1.4). Two interactions especially were assumed to play a significant role in the stabilization of the „closed“ state: a hydrogen bond between the residues Thr³⁰ and Asp²¹¹ and the hydrophobic interaction between residues Pro²⁹ and Phe²⁰⁸ (LEHWESS-LITZMANN, 2011; LEHWESS-LITZMANN *et al.*, 2011b).

Both of these interactions are not present in the „open“ state because of the spatial separation of the respective residues. The residues Pro²⁹ and Thr³⁰ are located in the helix α_2 , while their respective interaction partners Phe²⁰⁸ and Asp²¹¹ are located in the C-terminal α -helix of the neighboring subunit. The entrance of the active site in the „open“ state is ~ 3.8 Å wider compared to the active site in the „closed“ state (LEHWESS-LITZMANN, 2011).

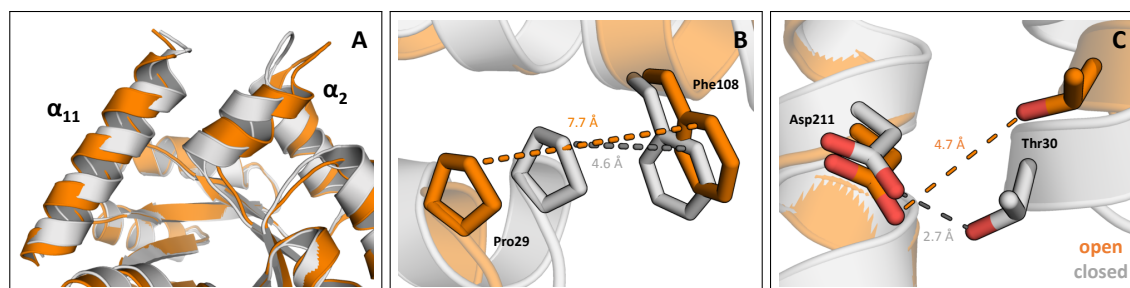
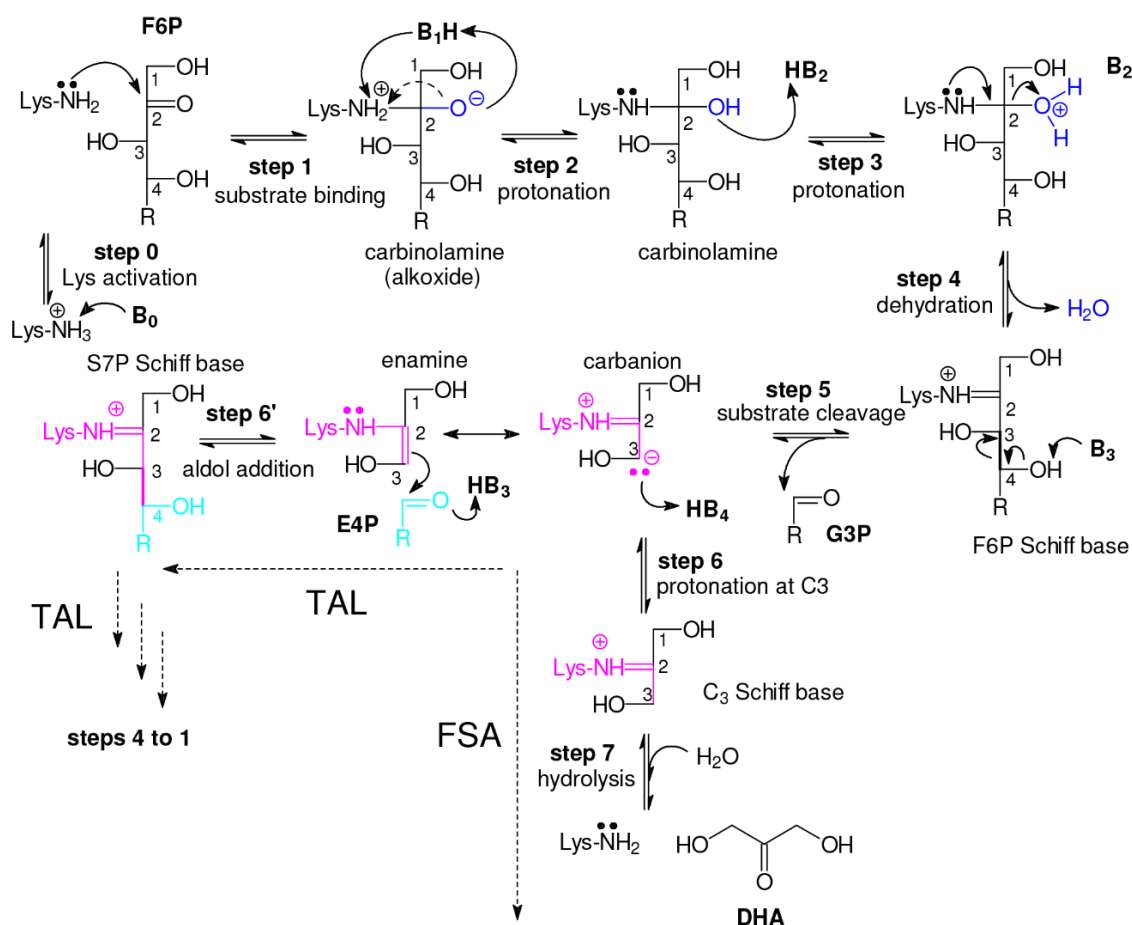


Figure 2.1.4: *TacTAL* monomer in its „open“ and „closed“ states. The polypeptide backbone is represented as cartoon, the interacting residues as sticks. Gray: „closed“ state; orange: „open“ state. **A:** The α -helices α_{11} and α_2 are close to each other in the „closed“ state, but separated in the „open“ state. **B:** The residue Phe²⁰⁸ of the α_{11} -helix interacts with the residue Pro²⁹ of the α_2 -helix in the „closed“ state but not in the „open“ state. **C:** The residue Asp²¹¹ of the α_{11} -helix interacts with the residue Thr³⁰ of the α_2 -helix in the „closed“ state but not in the „open“ state.

2.1.5 Active Site and the Reaction Mechanism of *TacTAL*

As a member of the class I aldolase family, transaldolase catalyzes its reaction using an active site lysine, which forms the SCHIFF base intermediate with the substrate (VENKATARAMAN AND RACKER, 1961). In *TacTAL*, this lysine (Lys⁸⁶) is located in the β_4 -strand of the barrel structure. Interestingly, the corresponding lysine residue of the mechanistically related class I fructose-1,6-bis(phosphate) aldolase (FBPA) is located in the β_6 -strand of the barrel (JIA *et al.*, 1996). In this context, a common ancestor was suggested, which evolved into the present-day aldolases and transaldolases. During the evolution, a circular permutation occurred on gene level resulting in circularly permuted TIM-barrel structures. The circular permutation events are suggested to be a common principle in the evolution of proteins belonging to the TIM-barrel family (NAGANO *et al.*, 2002) and were assumed to play a role in the evolution of non-TIM-barrel enzymes too, as it was suggested for the 1,3-1,4- β -glucanase (HEINEMANN AND HAHN, 1995).

For the reaction of *TacTAL*, the reactive lysine in the active site of transaldolase has to be deprotonated for the nucleophilic attack on the sugar's carbonyl group (STELLMACHER *et al.*, 2015). This is performed by a conserved glutamate residue (Glu⁶⁰ in *TacTAL*). This glutamate is the general



Scheme 2.3: Proposed reaction mechanism of transaldolase/aldolase. The transaldolase reaction (TAL) results in the reversible transfer of a dihydroxyacetone unit from ketose phosphates (donor substrate) to the C1 position of the aldose phosphates (acceptor substrate). The aldolase reaction (FSA) results in the reversible cleavage of the ketose-phosphate substrate. Both activities share the first half-reaction (steps 1 – 5) of the catalytic cycle. The main difference between the mechanisms is the protonation of the carbanion/enamine intermediate (SCHIFF base in FSA). Published in SAUTNER *et al.* (2015).

acid-base catalyst of transaldolase (LEHWESS-LITZMANN *et al.*, 2011b). Once deprotonated, the lysine residue can perform the nucleophilic attack on the carbonyl carbon of the donor-substrate, resulting in the formation of the carbinolamine intermediate (scheme 2.3, steps 1 and 2). The carbinolamine's C2 hydroxy group formed upon the nucleophilic attack and tautomerization step is protonated by the general acid-base catalyst Glu⁶⁰ and followed by dehydration (steps 3 and 4). After water elimination, the SCHIFF base intermediate is formed. Deprotonation of the C4 hydroxy group by the glutamate residue and the subsequent rearrangement result in the aldol cleavage of the intermediate (step 5). After product release, the reactive lysine remains modified as covalently linked carbanion/enamine intermediate. This reaction sequence describes the donor half-reaction

of the catalytic cycle. The acceptor half-reaction starts with the binding of the acceptor substrate followed by the nucleophilic attack of the carbanion/enamine intermediate on the carbonyl group of the acceptor substrate. Because of the reversible nature of the catalytic steps, the acceptor half-reaction corresponds to the reverse donor half-reaction.

The proton transfer reactions between the catalytic glutamate and the intermediates are facilitated by the catalytic water molecule observed in the active site, which is conserved in transaldolases (JIA *et al.*, 1997; THORELL *et al.*, 2002). However, the presence of this catalytic water molecule during all catalytic steps is in question (LEHWESS-LITZMANN, 2011; TITTMANN, 2014). This catalytic water molecule is coordinated by the residues Glu⁶⁰ and Thr¹¹⁰ (figure 2.1.5). In the structure containing the F6P-SCHIFF base intermediate in the active site this water is additionally coordinated by the C4 hydroxy group of the intermediate (LEHWESS-LITZMANN *et al.*, 2011b).

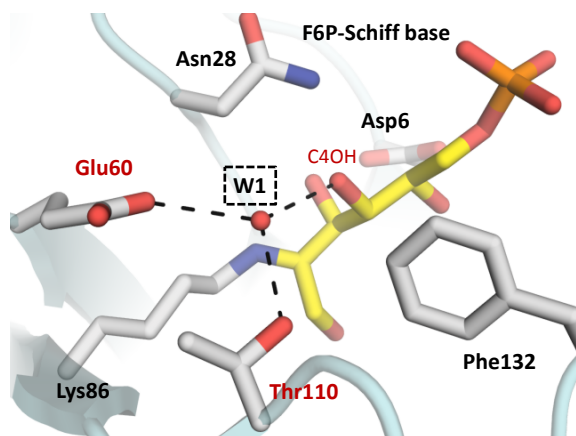


Figure 2.1.5: Catalytic water in the active site of *TacTAL*. The selected active site residues (gray) and the F6P-SCHIFF base intermediate (yellow) are represented as sticks. The polypeptide backbone (cyan) is shown as secondary structure. The catalytic water molecule (W1, framed) is shown as red sphere. The interaction partners of the water are labeled in red.

While most of the active site residues of *TacTAL* that are important for the catalysis and/or substrate binding are conserved in the related *EcFSA* (Asp⁶, Asn²⁸, Lys⁸⁶, Thr¹¹⁰, Arg¹³⁵ and Ser¹⁶⁷), some important active site residues are different and replaced in *EcFSA* by hydrophobic (Ser⁵⁸ → Phe, Asn¹⁰⁸ → Leu and Ser¹³⁰ → Ala) or homologous residues (Glu⁶⁰ → Gln, Phe¹³² → Tyr and Arg¹⁶⁹ → Lys). The absence of the transaldolase's general acid-base catalyst Glu⁶⁰ (Gln⁵⁹ in *EcFSA*) and the presence of a tyrosine residue at the position of Phe¹³² (Tyr¹³¹ in *EcFSA*) are of particular interest. It could be shown that a single mutation of the corresponding phenylalanine residue to tyrosine in the *E. coli* transaldolase and *TacTAL* results in a variant with stimulated aldolase activity (LEHWESS-LITZMANN, 2011; SCHNEIDER *et al.*, 2008).

According to the proposed reaction mechanisms (scheme 2.3) of *TacTAL* and *EcFSA*, both enzymes share the first half-reaction (donor half-reaction) of the catalytic cycle. In the case of *TacTAL*, those reactions are acid-base catalyzed by the residue Glu⁶⁰. The absence of the equivalent residue in

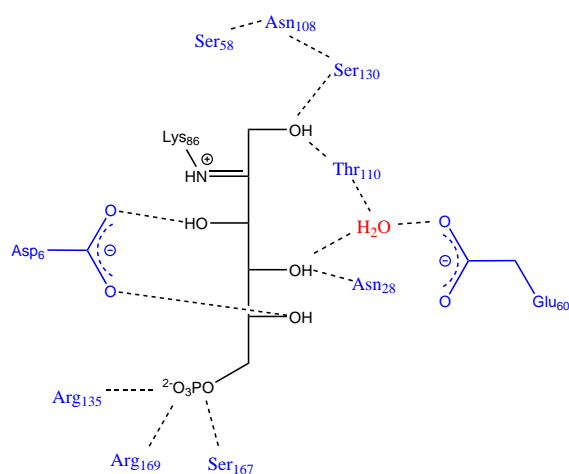
the active site of *EcFSA* is therefore surprising, since the acid-base catalyzed aldol-cleavage of the substrate is also a part of the reaction mechanism of this enzyme. With exception of Asp⁶, only the residue Tyr¹³¹ can perform the acid-base catalysis in the active site of *EcFSA*. The Asp⁶ is suggested to play an important role in the substrate binding and its correct orientation but does not sufficiently participate on the acid-base catalysis (LEHWESS-LITZMANN *et al.*, 2011b). In the *TacTAL* structure containing the F6P-SCHIFF base intermediate, this residue coordinates the C3 and C5 hydroxy groups of the intermediate. On this basis, one can assume that the Tyr¹³¹ residue takes over the role of the transaldolase's glutamate residue as the general acid-base catalyst.

The main difference in the catalytic mechanism of FSA compared to the reaction catalyzed by TAL is the protonation of the carbanion/enamine intermediate. In the case of TAL, this intermediate immediately reacts with the acceptor substrate (transaldolase reaction), while in FSA, the intermediate is protonated, forming a DHA-SCHIFF base intermediate (scheme 2.3). The DHA-SCHIFF base cannot attack the acceptor substrate nucleophilically but can be hydrolyzed (aldolase reaction). In this context, the Tyr¹³¹ residue in *EcFSA* is assumed to protonate the carbanion/enamine intermediate. On the other hand, the Glu⁶⁰ residue in *TacTAL* does not perform that protonation.

Tyrosine side chains are known to perform proton transfer reactions in other class I aldolases as in the case of the mammalian fructose-1,6-bis(phosphate) aldolase (FBPA). During the catalytic reaction of the rabbit muscle FBPA the C-terminal tyrosine residue (Tyr³⁶³) located on the flexible terminus acts together with Lys¹⁴⁶ and Glu¹⁸⁷ as the acid-base catalyst for the aldolytic cleavage of the substrate fructose 1,6-bis(phosphate) into the dihydroxyacetone phosphate and glyceraldehyde 3-phosphate (ST-JEAN AND SYGUSCH, 2007). Interestingly, the deletion of this tyrosine residue by treatment of the protein with carboxypeptidase results in a decrease of the aldolase activity and in an increase of the transaldolase activity (ROSE *et al.*, 1965).

The relative orientation of the tyrosine residue in the active site of *EcFSA* differs from that of the glutamate in *TacTAL*. While the transaldolase's glutamate residue is oriented in same direction as the reactive lysine residue (towards the active site entrance), the aldolase's tyrosine residue is oriented in the opposite direction (towards the reactive lysine). These two situations are common in different transaldolases and aldolases and are named as co-aligned and opposite-faced, respectively (TITTMANN, 2014).

TacTAL was the first transaldolase in whose active site a reactive F6P-SCHIFF base intermediate could be trapped *in crystallo* (LEHWESS-LITZMANN *et al.*, 2011b). The C3 and C5 hydroxy groups of



Scheme 2.4: Coordination of the F6P-SCHIFF base intermediate in the active site of *TacTAL*. Adapted from LEHWESS-LITZMANN *et al.* (2011b)

the intermediate are coordinated by Asp⁶ (figure 2.4). The C4 hydroxy group is coordinated by the Asn²⁸ residue and the catalytic water molecule. The phosphate group is coordinated by the residues Arg¹³⁵, Arg¹⁶⁹ and Ser¹⁶⁷.

The C1 hydroxy group exhibits two alternative conformations („up“ and „down“). This group in the „up“ conformation is coordinated by the residue Thr¹¹⁰ (figure 2.1.6 A) and the „down“ conformation is coordinated by the residue Ser¹³⁰ (figure 2.1.6 B). Both interactions were analyzed in previous works (LEHWESS-LITZMANN, 2011; SAUTNER, 2012). The *TacTAL*_{T110V} variant with interrupted „up“ coordination showed a greatly impaired transaldolase activity (LEHWESS-LITZMANN, 2011). Apart from the coordination of the C1 hydroxy group, this threonine coordinates the catalytic water molecule and is suggested to coordinate the C2 hydroxy group of the carbinolamine intermediate (SCHÖRKEN *et al.*, 2001). The *TacTAL*_{S130A} variant with interrupted „down“ coordination exhibits an impaired donor half-reaction activity (SAUTNER, 2012). However, crystallographic studies on this variant showed that the C1 hydroxy group of the F6P-SCHIFF base intermediate trapped in the active site adopts both alternative conformations despite the missing interaction partner (Ser¹³⁰) in the variant. In the case of the variant, the „down“ conformation is coordinated by the residue Asn¹⁰⁸, which is spatially close to the original interaction partner Ser¹³⁰. A corresponding variant of transaldolase from *Escherichia coli* (*EcTAL*_{S176A}) showed highly impaired transaldolase activity (SCHÖRKEN *et al.*, 2001).

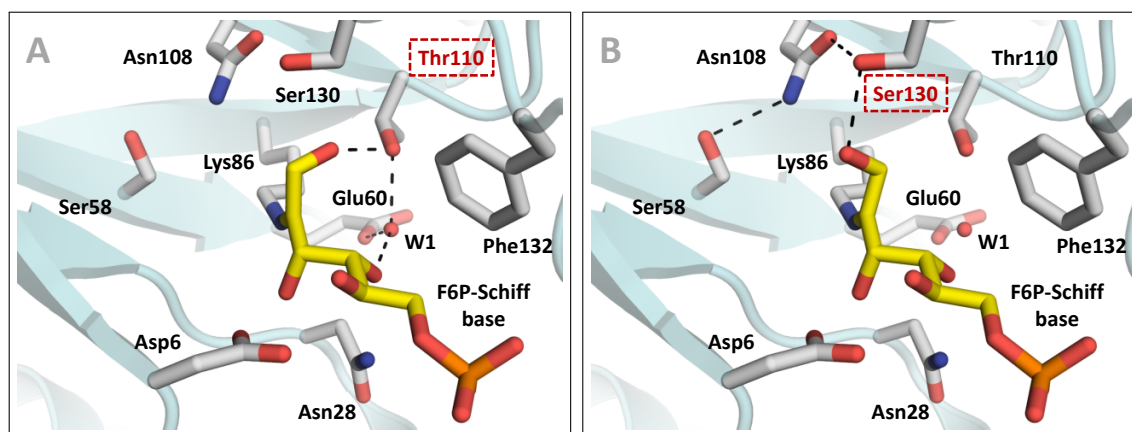


Figure 2.1.6: „Up“ and „down“ conformations of the C1 hydroxy group of the F6P-SCHIFF base intermediate in the active site of *TacTAL_{wt}* co-crystallized with F6P. The selected active site residues (gray) are represented as sticks. The polypeptide backbone is shown as secondary structure (cyan). The catalytic water molecule is shown as the red sphere. The respective hydrogen bond interactions are represented as black dashes. **A:** The „up“ conformation of the intermediate (yellow) is coordinated by Thr¹¹⁰ (framed). **B:** The „down“ conformation of the intermediate (yellow) is coordinated by Ser¹³⁰ (framed).

2.1.6 Motivation

Since the transaldolase activity was first described by HORECKER AND SMYRNIOTIS (1953), extensive information about the mechanism of action and the structure of the enzyme was gathered. More than half of this information was contributed during the last 20 years. During the last decade, studies on the transaldolase from *Thermoplasma acidophilum* enriched the structural basis for the understanding of the catalytic mechanism. The structure of *TacTAL* co-crystallized with the substrate F6P was the first observation of a reactive intermediate in the active site of transaldolase.

However, some important mechanistic and structural aspects remain unexplained. Due to the lack of structural information about the intermediates appearing prior to the SCHIFF base formation, the role of the active site residues, which do not participate directly on the acid-base catalysis but contribute to the binding process and presumably to the correct orientation of the substrate and/or intermediates, is unclear.

One of the tasks of the present work was to complement the previous efforts regarding the coordination of the substrate's C1 hydroxy group in its „down“ conformation. This group is located directly next to the substrate's carbonyl group, which is the reactive group in the course of the essential SCHIFF-base formation. The coordination of the C1 hydroxy group is assumed to be important for the correct orientation of the carbonyl group during the nucleophilic attack of the reactive lysine

(SCHÖRKEN *et al.*, 2001). Furthermore, this interaction is suggested to contribute to substrate binding and correct positioning of the intermediates.

A further aim of the thesis was to obtain structural information about the substrate bound in the active site of *TacTAL* as MICHAELIS complex and the carbinolamine intermediate, in order to provide a structural basis for a deeper understanding of the reaction mechanism.

In the beginning of the millennium, an enzyme with a novel activity was found in *Escherichia coli* (SCHÜRMAN AND SPRENGER, 2001). The enzyme catalyzes the reversible cleavage of fructose 6-phosphate and was referred to as fructose 6-phosphate aldolase (FSA). Although *EcFSA* is structurally similar to the *TacTAL* and catalyzes a mechanistically similar reaction, the determinant of the reaction selectivity remained unclear. Different *TacTAL* variants mimicking the situation in the active site of *EcFSA* should be designed, in order to investigate how both enzymes discriminate between transaldolase and aldolase activities.

Structural analysis of *TacTAL* showed the co-existence of two different conformational states („open“/„closed“) for single subunits of the homopentamer (LEHWESS-LITZMANN *et al.*, 2011b). Interestingly, the structures of *TacTAL* co-crystallized with the substrate F6P do not exhibit different conformations. All subunits, which bind the substrate in the active site, are present in the „closed“ conformation. Assuming the presence of different conformational states in solution, the conformational-selection mechanism for substrate binding was suggested (LEHWESS-LITZMANN *et al.*, 2011b). The role of these conformational changes in the catalysis can be investigated by introduction of a disulfide bond, cross-linking the flexible regions and arresting the „closed“ conformation. This conformational arrest can be unlocked by applying reducing agents such as DTT or β -mercaptoethanol giving the possibility to analyze the *TacTAL* in its constitutively „closed“ conformation.

2.2 Results

2.2.1 Crystallographic Studies on Enzyme Bound Intermediates

In order to gather deeper insights into the catalytic cycle of the transaldolase, the relative orientations of the intermediates occurring during the transaldolase reaction in the active site were analyzed using the crystallographic approach.

The crystal structure of *TacTAL*_{wt} co-crystallized with D-fructose 6-phosphate (F6P) was determined and refined as described in section 1.6.3. The initial model was refined against the experimental data to 1.51 Å resolution (table A.3 in the appendix). The final model corresponds to the diffraction data with $R_{\text{work}} = 15.98\%$ and $R_{\text{free}} = 18.58\%$ (table A.5 in the appendix). All subunits of the pentamer in the asymmetric unit are existent in the „closed“ conformation. An additional electron density was observed in all five active sites. This electron density was interpreted as F6P covalently linked to the reactive lysine (Lys⁸⁶) forming the F6P-SCHIFF base intermediate (figure 2.2.7 B) according to the proposed catalytic mechanism (scheme 2.3). The C1OH-group of the intermediate shows two alternative conformations, which were named in previous work as „up“ and „down“ conformations (LEHWESS-LITZMANN *et al.*, 2011b). The intermediate's C1OH-group in the „up“ conformation interacts with the Thr¹¹⁰ residue and participates in the hydrogen bond network between Thr¹¹⁰, Glu⁶⁰ (general acid-base catalyst in *TacTAL* reaction), the catalytic water and the C4OH-group of the intermediate (figure 2.2.7 A). In the „down“ conformation it interacts with Ser¹³⁰ and partakes in the hydrogen bond network between Ser¹³⁰, Asn¹⁰⁸ and Ser⁵⁸. This observation corresponds well to the previously published results of LEHWESS-LITZMANN *et al.* (2011a,b).

The Glu⁶⁰ residue in the active site of *TacTAL* is suggested to be the general acid-base catalyst for the transaldolase reaction (LEHWESS-LITZMANN, 2011; LEHWESS-LITZMANN *et al.*, 2011b). The proton transfer reactions are facilitated by the catalytic water molecule in the active site. This water molecule is coordinated by the Thr¹¹⁰ and Glu⁶⁰ residues as well as by the C4OH-group of the F6P-SCHIFF base intermediate. A single-mutation of the corresponding residue to glutamine in *E. coli* transaldolase (Glu⁹⁶ → Gln) results in a variant showing a highly affected transaldolase activity (SCHÖRKEN *et al.*, 2001). Likewise, the transaldolase activity of the *TacTAL*_{E60Q} variant was described as greatly impaired, considering the loss of the general acid-base catalyst (LEHWESS-LITZMANN, 2011; LEHWESS-LITZMANN *et al.*, 2011b). Moreover, the mass spectrometric analysis of the reaction intermediates showed a minor accumulation of the F6P-carbinolamine intermediate in

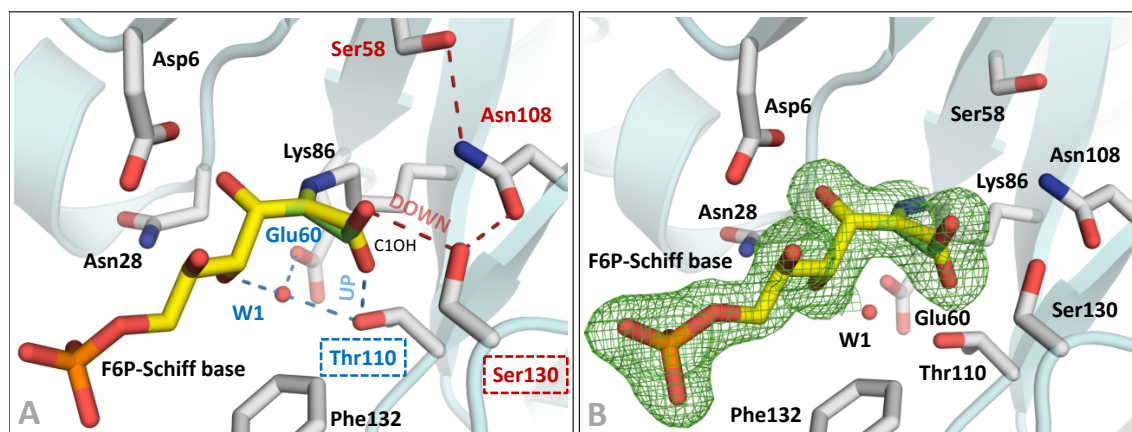


Figure 2.2.7: Active site of *TacTAL*_{wt} co-crystallized with F6P. The selected active site residues (gray) are represented as sticks. The polypeptide backbone is shown as secondary structure (cyan). **A:** The C1OH-group of the F6P-SCHIFF base intermediate (yellow) shows two alternative conformations („up“ and „down“). The intermediate’s C1OH-group in the „up“ conformation (yellow) interacts with Thr¹¹⁰ (framed) and partakes in the hydrogen bond network (blue dashes) between Thr¹¹⁰, catalytic water (W1), Glu⁶⁰ (labeled in blue) and the C4OH-group of the intermediate. The intermediate’s C1OH-group in the „down“ conformation (green) interacts with Ser¹³⁰ (framed) and participates in the hydrogen bond network (red dashes) between Ser¹³⁰, Asn¹⁰⁸ and Ser⁵⁸ (labeled in red). **B:** *mFO-DFC* simulated annealing omit map (green mesh, contour level 3 σ).

the variant, which was not detected neither for wild type enzyme nor for other analyzed variants (LEHWESS-LITZMANN, 2011). This finding is not surprising, since the protonation of the carbinolamine intermediate is performed via acid-base catalysis prior to water elimination resulting in the formation of the SCHIFF base intermediate, which was the only intermediate detected for the wild type enzyme. However, the major fraction of the observed intermediates appearing during the reaction of the *TacTAL*_{E60Q} variant in presence of F6P and E4P was represented by the F6P-SCHIFF base intermediate (LEHWESS-LITZMANN, 2011).

The observed rate constant for the donor half-reaction in absence of E4P (consisting of the binding of F6P, F6P-carbinolamine intermediate formation, F6P-SCHIFF base intermediate formation, F6P-SCHIFF base intermediate cleavage and GA3P-release) is two orders of magnitude lower compared to the wild type reaction according to the stopped-flow measurements (see figure C.4 in the appendix, for a representative progress curve). The observed first order rate constant for the reaction of *TacTAL*_{E60Q} after rapid mixing with F6P (final concentration 10 mM) was determined to $k_{\text{obs}} = 0.7 \text{ s}^{-1}$ ($k_{\text{obs}} = 55.9 \text{ s}^{-1}$, for the wild type reaction).

In order to obtain structural information about the covalently linked intermediate in the active site of *TacTAL*_{E60Q}, the variant was co-crystallized with F6P. The initial model was refined against the

diffraction data from a single crystal to 1.65 Å resolution (table A.3 in the appendix). The final model corresponds to the diffraction data with $R_{\text{work}} = 16.23\%$ and $R_{\text{free}} = 19.43\%$ (table A.5 in the appendix). An additional electron density was observed in all five active sites and interpreted as the F6P-SCHIFF base intermediate (figure C.6 in the appendix). A similar situation was recently reported for the corresponding variant (Glu⁹⁶ → Gln) of transaldolase from *E. coli* (STELLMACHER *et al.*, 2016).

The active site of the variant is superimposable with the active site of *TacTAL*_{wt} (rmsd = 0.133 Å based on C α atoms of a monomer, figure 2.2.8 B). Although the F6P-carbinolamine intermediate was previously detected by mass spectrometric analysis of the variant (LEHWESS-LITZMANN, 2011), the respective intermediate could not be trapped in the structure of the *TacTAL*_{E60Q} variant. The reasons are most probably the consequence of the relative long timeframe of the crystallization approach (7 – 14 days for crystallization compared to 10 min for the mass spectrometry measurements) and/or the relative small population of the F6P-carbinolamine intermediate compared to the F6P-SCHIFF base intermediate. The carbinolamine intermediate is another intermediate of interest appearing prior to the SCHIFF base formation.

In order to mimic the F6P-carbinolamine intermediate, *TacTAL*_{wt} was co-crystallized with D-mannitol 1-phosphate (M1P). The subject of interest was the relative orientation of the carbinol-

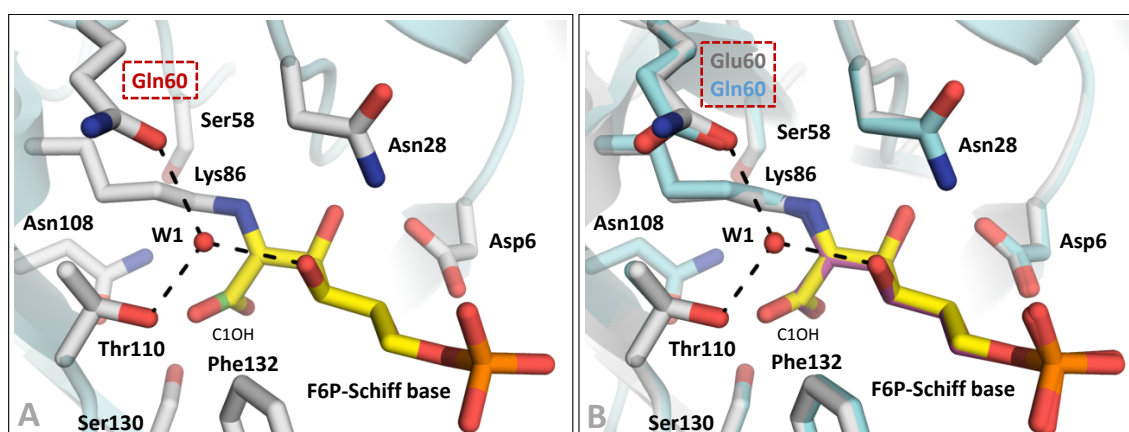
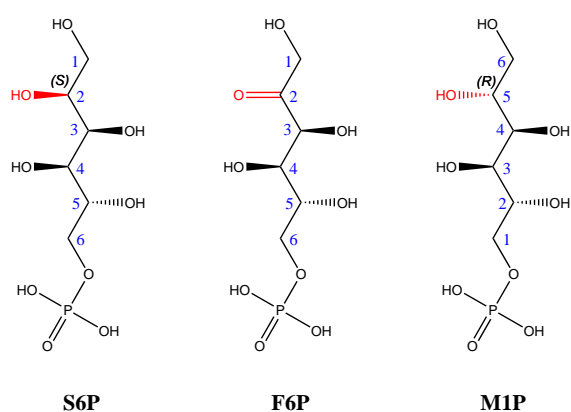


Figure 2.2.8: Active site of *TacTAL*_{E60Q} co-crystallized with F6P. **A:** The C1OH-group of the F6P-SCHIFF base intermediate (yellow) shows two alternative conformations („up“ and „down“). The mutated residue (Glu⁶⁰ → Gln, framed) is labeled in red. The catalytic water is coordinated by Thr¹¹⁰, Gln⁶⁰ and the intermediate's C4OH-group (black dashes). The selected active site residues (gray) are represented as sticks. The polypeptide backbone is shown as secondary structure (cyan). **B:** Superposition of the active sites of *TacTAL*_{E60Q} (gray; ligand: yellow) and *TacTAL*_{wt} (cyan, ligand: purple).

lamine's C2OH-group in the active site of transaldolase. M1P is a structural analogue of F6P differing in the formally reduced carbonyl group compared to the F6P structure (OH-group in M1P). This C5OH-group in the structure of M1P is assumed to mimic the C2OH-group of the F6P-carbinolamine intermediate formed after the nucleophilic attack of the reactive lysine on the substrate's C2-carbonyl group. The formation of the OH-group implies a change of the C2-atom's hybridization state (from sp^2 for a C2-carbonyl group to sp^3 for a C2OH group). This change results in the introduction of a new stereocenter. Since the chirality of the developing stereocenter is unknown, both enantiomers (*R* vs. *S*) are possible. The structural analogue of F6P with an *S*-stereocenter at C2 position is sorbitol 6-phosphate (S6P), whereas M1P mimics the (*2R*)-carbinolamine (scheme 2.5). Both substances are able to inhibit the physiological reaction of transaldolase (data not shown).



Scheme 2.5: Structural formula of S6P, F6P and M1P. While the F6P structure exhibits a carbonyl group at C2 position, the molecules of S6P and M1P contain a hydroxy group at the corresponding carbon atom (highlighted in red). The different (*S*)/(*R*)-configuration is denoted, respectively. Note the reverse atom numbering (blue numbers) in case of M1P nomenclature compared to S6P and F6P.

The interaction of S6P with the active site of *TacTAL*_{wt} was analyzed in previous studies. Unfortunately, the co-crystallized analogue did not bind properly into the active site of the wild type enzyme and showed multiple conformations (LEHWESS-LITZMANN, 2011).

The structure of *TacTAL*_{wt} co-crystallized with M1P was determined to 1.85 Å resolution (table A.3 in the appendix) and refined against the diffraction data with $R_{\text{work}} = 18.39\%$ and $R_{\text{free}} = 21.88\%$ (table A.5 in the appendix). While the subunits B, C and E were modeled as „closed“ conformation, the subunits A and D were modeled as mixed „open“/„closed“ alternative conformations. Additional electron densities observed in the active sites of subunits B, C, D and E were interpreted as the non-covalently bound M1P (figure C.7 in the appendix). In the active site of the subunit A only the phosphate group of M1P could be modeled into the electron density. The electron density around the ligand's C3-atom and the C3 hydroxy group is missing, implying a higher flexibility of this

group. Aldol cleavage of M1P is unfavorable, because the essential SCHIFF base formation is already impaired due to the lack of the carbonyl group in the structure of the ligand.

According to the refined structure, M1P is present in the active site with an occupancy of ~70 – 80 %. Furthermore, a resting state water molecule was modeled near the C5OH-group of M1P (figure 2.2.9 A). Since the distance between this water molecule and the C5OH-group of the ligand is too short for a co-existence of both (~1.6 Å), the water is assumed to be present only in active sites, which did not bind M1P. In this context, the water molecule was modeled and refined with an occupancy of ~20 – 30 %. A water molecule on this position is present in the resting state structure of *TacTAL*_{wt} (PDB entry: 3S0C (LEHWESS-LITZMANN *et al.*, 2011a,b)) and is coordinated by Thr¹¹⁰, Glu⁶⁰ and Lys⁸⁶. This water is displaced compared to the position of the catalytic water molecule observed in the structure of the wild type enzyme co-crystallized with F6P by ~0.7 Å.

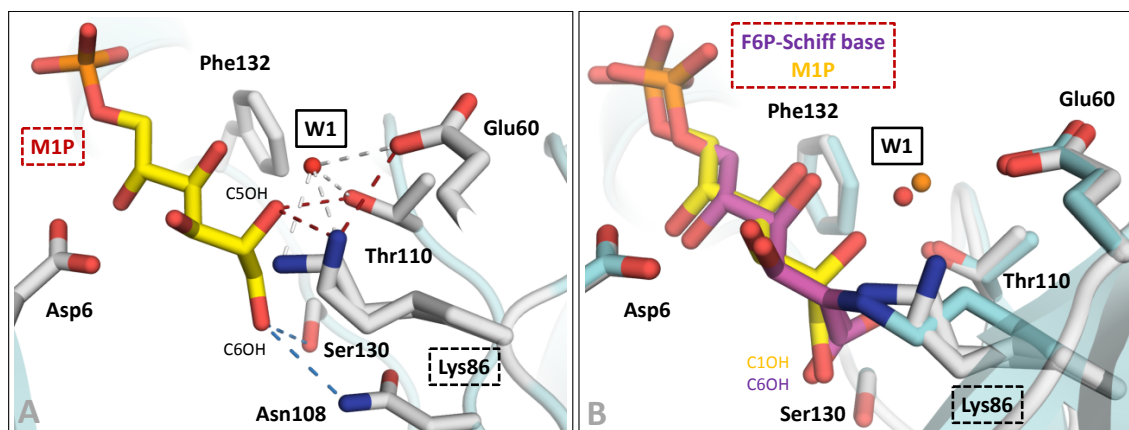


Figure 2.2.9: Active site of *TacTAL*_{wt} co-crystallized with M1P. **A:** M1P (yellow sticks) is present with partial occupancy in the active site of *TacTAL*_{wt} in a similar conformation as the F6P-SCHIFF base intermediate. The reactive lysine (framed) shows two alternative conformations. The C5OH-group of M1P presumably mimics the C2OH-group of the F6P-carbinolamine intermediate. This group is coordinated by Thr¹¹⁰ and one of the conformations of Lys⁸⁶, which is coordinated by Glu⁶⁰ (red dashes). A resting state water (W1, framed), corresponding to the catalytic water, is present near the C5OH-group of M1P. This water is in hydrogen bond distance to Thr¹¹⁰, Glu⁶⁰ and Lys⁸⁶ in both conformations (gray dashes). The C6OH-group of M1P is coordinated by Ser¹³⁰ and Asn¹⁰⁸ (blue dashes) corresponding to the „down“ conformation of the C1OH-group of the F6P-SCHIFF base intermediate. The selected active site residues (gray) are represented as sticks. The polypeptide backbone is shown as secondary structure (cyan). **B:** Superposition of the active sites of *TacTAL*_{wt} co-crystallized with M1P (gray) and F6P (cyan). The non-covalently bound M1P (yellow) is displaced relatively to the F6P-SCHIFF base intermediate (purple). The water molecules in the structures of *TacTAL*_{wt} co-crystallized with F6P or M1P are represented as orange or red spheres, respectively.

The reactive lysine (Lys⁸⁶) was modeled into the electron density in two alternative conformations (figure 2.2.9 A). One of the conformers is oriented towards the C5-atom of M1P. The distance

between the lysine's N ϵ and ligand's C5 atoms is ~ 1.8 Å, which is too long for a carbon-nitrogen covalent bond ($\sim 1.469 - 1.499$ Å (ALLEN *et al.*, 1987)) but too short for the co-existence of both atoms at their refined positions. Therefore, this conformer of the reactive lysine was assumed to be present in the fraction of the non-occupied active sites (occupancy of $\sim 20 - 30$ %). The second conformation of Lys⁸⁶ is coordinated by Glu⁶⁰. The interatomic distance between the ϵ -amino group of the lysine conformer and the C5OH-group of the ligand is sufficient for a hydrogen bond interaction (~ 2.8 Å). Furthermore, the ϵ -amino group of the reactive lysine in both conformations can interact with the main chain carbonyl of Thr²⁷ as in the case of the F6P-SCHIFF base intermediate trapped in the active site of *TacTAL*_{wt} co-crystallized with F6P (interatomic distances of $\sim 2.8 - 2.9$ Å; figure C.5 in the appendix).

The orientation of the C2, C3, and C4 hydroxy groups of the M1P molecule bound in the active site of *TacTAL*_{wt}, as well as the coordination of the phosphate group, is comparable to the binding mode of the corresponding groups of the F6P-SCHIFF base intermediate (figure 2.2.9 B). However, the M1P molecule is displaced towards the entrance of the active site compared to the SCHIFF base intermediate (displacement of the phosphate group by ~ 0.9 Å). The C6OH-group of the non-covalently bound M1P molecule is coordinated by the residues Asn¹⁰⁸ and Ser¹³⁰ corresponding to the „down“ conformer of the C1OH-group of the F6P-SCHIFF base intermediate.

The C5OH-group of the M1P molecule is oriented towards the position of the catalytic water molecule present in the active site of *TacTAL*_{wt} co-crystallized with F6P. This group is coordinated by the residues Thr¹¹⁰ and Lys⁸⁶. The C5OH-group is assumed to mimic the C2OH-group of the F6P-carbinolamine intermediate formed upon nucleophilic attack of the catalytic lysine on the C2 carbonyl group of the F6P substrate. In the case of the real F6P-carbinolamine intermediate, the interaction of the C2 hydroxy group with the ϵ -amino group of the lysine residue is not possible, because the lysine is covalently linked to the C2 atom. The residue Thr¹¹⁰ is conserved in all transaldolases (SAMLAND AND SPRENGER, 2009). Beside its role in the coordination of the catalytic water, this conserved threonine residue was already assumed to coordinate the C2 hydroxy group of the carbinolamine intermediate (SCHÖRKEN *et al.*, 2001). A single-mutation of the Thr¹¹⁰ to valine results in a *TacTAL* variant showing a two orders of magnitude lower turnover number and one order of magnitude higher apparent MICHAELIS constant for substrate F6P compared to the wild type enzyme (LEHWESS-LITZMANN, 2011).

The catalytic water molecule is assumed to mediate the proton transfer reactions between the general acid-base catalyst (Glu⁶⁰) and the substrate/intermediates during catalysis (LEHWESS-LITZMANN, 2011; LEHWESS-LITZMANN *et al.*, 2011b). A corresponding water molecule is not present in the active site of wild type enzyme co-crystallized with M1P. According to the proposed catalytic mechanism (scheme 2.3) the C2OH-group of the carbinolamine intermediate is protonated by Glu⁶⁰ prior to water elimination resulting in the formation of the F6P-SCHIFF base intermediate. In absence of the catalytic water, the observed distance between the C5 hydroxy group of M1P and the acid-base residue Glu⁶⁰ is too long for a direct proton transfer ($\sim 4.6 \text{ \AA}$) but could be possible assuming a local flexibility of the active site.

The carbinolamine intermediate is a result of the nucleophilic attack of the catalytic lysine on the carbonyl group of the donor substrate bound in the active site as MICHAELIS-complex. To elucidate the relative orientation of the substrate F6P in the MICHAELIS-complex an inactive *TacTAL* variant (*TacTAL*_{K86Q}) was generated and co-crystallized with F6P. The replacement of the reactive lysine (Lys⁸⁶) by glutamine results in a variant unable to form the carbinolamine- and the SCHIFF base intermediates.

The structure of *TacTAL*_{K86Q} co-crystallized with F6P was determined to 1.75 Å resolution (table A.3 in the appendix) and refined against the diffraction data with $R_{\text{work}} = 20.88 \%$ and $R_{\text{free}} = 25.04 \%$ (table A.5 in the appendix). All five subunits of the homopentamer in the crystallographic asymmetric unit were observed in „closed“ conformation. The donor substrate F6P was modeled in all five subunits into the observed electron density as non-covalent complex and refined to an occupancy of $\sim 70 - 80 \%$ (figure C.8 in the appendix). As in the case of wild type protein co-crystallized with M1P the middle part of the F6P molecule, especially the C4 hydroxy group (corresponding to the C3OH in M1P), is not represented by the corresponding difference electron density.

The C3, C4 and C5 hydroxy groups, as well as the phosphate group of the non-covalently bound F6P, are coordinated by the active site residues in similar way as the corresponding groups of the F6P-SCHIFF base intermediate (figure 2.2.10 B). Compared to the transaldolase structure containing the F6P-SCHIFF base intermediate in the active site, the non-covalently bound F6P is shifted towards the entrance of the active site by approximately one carbon position. The C1OH group is coordinated by Thr¹¹⁰ corresponding to the „up“ conformer of the C1OH-group of the F6P-SCHIFF base intermediate.

The C2 carbonyl of the non-covalently bound substrate is oriented towards the general acid-base catalyst Glu⁶⁰ but the interatomic distance between the side chain carboxyl group of the glutamate residue and the carbonyl oxygen of F6P is too long for a hydrogen bond interaction (~ 4.9 Å). The only active site residue placed in the hydrogen bond distance to the C2 carbonyl oxygen is the introduced Gln⁸⁶ (figure 2.2.10 A). In this context, a transient interaction between the lysine's ϵ -amino group and the carbonyl oxygen of F6P could be possible. The catalytic water observed in the active sites of *Tac*TAL structures containing the F6P-SCHIFF base intermediate is not present in the active site of the variant.

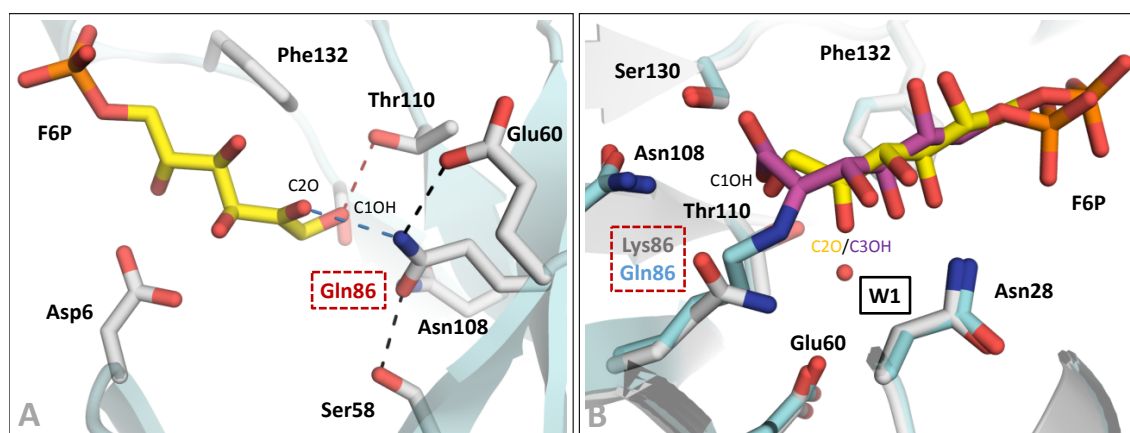


Figure 2.2.10: Active site of *Tac*TAL_{K86Q} co-crystallized with F6P. **A:** F6P (yellow sticks) is present with partial occupancy in the active site of *Tac*TAL_{K86Q}. The mutated residue (Lys⁸⁶ → Gln, framed) is labeled in red. This residue is coordinated by Glu⁶⁰ and Ser⁵⁸ (black dashes). The C2-carbonyl oxygen of F6P is coordinated by Gln⁸⁶ (blue dashes). The catalytic water is absent. The C1OH-group of F6P is coordinated by Thr¹¹⁰ (red dashes) corresponding to the „up“ conformation of the C1OH-group of the F6P-SCHIFF base intermediate. The selected active site residues (gray) are represented as sticks. The polypeptide backbone is shown as secondary structure (cyan). **B:** Superposition of the active sites of *Tac*TAL_{K86Q} (gray) and *Tac*TAL_{wt} (cyan) co-crystallized with F6P. The non-covalently bound F6P (yellow) is displaced relatively to the F6P-SCHIFF base intermediate (purple). The catalytic water molecule in the structure of *Tac*TAL_{wt} is represented as red sphere.

According to the BÜRGI-DUNITZ trajectory for the nucleophilic attack on a sp^2 electrophile, the perfect trajectory angle between the nucleophile and the plane defined by the carbonyl group (direction: nucleophile→C→O) is $\sim 105 \pm 5^\circ$ (figure 2.2.11 C; (BÜRGI *et al.*, 1973, 1974)). When transferring the non-covalently bound F6P from the structure of the *Tac*TAL_{K86Q} variant into the active site of the structure of wild type protein, the corresponding angle for the nucleophilic attack of the lysine residue on the sugar's carbonyl group is $\sim 58.7^\circ$ (figure 2.2.11 A). Consequently, a reorientation of the substrate's carbonyl group (e.g. by rotation of the carbonyl group around the C2-C3 bond axis in the F6P molecule) and/or of the flexible lysine residue is necessary for a

nucleophilic attack of the lysine's N ϵ -atom on the carbonyl group. At this point, it should be noted, that the relative orientation of the substrate's carbonyl group in the active site of *Tac*TAL_{K86Q} could differ from the orientation of this group in the environment of the wild type protein. The only interaction partner of the carbonyl's oxygen in the active site of the variant is Gln⁸⁶, which is not present in the active site of *Tac*TAL_{wt}.

LIGHT *et al.* (2014) determined the crystal structure of an inactive variant of transaldolase from *Francisella tularensis* (*Ftu*TAL) co-crystallized with F6P. In this study, the reactive lysine was mutated to a methionine giving an inactive *Ftu*TAL_{K135M} variant. When transferring the non-covalently bound F6P molecule observed in the active site of the variant (PDB entry: 3te9) into the active site of the *Ftu*TAL wild type enzyme (PDB entry: 3tk7), the relative orientation of the reactive lysine to the plane of the carbonyl group shows an obtuse N ϵ -C2-O2 angle of $\sim 118.7^\circ$ (figure 2.2.11 B) close to the ideal BÜRGI-DUNITZ angle of $\sim 105 \pm 5^\circ$ (figure 2.2.11 C; (BÜRGI *et al.*, 1973, 1974)). Furthermore, they suggested larger conformational changes in the C1-C2-C3 region of the substrate molecule taking place along with the formation of the SCHIFF base intermediate.

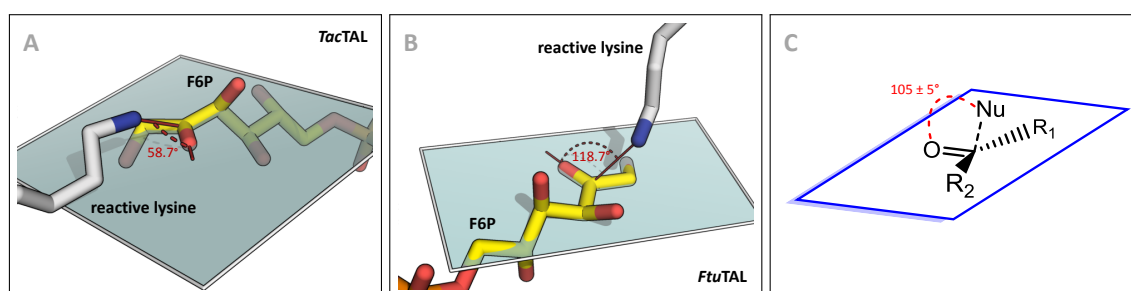
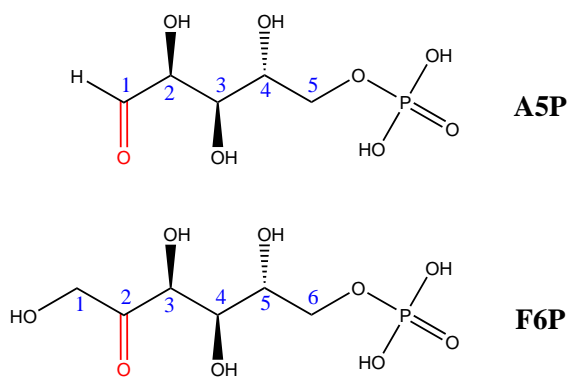


Figure 2.2.11: Ideal BÜRGI-DUNITZ angle compared to the non-covalently bound F6P in *Tac*TAL and *Ftu*TAL (LIGHT *et al.*, 2014). **A:** Non-covalently bound F6P (yellow sticks) from the *Tac*TAL_{K86Q} structure modeled into the active site of the wild type protein. The reactive lysine (gray sticks) is placed relatively to the plane of the carbonyl group (cyan) in an acute N ϵ -C2-O2 angle (red dashes) that is unfavorable for the nucleophilic attack. **B:** Non-covalently bound F6P (yellow sticks) from the *Ftu*TAL_{K135M} structure (PDB entry: 3te9 (LIGHT *et al.*, 2014)) modeled into the active site of the wild type protein (PDB entry: 3tk7 (LIGHT *et al.*, 2014)). The reactive lysine (gray sticks) is placed relatively to the plane of the carbonyl group (cyan) in an obtuse N ϵ -C2-O2 angle (red dashes) that is convenient for the nucleophilic attack. **C:** A scheme of the perfect orientated nucleophile (Nu) relatively to the plane of the carbonyl group (blue) with a BÜRGI-DUNITZ Nu-C-O angle (red dashes) of $\sim 105 \pm 5^\circ$ (BÜRGI *et al.*, 1973, 1974).

2.2.2 Interactions of the Intermediate's C1OH-Group with the Active Site of TacTAL

The SCHIFF base formation is the central and most important event in the catalytic cycle of TacTAL. The reactive groups directly involved in the SCHIFF base formation are the ϵ -amino group of the enzyme's reactive lysine and the carbonyl group of the sugar substrate. The C1 hydroxy group is the direct neighbor of the carbonyl group in the F6P molecule (scheme 2.6). The interaction of the active site with this group is suggested to contribute to efficient catalysis of the transaldolase reaction. The coordination of the C1 hydroxy group assures the correct orientation of the substrate molecule (especially the orientation of the carbonyl group in a position favorable for the nucleophilic attack) or the orientation of the intermediates appearing along the catalytic cycle in the active site.



Scheme 2.6: Structural formula of A5P and F6P. A5P lacks the carbon atom and the hydroxy group at the first position compared to the F6P structure. In contrast to F6P (ketose sugar), A5P is an aldose sugar. The remaining atoms in both structures are stereochemically equivalent.

As previously described (section 2.2.1 and (LEHWESS-LITZMANN, 2011; LEHWESS-LITZMANN *et al.*, 2011b)), the C1OH-group of the F6P-SCHIFF base intermediate adopts two alternative conformations („up“ and „down“) in the active site of TacTAL. In its „up“ conformation the C1 hydroxy group interacts with the hydroxy group of the Thr¹¹⁰ residue. A replacement of this threonine by an isosteric valine residue results in a variant showing a greatly impaired transaldolase activity (LEHWESS-LITZMANN, 2011). This effect cannot be strictly assigned to the interruption of the hydrogen bond with the C1OH-group in its „up“ conformation alone. Besides the coordination of the C1OH-group in its „up“ conformation, the residue Thr¹¹⁰ coordinates the catalytic water molecule and is assumed to coordinate the C2 hydroxy group of the carbinolamine intermediate (SCHÖRKEN *et al.*, 2001).

The interaction partner of the „down“ conformation of the intermediate's C1OH-group in the active site of TacTAL is the residue Ser¹³⁰. In a previous work, this residue was replaced by an alanine residue giving a variant showing a moderate loss in activity of the donor half-reaction in

single-turnover experiments (SAUTNER, 2012). The C1OH-group of the intermediate in the active site of this variant is coordinated by the residue Asn¹⁰⁸ located closely to the mutated serine residue.

Complementary, the influence of the interaction of the C1OH-group with the active site can be analyzed using arabinose 5-phosphate (A5P) as a donor substrate. A5P is an aldose sugar showing the same stereochemistry as the natural ketose sugar substrate F6P. In contrast to the F6P molecule, A5P does not contain an equivalent for the C1OH-group in its structure (scheme 2.6).

A5P was described as competitive inhibitor of transaldolases from different organisms (CAILLAU AND PAUL QUICK, 2005; SPRENGER *et al.*, 1995; WILLIAMS *et al.*, 1978) and as a substrate for the structurally and mechanistically related enzyme fructose 6-phosphate aldolase (GARRABOU *et al.*, 2009; GUÉRARD-HÉLAINE *et al.*, 2015). Single-turnover analysis of the *TacTAL* reaction with A5P as donor substrate using a coupled spectrophotometric assay detecting the formation of glyceraldehyde 3-phosphate (GA3P) showed the formation of the product (SAUTNER, 2012). This finding implies the conversion of A5P as substrate at least in the donor half-reaction of the catalytic cycle of *TacTAL*.

In the present work, both possible interaction partners (Asn¹⁰⁸ and Ser¹³⁰) of the C1 hydroxy group's „down“ conformation were replaced by alanine giving the double-mutation variant *TacTAL*_{N108A/S130A}. The single-turnover reaction of the variant after rapid mixing with F6P as donor substrate was analyzed using stopped-flow spectroscopy. The crystal structures of the variant co-crystallized with F6P and the wild type enzyme co-crystallized with A5P were determined.

2.2.2.1 Perturbation of the Interaction between the Intermediate's C1OH-Group and the Active Site of *TacTAL* impairs the donor half-reaction

The importance of the interaction of the C1OH-group of the donor substrate with the active site residues of *TacTAL* was investigated analyzing the donor half-reaction of wild type enzyme and variants using the stopped-flow technique. The reaction was performed in single-turnover mode. To do so, the acceptor substrate is not present in the reaction mixture. Thus, each active site can interact with the substrate only once after rapid mixing of the enzyme with the donor substrate and can catalyze the cleavage of only one substrate molecule assuming the very slow aldolase side-reaction of transaldolase as negligible. The reactive lysine residue remains as carbanion/enamine-conjugate after the first product glyceraldehyde 3-phosphate (GA3P) is released. In this state, the lysine residue is not able to perform a nucleophilic attack on the next donor substrate molecule resulting

Table 2.2.1: Overview of microscopic kinetic constants for the donor half-reaction of *TacTAL_{wt}* and variants. $k_{\text{obs}}^{\text{max}}$ =first order rate constant at substrate saturation; $K_{\text{S}}^{\text{app}}$ =apparent equilibrium constant of the fast pre-equilibrium; K_{I} =apparent inhibition equilibrium constant of the putative substrate inhibition. ND=not determined. The margin of error is given as the standard deviation of the fitted data (sets of triplicates). *taken from SAUTNER (2012).

Constant	S130A*	N108A*	N108A/S130A	wt+A5P*	wt+F6P*
$k_{\text{obs}}^{\text{max}}$ (s^{-1})	18.11 \pm 1.22	1.63 \pm 0.10	0.37 \pm 0.07	0.34 \pm 0.01	60.31 \pm 4.12
$K_{\text{S}}^{\text{app}}$ (mM)	2.19 \pm 0.36	0.59 \pm 0.24	1.60 \pm 0.65	0.029 \pm 0.004	0.70 \pm 0.17
K_{I} (mM)	203.1 \pm 95.2	ND	13.28 \pm 5.53	–	40.42 \pm 10.27

ure 2.2.12), while the rate constants are getting lower at higher substrate concentrations. This observation correlates well with the situation in the case of the donor half-reaction of *TacTAL_{wt}* with F6P (LEHWESS-LITZMANN, 2011; SAUTNER, 2012; SAUTNER *et al.*, 2015). However, the data for the donor half-reaction of *TacTAL_{wt}* with A5P show a hyperbolic dependency on substrate concentration with a saturation at lower millimolar range.

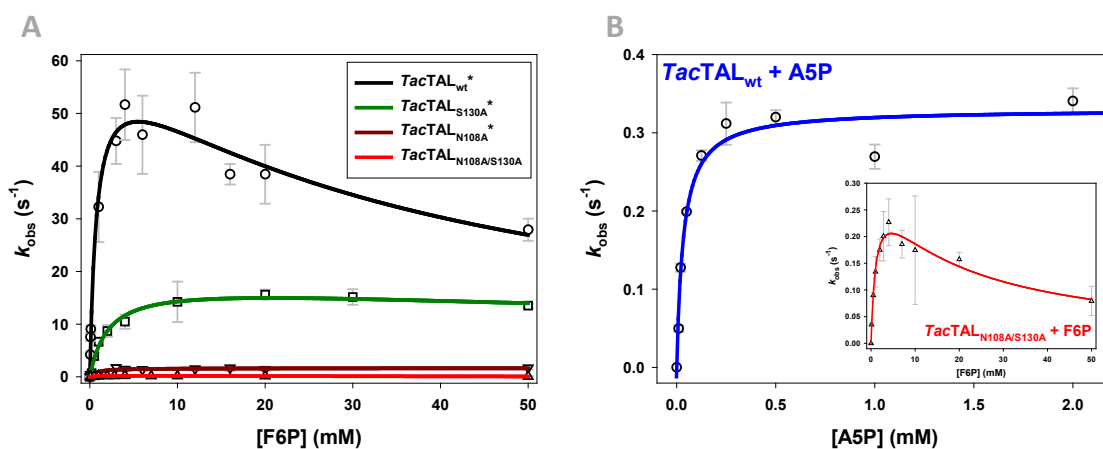


Figure 2.2.12: Pre-steady-state analysis of the donor half-reaction of *TacTAL_{wt}* and variants. The measurements were performed at 30 °C. The error bars represent the standard deviation of the mean value calculated from the measurement of triplicates. **A:** Dependency of the observed rate constant (k_{obs}) on F6P concentration (0.05 – 50 mM) for *TacTAL_{wt}* and variants. The data were fitted according to eq. 1.6.8 (solid line). *data from SAUTNER (2012) **B:** Dependency of k_{obs} on A5P concentration for *TacTAL_{wt}* (SAUTNER, 2012). The data were fitted according to eq. 1.6.9 (solid line). Inset: Dependency of k_{obs} on F6P concentration for *TacTAL_{N108A/S130A}*.

In summary, a mutation of Asn¹⁰⁸ and/or Ser¹³⁰ to alanine greatly impairs the donor half-reaction of *TacTAL*. The analysis of the single-turnover measurements of the donor half-reaction of the *TacTAL_{N108A/S130A}* variant with F6P in comparison to the single-mutation variants and the wild

type protein underlines that the deletion of both interaction partners of the substrate's C1OH-group results in the highest effect on the first order rate constant of the single-turnover reaction. The determined first order rate constant for the donor half-reaction of the *TacTAL*_{N108A/S130A} variant with F6P is comparable to that of wild type reaction with A5P. Note that in the latter case, the corresponding interaction is interrupted because of the absence of the C1OH-group in the A5P substrate.

2.2.2.2 An Additional Water Molecule is Present in the Active Sites of *TacTAL*_{wt} and *TacTAL*_{N108A/S130A} Co-Crystallized with A5P and F6P, Respectively

In order to obtain structural insights with regard to the interaction of substrate's C1OH-group with the active site, the *TacTAL*_{wt} protein and the *TacTAL*_{N108A/S130A} variant were co-crystallized with A5P and F6P, respectively.

In the refined structure of *TacTAL*_{wt} co-crystallized with A5P (1.82 Å resolution, $R_{\text{work}} = 15.65\%$ and $R_{\text{free}} = 18.16\%$, tables A.3 and A.5 in the appendix) an additional electron density was observed in all five active sites and interpreted as the A5P-SCHIFF base intermediate (figure C.9 in the appendix). The intermediate is coordinated by the active site residues in a similar way as the F6P-SCHIFF base except for the absent C1OH-group. The A5P-SCHIFF base intermediate is displaced towards the entrance of the active site by approximately 0.5 Å compared to the F6P-SCHIFF base intermediate in the active site of the *TacTAL*_{wt} protein (figure 2.2.14 A). This displacement causes the more relaxed all-*trans* conformation of the reactive lysine, which is nearly fully expanded in the A5P-SCHIFF base intermediate structure and „U-shaped“ in the F6P-SCHIFF base intermediate structure (figure C.11 in the appendix).

An additional water molecule was observed in the active site occupying the position of the C1 hydroxy group of the F6P-SCHIFF base intermediate in its „down“ conformation in the active site of *TacTAL*_{wt} (figure 2.2.13 A and B). This water molecule is displaced from the exact position of the C1 hydroxy group (~0.9 Å) and is coordinated by the residues Asn¹⁰⁸ and Ser¹³⁰ (figure 2.2.14 A).

The catalytic water molecule in the structure containing the A5P-SCHIFF base intermediate is displaced towards the intermediate by ~0.4 Å from its position in the structure with the F6P-SCHIFF base intermediate.

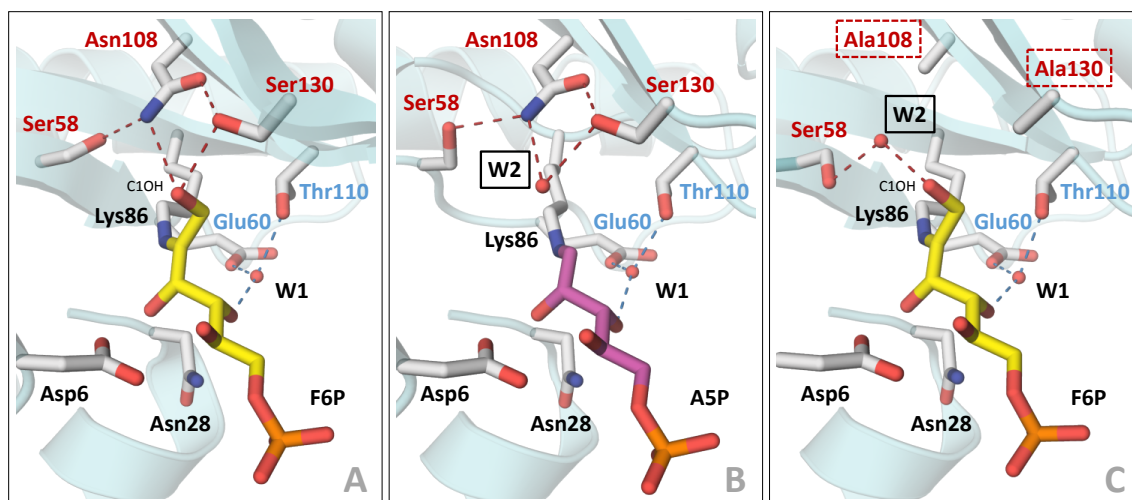


Figure 2.2.13: Active sites of *TacTAL*_{wt} and *TacTAL*_{N108A/S130A} co-crystallized with F6P and/or A5P. The C1OH-group of the F6P-SCHIFF base intermediate is shown in the „down“ conformation (the „up“ conformation is omitted). The active site residues partaking in the hydrogen bond network (dashed lines) of the „down“ or „up“ conformation are labeled in red or blue, respectively. The selected active site residues are represented as gray sticks. The polypeptide backbone is shown as secondary structure (cyan). **A:** *TacTAL*_{wt} co-crystallized with F6P. The F6P-SCHIFF base intermediate is represented as yellow sticks. **B:** *TacTAL*_{wt} co-crystallized with A5P. The A5P-SCHIFF base intermediate is represented as purple sticks. The space of the absent C1OH-group of the intermediate is occupied by an additional water molecule (framed). **C:** *TacTAL*_{N108A/S130A} co-crystallized with F6P. The F6P-SCHIFF base intermediate is represented as yellow sticks. The mutated residues Asn¹⁰⁸ → Ala and Ser¹³⁰ → Ala are framed (dashed). The space of the absent side chains is occupied by an additional water molecule (framed).

The structure of *TacTAL*_{N108A/S130A} co-crystallized with F6P was determined to 1.63 Å resolution (table A.3 in the appendix) and refined against the diffraction data with $R_{\text{work}} = 16.56\%$ and $R_{\text{free}} = 19.27\%$ (table A.6 in the appendix). An additional electron density was observed in all five active sites and interpreted as the F6P-SCHIFF base intermediate (figure C.10 in the appendix).

The relative orientation of the F6P-SCHIFF base intermediate in the active site of the variant is comparable to that of the intermediate in the active site of the wild type enzyme (figure 2.2.14 B). In contrast to the A5P-SCHIFF base intermediate in *TacTAL*_{wt}, the F6P-SCHIFF base intermediate is only slightly displaced (~ 0.2 Å) towards the reactive lysine in the active site of the variant compared to its position observed in the active site of the wild type protein.

In spite of the lacking interaction partners of the C1OH-group in its „down“ conformation in the variant, this group could be observed in both conformations („up“ and „down“) as in the case of *TacTAL*_{wt} co-crystallized with F6P. According to the occupancy refinement, the „down“ conformation of the hydroxy group is present in the active site of the variant to 44 – 55 % (depending

on the pentamer's subunit), while the corresponding occupancy values in the active site of the wild type protein were determined to 48 – 60 %.

As in the case of the *TacTAL_{wt}* structure co-crystallized with A5P, an additional water molecule is present in the active site of the variant occupying the area near the side chain of Asn¹⁰⁸ residue (Ala in the variant). This water molecule is coordinated by the residue Ser⁵⁸ and the intermediate's C1 hydroxy group („down“ conformation). Compared to the position of the additional water molecule observed in the active site of *TacTAL_{wt}* co-crystallized with A5P, the corresponding water molecule present in the active site of the variant is displaced by ~2.5 Å away from the intermediate (figure 2.2.14 C). The position of the catalytic water molecule in the active site of the variant is comparable to its position observed in the wild type enzyme.

In contrast to the structure of the A5P-SCHIFF base intermediate, the conformation of the SCHIFF base-forming lysine residue in the active site of the variant is similar to the corresponding conformation in the structure of wild type protein.

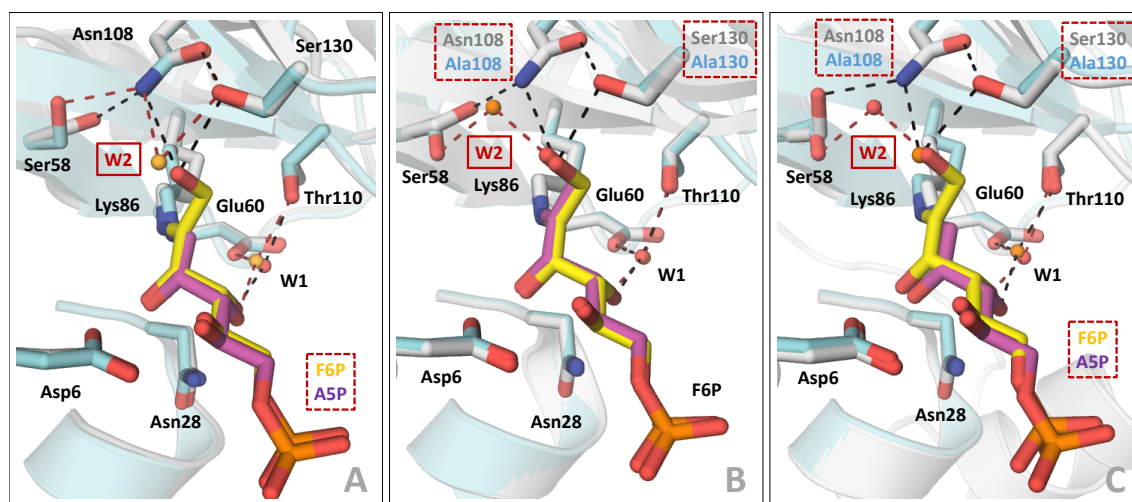
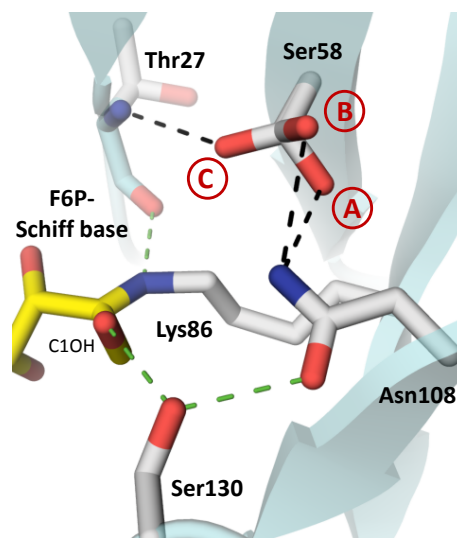


Figure 2.2.14: Superposition of active sites of *TacTAL_{wt}* and *TacTAL_{N108A/S130A}* co-crystallized with F6P and/or A5P. The C1OH-group of the F6P-SCHIFF base intermediate is shown in the „down“ conformation (the „up“ conformation is omitted). The selected active site residues are represented as sticks. The polypeptide backbone is shown as secondary structure. **A:** *TacTAL_{wt}* (gray) co-crystallized with F6P (yellow sticks) superposed with *TacTAL_{wt}* (cyan) co-crystallized with A5P (purple sticks). The water molecules are represented as red or orange spheres, respectively. **B:** *TacTAL_{wt}* (gray) co-crystallized with F6P (yellow sticks) superposed with *TacTAL_{N108A/S130A}* (cyan) co-crystallized with F6P (purple sticks). The water molecules are represented as red or orange spheres, respectively. **C:** *TacTAL_{wt}* (gray) co-crystallized with A5P (purple sticks) superposed with *TacTAL_{N108A/S130A}* (cyan) co-crystallized with F6P (yellow sticks). The water molecules are represented as orange or red spheres, respectively.

The residue Ser⁵⁸ participates in the hydrogen bond network relating to the „down“ conformation of the intermediate’s C1OH-group. This residue is conserved in a number of transaldolases from different origins (plants, mammals, insects, fungi, bacteria and archaea; [figure C.17] in the appendix). Ser⁵⁸ can adopt three different conformations (A, B and C) as it could be shown in one of the five subunits of *TacTAL*_{wt} structure co-crystallized with F6P (figure 2.2.15). In the remaining four subunits this residue exhibits only two alternative conformations (A and B), while the C-conformation is not present. In the structures of the *TacTAL*_{wt} co-crystallized with A5P and *TacTAL*_{N108A/S130A} co-crystallized with F6P, this residue is present in all five subunits mainly in its B- or C-conformation, respectively. While the Ser⁵⁸ residue does not interact with the SCHIFF base intermediate directly, it is located in hydrogen bond distance either to the side chain of the Asn¹⁰⁸ residue (conformations A and B) or to the backbone nitrogen of the Thr²⁷ residue (conformation C). In this context, the A- and B-conformations of the serine residue contribute to the hydrogen bond network corresponding to the „down“ conformation of the SCHIFF base intermediate’s C1OH-group. On the other hand, the C-conformation of the residue could indirectly communicate with the Nε-atom of the SCHIFF base-forming lysine via the interaction with the backbone of the Thr²⁷ residue (figure C.5 in the appendix).

Figure 2.2.15: Different conformations of Ser⁵⁸ in the structure of *TacTAL*_{wt} co-crystallized with F6P. The conformations A and B are in hydrogen bond distance to the side chain of Asn¹⁰⁸ (black dashes), which contributes to the hydrogen bond network relating to the „down“ conformation of the intermediate’s C1OH-group (green dashes). The conformation C interacts with the backbone nitrogen of the Thr²⁷ residue (black dashes), whose backbone carbonyl oxygen is in hydrogen bond distance to the Nε-atom of the SCHIFF base-forming lysine (green dashes). The selected active site residues (gray) and the F6P-SCHIFF base intermediate (yellow) are represented as sticks. The polypeptide backbone is colored in cyan.



Interestingly, a serine residue at the corresponding position is not present in the related enzyme fructose 6-phosphate aldolase (FSA). The sequence and structure of FSA are highly similar to those of *TacTAL*. This enzyme catalyzes the reversible aldolytic cleavage of F6P via SCHIFF base chemistry and is mechanistically related to *TacTAL* (scheme 2.3). According to the multiple sequence alignment of known FSA proteins the position of the Ser⁵⁸ in the sequence of *TacTAL* is

occupied by either phenylalanine or histidine in the analyzed FSA sequences (figure C.18 in the appendix).

2.2.3 Analysis of *Tac*TAL Variants with Enhanced Aldolase Activity

Although FSA is mechanistically related to *Tac*TAL, the direct environments of the reactive lysines in both enzymes are not comparable. On one hand, the hydrogen bond network corresponding to the „up“ conformation of the intermediate in the active site of *Tac*TAL is different in FSA from *Escherichia coli* (*Ec*FSA). The catalytic water molecule participating in this hydrogen bond network is additionally coordinated by a tyrosine residue, which is not present in the active site of *Tac*TAL (phenylalanine in TAL). Furthermore, the general acid-base catalyst in *Tac*TAL (Glu⁶⁰) is replaced in the active site of *Ec*FSA by an acid-base neutral glutamine residue (figure 2.2.16). The absence of a residue corresponding to the transaldolase's general acid-base catalyst in the active site of *Ec*FSA is surprising, since FSA is assumed to catalyze its reaction via acid-base catalysis as in the case of TAL. As previously published by SCHNEIDER *et al.* (2008) a single-mutation of a phenylalanine residue (tyrosine in FSA, *vide supra*) by a tyrosine in the active site of transaldolase from *Escherichia coli* or human, provides an enhanced aldolase activity compared to the wild type proteins. A similar observation was described by LEHWESS-LITZMANN (2011) for *Tac*TAL. A replacement of Phe¹³² residue in the active site of *Tac*TAL by a tyrosine results in a highly stimulated aldolase activity of the variant.

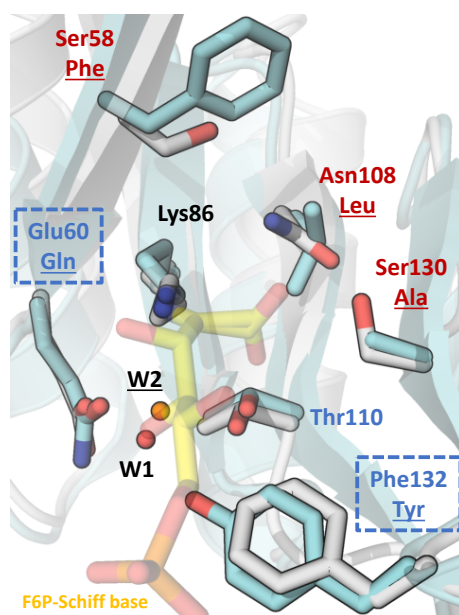


Figure 2.2.16: Superposition of the active sites of *Tac*TAL_{wt} and *Ec*FSA. The residues present in the *Ec*FSA are underlined. Residues are numbered according to their position in *Tac*TAL. The selected active site residues and the F6P-SCHIFF base intermediate in *Tac*TAL (transparent yellow) are represented as sticks. The polypeptide backbone is shown as secondary structure (gray: *Tac*TAL, cyan: *Ec*FSA). Residues corresponding to the „down“ or „up“ conformation (hydrogen bond network) are labeled in red or blue, respectively. Residues relevant for the acid-base catalysis are framed. The catalytic (W1) or resting state (W2) water molecules in the active sites of *Tac*TAL or *Ec*FSA are shown as red or orange spheres, respectively. PDB entry for *Ec*FSA: 1L6W, (THORELL *et al.*, 2002).

Taking into account the absence of an acid-base catalyst, equivalent to the *TacTAL*'s Glu⁶⁰ residue and the presence of the aforementioned tyrosine in the active site of *EcFSA*, one can assume that the tyrosine residue takes over the role of the general acid-base catalyst in *EcFSA*. In the present work, a variant of *TacTAL* was generated and analyzed, in which the residues Glu⁶⁰ and Phe¹³² were replaced by glutamine and tyrosine residues, respectively. The resulting *TacTAL*_{E60Q/F132Y} variant shows the identical acid-base constellation as in the active site of *EcFSA*.

On the other hand, the residues involved in the hydrogen bond network of the „down“ conformation in the active site of *TacTAL* are hydrophobic residues in the active site of *EcFSA* (Ser⁵⁸ → Phe, Asn¹⁰⁸ → Leu and Ser¹³⁰ → Ala). In order to mimic the direct environment of the reactive lysine of *EcFSA* in the active site of *TacTAL*, a fivefold variant was generated (*TacTAL*_{FSA-mimic}). The active site of the variant contains the previously introduced mutations Glu⁶⁰ → Gln and Phe¹³² → Tyr as well as the hydrophobic residues as described before (Ser⁵⁸ → Phe, Asn¹⁰⁸ → Leu and Ser¹³⁰ → Ala).

2.2.3.1 Introduction of a Phe/Tyr-Mutation and Simultaneous Removal of the General Acid-Base Catalyst Glu⁶⁰ in *TacTAL*'s Active Site Results in a Highly Efficient Aldolase

The steady-state kinetic measurements for the *TacTAL* variants with enhanced aldolase activity were performed as described in section 1.6.4.2. The used coupled spectrophotometric assay detects the formation of the first product glyceraldehyde 3-phosphate (GA3P). The both activities (transaldolase and aldolase) result in the formation of this product. Therefore, in presence of acceptor substrate E4P it cannot be discriminated between transaldolase and aldolase reaction. However, in absence of acceptor substrate only the aldolase activity can occur. The measured activity was plotted against the substrate concentration (figure 2.2.17) and fitted according to the MICHAELIS-MENTEN-equation (eq. 1.6.2).

*TacTAL*_{wt} catalyzes the aldolytic cleavage of the donor substrate F6P as a very slow side reaction. The turnover number for this reaction was determined to $k_{\text{cat}} = \sim(2.25 \pm 0.01) \cdot 10^{-3} \text{ s}^{-1}$ (data not shown). The introduction of a tyrosine residue in the active site of *TacTAL* giving the *TacTAL*_{F132Y} variant results in an increase of the aldolase activity in terms of k_{cat} by two orders of magnitude compared to wild type (table 2.2.2). The second mutation of Glu⁶⁰ to glutamine enhanced this activity by an additional factor of three. Further introduction of bulky hydrophobic residues in

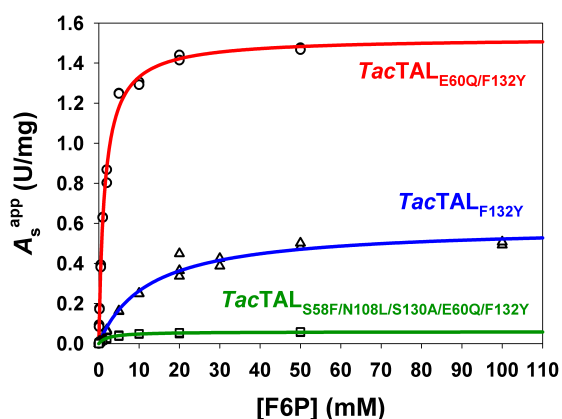


Figure 2.2.17: Dependency of the aldolase activity (cleavage of F6P into GA3P and DHA) of *TacTAL* variants on F6P concentration.

The steady-state measurements were performed at 30 °C. The substrate concentration was varied (0.1 – 100 mM). The rectangles, triangles and circles indicate the measured aldolase activity of *TacTAL*_{FSA-mimic} (125 µg/mL), *TacTAL*_{F132Y} (120 µg/mL) and *TacTAL*_{E60Q/F132Y} (35 µg/mL), respectively. The MICHAELIS-MENTEN fits (eq. 1.6.2, solid line) are depicted by green, blue and red lines, respectively.

Table 2.2.2: Overview of macroscopic kinetic constants for aldolase activity (cleavage of F6P into GA3P and DHA) of *EcFSA*_{wt}, *TacTAL*_{wt} and *TacTAL* variants. The margin of error is given as the standard deviation of the fitted data (sets of triplicates). nd = not detectable. *taken from SCHNEIDER *et al.* (2008), **published in SAUTNER *et al.* (2015), ***data provided by LIETZOW (2015).

Protein	k_{cat} (s ⁻¹)	K_M^{app} (mM)	k_{cat}/K_M^{app} (s ⁻¹ M ⁻¹)
<i>TacTAL</i> _{wt}	(2.25 ± 0.01)·10 ⁻³	nd	nd
<i>TacTAL</i> _{FSA-mimic} ***	(2.41 ± 0.02)·10 ⁻²	2.41 ± 0.09	10.00
<i>TacTAL</i> _{F132Y} **	0.24 ± 0.01	12.30 ± 1.50	19.51
<i>TacTAL</i> _{E60Q/F132Y} **	0.62 ± 0.01	1.50 ± 0.10	413.33
<i>EcFSA</i> _{wt} *	1.30 ± 0.30	12.00 ± 3.00	108.33

the „down“ site of the active site (Ser⁵⁸ → Phe, Asn¹⁰⁸ → Leu and Ser¹³⁰ → Ala) results in a 5x-variant (*TacTAL*_{FSA-mimic}) with a greatly impaired aldolase activity compared to the double variant (*TacTAL*_{E60Q/F132Y}). The aldolase activity of the *TacTAL*_{FSA-mimic} variant is one order of magnitude lower than that of the *TacTAL*_{F132Y} variant. This result is surprising since the *TacTAL*_{FSA-mimic} variant reflects the situation in the active site of *EcFSA* better than the double variant regarding the relative positions of particular amino acid residues in the active site. However, the *TacTAL*_{FSA-mimic} variant still shows one order of magnitude higher aldolase activity compared to *TacTAL*_{wt}.

In order to estimate the transaldolase activity (reversible transfer of a DHA-unit from the donor F6P to the acceptor E4P) of the variants, the steady-state measurements were performed in presence of 2 mM E4P. The presence of the acceptor substrate (E4P) does not influence the activity of the *TacTAL*_{F132Y} variant and inhibits only slightly the activity of the *TacTAL*_{E60Q/F132Y} variant (decrease in activity by ~10 %). In other words, the transaldolase activity of the variants is either lower than the respective aldolase activity or equal to that. Thus, the transaldolase activity of the

Table 2.2.3: Overview of macroscopic kinetic constants for transaldolase activity (reversible transfer of a DHA-unit from F6P to E4P) of *TacTAL*_{wt} and variants. The margin of error is given as the standard deviation of the fitted data (sets of triplicates). ND = not determined. *taken from LEHWESS-LITZMANN (2011), **published in SAUTNER *et al.* (2015), ***data provided by LIETZOW (2015).

Protein	k_{cat} (s ⁻¹)	$K_{\text{M}}^{\text{app}}$ (mM)	$k_{\text{cat}}/K_{\text{M}}^{\text{app}}$ (s ⁻¹ M ⁻¹)
<i>TacTAL</i> _{wt} *	13.86 ± 0.65	2.30 ± 0.36	6026.1
<i>TacTAL</i> _{FSA-mimic} ***	≤ 2.82 · 10 ⁻²	ND	ND
<i>TacTAL</i> _{F132Y} **	≤ 0.24	ND	ND
<i>TacTAL</i> _{E60Q/F132Y} **	< 0.62	ND	ND
<i>TacTAL</i> _{E60Q} *	0.12 ± 0.01	0.49 ± 0.13	244.90

variants is much lower than the corresponding activity of the wild type protein (table 2.2.3). The addition of E4P slightly stimulates the activity of the *TacTAL*_{FSA-mimic} variant (increase in activity by ~10 %). This activation effect in presence of E4P could mean that the *TacTAL*_{FSA-mimic} variant catalyzes the transaldolase reaction slightly better than the aldolase reaction and could be a hint for the impaired protonation of the carbanion/enamine intermediate in this variant compared to the *TacTAL*_{E60Q/F132Y} variant, which is essential for the aldolase reaction.

The apparent MICHAELIS constant ($K_{\text{M}}^{\text{app}}$) for the aldolase reaction of *TacTAL*_{F132Y} is approximately equal to that of *EcFSA*_{wt} (table 2.2.2). This value is fivefold higher than the corresponding constant for the transaldolase reaction of *TacTAL*_{wt}. The introduction of the second mutation (Glu⁶⁰ → Gln) leads to lower $K_{\text{M}}^{\text{app}}$ (~8x lower compared to the single-mutation variant) as well as to a higher turnover number. Both effects give a *TacTAL* variant with a higher catalytic efficiency ($k_{\text{cat}}/K_{\text{M}}^{\text{app}} = 413.33 \text{ s}^{-1}\text{M}^{-1}$) than in case of the native fructose 6-phosphate aldolase from *E. coli* ($k_{\text{cat}}/K_{\text{M}}^{\text{app}} = 108.33 \text{ s}^{-1}\text{M}^{-1}$, (SCHNEIDER *et al.*, 2008)). The $K_{\text{M}}^{\text{app}}$ value for F6P conversion catalyzed by the *TacTAL*_{FSA-mimic} variant is similar to that of *TacTAL*_{wt} but because of the low turnover number the catalytic efficiency of this variant is one order of magnitude lower compared to *EcFSA*_{wt}.

In other words, the introduction of a single Phe → Tyr mutation in the active site of transaldolase (*E. coli*: Phe¹⁷⁸, human: Phe¹⁸⁹, *Thermoplasma acidophilum*: Phe¹³²) is the minimum requirement to induce the aldolase activity (LEHWESS-LITZMANN, 2011; SAUTNER *et al.*, 2015; SCHNEIDER *et al.*, 2008). The additional mutation of the original general acid-base catalyst of *TacTAL* (Glu⁶⁰) to glutamine results in a variant with a greatly improved catalytic efficiency towards the aldolase reaction. This double-variant (*TacTAL*_{E60Q/F132Y}) shows the best results in terms of k_{cat} , $K_{\text{M}}^{\text{app}}$ and

$k_{\text{cat}}/K_{\text{M}}^{\text{app}}$ for the aldolase activity compared to other variants introduced in this section. Further introduction of a hydrophobic surface in the „down“ site of the *TacTAL*'s active site (mutations: Ser⁵⁸ → Phe, Asn¹⁰⁸ → Leu and Ser¹³⁰ → Ala) to mimic the situation in the active site of *EcFSA_{wt}* results in the worst „aldolase“ analyzed in this work.

2.2.3.2 The Active Site of *TacTAL_{FSA-mimic}* Variant Shows a Different $\text{p}K_{\text{a}}$ Behavior Compared to Other Variants with Enhanced Aldolase Activity

Glu⁶⁰ is the general acid base catalyst in the active site of *TacTAL* (LEHWESS-LITZMANN *et al.*, 2011b). Replacement of this residue by glutamine and subsequent introduction of the Phe¹³² → Tyr mutation results in a *TacTAL* variant showing high aldolase efficiency. Since the original general acid-base catalyst is not present in the active site of the variant, the newly introduced tyrosine residue is assumed to take over the role of Glu⁶⁰ in acid-base catalysis. In order to analyze the $\text{p}K_{\text{a}}$ behavior in the active site of the variants with enhanced aldolase activity, the dependency of the turnover number on the pH was measured under the steady-state conditions.

The observed aldolase activity plotted versus pH shows bell-shaped curves in the case of the *TacTAL_{F132Y}* and *TacTAL_{E60Q/F132Y}* variants (figure: 2.2.18A) and sigmoidal curve in the case of the *TacTAL_{FSA-mimic}* variant (figure: 2.2.18 B).

The estimated $\text{p}K_{\text{ES}}$ values for the *TacTAL_{F132Y}* and *TacTAL_{E60Q/F132Y}* variants are similar to the constants estimated for the transaldolase reaction of *TacTAL_{wt}* (LEHWESS-LITZMANN, 2011) and show the highest aldolase activity at pH around 7.9 (table: 2.2.4).

The $\text{p}K_{\text{a}}$ behavior in the active site of the *TacTAL_{FSA-mimic}* variant is different compared to the variants discussed above. The pH-dependency plot of this variant shows a sigmoidal progression. The highest aldolase activity of this variant was measured at $\text{pH} \geq 8.5$. The activity optimum of this variant at alkaline pH corresponds well to the published activity optimum of *EcFSA_{wt}* (optimal activity at pH around 8.5, SCHÜRMAN AND SPRENGER (2001)).

SCHÜRMAN AND SPRENGER (2001) described a significant inactivation effect of *EcFSA_{wt}* by Tris in concentrations >10 mM. Tris is one component of the three-component buffer system, which was used for the pH-dependency measurements in order to keep the ionic strength constant at different pH. In the case of *TacTAL_{E60Q/F132Y}* as representative variant with enhanced aldolase activity, Tris was assumed as non-inhibiting substance, since a replacement of GlyGly as the standard buffer

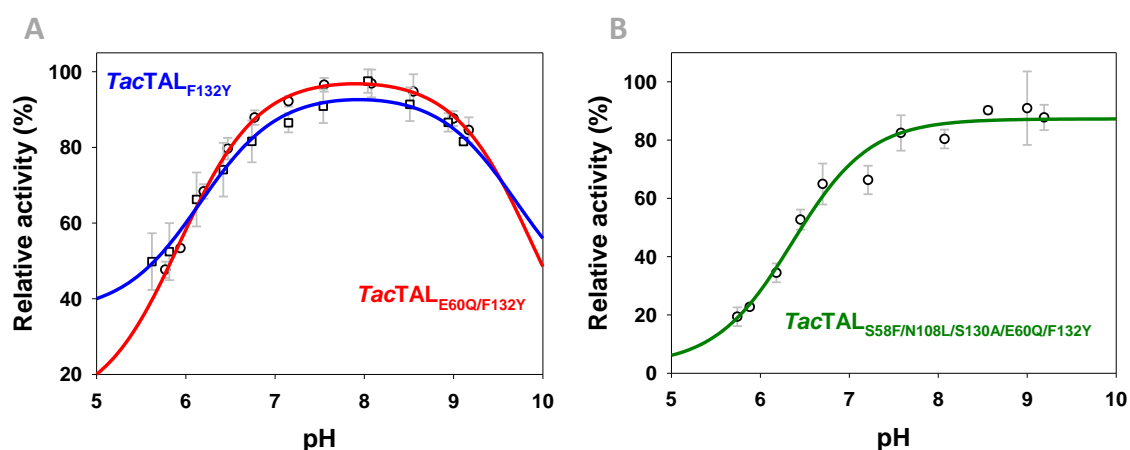


Figure 2.2.18: pH-dependency of aldolase activity (cleavage of F6P into GA3P and DHA) of *TacTAL* variants. The measurements were performed at 30 °C. The F6P concentration was 50 mM. The error bars represent the standard deviation of the mean value calculated from the measurement of triplicates. **A:** *TacTAL*_{F132Y} and *TacTAL*_{E60Q/F132Y} (final concentrations 0.1 mg/mL and 0.025 mg/mL, respectively). Bell-shaped curves showing an optimum at pH around 7.9 **B:** *TacTAL*_{FSA-mimic} (final concentration 0.125 mg/mL), data provided by LIETZOW (2015). Sigmoidal curve showing the highest aldolase activity at pH \geq 8.5.

compound in the activity assay (see previous section) by 20 mM Tris does not show any effect on the activity.

To rule out denaturation effects, stability of the protein at different pH was tested by recording far-UV-CD-spectra at respective pH. The variants were assumed as stable in the used pH range, since only minor changes in secondary structure occur, first at a pH below 5.9 (figure: C.1 in the appendix).

Table 2.2.4: Overview of the estimated pK_a values for the enzyme-substrate complex of *TacTAL*_{wt} and variants. The aldolase reaction (cleavage of F6P into GA3P and DHA) was measured. The margin of error is given as the standard deviation of the fitted data (sets of triplicates). nd = Not detected. *LEHWESS-LITZMANN (2011), values for transaldolase reaction (reversible transfer of a DHA-unit from F6P to E4P), **data provided by LIETZOW (2015).

Protein	pK_{ES1}	pK_{ES2}
<i>TacTAL</i> _{wt} *	6.4	9.5
<i>TacTAL</i> _{FSA-mimic} **	6.4 \pm 0.1	nd
<i>TacTAL</i> _{F132Y}	6.2 \pm 0.1	9.7 \pm 0.2
<i>TacTAL</i> _{E60Q/F132Y}	5.9 \pm 0.1	9.9 \pm 0.1

2.2.3.3 Co-Existence of Two Potential Acid-Base Catalysts (Glu⁶⁰ and Tyr¹³²) in the Active Site Perturbs the Donor Half-Reaction of *Tac*TAL

In addition to the steady-state analysis of *Tac*TAL variants with enhanced aldolase activity, the donor half-reaction was analyzed, using the stopped-flow technique. In contrast to the steady-state measurements, giving information about macroscopic kinetic constants, this rapid mixing absorbance spectroscopy method allows to resolve the pre-steady-state region of the reaction and to obtain information about the microscopic kinetic constants for transient kinetic processes.

Measurement of the NADH oxidation coupled to the transaldolase/aldolase reaction after rapid mixing of *Tac*TAL_{wt} with F6P results in a progress curve consisting of an exponential burst phase followed by a linear phase (figure 2.2.19 A). The linear phase corresponds to the steady state of the aldolase side-reaction and the exponential burst phase corresponds to the initial transient carbanion/enamine intermediate formation. Fitting of the progress curve according to equations 1.6.6 and 1.6.7 gives an observed first order rate constant (k_{obs}) for the exponential burst phase and the slope of the linear phase. The apparent turnover number per active site for the aldolase reaction ($k_{\text{cat}}^{\text{app}}$) can be calculated from the linear slope, considering the enzyme concentration. The exponential burst phase represents the carbanion/enamine intermediate accumulation ($k_{\text{obs}} > k_{\text{cat}}^{\text{app}}$) and describes all processes until the GA3P release (binding of F6P, F6P-carbinolamine intermediate formation, F6P-SCHIFF base intermediate formation, F6P-SCHIFF base intermediate cleavage and GA3P-release; see scheme 2.7).

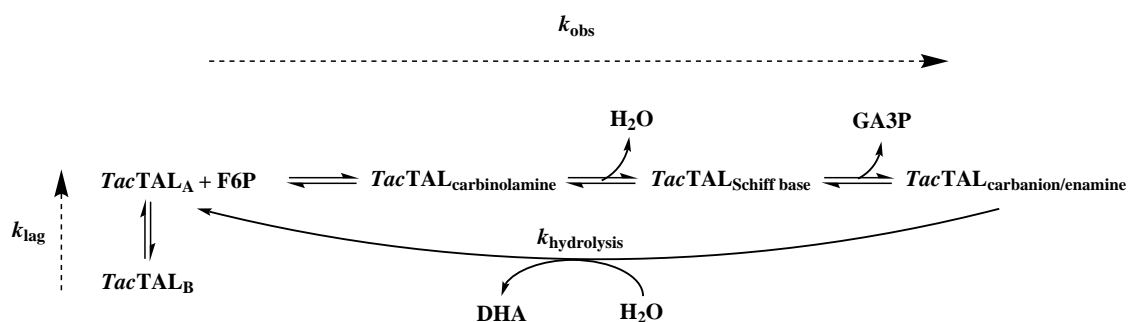
The progress curve for the reaction of the *Tac*TAL_{F132Y} variant after rapid mixing with the substrate does not show an exponential burst phase and describes only the linear steady-state of the aldolase reaction (figure 2.2.19 B). The absence of a burst phase suggests that the rate limiting step is situated before GA3P is released ($k_{\text{obs}} < k_{\text{hydrolysis}}$). Since the observed first order rate constant for the donor half-reaction of *Tac*TAL_{wt} with F6P was determined to $k_{\text{obs}}^{\text{max}} = 60.31 \pm 4.12 \text{ s}^{-1}$ (SAUTNER, 2012) and k_{cat} for the *Tac*TAL_{F132Y} variant to $0.24 \pm 0.01 \text{ s}^{-1}$ (section 2.2.3.1), the introduction of a Phe¹³² → Tyr mutation in the active site of *Tac*TAL impairs the donor half-reaction by a factor of at least 250.

An additional mutation (Glu⁶⁰ → Gln) resulting in the *Tac*TAL_{E60Q/F132Y} variant restores the activity of the donor half-reaction. The progress curves of this variant consist of an exponential phase prior to a linear aldolase steady-state phase (figure 2.2.19 C). The corresponding k_{obs} of the burst phase for this variant after mixing with 10 mM F6P (final concentration) is comparable to the k_{obs}

determined for the wild type protein under the same conditions ($46.9 \pm 1.4 \text{ s}^{-1}$ and $55.9 \pm 0.5 \text{ s}^{-1}$, respectively). Furthermore, the progress curve of the variant shows an additional lag phase during the first 40 – 50 ms of the reaction, which could not be detected for the wild type in a similar experiment. The duration of this lag phase is independent from the substrate concentration (figure 2.2.19 D).

The previous crystallographic structural studies showed that *TacTAL* can exist in two conformational states („open“ and „closed“; LEHWESS-LITZMANN *et al.* (2011b)). Furthermore, a conformational selection mechanism was suggested for substrate binding assuming the existence of the conformational states in solution (LEHWESS-LITZMANN *et al.*, 2011b). In contrast to the induced fit mechanism, in which the substrate binding event induces the conformational adaptation of the active site (as suggested for a broad range of different enzymes (FAN *et al.*, 2014; GONÇALVES *et al.*, 2012; MOSCATO *et al.*, 2016; ST-JEAN *et al.*, 2005)), the conformational selection mechanism postulates an equilibrium between different conformational states of the protein with different affinities for the substrate (BOEHR *et al.*, 2009; HAMMES *et al.*, 2009).

Assuming the conformational selection mechanism for the substrate binding (the substrate binds preferentially to either „open“ or „closed“ state giving a productive enzyme-substrate complex), the substrate binding event, followed by the reaction, would result in an „open“/„closed“ equilibrium shift under single-turnover conditions. In this case, the lag phase would describe the „open“/„closed“ conformational change of the protein before substrate binding (scheme 2.8). A similar situation was described for the *Bacillus* 1,3-1,4- β -glucanase (ABEL *et al.*, 2001).



Scheme 2.8: Minimal reaction sequence of aldolase reaction catalyzed by transaldolase. F6P binds preferentially to a distinct *TacTAL* conformation („open“ or „closed“). The cleavage of F6P by *TacTAL* results in the formation of GA3P. The auxiliary enzyme TIM converts GA3P to DHAP. Subsequently, GDH reduces DHAP to G3P. The simultaneous oxidation of NADH monitors the accumulation of the carbanion/enamine intermediate (decrease in absorbance at 340 nm). After the protonation of carbanion/enamine intermediate, a hydrolysis reaction can occur (steady state of aldolase reaction).

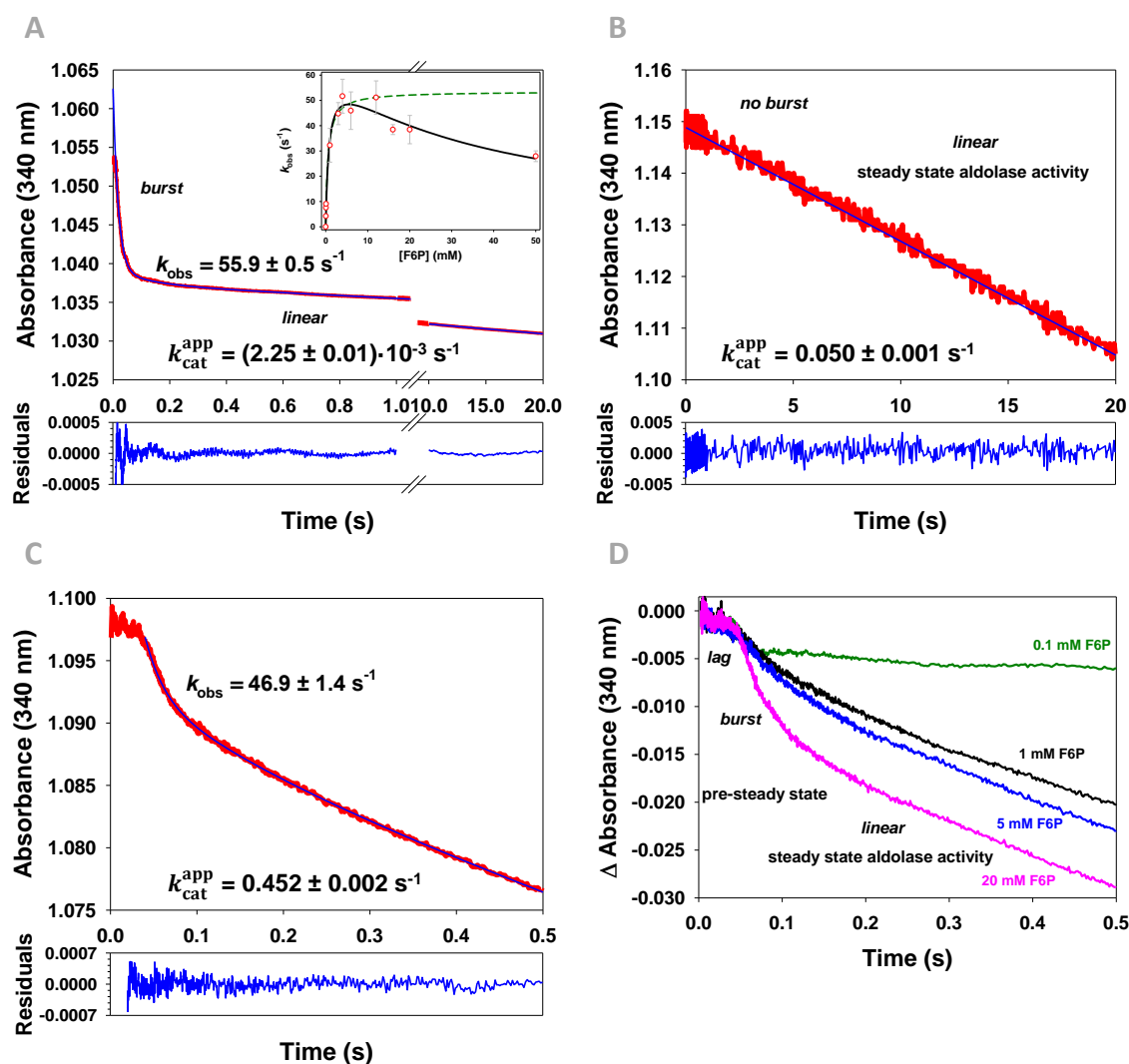


Figure 2.2.19: Representative stopped-flow progress curves (cleavage of F6P into GA3P and DHA) of $TacTAL_{wt}$ and variants recorded at 340 nm. The measurements were performed at 30 °C. The F6P concentration was 10 mM after mixing with the enzyme. The deviation of the applied fit (for details, see Materials and Methods) from the data is shown as residuals-plot. k_{obs} = observed rate constant of the burst phase. k_{cat}^{app} = apparent rate constant in steady state. **A:** $TacTAL_{wt}$ (final concentration 0.22 mg/mL). The progress curve shows a burst phase (first order reaction) and a linear phase (steady-state depletion of substrate). The observed rate constant of the burst phase (k_{obs}) plotted against the applied F6P concentration shows an optimum curve progression (inset, eq. 1.6.8, section: 1.6.4.4, data from SAUTNER (2012)). The green dashed line corresponds to the hyperbolic fit for $F6P \leq 12$ mM. **B:** $TacTAL_{F132Y}$ (final concentration 0.17 mg/mL). The progress curve shows only the linear phase (steady-state depletion of substrate) and no burst phase (rate limiting step before hydrolysis). The data was taken from LEHWESS-LITZMANN (2011). **C and D:** $TacTAL_{E60Q/F132Y}$ (final concentration 0.22 mg/mL). The progress curves (final concentrations of F6P: 0.1 mM, 1 mM, 5 mM and 20 mM) show a lag phase independent from the substrate concentration prior to a burst phase and a subsequent linear phase (for explanation, see text). Published in SAUTNER *et al.* (2015).

The same situation was observed for the reaction of the *TacTAL*_{FSA-mimic} variant with F6P. The respective progress curves comprise a lag-phase (first 40 – 50 ms) prior to an exponential burst phase ($k_{\text{obs}} = 57.9 \pm 1.65 \text{ s}^{-1}$) followed by the linear aldolase steady-state phase (see figure C.3 in the appendix for a representative progress curve). The *TacTAL*_{FSA-mimic} is the variant showing the lowest steady-state aldolase activity compared to related variants (*TacTAL*_{F132Y} and *TacTAL*_{E60Q/F132Y}), but the donor half-reaction of the variant is not impaired compared to the wild type enzyme and the *TacTAL*_{E60Q/F132Y} variant. Therefore, the introduction of a hydrophobic surface in the „down“ site of the active site of the *TacTAL*_{E60Q/F132Y} giving the *TacTAL*_{FSA-mimic} variant impairs at least one of the reaction steps after GA3P-release (protonation of the carbanion/enamine intermediate, hydrolysis of the DHA-SCHIFF base intermediate or the release of DHA).

Assuming the „open“/„closed“ equilibrium is present in the case of *TacTAL*_{wt} as well, the absence of the lag phase in the respective stopped-flow progress curves can be explained by suggesting a very fast conformational change process, making the duration of the lag phase shorter than the dead time of the experiment (~1.5 ms). In this context, the process of conformational changes is presumably impaired in the *TacTAL*_{E60Q/F132Y} and *TacTAL*_{FSA-mimic} variants compared to the wild type enzyme.

2.2.3.4 Relative Orientation of the Catalytic Tyrosine is Geometrically Favorable for a Direct Protonation of the Central Intermediate

The structure of the *TacTAL*_{E60Q/F132Y} variant co-crystallized with F6P was determined to 1.80 Å resolution (table A.3 in the appendix) and refined against the diffraction data with $R_{\text{work}} = 16.22 \%$ and $R_{\text{free}} = 19.38 \%$ (table A.6 in the appendix). In this structure, two of the five subunits (B and C) of the pentamer in the asymmetric unit exhibit the „closed“ conformation. One subunit (E) is present mainly in the „open“ conformation. The remaining two subunits (A and D) exhibit mixed conformational states. In the active sites of subunits with the „closed“ conformation an additional discontinuous electron difference density was observed (figure 2.2.20 A). The part of the electron density, which is fused with the density of the reactive lysine was interpreted as the covalently linked dihydroxyacetone unit (DHA-SCHIFF base intermediate). The remaining electron density was interpreted as the enzyme bound product glyceraldehyde 3-phosphate (GA3P) formed upon the F6P cleavage. The carbonyl moiety of GA3P was not modeled because of the absence of the corresponding electron density. The phosphate moiety of GA3P is displaced towards the active site

entrance by ~ 0.75 Å (~ 0.90 Å in subunit C) compared to the F6P-SCHIFF base intermediate observed in the wild type protein (figure 2.2.20 B). For this reason, an attempt to model the F6P-SCHIFF base intermediate into the electron density observed in the active site of the variant was not successful.

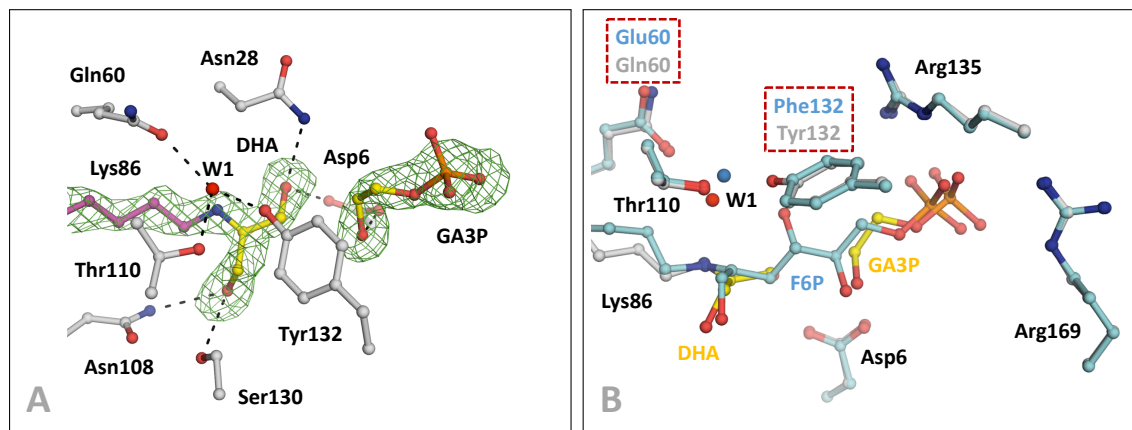


Figure 2.2.20: Active site of *TacTAL*_{E60Q/F132Y} co-crystallized with F6P. **A:** *mF*₀-*DF*_C simulated annealing omit map (green mesh, contour level 2.5σ). The selected active site residues (gray) and the DHA-SCHIFF base intermediate (yellow) are shown in ball-and-stick representation. The SCHIFF base-forming lysine residue is colored in purple. The catalytic water molecule (W1) is shown as red sphere. **B:** Superposition of the active sites of *TacTAL*_{E60Q/F132Y} (gray; ligands: yellow) and *TacTAL*_{wt} (cyan). The mutated residues (Glu⁶⁰ → Gln and Phe¹³² → Tyr) are framed (dashed). The catalytic water molecule (W1) is shown as red or blue sphere in *TacTAL*_{E60Q/F132Y} and *TacTAL*_{wt}, respectively. Published in SAUTNER *et al.* (2015).

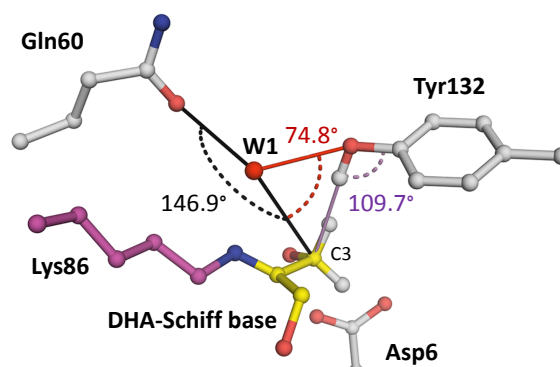
According to the proposed catalytic mechanism for the transaldolase/aldolase reaction (scheme 2.3), the protonation state of the DHA-SCHIFF base intermediate discriminates between the two activities (transaldolase vs. aldolase). If the intermediate is present in its carbanion/enamine form, the transaldolase reaction will take place (reversible transfer of a DHA-unit to the carbonyl carbon of the acceptor aldose phosphate). In the case of the protonated DHA-SCHIFF base intermediate, aldolase reaction will occur (reversible cleavage).

A further analysis of the relative orientation of the DHA-SCHIFF base intermediate in the active site of the variant underlines the role of the introduced Tyr¹³² residue as the general acid-base catalyst in the variant. The tyrosine's hydroxy group is perfectly oriented for a direct proton transfer onto the intermediate's C3-atom, whereas the position of the introduced Gln⁶⁰ residue in place of the transaldolase specific general acid-base catalyst (Glu⁶⁰) is unfavorable for a direct or water mediated protonation (figure 2.2.21).

The catalytic water molecule present in the active site of the variant is displaced towards the intermediate by ~ 1.0 Å (~ 0.6 Å in subunit C) compared to its position in the active site of the

Figure 2.2.21: DHA-SCHIFF base intermediate in the active site of *TacTAL*_{E60Q/F132Y}.

The selected active site residues (gray) and the intermediate (yellow) are shown in ball-and-stick representation, the catalytic water molecule as red sphere. The SCHIFF base-forming lysine is colored in purple. The relative orientation of Gln⁶⁰ (Glu in *TacTAL*_{wt}) to the intermediate's C3-atom is unfavorable for a direct or water mediated proton transfer, other than the position of the Tyr¹³² residue, which is geometrically convenient for the direct protonation. The hydrogen atoms were added in their riding positions for the purpose of representation. Published in SAUTNER *et al.* (2015).



wild type protein co-crystallized with F6P. The water molecule in the active site of the variant is coordinated by the active site residues Thr¹¹⁰, Gln⁶⁰ and Tyr¹³². This is in contrast to the coordination of the water molecule in the active site of the wild type protein, which is coordinated by only two active site residues Thr¹¹⁰ and Glu⁶⁰ because it lacks the Tyr¹³² side chain (Phe¹³² in the wild type protein). These residues are corresponding to the hydrogen bond network including the C1OH-group of the F6P-SCHIFF base intermediate in its „up“ conformation in the active site of wild type enzyme.

The C1OH-group of the DHA-SCHIFF base intermediate in the active site of the *TacTAL*_{E60Q/F132Y} variant is coordinated by the residues Asn¹⁰⁸ and Ser¹³⁰ corresponding to the „down“ conformation of the same group in the F6P-SCHIFF base intermediate structure. This hydrogen bond network is not present in the active site of *EcFSA* (figure 2.2.22 A). The *TacTAL*_{FSA-mimic} variant mimics the situation in the active site of *EcFSA* (figure 2.2.22 B). In the active site of this variant, only one residue (Arg¹⁶⁹ →Lys in *EcFSA*) is different compared to the active site of *EcFSA*.

The structure of the *TacTAL*_{FSA-mimic} variant co-crystallized with F6P was determined to 1.90 Å resolution (table A.3 in the appendix) and refined against the diffraction data with $R_{\text{work}} = 17.80\%$ and $R_{\text{free}} = 20.99\%$ (table A.6 in the appendix). Two of the five subunits (D and E) of the pentamer in the asymmetric unit exhibit mixed conformational states. The remaining three subunits (A, B and C) are present in the „closed“ conformation. An additional electron difference density was observed in all five active sites of the pentamer (figure C.12 A in the appendix). This electron density was interpreted as the F6P-SCHIFF base intermediate (figure 2.2.23 A).

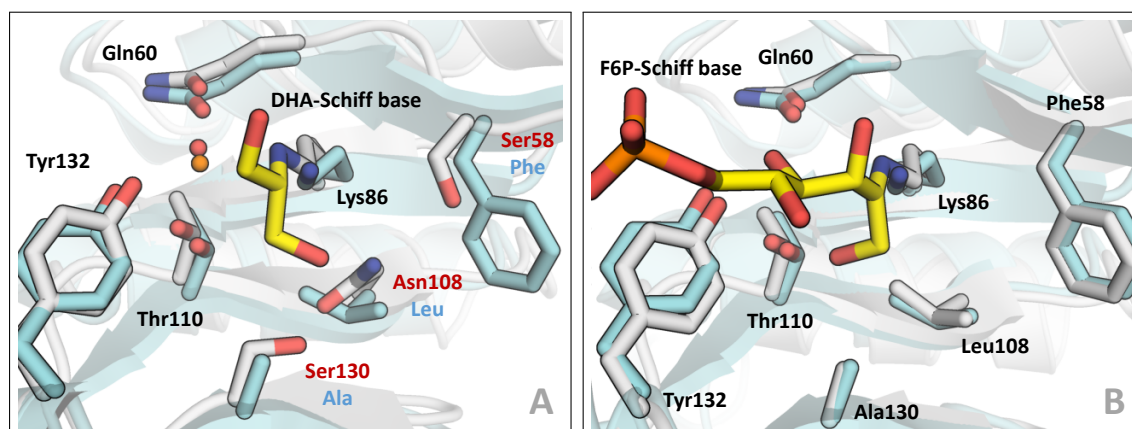


Figure 2.2.22: Superposition of the active sites of variants with enhanced aldolase activity co-crystallized with F6P and *EcFSA*. **A:** $TacTAL_{E60Q/F132Y}$ (gray) containing DHA-SCHIFF base intermediate (yellow sticks). The selected active site residues are shown as sticks, the catalytic water molecule as red (variant) or orange (*EcFSA*) sphere. While the residues related to the „up“ conformation of the intermediate’s C1OH-group in the variant are identical with the corresponding residues in *EcFSA* (cyan; PDB entry: 1L6W, (THORELL *et al.*, 2002)), the residues corresponding to the „down“ conformation are different (red labels: $TacTAL_{E60Q/F132Y}$, blue labels: *EcFSA*). **B:** $TacTAL_{FSA-mimic}$ (gray) containing F6P-SCHIFF base intermediate (yellow sticks). The environment of the reactive lysine in the variant and *EcFSA* (cyan) is identical. The residues are numbered according to their position in $TacTAL_{FSA-mimic}$.

The relative orientation of the F6P-SCHIFF base intermediate in the active site of the variant is comparable to the wild type situation (figure 2.2.23 B). However, the C1 hydroxy group is coordinated by Thr¹¹⁰ corresponding to its „up“ conformation (figure 2.2.23 A). The conformation of the reactive lysine residue in the active site of the variant is different compared to the wild type enzyme, with the highest difference in the C-C α -C β -C γ torsion angle. This angle was determined to 70.8 – 80.8° (depending on the analyzed subunit) in the structure of the F6P-SCHIFF base intermediate in the active site of $TacTAL_{wt}$ and to 170.3 – 177.2° in the $TacTAL_{FSA-mimic}$ variant.

Surprisingly, no proper electron density for the catalytic water molecule was present in the active site of the variant as in the case of the wild type enzyme. Only a weak mF_O-DF_C electron density appearing first at a contour level of 3.5σ could be observed in the active site of the variant implying a low occupancy of the water molecule. For this reason, the catalytic water molecule was not modeled into the active site of the variant (figure C.12 B in the appendix).

The structure of the F6P-SCHIFF base intermediate in the active site of the previously discussed $TacTAL_{E60Q/F132Y}$ variant was determined from another crystal of the variant co-crystallized with F6P (1.90 Å resolution, $R_{work} = 18.23\%$ and $R_{free} = 22.01\%$; tables A.4 and A.8 in the ap-

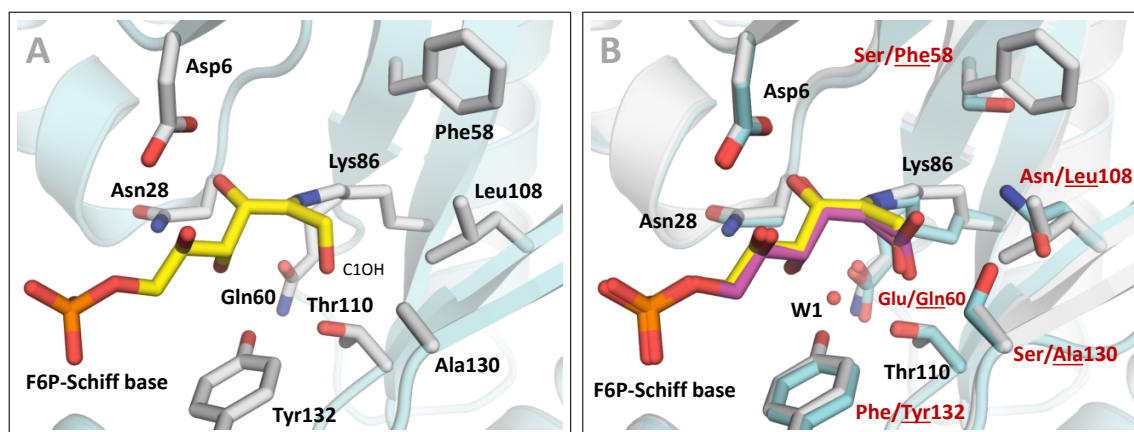
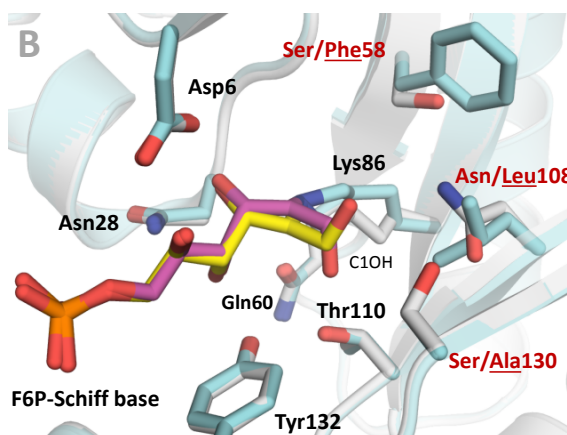


Figure 2.2.23: Active site of *TacTAL*_{FSA-mimic} co-crystallized with F6P. **A:** The selected active site residues (gray) and the F6P-SCHIFF base intermediate (yellow) are represented as sticks. The polypeptide backbone is shown as secondary structure (cyan). The C1OH-group is oriented towards Thr¹¹⁰ corresponding to the „up“ conformation. **B:** Superposition of the active sites of *TacTAL*_{FSA-mimic} (gray, ligand: yellow) and *TacTAL*_{wt} (cyan, ligand: purple) co-crystallized with F6P. The mutated residues are labeled in red. The residues present in the variant are underlined. The catalytic water molecule (W1) in *TacTAL*_{wt} is shown as red sphere.

pendix). The relative orientation of the F6P-SCHIFF base intermediate in the active site of the *TacTAL*_{E60Q/F132Y} variant is comparable to the situation in the active site of *TacTAL*_{FSA-mimic} (figure 2.2.24). In contrast to the *TacTAL*_{FSA-mimic} variant, the C1OH-group of the intermediate in the active site of the *TacTAL*_{E60Q/F132Y} variant is present mainly in its „down“ conformation. Although a mF_O - DF_C difference density corresponding to the alternative „up“ conformation could be observed in the active site of the variant, the alternative conformation was not modeled because of the weak electron density (figure C.13 B in the appendix). The same is true for the mF_O - DF_C difference density corresponding to the catalytic water molecule as in the case of the *TacTAL*_{FSA-mimic} variant (figure C.13 A in the appendix).

Figure 2.2.24: Superposition of the active sites of *TacTAL*_{FSA-mimic} and *TacTAL*_{E60Q/F132Y} co-crystallized with F6P. The mutated residues are labeled in red. The residues present in the *TacTAL*_{FSA-mimic} are underlined. The selected active site residues and the F6P-SCHIFF base intermediate (yellow: *TacTAL*_{E60Q/F132Y}, purple: *TacTAL*_{FSA-mimic}) are represented as sticks. The polypeptide backbone is shown as secondary structure (gray: *TacTAL*_{E60Q/F132Y}, cyan: *TacTAL*_{FSA-mimic}).



As previously described, the *TacTAL*_{E60Q/F132Y} variant shows a lag-phase during the first 50 ms after rapid mixing with substrate F6P using a stopped-flow device, which is independent from the substrate concentration. This lag-phase was interpreted to correspond to the conformational „open“/„closed“ change of the variant’s active sites. The subunit B of *TacTAL*_{E60Q/F132Y} variant containing DHA-SCHIFF base intermediate exhibits the „closed“ conformation, while the subunit E from the same structure exists mainly in the „open“ conformation. The superposition of both subunits shows that the conformational change indeed could play a role in the catalysis. Active site residues interacting with the intermediate or catalytic water in the „closed“ conformation, do not perform this interaction in the case of the „open“ conformation (figure 2.2.25).

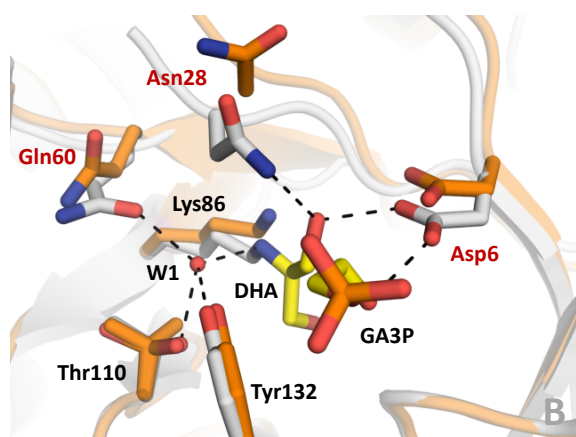


Figure 2.2.25: Superposition of the active sites of *TacTAL*_{E60Q/F132Y} co-crystallized with F6P in their „open“ and „closed“ states. The selected active site residues, the DHA-SCHIFF base intermediate (yellow) and the product GA3P (yellow) are represented as sticks, the catalytic water molecule (W1, „closed“ conformation) as red sphere. The polypeptide backbone is shown as secondary structure (gray: „closed“ subunit B, orange: „open“ subunit E). Residues interacting with the intermediate (black dashes), which have different position in „open“ or „closed“ conformations are labeled in red. Published in SAUTNER *et al.* (2015).

2.2.4 Studies on „Open“/„Closed“ Conformations of *TacTAL*

The structure of transaldolase from *Thermoplasma acidophilum* contains a homopentamer in the crystallographic asymmetric unit and is suggested to form homodecamers (dimer of pentamers) in solution (LEHWESS-LITZMANN, 2011; LEHWESS-LITZMANN *et al.*, 2011b). A prominent feature of the interaction of the pentamer’s subunits with each other is the inter-subunit helix swapping, in which a C-terminal α -helix of a subunit interacts with the TIM-barrel of the neighboring subunit. The subunits of the pentamer in the resting state structure of wild type *TacTAL* are not equivalent and exhibit „closed“ or „open“ conformations, while in the structure co-crystallized with substrate F6P all five subunits are present in the „closed“ conformation. The major difference between the „open“ and „closed“ conformations is the orientation of the flexible N-terminal part (residues 6 – 55) relative to the remaining chain. This part interacts with the C-terminal α -helix in the „closed“ but

not in the „open“ conformation. Additionally, a minor flexibility of the C-terminal α -helix could be observed as well.

In the crystal structure of the *TacTAL*_{E60Q/F132Y} variant, containing the DHA-SCHIFF base intermediate in two of five active sites, the subunits with bound intermediate were observed in „closed“ conformation, while the remaining subunits exhibit mainly „open“ conformation or mixed conformations (figure 2.2.26). The presence of a substrate-independent lag-phase in the pre-steady state of the aldolase reaction catalyzed by the variant could be the first indication that the conformational changes are present in solution as well and could be important for the catalysis.

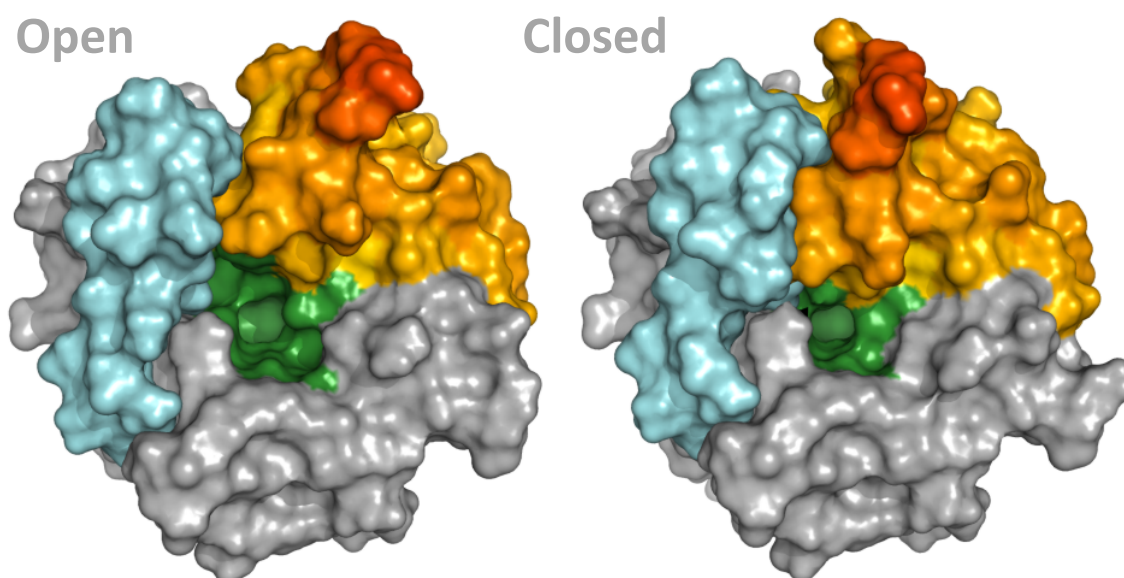


Figure 2.2.26: „Open“ and „closed“ conformations of functional subunits in *TacTAL*_{E60Q/F132Y}. The functional subunits B („closed“) and E („open“) are shown as surface model. The C-terminal α -helix of the neighboring subunit (C and A, respectively) is colored in cyan. The flexible N-terminal part (residues 6 – 55) is colored in orange/red (red: highest amplitude of flexibility). The active site cavity is indicated in green.

The residue Asp²¹¹ located at the C-terminal helix interacts with the Thr³⁰ located in the flexible N-terminal region of the neighboring subunit (figure 2.2.27). As described by LEHWESS-LITZMANN (2011), both residues are located in hydrogen bond distance to each other in the „closed“ conformation (the interatomic distance between the threonine’s hydroxy group and aspartate’s carboxyl is 2.7 Å), while these residues are separated from each other in the „open“ conformation (4.7 Å).

The residues Asp²¹¹ and Thr³⁰ were replaced by cysteine residues giving the *TacTAL*_{T30C/D211C} variant, in order to arrest the „closed“ conformation in all five subunits by formation of a disulfide bridge between the introduced residues Cys²¹¹ and Cys³⁰. Since the disulfide bridge forming

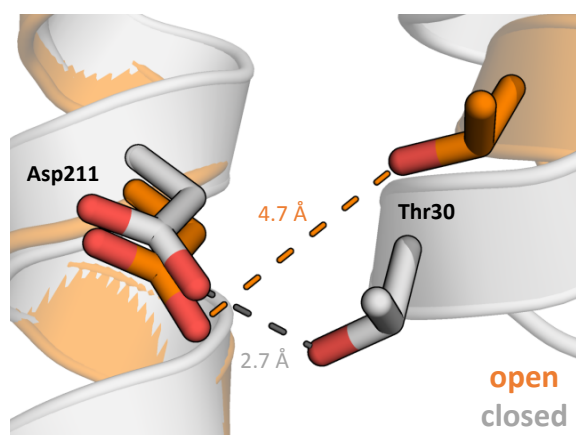


Figure 2.2.27: Relative orientation of Asp²¹¹ and Thr³⁰ to each other in the „open“ and „closed“ conformation. In the „closed“ conformation, both residues form a hydrogen bond (interatomic distance between the threonine's hydroxy group and aspartate's carboxyl: 2.7 Å). In the „open“ conformation this distance is elongated to 4.7 Å.

residues are located at neighboring subunits, the homopentamer of the *TacTAL*_{T30C/D211C} variant is covalently cross-linked. Importantly, the arrest of the „closed“ conformation in the variant can be unlocked using reducing agents (e.g. in presence of DTT or β -mercaptoethanol).

The structure of the *TacTAL*_{T30C/D211C} variant in resting state was determined to a resolution of 2.25 Å ($R_{\text{work}} = 16.84\%$ and $R_{\text{free}} = 20.98\%$; tables A.3 and A.6 in the appendix). A continuous electron density between the sulfur atoms of introduced cysteines residues, as well as the interatomic distance of ~ 2.05 Å, clearly indicates an intersubunit disulfide bridge formed in all five subunits of the variant (figure 2.2.28). The torsion angle C-S-S-C (τ) is 94.9 – 104.6° (depending on the subunit), which fits well to the natural distribution of τ -angles as described by BHATTACHARYYA *et al.* (2004). The usual interatomic distance for a disulfide bond with τ -angles of 75.0 – 105.0° is 2.031 ± 0.015 Å as reported by ALLEN *et al.* (1987).

When superposing subunits of *TacTAL*_{T30C/D211C} with the subunits from the wild type protein co-crystallized with F6P, in which all five subunits are present in the „closed“ conformation, the distance between the corresponding backbone's C α atoms of the compared subunits is lower than 1 Å (figure 2.2.29). On the other hand, when plotting the corresponding distance for the subunits of the resting state structure of *TacTAL*_{T30C/D211C} compared to the subunit in the „open“ conformation observed in the resting state structure of the wild type enzyme (PDB entry: 3S0C, (LEHWESS-LITZMANN *et al.*, 2011b)) against the residue number, the plot shape is similar to the plot resulting from the comparison between the „open“ and „closed“ conformations of subunits from the wild type protein. This plot clearly shows the difference between the „open“ and „closed“ conformations in their N-terminal part with a maximal deviation in corresponding C α -positions of ~ 7 Å. In other words, the subunits of the resting state structure of *TacTAL*_{T30C/D211C} variant are comparable to the subunits in the „closed“ conformation of wild type enzyme (rmsd = 0.257 Å,

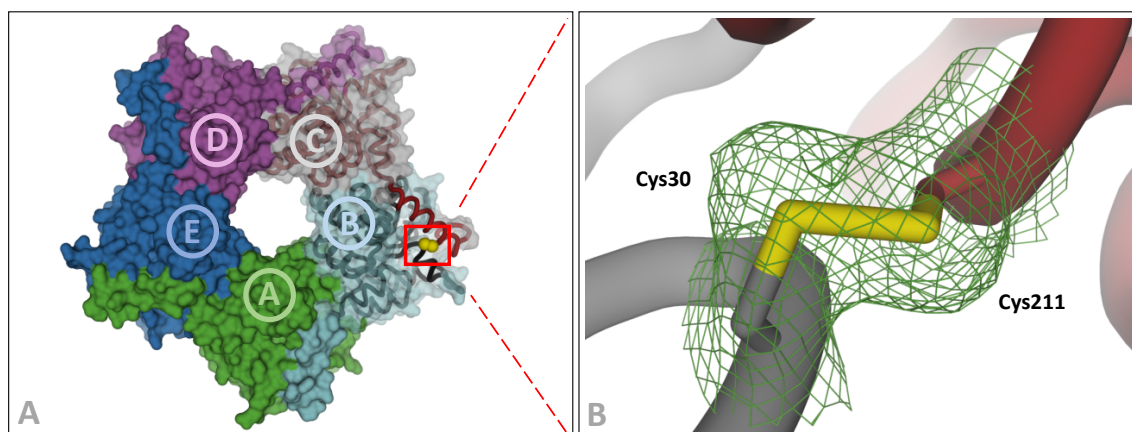


Figure 2.2.28: Introduction of an intersubunit disulfide bridge in *TacTAL*. **A:** The introduced cysteine residues at positions 30 and 211 (Thr and Asp in wild type enzyme, respectively) form a disulfide bridge between the flexible N-terminal part and the C-terminal α -helix of the neighboring subunit. The pentamer's subunits (A – E) are represented as surface and indicated by different colors. The polypeptide backbone of subunits C and B is shown in tube representation in black and red, respectively. The sulfur atoms of the introduced disulfide bridge (red frame) are shown as yellow spheres. **B:** *mF_O-DF_C* simulated annealing omit map of *TacTAL*_{T30C/D211C} in resting state. The difference electron density map is shown as green mesh (contour level 3 σ). The polypeptide backbone of subunits C and B is shown in tube representation in black and red, respectively. The introduced cysteine residues are represented as sticks.

based on C α atoms of a monomer) and differ from the „open“ state (rmsd = 1.221 Å) in a similar way as in the case of the wild type („open“) to wild type („closed“) comparison (rmsd = 1.290 Å).

The structure of the variant co-crystallized with F6P was determined to a resolution of 2.05 Å ($R_{\text{work}} = 16.64\%$ and $R_{\text{free}} = 20.62\%$; tables A.3 and A.6 in the appendix). As in the case of the resting state structure, the introduced disulfide is present in its oxidized form (disulfide bridge) and all five subunits of the homopentamer exhibit the „closed“ conformation. The F6P-SCHIFF base intermediate could be observed in the active site of all five subunits (figure 2.2.30 A). The active site of the variant co-crystallized with F6P is superimposable with the active site of the corresponding wild type structure (figure 2.2.30 B).

In order to obtain a structure of the variant containing reduced cysteines (unlock of the conformational arrest), the protein was co-crystallized with 1 – 2 mM DTT. Unfortunately, no crystals of the *TacTAL*_{T30C/D211C} variant could be observed under reducing conditions. For this reason, the previously obtained resting state crystals were soaked with the reservoir solution supplemented with 50 mM DTT for 10 min at 20 °C. The structure was determined to a resolution of 2.15 Å ($R_{\text{work}} = 17.98\%$ and $R_{\text{free}} = 21.40\%$; tables A.4 and A.7 in the appendix). Surprisingly, the intro-

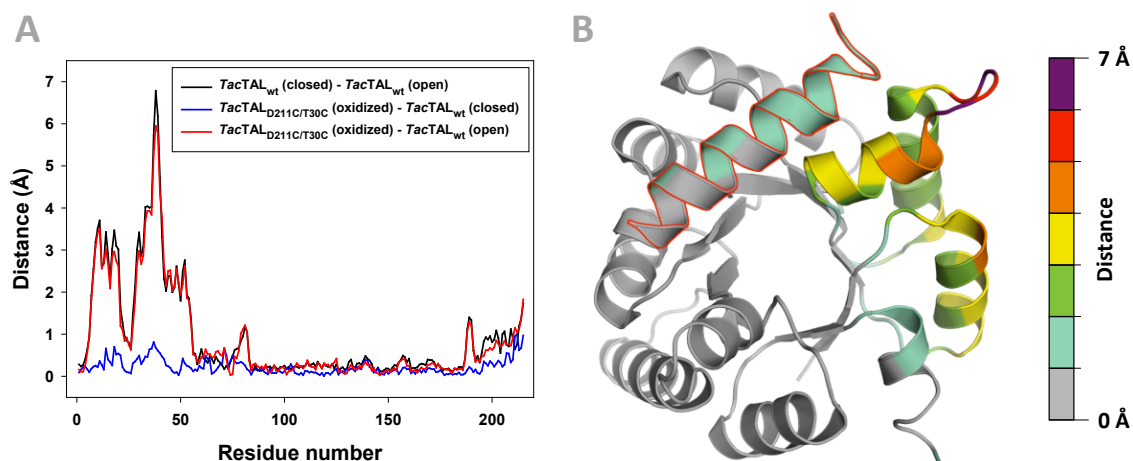


Figure 2.2.29: Comparison of the „open“/„closed“ conformations observed in resting state wild type structure with the resting state of *TacTAL*_{T30C/D211C}. **A:** Distance (Å) between the backbone C α atoms of compared subunits plotted vs. residue number (calculated using (KLEYWEGT, 1996)). Black solid line: „open“ vs. „closed“ conformation in resting state of *TacTAL*_{wt} (PDB entry: 3S0C, (LEHWESS-LITZMANN *et al.*, 2011b)), blue solid line: „closed“ conformation of *TacTAL*_{wt} vs. resting state of *TacTAL*_{T30C/D211C}, red solid line: „open“ conformation in resting state of *TacTAL*_{wt} vs. resting state of *TacTAL*_{T30C/D211C}. The conformational state of *TacTAL*_{T30C/D211C} is similar to the „closed“ conformation in wild type. **B:** Functional subunit of *TacTAL*_{wt} in „closed“ conformation as secondary structure. The C-terminal α -helix of the neighboring subunit is contoured in red. The color scale indicates the difference in the interatomic distance (Å) between backbone C α atoms compared to the „open“ conformation.

duced cysteines were inspected to form disulfide bonds in all five subunits and were not reduced as expected. The cause of this observation is unclear. The introduced disulfide is located on the surface of the homopentamer in a region, which does not contribute to the crystallographic contacts. Consequently, the introduced disulfide bridge was assumed to be accessible for the reducing agent DTT. A longer incubation of the crystal in the soaking solution was not possible, because the crystals started to dissolve after 10 min.

Another resting state crystal was soaked with the reservoir solution containing 50 mM DTT and 100 mM F6P for 2 min at 20 °C. The structure was determined to a resolution of 2.10 Å ($R_{\text{work}} = 19.56\%$ and $R_{\text{free}} = 23.02\%$; tables A.4 and A.7 in the appendix). In this case as well, the introduced residues Cys²¹¹ and Cys³⁰ are present as oxidized disulfides in all subunits, in spite of the presence of DTT in the soaking solution. An additional electron difference density was observed in the active sites of all five subunits. This electron density was interpreted as the F6P-SCHIFF base intermediate (figure C.15 in the appendix). The intermediate is coordinated by the active site residues in a similar way as observed in the active site of the variant co-crystallized without DTT (figure 2.2.31). The C1OH-group of the intermediate is oriented in the „down“ conformation. The

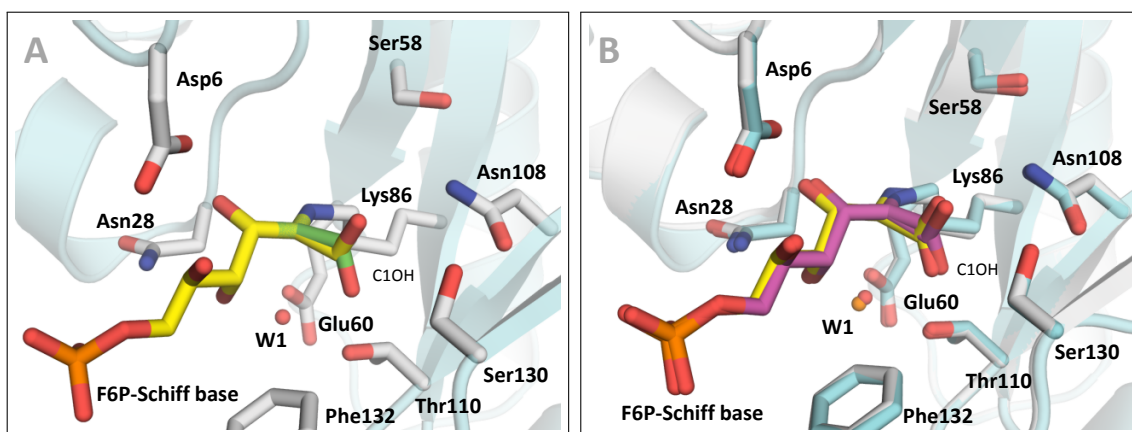


Figure 2.2.30: Active site of *TacTAL*_{T30C/D211C} co-crystallized with F6P. **A:** The selected active site residues (gray) and the F6P-SCHIFF base intermediate (yellow) are represented as sticks, the catalytic water molecule as red sphere. The polypeptide backbone is shown as secondary structure (cyan). The C1OH-group is present in two alternative conformations (green: „up“, yellow: „down“). **B:** Superposition of the active sites of *TacTAL*_{T30C/D211C} (gray, ligand: yellow) and *TacTAL*_{wt} (cyan, ligand: purple) co-crystallized with F6P. The catalytic water molecule is shown as orange (*TacTAL*_{wt}) or red (*TacTAL*_{T30C/D211C}) sphere.

SCHIFF base-forming lysine adopts its all-*trans* conformation, comparable to the lysine observed in the wild type structure co-crystallized with A5P.

The presence of the F6P-SCHIFF base intermediate in the active site of the variant after soaking indicates that two minutes of soaking, seem to be sufficient for the diffusion of F6P into the crystal. In this context, ten minutes of treatment with the DTT containing solution were assumed to be sufficient as well. However, a different behavior in diffusion of different substances to the different positions in the crystal lattice cannot be excluded.

Soaking of a resting state crystal with F6P containing solution without addition of DTT resulted in a structure (resolution=2.50 Å, $R_{\text{work}} = 19.77\%$ and $R_{\text{free}} = 23.40\%$; tables A.4 and A.7 in the appendix) with an additional electron difference density in the active site, which was interpreted as covalently linked F6P-carbinolamine intermediate in the active sites of subunits C, D and E (figure C.16 in the appendix). In the active sites of the remaining two subunits (A and B), the F6P-SCHIFF base intermediate was modeled.

The relative orientation of the F6P-carbinolamine intermediate in the active site of the variant is comparable to the orientation of the carbinolamine-mimic M1P in the active site of the wild type enzyme (figure 2.2.32 B). While the phosphate groups of the intermediate and the enzyme bound M1P are superimposable, the C2-atom of the intermediate is displaced by ~ 0.7 Å compared to

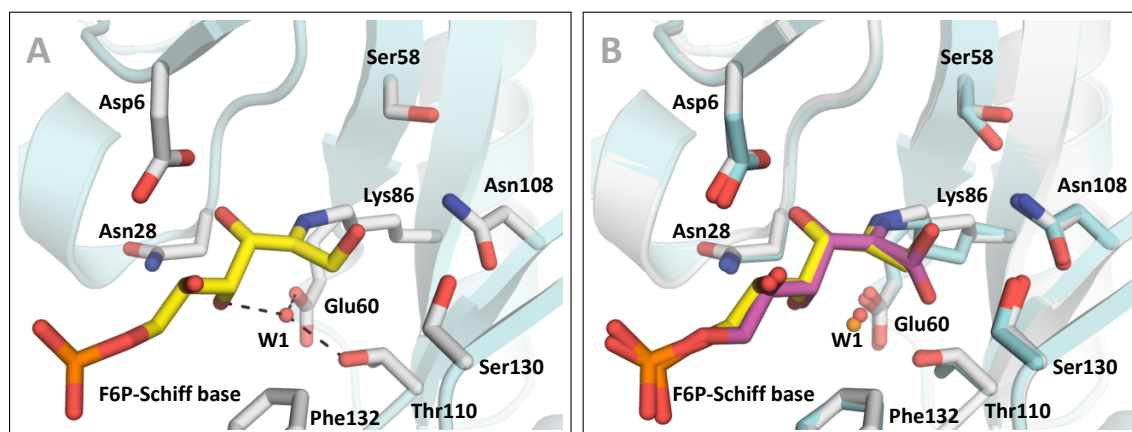


Figure 2.2.31: Active site of *TacTAL*_{T30C/D211C} soaked simultaneously with F6P and DTT. **A:** The selected active site residues (gray) and the F6P-SCHIFF base intermediate (yellow) are represented as sticks, the catalytic water molecule as red sphere. The polypeptide backbone is shown as secondary structure (cyan). The C1OH-group is coordinated by Ser¹³⁰ corresponding to the „down“ conformation. **B:** Superposition of the active sites of *TacTAL*_{T30C/D211C} soaked (gray, ligand: yellow) with DTT/F6P and co-crystallized (cyan, ligand: purple) with F6P. Orange sphere: catalytic water molecule in structure co-crystallized with F6P, red sphere: catalytic water molecule in structure soaked with F6P and DTT.

the M1P structure. The C1OH-group adopts the „down“ conformation. The C2 hydroxy group is coordinated by Thr¹¹⁰. The catalytic water molecule is not present in the active site of the F6P-carbinolamine intermediate containing structure.

Compared to the structure of the F6P-SCHIFF base intermediate observed in the structure of the variant co-crystallized with F6P, the carbinolamine intermediate is displaced by ~ 0.7 Å towards the entrance of the active site (figure 2.2.32). The C2-atom of the carbinolamine intermediate is displaced by ~ 1.0 Å caused *inter alia* by the sp^3 -hybridization of the carbon in the carbinolamine compared to the sp^2 -hybridized carbon of the SCHIFF base. The catalytic lysine residue adopts the all-*trans* conformation in the structure of the F6P-carbinolamine intermediate.

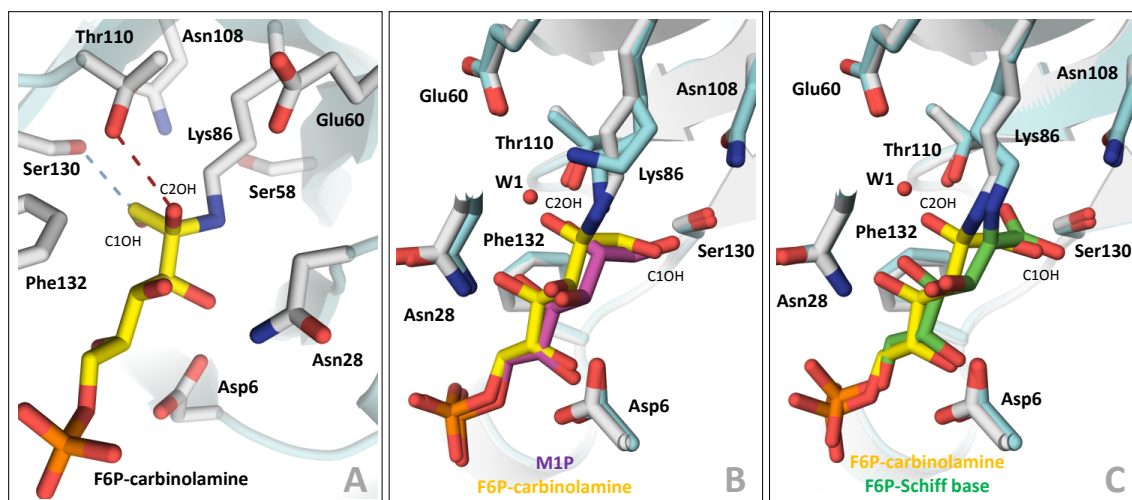


Figure 2.2.32: Active site of *TacTAL*_{T30C/D211C} soaked with F6P. **A:** The selected active site residues (gray) and the F6P-carbinolamine intermediate (yellow) are represented as sticks. The polypeptide backbone is shown as secondary structure (cyan). The C1OH-group is coordinated by Ser¹³⁰ corresponding to the „down“ conformation. **B:** Superposition of the active sites of *TacTAL*_{T30C/D211C} (gray, ligand: yellow) soaked with F6P and *TacTAL*_{wt} (cyan, ligand: purple) co-crystallized with M1P. The relative orientation of the F6P-carbinolamine intermediate trapped in *TacTAL*_{T30C/D211C} is comparable to that of the carbinolamine-mimic M1P in the active site of *TacTAL*_{wt}. Red sphere: resting state water molecule in *TacTAL*_{wt} (absent in *TacTAL*_{T30C/D211C}). **C:** Superposition of the active sites of *TacTAL*_{T30C/D211C} soaked (gray, F6P-carbinolamine intermediate: yellow) and co-crystallized (cyan, F6P-Schiff base intermediate: green) with F6P. Red sphere: catalytic water molecule in F6P-Schiff base intermediate containing structure (absent in the case of F6P-carbinolamine intermediate).

In order to analyze, if the „closed“-state arrest of the subunits in the *TacTAL*_{T30C/D211C} variant influences the catalysis, steady-state measurements, as well as single-turnover analysis, were performed.

The steady-state measurements for the *TacTAL*_{T30C/D211C} variant were performed under oxidizing (absence of DTT) and reducing (presence of 1 mM DTT [final concentration]) conditions (figure 2.2.33). The turnover number for the oxidized form (the „closed“ conformation is stabilized by an inter-subunit disulfide bound) of the variant was determined to $k_{\text{cat}} = 1.1 \pm 0.3 \text{ s}^{-1}$ and the apparent MICHAELIS constant to $K_{\text{M}}^{\text{app}} = 0.60 \pm 0.08 \text{ mM}$. The treatment of the variant with 20 mM DTT (final concentration of 1 mM DTT in reaction mixture; for details, see section 1.6.4.2) results in a ~4 fold higher turnover number and a ~50 fold higher apparent MICHAELIS constant. However, because of this high increase of the apparent MICHAELIS constant, the catalytic efficiency of the variant under reducing conditions ($k_{\text{cat}}/K_{\text{M}}^{\text{app}} = 0.14 \text{ s}^{-1}\text{M}^{-1}$) is one order of magnitude lower compared to the oxidizing conditions ($k_{\text{cat}}/K_{\text{M}}^{\text{app}} = 1.83 \text{ s}^{-1}\text{M}^{-1}$), while the turnover number is higher.

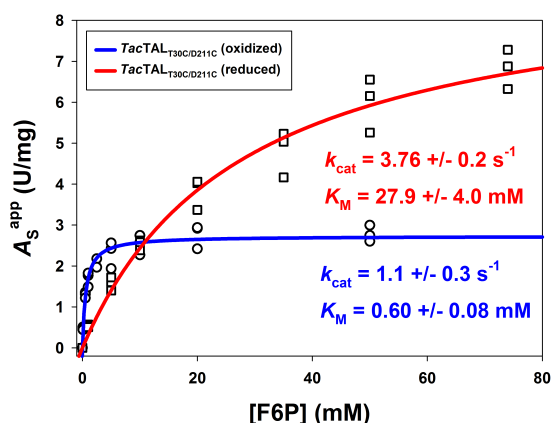


Figure 2.2.33: Dependency of the transaldolase activity of *TacTAL*_{T30C/D211C} on F6P concentration (0.1 – 74 mM). The rectangles and circles indicate the measured transaldolase steady-state activity of *TacTAL*_{T30C/D211C} (50 $\mu\text{g}/\text{mL}$, 30 $^{\circ}\text{C}$) in its reduced (pre-incubated with DTT) and oxidized form, respectively. The MICHAELIS-MENTEN fits (eq. 1.6.2, solid line) are indicated by red and blue, respectively. The margin of error for the macroscopic kinetic constants is given as the standard deviation of the fitted data (sets of triplicates). Data provided by LIETZOW (2015).

In order to satisfy the complete reduction of all cysteines in the molecule, the variant was pre-incubated with 20 mM DTT for at least 10 min. Because the incubation of the enzyme in DTT containing buffer for 4 h results in 40 – 50 % loss in transaldolase activity, the enzyme/DTT pre-mix was prepared freshly every 40 min during the experiment (loss in activity of ~ 5 %). The origin of the inactivating effect of DTT on the variant is unclear. However, the incubation of the variant with 1 mM DTT for 10 min does not influence the secondary structure of the protein according to CD measurements (figure C.2 in the appendix).

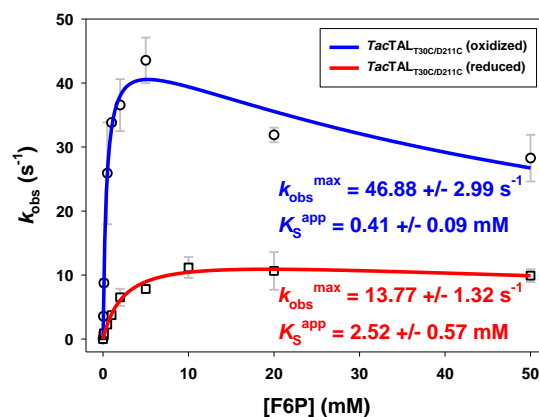
The transaldolase activity of the *TacTAL*_{T30C/D211C} variant is ~ 4 or ~ 15 fold lower (under reducing or oxidizing conditions, respectively) than the activity of the wild type enzyme ($k_{\text{cat}} = 13.86 \pm 0.65 \text{ s}^{-1}$, (LEHWESS-LITZMANN, 2011)). The apparent MICHAELIS constant of the variant determined under oxidizing conditions is ~ 4 fold lower, while the same constant determined under reducing conditions is ~ 12 fold higher compared to the wild type enzyme ($K_{\text{M}}^{\text{app}} = 2.30 \pm 0.36 \text{ mM}$, (LEHWESS-LITZMANN, 2011)). The treatment of the wild type enzyme with DTT did not show any effect on the turnover number or apparent MICHAELIS constant of transaldolase reaction.

In addition to the steady-state measurements the pre-steady-state analysis of the variant was performed under oxidizing (absence of DTT) and reducing (presence of 1 mM DTT after mixing with F6P in a 1:1 volume ratio) conditions using stopped-flow technique (figure 2.2.34).

The dependency of the observed first order rate constant (k_{obs}) on the substrate concentration of the variant in its oxidized form is comparable to the single-turnover kinetics of the wild type. The first order rate constant ($k_{\text{obs}}^{\text{max}}$) was determined to $46.88 \pm 2.99 \text{ s}^{-1}$ (for wild type: $60.31 \pm 4.12 \text{ s}^{-1}$ (SAUTNER, 2012)). The apparent equilibrium constant of the fast pre-equilibrium ($K_{\text{S}}^{\text{app}}$) for the

Figure 2.2.34: Pre-steady-state analysis of the donor half-reaction of *TacTAL*_{T30C/D211C} in its reduced and oxidized forms.

The measurements were performed at 30 °C. The error bars represent the standard deviation of the mean value calculated from the measurement of triplicates. The rectangles and circles indicate the observed rate constants (k_{obs}) depending on F6P concentration (0.05 – 50 mM) for reduced (pre-incubated with DTT) and oxidized form, respectively. The data were fitted according to eq. 1.6.8 (red and blue, respectively). Data provided by LIETZOW (2015) and LISA-MARIE FUNK.



donor half-reaction of the variant in its oxidized form was determined to 0.41 ± 0.09 mM which is ~ 2 fold lower than the corresponding constant for the wild type enzyme (0.70 ± 0.17 mM (SAUTNER, 2012)). The respective constants for the reduced form of the variant were determined to $k_{\text{obs}}^{\text{max}} = 13.77 \pm 1.32 \text{ s}^{-1}$ and $K_{\text{S}}^{\text{app}} = 2.52 \pm 0.57$ mM. In contrast to the steady-state results, the arrest of conformational „open“/„closed“ dynamics in the oxidized form of the *TacTAL*_{T30C/D211C} variant influences the donor half-reaction only marginal. The reduction of the disulfide bond between Cys³⁰ and Cys²¹¹ impairs the first order rate constant ($k_{\text{obs}}^{\text{max}}$) at least by a factor of three. The apparent equilibrium constant of the fast pre-equilibrium ($K_{\text{S}}^{\text{app}}$) of the donor half-reaction under reducing conditions is increased by a factor of six.

2.3 Discussion

During the last few decades, an extensive knowledge regarding the mechanism of action of transaldolase was obtained. Previous investigations on transaldolase from *Escherichia coli* contributed information about the geometry of the active site (JIA *et al.*, 1996). In further studies, catalytically important residues could be identified by mutagenesis and structural analysis of invariant residues located in the active site (SCHÖRKEN *et al.*, 2001). Finally, the transaldolase from *Thermoplasma acidophilum* emerged as a good model enzyme for further investigations on the mechanism of catalysis. Crystallographic analysis of this thermostable transaldolase contributed the structural information about the orientation of the F6P-SCHIFF base intermediate in the active site, which was the first observation of a reactive intermediate *in crystallo* for this class of enzymes (LEHWESS-LITZMANN *et al.*, 2011b). In these studies, the Glu⁶⁰ residue was identified as the general acid-base catalyst, which contrasts the previous assumption that an aspartate residue (Asp⁶ in *TacTAL*) participates in the acid-base catalyzed aldol cleavage as well (SCHÖRKEN *et al.*, 2001). However, the impact of the different conformational states observed in the structure of *TacTAL* („open“ and „closed“) on the catalysis remained unclear.

Intrinsic dynamic processes in enzymes are reported to play an important role during catalysis or for substrate recognition (BOEHR *et al.*, 2009; EISENMESSER *et al.*, 2005; HAMMES *et al.*, 2011). A mechanism in which the enzyme adopts different conformational states convenient for the respective catalysis step was described for the dihydrofolate reductase from *Escherichia coli* (BOEHR *et al.*, 2006). This strategy allows the enzyme to catalyze its reaction in the most efficient way and was reported for a number of different enzymes (HAMMES *et al.*, 2011; HAMMES-SCHIFFER AND BENKOVIC, 2006; HENZLER-WILDMAN *et al.*, 2007; WOLF-WATZ *et al.*, 2004). Intrinsic dynamic processes take place during the catalytic cycle of aldolase from rabbit muscle, an enzyme structurally and mechanistically related to transaldolase. A tyrosine residue acting as the acid-base catalyst for the protonation of the central DHAP-carbanion/enamine intermediate prior to the hydrolysis reaction is located in the flexible C-terminus of the protein. This residue is not present in the active site during the DHAP-carbanion/enamine intermediate formation, which is acid-base catalyzed by a glutamate residue similar to the transaldolase reaction. When the DHAP-carbanion/enamine intermediate is formed and the first product is released, the C-terminus adopts a conformation, in which the tyrosine's hydroxy group is perfectly oriented for the proton transfer onto the intermediate (ST-JEAN AND SYGUSCH, 2007). Protonation of the intermediate is necessary for the hydrolysis reaction to

occur. In this case, the dynamic process provides a spatial separation of the reactants along the catalytic cycle.

In the case of *Tac*TAL, two different conformational states („open“ and „closed“) were observed in the crystal structure of the protein in resting state (LEHWESS-LITZMANN, 2011). In the „closed“ state the flexible N-terminal part (6 – 55 aa) interacts with the C-terminal α -helix of the neighboring subunit. The active site entrance of the subunits in „closed“ conformation is ~ 3.8 Å narrower compared to the active site in the „open“ conformation (LEHWESS-LITZMANN, 2011). In order to investigate the importance of the conformational changes in *Tac*TAL for the catalysis, the enzyme was covalently arrested in its „closed“ conformation by the introduction of an intersubunit disulfide bond. A double-mutation variant (*Tac*TAL_{T30C/D211C}) was generated and analyzed structurally and kinetically.

The use of designed disulfide bridges is a convenient method to cross-link protein molecules or protein domains (CEDERVALL *et al.*, 2015; KUFAREVA *et al.*, 2016). In contrast to chemical cross-linking (e.g. by the use of glutaraldehyde as cross-linker), cysteine residues and disulfide bonds are common in natural proteins and they can be introduced in a selective manner. Furthermore, the designed disulfide bridges can be used to provide thermal stability to mesophilic proteins as it was described for 1,3-1,4- β -glucanase from *Bacillus terquilensis* (NIU *et al.*, 2016). In the present work, the disulfide bridge was introduced in *Tac*TAL in order to arrest the protein in a distinct conformation as recently published for other enzymes (GIGANTI *et al.*, 2015; ZAREMBA AND SIKSNYS, 2015)

In the resting state structure of the variant, the introduced cysteine residues were found to form a disulfide bond cross-linking the C-terminal α -helix with the flexible N-terminal part of the neighboring subunit. The geometry of this disulfide bond corresponds well with the preferred geometries of disulfide bonds as observed in numerous structures (ALLEN *et al.*, 1987; BHATTACHARYYA *et al.*, 2004; PELLEQUER AND CHEN, 2006).

According to the fact that the monomers of *Tac*TAL's homodecamer (dimer of pentamers) are unable to adopt the „open“ conformation without the breaking of the disulfide bridge, all five subunits of the homopentamer in the asymmetric unit were observed in the „closed“ conformation although the variant was crystallized in resting state (figure 2.3.35). This is in contrast to the wild type protein, whose resting state structure shows different conformations.

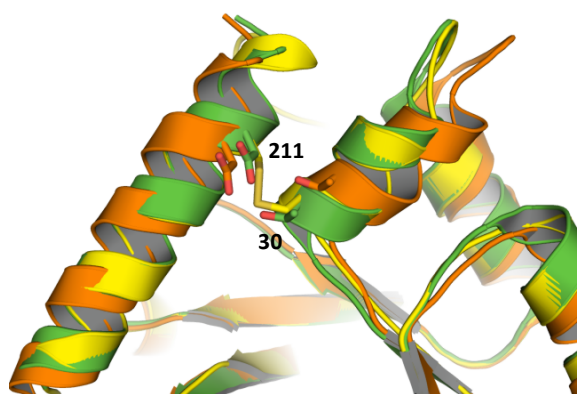


Figure 2.3.35: Superposition of „open“ and „closed“ conformations of *TacTAL*_{wt} (orange and green, respectively) with a subunit of *TacTAL*_{T30C/D211C} (yellow). The main chain is represented as secondary structure. The side chains of the interacting residues are shown as sticks.

Although the introduced disulfide bond preserves the „closed“ conformation by covalent linkage, an absolute arrest of protein dynamics cannot be assumed for sure. The flexible region of *TacTAL* contains 50 amino acid residues (residues 6-55). A local arrest of the flexibility by the introduced disulfide bond is most probably insufficient to prevent remaining regional flexibility. However, the conformational equilibrium in this region is assumed to be shifted towards the „closed“ state. The introduced cysteines replace the residues Asp²¹¹ and Thr³⁰, which interact with each other in the „closed“ state of the wild type protein by hydrogen bonding. In presence of a reducing agent (e.g. DTT or β -mercaptoethanol) the cysteines are existent as thiols and do not form a covalent bond. The „closed“ state is suggested to be destabilized under reducing conditions, because of the lacking hydrogen bond between the mutated residues Asp²¹¹ and Thr³⁰ as in the case of wild type situation. Consequently, the „open“/„closed“ equilibrium of the reduced variant is suggested to be shifted towards the „open“ state. In other words, the designed variant is assumed to be present mainly in the „closed“ conformation under oxidizing conditions and mainly in the „open“ conformation under reducing conditions but the occurrence of regional flexibility cannot be excluded in both cases.

According to the single-turnover analysis of the variant, the „closed“ conformation is important for the donor half-reaction consisting of the catalytic steps from substrate binding (F6P) to the release of the first product (GA3P). The reaction rates determined for the variant are comparable to those of the wild type protein, other than the rates in presence of DTT unlocking the conformational arrest and destabilizing the „closed“ state. In the latter case, the rate constant is significantly decreased. In steady-state experiments, the addition of DTT results in a higher turnover number and higher MICHAELIS-constant compared to the oxidizing conditions. Based on these results, a model can be proposed, in which substrate binding and catalysis of the donor half-reaction are performed by the enzyme in its „closed“ conformation. On the other hand, the adoption of the „open“ conformation is

necessary for efficient catalysis of the acceptor half-reaction (DHA-unit transfer to the C1-position of E4P and release of the second product S7P). This corresponds well to the previous suggestion of the conformational-selection mechanism for the substrate binding (LEHWESS-LITZMANN *et al.*, 2011b). In this case, the protein is present in different conformational states showing different affinities for the substrate (VOGT AND DI CERA, 2012; VOGT *et al.*, 2014). VOGT AND DI CERA (2013) suggested a preeminent role of the conformational selection mechanism for ligand binding in nature. An alternative mechanism for the substrate binding is the induced-fit mechanism, in which the substrate-binding event induces the conformational adaptation of the active site. The conformational-selection and induced-fit mechanisms are edge cases in the natural complexity regarding the ligand binding and dynamic processes. In this context, mixed situations were proposed as well (VOGT AND DI CERA, 2013).

The residues Thr³⁰ and Asp²¹¹ are not a part of the active site. A virtual rotamer of Thr³⁰ could interact with the active site's residue Asn²⁸, which coordinates the C4 hydroxy group of the F6P-SCHIFF base intermediate but this conformation of Thr³⁰ was not observed in any structure of *TacTAL* so far. Although both introduced mutations are not located in the active site, the steady-state activity of the variant is significantly impaired compared to the wild type activity irrespective of the redox-state of the disulfide. This underlines the importance of the dynamic processes (*per se*) for the catalysis, which is assumed to be perturbed for the variant in both cases (reducing or oxidizing conditions).

The incubation of the *TacTAL*_{T30C/D211C} variant with 20 mM DTT for four hours results in ~50 % loss in activity. This effect remains unexplained. One possibility could be a covalent modification of the cysteine residues by DTT over the time destabilizing the correct fold. Another explanation could be the potential lower stability of the enzyme in its „open“ state. Furthermore, a perturbation of the homopentamer formation because of the missing interaction between the side chains of Thr³⁰ and Asp²¹¹ is assumable but unlikely, since the pentamer is stabilized by a number of interactions and the removed interaction is only present in the „closed“ state of the protein. The oligomerization state of the variant under reducing conditions could be analyzed using analytical gel-filtration or the size exclusion chromatography coupled multiangle light scattering. Another method giving the information about the oligomerization state is the analytical ultracentrifugation as it was performed for *TacTAL*_{wt} in previous work (LEHWESS-LITZMANN, 2011).

The analysis of the pre-steady state kinetics of the aldolase active variant *TacTAL*_{E60Q/F132Y} in reaction with F6P provides further evidence for conformational changes of the enzyme in solution. The progress curves of the pre-steady-state kinetics of the aldolase-active variant *TacTAL*_{E60Q/F132Y} in reaction with F6P show a lag phase during the first 50 ms. The duration of this phase is independent from the substrate concentration. This lag phase could be a further evidence that *TacTAL* undergoes conformational changes in solution, which are important for the catalysis. According to the conformational selection mechanism, the substrate is assumed to bind preferentially to the „closed“ state of *TacTAL* giving a productive enzyme-substrate complex. The aldol cleavage of the substrate after the binding event results in an „open“/„closed“ equilibrium shift under single-turnover conditions. In this case, the lag phase would describe the „open“/„closed“ conformational change of the protein before substrate binding. A similar observation was published for the 1,3-1,4- β -glucanase from *Bacillus licheniformis* (ABEL *et al.*, 2001). A lag phase in the very beginning of the progress curves of the single-turnover reaction of the disulfide variant *TacTAL*_{T30C/D211C} could be observed, but was not discussed in the present work because of the poor data quality in this sensible region of the curve. However, under oxidizing conditions the lag phase was observed only at low substrate concentration (≤ 1 mM). The duration of this lag phase was supposed to depend on substrate concentration and could describe the substrate binding process. Under the reducing conditions, the duration of the lag phase was supposed to be independent from the substrate concentration.

The *TacTAL*_{E60Q/F132Y} variant mimics the acid-base constellation of the active site of fructose 6-phosphate aldolase from *Escherichia coli* (*EcFSA*), which is structurally and mechanistically related to transaldolase. Other than transaldolase, which catalyzes the reversible transfer of a dihydroxyacetone-unit from a donor-substrate (e.g. F6P) to the carbonyl-carbon of an acceptor-substrate (e.g. E4P), fructose 6-phosphate aldolase catalyzes the reversible cleavage of the sugar substrate (SCHÜRMAN AND SPRENGER, 2001). As previously published, a single-mutation of the particular phenylalanine residue in the active site of transaldolase (*Thermoplasma acidophilum*: Phe¹³², *Escherichia coli*: Phe¹⁷⁸, human: Phe¹⁸⁹) by tyrosine enhances the aldolase activity of transaldolase and impairs the transaldolase activity (LEHWESS-LITZMANN, 2011; SCHNEIDER *et al.*, 2008).

Although *EcFSA* catalyzes its reaction via acid-base catalysis akin transaldolase, an equivalent for the general acid-base catalyst of *TacTAL* (Glu⁶⁰) is substituted by a glutamine residue in the active

site of *EcFSA*. In this context, the aforementioned tyrosine residue was suggested to take over the role of the transaldolase specific glutamate as the general acid-base catalyst.

Tyrosine residues were indicated as the acid-base catalysts for a number of enzymes (DANIELS *et al.*, 2014; SCHWANS *et al.*, 2013; SUN AND TONEY, 1999). Moreover, a tyrosine residue emerged as the acid-base catalyst in the designed non-natural aldolases (BJELIC *et al.*, 2014; GIGER *et al.*, 2013; ZHU *et al.*, 2009). Although the tyrosine side chain is a weak acid with a pK_a of 9.7 ± 0.5 in aqueous solution (HARRIS AND TURNER, 2002), this pK_a can be lowered in the environment of the active site by up to 4 units, caused by the stabilization of the negative charge of the phenolate anion via hydrogen bonds or positively charged residues such as arginine (SCHWANS *et al.*, 2013; SUN AND TONEY, 1999). In the active site of *EcFSA* an arginine residue (Arg¹³⁴) is placed in the direct environment of the catalytic tyrosine (Tyr¹³¹), which is conserved in *TacTAL* (Arg¹³⁵) as well (STELLMACHER *et al.*, 2015). As suggested by STELLMACHER *et al.* (2015), this arginine residue could lower the pK_a of the catalytic tyrosine in *EcFSA* as well as in the transaldolase variants with enhanced aldolase activity (variants containing Phe¹³² → Tyr mutation, referring to *TacTAL*).

The protonation state of the DHA-SCHIFF base intermediate (or carbanion/enamine intermediate, respectively) formed upon the aldol cleavage reaction discriminates between the two activities (transaldolase vs. aldolase). If the intermediate is present in its carbanion/enamine form, the transaldolase reaction will take place (reversible transfer of a DHA-unit to the carbonyl carbon of the acceptor aldose phosphate). In the case of the protonated intermediate (DHA-SCHIFF base), the aldolase reaction will occur (reversible cleavage). According to the analysis of the DHA-SCHIFF base intermediate trapped in the active site of the *TacTAL*_{E60Q/F132Y} variant, the relative orientation of the hydroxy group of the introduced tyrosine residue is favorable for direct proton transfer onto the intermediate's C3-atom. On the other hand, the geometry of the active site is unfavorable for a direct or water mediated protonation of this atom by the transaldolase specific acid-base catalyst glutamate. This observation explains why a single mutation of the phenylalanine residue to tyrosine in the active site of transaldolase provides the aldolase activity. When comparing the available structures of different transaldolases and aldolases, the respective acid-base catalysts can be subdivided in two groups: co-aligned (acid-base catalyst is oriented in same direction as the reactive lysine) and opposite-faced (acid-base catalyst is oriented towards the reactive lysine (TITTMANN, 2014)).

In this context, the single-mutation variant *TacTAL*_{F132Y} contains two potential acid-base catalysts in the active site: the co-aligned transaldolase specific Glu⁶⁰ and the opposite-faced aldolase specific Tyr¹³². This variant shows a stimulated aldolase activity and greatly impaired transaldolase activity. According to the pre-steady-state analysis the hydrolysis of the central DHA-SCHIFF base intermediate is not rate limiting for the conversion of F6P but one of the previous steps including F6P binding, formation of the intermediates (F6P-carbinolamine, F6P-SCHIFF base) and the release of the first product GA3P (first half-reaction). Compared to *TacTAL*_{wt}, the first half-reaction of the variant is at least three orders of magnitude slower. The additional replacement of the Glu⁶⁰ residue to glutamine restores the activity of the first half-reaction. The rate constant of this reaction for the *TacTAL*_{E60Q/F132Y} variant is comparable to that of the wild type enzyme and is not rate limiting anymore. Remarkably, the catalytic efficiency of the variant under the steady-state conditions is higher than that of the natural *EcFSA*. A similar situation was published for the transaldolase from *Escherichia coli* (STELLMACHER *et al.*, 2015). Here as well, an additional mutation of the transaldolase specific general acid-base catalyst (Glu⁹⁶) to a glutamine together with the introduced tyrosine residue (Tyr¹⁷⁸) results in a double-mutation variant (*EcTAL*_{E96Q/F178Y}) with higher aldolase activity compared to the single-mutation variant (*EcTAL*_{F178Y}).

While the replacement of Glu⁶⁰ by glutamine together with the introduced Phe¹³² → Tyr mutation improves the rates of the first half-reaction in the *TacTAL*_{E60Q/F132Y} variant compared to *TacTAL*_{F132Y}, a single Glu⁶⁰ → Gln mutation in the active site of *TacTAL* impairs the first half-reaction by two orders of magnitude in *TacTAL*_{E60Q} compared to the wild type. Furthermore, the *TacTAL*_{E60Q} variant was previously described to show greatly impaired transaldolase steady-state activity, without the stimulation of the aldolase activity (LEHWESS-LITZMANN, 2011; LEHWESS-LITZMANN *et al.*, 2011b). A complementary replacement of the corresponding glutamine residue by a glutamate in the active site of *EcFSA* would result in an *EcFSA*_{Q59E} variant with similar acid-base situation as in the case of the *TacTAL*_{F132Y} variant (two potential acid-base catalysts Glu and Tyr are present in the active site). The aldolase activity of this variant is reported to be impaired compared to the wild type *EcFSA* (STELLMACHER *et al.*, 2015). The relation between *EcFSA*_{Q59E} and *EcFSA*_{wt} is the same as the relation between *TacTAL*_{F132Y} and *TacTAL*_{E60Q/F132Y}. Surprisingly, the double-mutation variant of *EcFSA* (*EcFSA*_{Q59E/Y131F}) did not show any transaldolase activity, although the acid-base situation in this variant is the same as in *TacTAL* (STELLMACHER *et al.*, 2015). Moreover, this variant is not able to catalyze the aldolase reaction anymore.

In other words, the presence of both potential acid-base catalysts (co-aligned glutamate and opposite-faced tyrosine) impairs catalysis of the aldolase reaction, especially its first half-reaction (all steps until the release of the first product), which becomes rate limiting. A prominent exception is the mammalian glycolytic enzyme fructose-1,6-bis(phosphate) aldolase (FBPA) which contains both: a glutamate residue at the position corresponding to the transaldolase specific general acid-base glutamate and a tyrosine residue positioned equivalently to the FSA specific general acid-base tyrosine (TITTMANN, 2014). Nevertheless, the mammalian FBPA efficiently catalyzes the cleavage of the substrate fructose 1,6-bis(phosphate). During the catalysis of the first half-reaction of the mammalian FBPA, the glutamate residue acts as the acid-base catalyst akin to the catalysis of the corresponding reaction by transaldolase (figure 2.3.36), while the catalytic tyrosine residue located at the C-terminal position of the flexible C-terminus is not present in the active site (MAURADY *et al.*, 2002; ST-JEAN *et al.*, 2005). Once the first half-reaction is completed and the first product GA3P is released, the C-terminal tyrosine enters the active site at a position favorable for the protonation of the central DHAP-carbanion/enamine intermediate similar to the reaction of FSA (ST-JEAN AND SYGUSCH, 2007). Interestingly, the treatment of the FBPA enzyme with carboxypeptidase giving a truncated version of the enzyme, which does not contain the C-terminal tyrosine residue, results in loss of the aldolase activity but in stimulation of the transaldolase activity (ROSE *et al.*, 1965). However, archeal fructose-1,6-bis(phosphate) aldolases catalyze the reaction using only a tyrosine residue as multi-functional acid-base catalyst similar to *EcFSA* (TITTMANN, 2014). The reason for the impaired donor half-reaction in presence of both acid-base catalysts is unclear. One possible explanation could be the re-orientation of the hydrogen bond network in the active site of the variants with both acid-base catalysts, resulting in a for the catalysis unfavorable orientation of the hydrogen atoms.

Aside from the difference in the acid-base situations in the active sites of *TacTAL* and *EcFSA*, the direct environment of the reactive lysine differs in both enzymes as well. While the transaldolase contains the hydrophilic residues Ser⁵⁸, Asn¹⁰⁸ and Ser¹³⁰, in the active site of *EcFSA* these residues are replaced by the hydrophobic residues Phe, Ala and Leu, respectively. In order to investigate the impact of these residues for the catalysis, a five-fold variant was generated (*TacTAL*_{FSA-mimic}). The active site of the variant contains the previously introduced mutations Glu⁶⁰ → Gln and Phe¹³² → Tyr as well as the hydrophobic residues as described before (Ser⁵⁸ → Phe, Asn¹⁰⁸ → Leu and Ser¹³⁰ → Ala).

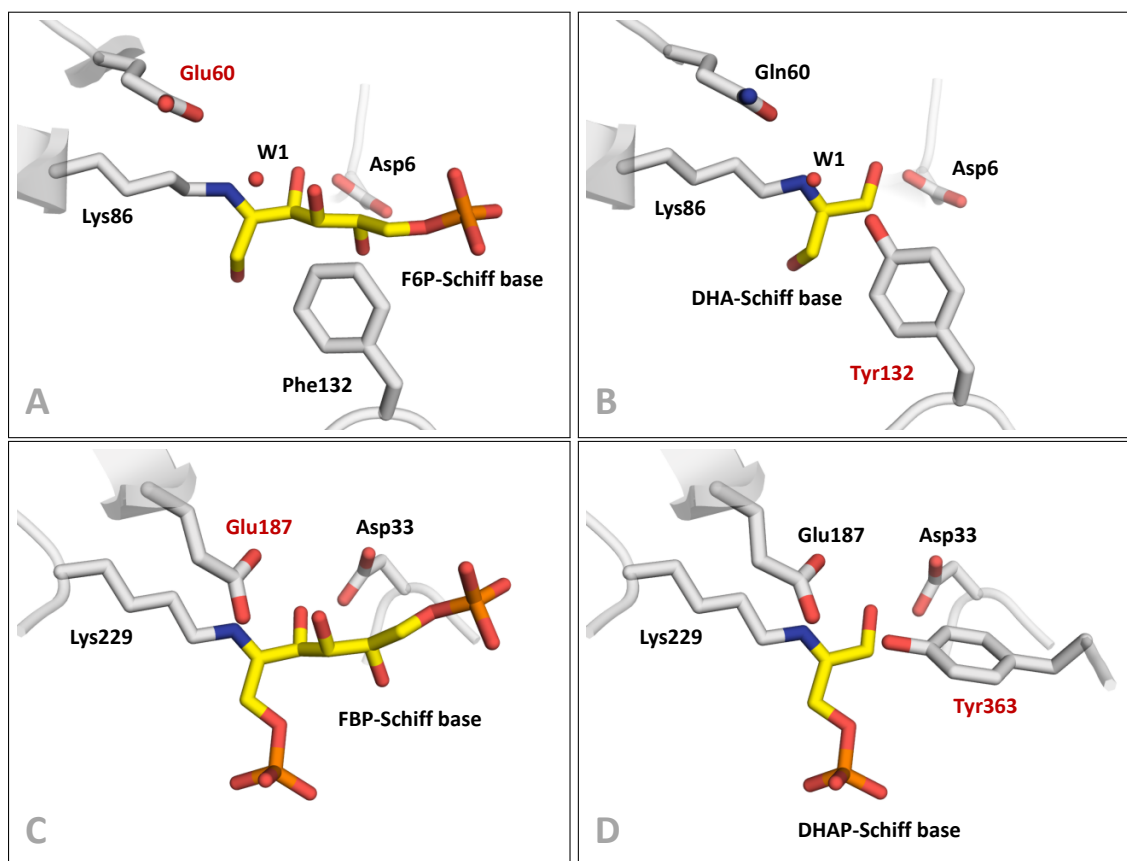


Figure 2.3.36: Comparison of the active sites of *TacTAL*_{wt} and *TacTAL*_{E60Q/F132Y} with the mammalian FBPA. The selected active site residues (gray) and the respective intermediates (yellow) are shown as sticks. The catalytic water molecule (W1) is shown as red sphere. The residue acting as acid-base catalyst is highlighted in red. **A:** *TacTAL*_{wt} with F6P-Schiff base intermediate. The co-aligned glutamate is the multi-functional acid-base catalyst for all steps of the catalysis. **B:** *TacTAL*_{E60Q/F132Y} with DHA-Schiff base intermediate. The opposite-faced tyrosine is the multi-functional acid-base catalyst for all steps of the catalysis. **C:** Mammalian FBPA with FBP-Schiff base intermediate. The co-aligned glutamate is the acid-base catalyst for the first half-reaction of the catalysis. The catalytic tyrosine is absent in the active site. PDB entry: 1ZAI (ST-JEAN *et al.*, 2005). **D:** Mammalian FBPA with DHAP-Schiff base intermediate. The opposite-faced tyrosine is now present in the active site to perform the protonation of the carbanion/enamine intermediate, which is necessary for the hydrolysis. PDB entry: 2QUU (ST-JEAN AND SYGUSCH, 2007).

Surprisingly, the *TacTAL*_{FSA-mimic} variant shows the lowest aldolase activity compared to other variants analyzed in this work, although the topology of the active site of the variant is nearly equal to that of *EcFSA*. However, the aldolase activity of the variant is one order of magnitude higher than the aldolase side reaction of *TacTAL*_{wt}. The first half-reaction for the conversion of F6P by *TacTAL*_{FSA-mimic} is not impaired, according to the pre-steady-state analysis. This finding implies that the introduction of the hydrophobic surface in the direct environment of the catalytic lysine

affects at least one step in the catalysis after the release of the first product (protonation of the carbanion/enamine intermediate, hydrolysis of the DHA-SCHIFF base intermediate and/or the release of the second product DHA).

The variant shows a different pH dependency of the turnover number under steady-state conditions. While the observed aldolase activities of the *TacTAL*_{F132Y} and *TacTAL*_{E60Q/F132Y} variants plotted versus pH exhibit bell-shaped curves with an optimum at pH around 7.9, the *TacTAL*_{FSA-mimic} variant shows a sigmoidal progression with the highest aldolase activity at pH ≥ 8.5 . A measurement of the steady-state activity at the pH values higher than 9.5 was not possible because of the limitations of the three-component buffer system used in the assay. Regarding this pH properties, the *TacTAL*_{FSA-mimic} variant behaves similar to the natural *EcFSA* (STELLMACHER *et al.*, 2015).

The hydrophobic environment of the reactive lysine in *EcFSA* is suggested to lower the pK_a of the lysine (STELLMACHER *et al.*, 2015). However, a mutation of the alanine residue located in this environment (Ala¹²⁹) to a serine residue as present in the active site of transaldolase (Ser¹³⁰) results in an *EcFSA*_{A129S} variant with significantly improved catalytic efficiency (CASTILLO *et al.*, 2010). Recently, a number of variants with regard to this area of the active site of *EcFSA* were designed and analyzed (GÜCLÜ *et al.*, 2016; SZEKRENYI *et al.*, 2014). In these studies, the examined variants showed a broad range of selectivity for different donor-substrates giving a good tool for applications in synthetic chemistry.

In contrast to *EcFSA*, the corresponding residues in the active site of *TacTAL* are substituted by the hydrophilic residues Ser⁵⁸ (Phe in *EcFSA*), Asn¹⁰⁸ (Leu) and Ser¹³⁰ (Ala). This residues form a hydrogen bond network with each other. Moreover, Ser¹³⁰ coordinates the C1 hydroxy group of the intermediate. The C1OH-group of the F6P-SCHIFF base intermediate trapped in the active site of *TacTAL*_{wt} exhibits two alternative conformations („up“ and „down“). In its „up“ conformation the C1OH-group is coordinated by Thr¹¹⁰, while the aforementioned residue Ser¹³⁰ coordinates the „down“ conformation.

The C1 hydroxy group is the direct neighbor of the carbonyl group in the F6P molecule. This carbonyl group is directly involved in the formation of the covalent intermediate, which is essential for the catalysis. The covalent intermediate such as carbinolamine is formed upon the nucleophilic attack of the ϵ -amino group of the enzyme's reactive lysine onto the substrate's carbonyl group. In this context, the coordination of the neighboring C1 hydroxy group could be important for the

correct orientation of the carbonyl group for the nucleophilic attack and for the proper positioning of the intermediates appearing during the catalytic cycle (SCHÖRKEN *et al.*, 2001).

In the present work, the interaction of the substrate's „down“ conformer with the active site was investigated. This interaction was interrupted by removing the interaction partners in the direct environment of the C1 hydroxy group in the *TacTAL*_{N108A/S130A} variant, or by removing the C1OH-group using A5P as donor-substrate.

In previous work, it could be shown that A5P can be converted by transaldolase and acts as alternative substrate at least during the donor half-reaction (SAUTNER, 2012). The conversion of A5P by *EcFSA* was described as well (GARRABOU *et al.*, 2009; GUÉRARD-HÉLAINE *et al.*, 2015).

The analysis of the donor half-reaction of the *TacTAL*_{N108A/S130A} variant in a single-turnover reaction with F6P and of the wild type in reaction with A5P showed that in both cases the reaction is greatly impaired. Importantly, the observed first order rate constants for both reactions are nearly equal to each other. These constants are two orders of magnitude lower than the corresponding rate constant for single-turnover conversion of the natural donor-substrate by the wild type enzyme. These results demonstrate the importance of the interactions between the substrate's C1OH-group and the active site for the catalysis.

The structure of the A5P-SCHIFF base intermediate trapped in the active site of the wild type enzyme is comparable to that of the F6P-SCHIFF base intermediate. However, the intermediate is shifted towards the entrance of the active site resulting in a relaxed all-*trans* conformation of the SCHIFF base-forming lysine residue. Compared to the structure of the wild type enzyme with the F6P-SCHIFF base intermediate in the active site, the catalytic water molecule in the structure containing A5P-SCHIFF base intermediate is displaced as well. These minor differences in the relative orientation of the SCHIFF base intermediate and the catalytic water could contribute to the low reactivity of A5P in reaction of *TacTAL*. The position of the catalytic water molecule relatively to the intermediate is assumed to be important for the catalysis, since this water facilitates the proton transfer between the general acid-base catalyst and the intermediate (SCHÖRKEN *et al.*, 2001). A comparable A5P-SCHIFF base intermediate structure observed in the active site of the transaldolase from *Francisella tularensis* (*FtuTAL*) was recently published by LIGHT AND ANDERSON (2014).

A5P was described as competitive inhibitor of transaldolases from different organisms (CAILLAU AND PAUL QUICK, 2005; SPRENGER *et al.*, 1995; WILLIAMS *et al.*, 1978). Taking into account the present

results, A5P is most likely a competitive high affinity but low activity substrate of transaldolase as previously suggested (LIGHT AND ANDERSON, 2014; SAUTNER, 2012). In the single-turnover reaction of wild type with A5P, the enzyme is already saturated at A5P concentration of ~ 0.5 mM, which is one order of magnitude lower than the concentration of F6P needed to saturate the enzyme under comparable conditions.

Although the *TacTAL*_{N108A/S130A} variant showed a similar decrease in activity in single-turnover reaction with F6P as in the case of the reaction of wild type with A5P, the structure of the F6P-SCHIFF base intermediate observed in the active site of the variant is comparable to that of the intermediate in the active site of the wild type enzyme.

Remarkably, in the active sites of both structures with perturbed C1 hydroxy group coordination (*TacTAL*_{N108A/S130A} + F6P and *TacTAL*_{wt} + A5P) an additional water molecule was observed occupying the positions of the absent groups, which is not present in the active site of the wild type enzyme with F6P-SCHIFF base intermediate. However, the positions of these water molecules are not equivalent in both structures. The contribution of this water molecule to the perturbation of the activity remains unclear.

Previously, the single-mutation variants (*TacTAL*_{N108A} and *TacTAL*_{S130A}) were analyzed structurally and kinetically (SAUTNER, 2012). Both variants showed significantly affected single-turnover conversion of F6P. Surprisingly, this effect was much stronger in the case of the *TacTAL*_{N108A}-variant, although the residue Asn¹⁰⁸ in the structure of the wild type does not directly interact with the SCHIFF base intermediate but coordinates the residue Ser¹³⁰. Notably, in the active site of the *TacTAL*_{N108A}-variant an additional water molecule could be observed as well. In the structure of the *TacTAL*_{S130A} variant, the C1 hydroxy group of the intermediate was coordinated by the Asn¹⁰⁸ residue. This observation implies that the Asn¹⁰⁸ residue can transiently coordinate the intermediate's hydroxy group in the wild type enzyme, for example during the conformational change from „up“ to „down“ conformation (rotation around the C1-C2 bond).

In the active sites of all these structures, the C1 hydroxy group was present in both conformations, even in the *TacTAL*_{N108A/S130A} variant, in which both possible interaction partners are absent. The only exception is the F6P-SCHIFF base intermediate observed in the active site of the *TacTAL*_{FSA-mimic} variant, where the C1 hydroxy group was coordinated only by the Thr¹¹⁰ residue, corresponding to the „up“ conformation. In the case of the *TacTAL*_{FSA-mimic} variant, the coordination of the „down“ conformation is not possible because of the introduced mutations

(Ser⁵⁸ → Phe, Asn¹⁰⁸ → Leu and Ser¹³⁰ → Ala). Interestingly, the single-turnover conversion of F6P was not significantly affected in the variant, but the aldolase specific second half-reaction.

The residue Ser¹⁷⁶ in the active site of *Escherichia coli* transaldolase (*EcTAL*) corresponding to the Ser¹³⁰ of *TacTAL* was analyzed by SCHÖRKEN *et al.* (2001). A replacement of this residue by alanine results in an *EcTAL* variant showing only 2.5 % residual transaldolase activity. The importance of this residue for the coordination of the substrate's C1 hydroxy group and for the correct orientation of the intermediates was proposed. This serine residue is conserved in transaldolases as well as in fructose-1,6-bis(phosphate) aldolases (JIA *et al.*, 1996).

The investigation of the impact of the interaction of the substrate's „up“ conformer with the residue Thr¹¹⁰ for the catalysis is difficult. This residue is strictly conserved in transaldolases and suggested to play a multi-functional role in substrate binding and catalysis, such as the coordination of the catalytic water molecule (SCHÖRKEN *et al.*, 2001). Furthermore, this threonine residue was suggested to coordinate the C2 hydroxy group of the covalently linked carbinolamine intermediate formed upon nucleophilic attack on the carbonyl group by the reactive lysine. In previous works, this residue was replaced by an isosteric valine residue (LEHWESS-LITZMANN, 2011). The resulting variant showed a greatly impaired transaldolase activity. However, this effect cannot be strictly assigned to the interruption of the hydrogen bond with the C1 hydroxy group in its „up“ conformation alone, because of the multi-functionality of the threonine residue.

In the wild type structure co-crystallized with M1P as carbinolamine mimic the corresponding group is indeed coordinated by Thr¹¹⁰. The relative orientation of M1P fits well to the orientation of the F6P-carbinolamine intermediate observed in the active site of *TacTAL*_{T30C/D211C} variant soaked with F6P. A catalytic water molecule is not present in the active sites occupied by the carbinolamine intermediate or mimic M1P. A resting state water molecule located in the area between the position of the carbinolamine's C2 hydroxy group and the position of the catalytic water molecule observed in the structure containing F6P-SCHIFF base intermediate is most probably replaced by the substrate's C2 oxygen along with the binding process and the carbinolamine formation as previously assumed by LEHWESS-LITZMANN (2011) and TITTMANN (2014) for the transaldolase. A similar situation was reported for the 2-keto-3-deoxy-6-phosphogluconate aldolase (FULLERTON *et al.*, 2006). In the latter case, the eliminated water molecule transiently co-exists with the catalytic water molecule in the active site. Both water molecules act as separated proton relays in different catalytic steps.

According to the proposed mechanism of catalysis of transaldolase, the carbinolamine's C2 hydroxy group is protonated by the general acid-base catalyst Glu⁶⁰ necessary for the SCHIFF base intermediate formation upon water elimination. In the structure of the carbinolamine intermediate, there is not enough space for a catalytic water molecule between the carbinolamine's C2 hydroxy group and the general acid-base catalyst Glu⁶⁰. Therefore, the direct protonation of the hydroxy group by the glutamate is assumable. This however, would require locale flexibility of the intermediate and/or catalytic glutamate because the distance between the respective groups is too long for an interaction. It should be noted that a mechanism, in which a water molecule facilitates the proton transfer before the SCHIFF base is formed, cannot be excluded for sure. However, in this case the regional flexibility is also necessary, which would allow enough space between the catalytic glutamate and the hydroxy group of the intermediate for the transient presence of such a water molecule.

Similar crystallographic studies were performed for fructose-1,6-bis(phosphate) aldolase (FBPA; (LAFRANCE-VANASSE AND SYGUSCH, 2007; ST-JEAN *et al.*, 2005)). In these studies, mannitol-1,6-bis(phosphate) (MBP) was used as the mimic for the carbinolamine intermediate. In contrast to *TacTAL*_{wt} co-crystallized with MIP, the carbinolamine specific hydroxy group of MBP trapped in the active site of rabbit muscle FBPA is located in hydrogen bond distance from the acid-base catalyst glutamate (ST-JEAN *et al.*, 2005).

In the structure of the disulfide variant *TacTAL*_{T30C/D211C} soaked with the substrate F6P the F6P-carbinolamine intermediate could be observed. Albeit the moderate resolution (2.5 Å), this is the first observation of a natural carbinolamine intermediate for the class of enzymes. The relative orientation of the intermediate in the active site corresponds well to that of the carbinolamine mimic MIP bound in the active site of *TacTAL*_{wt}.

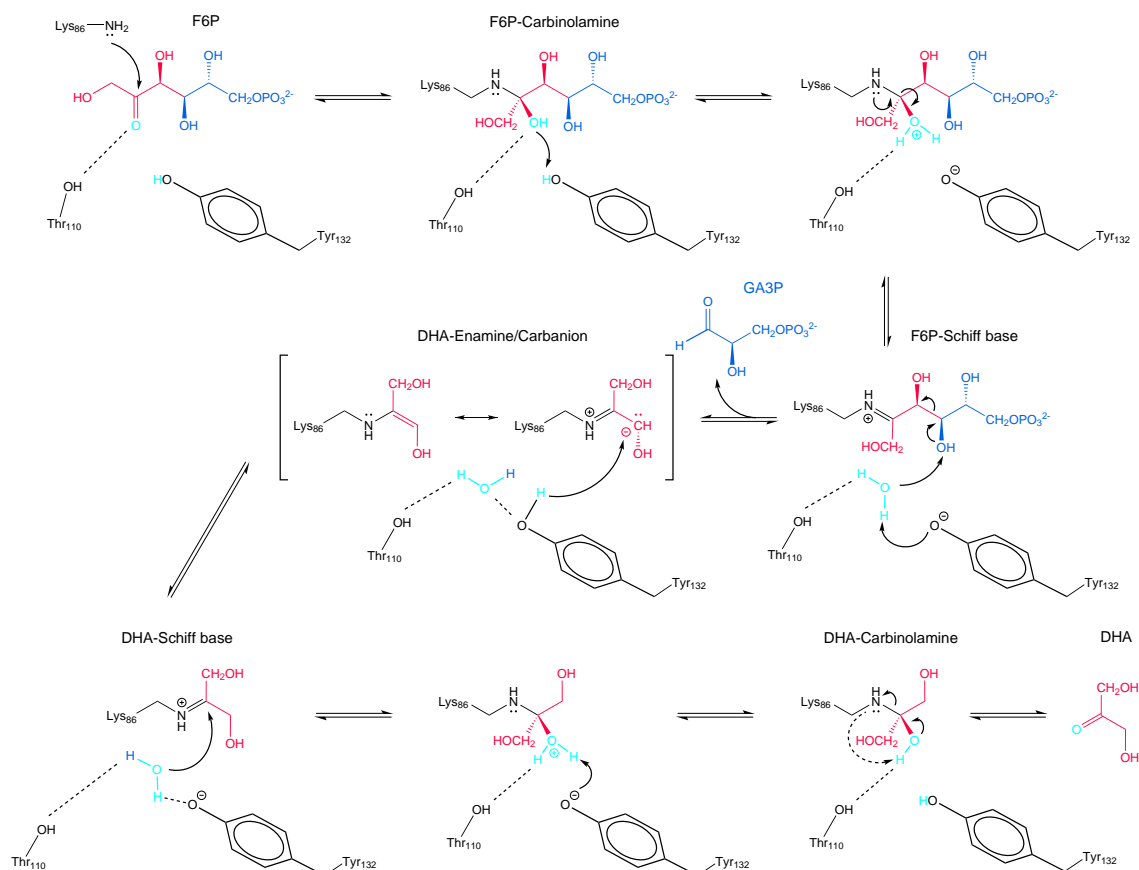
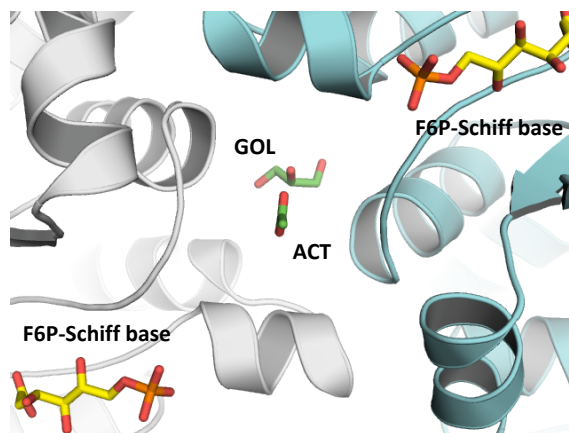
In the structure of the catalytically inactive *TacTAL*_{K86Q} variant with the F6P-MICHAELIS-complex, a catalytic water molecule is absent as well. The sugar's carbonyl oxygen is oriented towards the virtual position of this water molecule. This observation supports the suggestion that the catalytic water molecule is not present in the active site before the SCHIFF base intermediate is formed. Most likely, the catalytic water is a result of the water elimination upon the protonation of the C2 hydroxy group of the carbinolamine intermediate. Once formed, this water molecule can facilitate the proton transfer during the catalysis of the further reaction steps such as water-mediated deprotonation of the C4 hydroxy group of the intermediate by the acid-base Glu⁶⁰.

In the active sites of the *TacTAL* variants with enhanced aldolase activity *TacTAL*_{E60Q/F132Y} and *TacTAL*_{FSA-mimic} containing F6P-SCHIFF base intermediate, the catalytic water molecule is absent as well (or present with low occupancy). In the case of these variants, the introduced general acid-base Tyr¹³² can participate in all proton transfer reactions directly, in contrast to the transaldolase specific catalyst Glu⁶⁰.

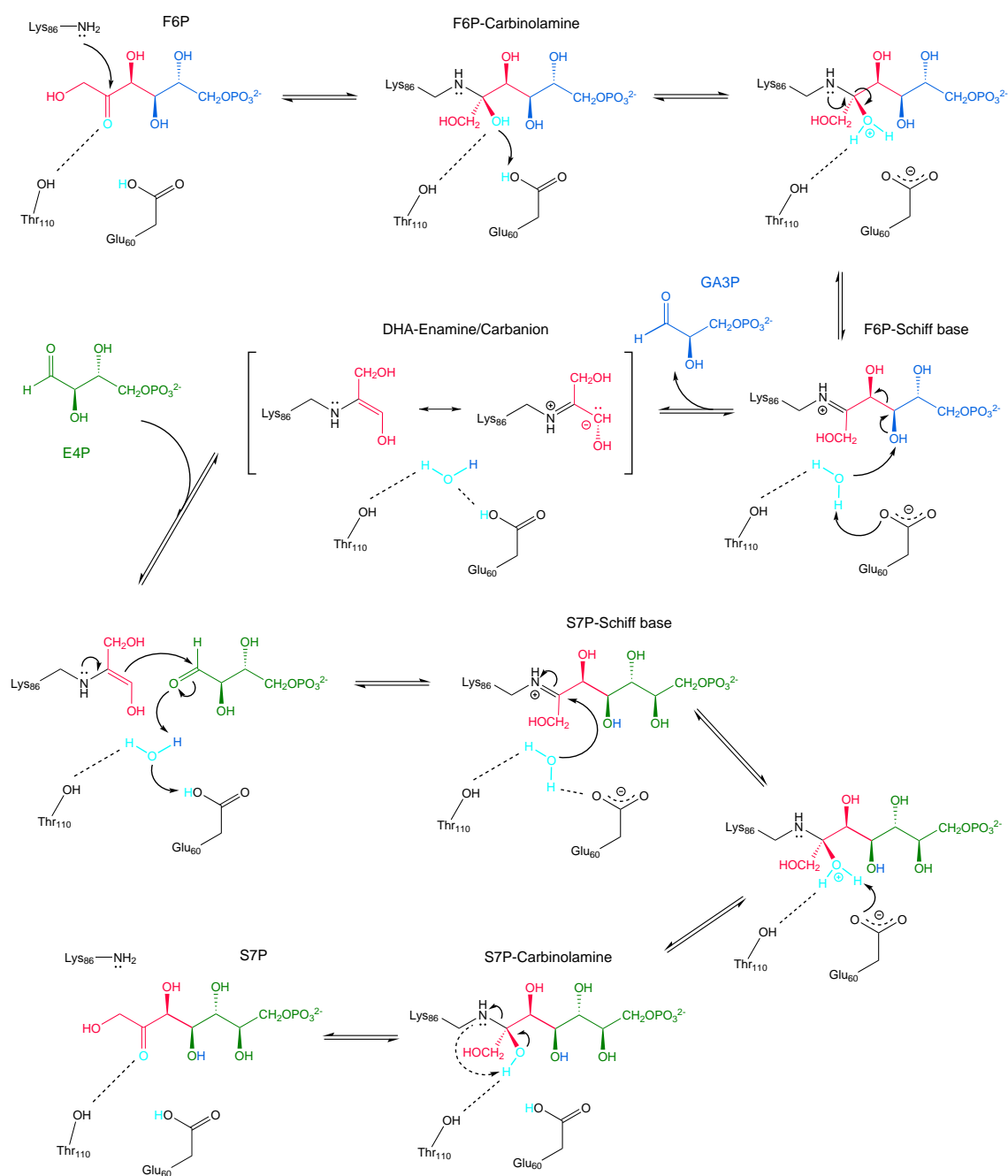
The proposed mechanisms for the reactions catalyzed by *TacTAL* and FSA (illustrated on *TacTAL*_{E60Q/F132Y}) are shown in schemes 2.10 and 2.9, respectively. These catalytic mechanisms are comparable to the mechanisms reported by LEHWESS-LITZMANN (2011) and STELLMACHER *et al.* (2015).

The single-turnover analysis of the wild type enzyme shows a non-hyperbolic dependency of the observed first order rate constants on the substrate concentration. While the rate constants increase with increasing substrate concentration up to ~5 mM, the rate constants are decreasing at higher concentrations of F6P. The origin of this observed substrate induced inactivation remains unclear. A possible explanation could be a negative cooperativity between the monomers of the homopentamer or homodecamer as previously suggested by LEHWESS-LITZMANN *et al.* (2011b). An allosteric inhibition, in which the substrate binds to an additional binding site, would be another explanation. However, in the available structures of *TacTAL* co-crystallized or soaked with F6P the substrate was never observed bound at a different location as the active site. In all available structures of *TacTAL*, a glycerol and an acetate molecules are bound between the entrances of the opposite active sites of the homodecamer (figure 2.3.37). Both substances are present in the crystallization solution. The glycerol molecule is coordinated by the residues Asp¹³⁷ and Arg¹⁷⁶. The acetate molecule is coordinated by Asn¹⁷⁰. This cavity could be a potential allosteric binding site for the acceptor substrate E4P or product GA3P. However, there is no evidence for binding of F6P to this site. The presence of these additional ligands could be a crystallographic artifact. Further studies with this regard are required.

Figure 2.3.37: Glycerol and acetate molecules bound between two opposite active sites of the homodecamer. Glycerol and acetate molecules (green) and F6P bound as SCHIFF base (yellow) in the active sites of the opposite subunits in the homodecamer are represented as sticks. The subunits belonging to the interacting homopentamers (gray/cyan) are represented as secondary structure.



Scheme 2.9: Proposed mechanism for the catalysis of the FSA reaction illustrated on *TacTAL*_{E60Q/F132Y} variant. A tyrosine residue is the general acid-base catalyst.



Scheme 2.10: Proposed mechanism for the catalysis of the *TacTAL* reaction. A glutamate residue is the general acid-base catalyst.

2.4 Outlook

The results reported in the present work together with those of the preceding works of LEHWESS-LITZMANN (2011) form a good basis for further investigations on transaldolase from *Thermoplasma acidophilum*. Especially the dynamic process of the „open“/„closed“ conformational change should be analyzed in more detail. The observed rate constants for the equilibrium of the conformational change could be determined using temperature jump approach. The sequence of *TacTAL* contains two tryptophan residues. Both residues are located in the regions relevant for the „open“/„closed“ conformational change. The Trp¹⁹ residue is located in the flexible N-terminal part and the Trp²¹² residue in the C-terminal α -helix, which interacts with the flexible part. Preliminary temperature jump experiments using the fluorescence signal of these tryptophan side chains showed a time depending exponential change of the fluorescence after temperature jump.

The progress curves recorded in pre-steady-state region of the reaction of the *TacTAL*_{E60Q/F132Y} variant with F6P exhibit a lag phase, which is independent from the substrate concentration. This lag phase is assumed to describe the „open“/„closed“ conformational change process in solution. In order to prove this assumption, a disulfide bridge can be introduced in the *TacTAL*_{E60Q/F132Y} variant. The resulting *TacTAL*_{E60Q/F132Y/T30C/D211C} variant, which is arrested in the „closed“ state, should not show such a lag phase in the beginning of the pre-steady state. However, the limitations of the local-arrest approach should be taken into account (regional flexibility could be possible).

Control measurements regarding the reduced form of *TacTAL*_{T30C/D211C} variant can be performed analyzing the *TacTAL*_{D211A} or *TacTAL*_{T30A} variants. These variants do not contain a disulfide bridge cross-linking the „closed“ conformation, but the hydrogen bond between the residues Thr³⁰ and Asp²¹¹ is absent too. Because this interaction is assumed to be important for the stabilization of the „closed“ state of the protein, the „open“/„closed“ equilibrium would be shifted towards the „open“ state as suggested for the *TacTAL*_{T30C/D211C} variant in its reduced form.

The communication between the subunits of *TacTAL* remain uninvestigated. Variants with regard to the binding site of glycerol and acetate *in crystallo* could be analyzed structurally and kinetically. If this binding site is not a crystallographic artifact, the variants *TacTAL*_{R176A} or *TacTAL*_{D137A} would show affected kinetic properties compared to the wild type enzyme. The residues Asp¹³⁷ and Arg¹⁷⁶ coordinate the glycerol molecule in *TacTAL* structures and are located between the entrances of the two opposite active sites of the homodecamer.

2.5 Summary

The results introduced in the present work are mainly based on the pre-steady state and steady-state analysis supported by structural information from crystallographic studies. Different variants of *TacTAL* were generated and analyzed, using these methods. The „closed“ conformation of *TacTAL* could be arrested in the *TacTAL*_{T30C/D211C} variant. It could be shown that the „closed“ state is important for the binding of the substrate F6P and the catalysis of the donor half-reaction (until the release of the first product GA3P). On the other hand, the „open“ conformation is necessary for the acceptor half-reaction (reaction with E4P and/or release of the second product S7P).

Furthermore, the transaldolase activity of *TacTAL* could be transformed into fructose-6-phosphate aldolase activity of the *TacTAL*_{E60Q/F132Y} variant. The acid-base situation in the active site of the variant is the same as in the active site of natural *EcFSA*. It could be shown, that the introduced Tyr¹³² residue takes over the role of the general acid-base catalyst Glu⁶⁰. This tyrosine residue is placed in favorable orientation for the direct protonation of the central carbanion/enamine intermediate, which discriminates between the aldolase and transaldolase activity.

The analysis of the interaction between the substrate's C1 hydroxy group and the active site showed that the deletion of the respective interaction partner on the part of the enzyme (*TacTAL*_{N108A/S130A} variant) or on the part of the substrate (A5P as substrate) results in comparable decrease of the donor half-reaction activity.

The binding mode of the substrate F6P in the active site of *TacTAL* as MICHAELIS complex was analyzed. To do so, the catalytically inactive variant *TacTAL*_{K86Q} was generated and co-crystallized with F6P. The carbonyl group of the substrate is oriented in an acute attacking angle relative to the lysine in the active site of the wild type enzyme. This angle is unfavorable for the nucleophilic attack of lysine's ε-nitrogen on the electrophilic carbonyl. However, the orientation of the substrate's carbonyl group in the active site of *TacTAL*_{K86Q} could be affected by the variant specific interaction.

Finally, the relative orientation of the F6P-carbinolamine intermediate in the active site was analyzed in the structure of *TacTAL*_{wt} co-crystallized with the carbinolamine mimic M1P. This structure corresponds well to those of the F6P-carbinolamine intermediate trapped in the active site of the *TacTAL*_{T30C/D211C} variant soaked with F6P. According to these structures, the C2 hydroxy group formed upon the nucleophilic attack of the catalytic lysine residue on the substrate's carbonyl group is coordinated by the active-site residue Thr¹¹⁰. The catalytic water molecule is absent

in the active sites of those structures. This water molecule is present in structures containing the F6P-SCHIFF base intermediate and is assumed to mediate the proton transfer reactions during catalysis. The fact that the corresponding water molecule could not be observed in the active sites containing the F6P-carbinolamine intermediate or carbinolamine mimic underlines the previous suggestion that the catalytic water is a result of water elimination prior to the SCHIFF base formation (LEHWESS-LITZMANN, 2011; TITTMANN, 2014). Therefore, this water molecule cannot be present in steps before the SCHIFF base intermediate is formed. However, a transient presence of an equivalent resting state water molecule in the active site, which facilitates the protonation of the carbinolamine, cannot be excluded.

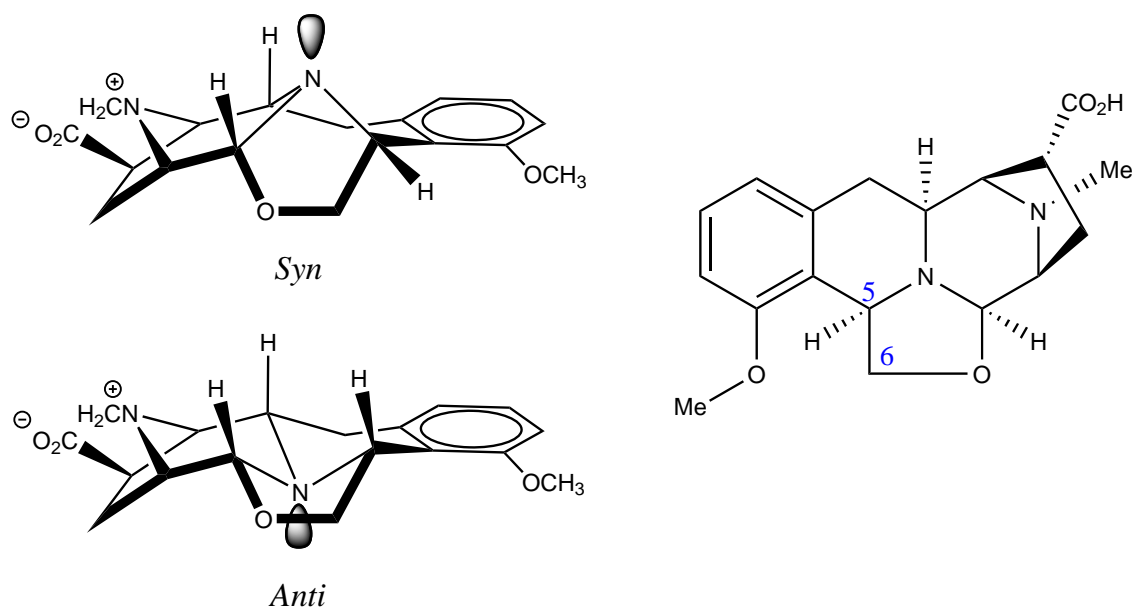
3 Preliminary Analysis of the QncN/L-M Protein System from *Streptomyces Melanovinaceus*

3.1 Introduction

3.1.1 Quinocarcin

Streptomyces melanovinaceus is a bacterium, which was first isolated from a soil sample and described by TOMITA *et al.* (1983). The strain produces a pigment resulting in a characteristic mauve wine color of the culture. This property is name giving for the organism. Furthermore, *Streptomyces melanovinaceus* produces and excretes the antibiotic quinocarcin.

Quinocarcin was first isolated from *Streptomyces melanovinaceus* culture broth by TAKAHASHI AND TOMITA (1983). The structure of the antibiotic (scheme 3.1) was determined by NMR spectroscopy and X-ray crystallography (HIRAYAMA AND SHIRAHATA, 1983; TAKAHASHI AND TOMITA, 1983). Quinocarcin belongs to the tetrahydroisoquinoline family of antibiotics. It exhibits an activity against gram-positive bacteria and an antitumor activity (SCOTT AND WILLIAMS, 2002).



Scheme 3.1: Structural formula of quinocarcin. Adapted from WILLIAMS *et al.* (1992).

Quinocarcin can adopt two alternative conformations (HILL *et al.*, 1988). The *syn* and *anti* conformations are shown in scheme 3.1. It could be shown that the *anti*-conformer can form an oxazolidinyl

radical (WILLIAMS *et al.*, 1992). The formation of this radical is necessary for the self-redox disproportionation resulting in the formation of superoxide followed by oxidative DNA cleavage (TOMITA *et al.*, 1984; WILLIAMS *et al.*, 1992). Furthermore, it was suggested that quinocarcin can directly interact with the DNA molecule (TOMITA *et al.*, 1984).

Since the first total synthesis for the quinocarcin was published by FUKUYAMA AND NUNES (1988) a number of synthesis strategies were reported (CHIBA *et al.*, 2012; SCOTT AND WILLIAMS, 2002; WU *et al.*, 2008). The most recent organic synthesis for quinocarcin was published by CHIBA *et al.* (2013).

3.1.2 The Role of the QncN/L-M Protein System in the Biosynthesis of Quinocarcin

The *in vivo* biosynthesis of the quinocarcin is catalyzed in a nonribosomal peptide assembly line (HIRATSUKA *et al.*, 2013; PENG *et al.*, 2012). Nonribosomal peptide assembly lines consist of nonribosomal peptide synthetases (NRPS). These enzymes catalyze peptide synthesis from single amino acids. Additionally, non-amino acids building blocks such as polyketides can be incorporated into the nonribosomal peptide assembly line (WINN *et al.*, 2016). The nonribosomal peptide synthetases are assembled from different modules. In general, a single module catalyzes the incorporation of one single building unit. Usually, each module is subdivided into three domains: the adenylation domain, the peptidyl carrier protein (PCP) domain and the condensation domain. The adenylation domain recognizes amino acids and activates the substrate as aminoacyl-AMP intermediate using ATP. Once activated, the building block can be transferred onto the thiol group of the phosphopantetheine moiety of the PCP domain. This results in a PCP-bound aminoacyl thioester. The PCP domain functionally related to the acyl carrier protein (ACP), a protein from fatty acid synthesis. The reactive group of these proteins is a phosphopantetheine moiety, which is covalently linked to a conserved Ser residue. The condensation domain catalyzes peptide bond formation between two activated PCP-bound aminoacyl thioester resulting in the formation of a PCP-bound dipeptidyl thioester, which can be further elongated in a similar way. The intermediates of the nonribosomal peptide assembly lines are always covalently linked to the PCP domain during synthesis, until the final product is formed. In many prokaryotes, the single modules are present as protein subunits, which interact with each other, rather than existing as a large multi-domain protein (WINN *et al.*, 2016). Beside this basic domain architecture, many assembly lines contain auxiliary

domains/proteins, which provide additional activities such as epimerization or redox reactions (WALSH, 2008).

The gene cluster of the nonribosomal peptide assembly line of the quinocarcin synthesis in *Streptomyces melanovinaceus* was recently identified and analyzed by HIRATSUKA *et al.* (2013). They proposed a biosynthetic pathway for quinocarcin based on results from bioinformatic, cell biological and kinetic methods. This pathway involves a group of proteins, which were previously described by PENG *et al.* (2012), namely the proteins QncN, QncL and QncM. These proteins are of particular interest, since they incorporate an unusual building unit (hydroxyacetyl moiety) derived from an unusual precursor (ketose phosphate) into the nonribosomal peptide assembly line of quinocarcin.

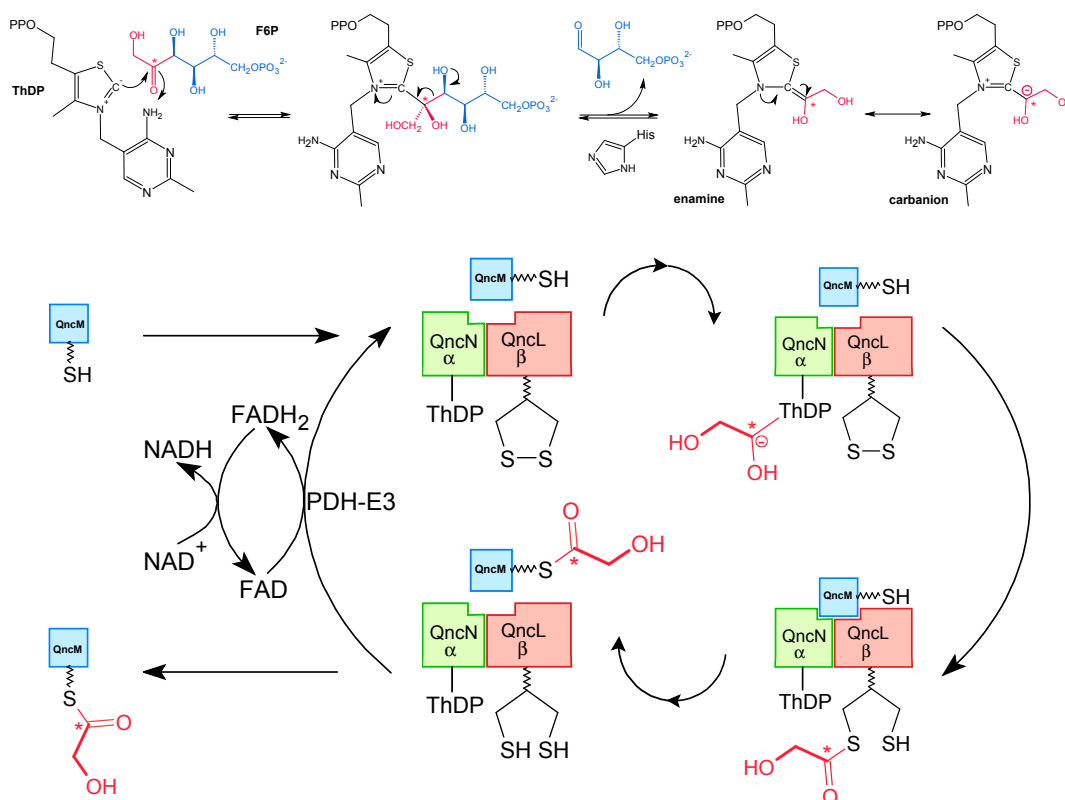
According to the sequence analysis, QncN, QncL and QncM proteins are similar to enzymes from central sugar metabolism. The QncN protein shows 64 % identity and 74 % similarity to the E1 α subunit of pyruvate dehydrogenase (PDH; EC 1.2.4.1) from *Streptomyces coelicolor* and is similar to the pyrophosphate-binding domain of transketolase (PENG *et al.*, 2012). The QncL protein can be subdivided in four domains (D1 – D4). The N-terminal D1 domain corresponds to the aminopyrimidine-binding domain of transketolase and the E1 β subunit of PDH. The D2 domain is similar to the C-terminal domain of transketolase. The D3 and D4 domains correspond to the lipoyl attachment and the catalytic domains of the E2 component of PDH complex (PDHc), respectively.

It was suggested, that the QncN and QncL components form a heterodimer similar to the $\alpha\beta$ heterodimer of the E1 component from PDHc. The human E1 component forms a dimer of $\alpha\beta$ heterodimers (CISZAK *et al.*, 2003). Two cofactor molecules (ThDP) bind on the interface between the two $\alpha\beta$ heterodimers. The cofactor binding is necessary for the catalysis of the decarboxylation of pyruvate, resulting in the formation of the 2-hydroxyethyl ThDP. This kind of higher oligomerization can be assumed for the QncN/L component as well.

The D3 and D4 domains of the QncL subunit are similar to the domains of the E2 component. This component of the PDHc is a dihydrolipoyl transacetylase (EC 2.3.1.12) and catalyzes the transfer of the C2 unit from the intermediate of the E1 reaction to the thiol group of the phosphopantetheine moiety of coenzyme A. The covalently bound lipoyl moiety is essential for the transfer reaction. This prosthetic group is located at the lipoyl attachment domain (D3 in QncL). The E2 component of the PDHc forms homotrimers (MATTEVI *et al.*, 1992). The active sites of the catalytic domains (D4 in QncL) are formed on the trimer interface. The E2 trimers are organized to oligomerization states of higher degree such as 20-mers or octamers of homotrimers (IZARD *et al.*, 1999; PERHAM

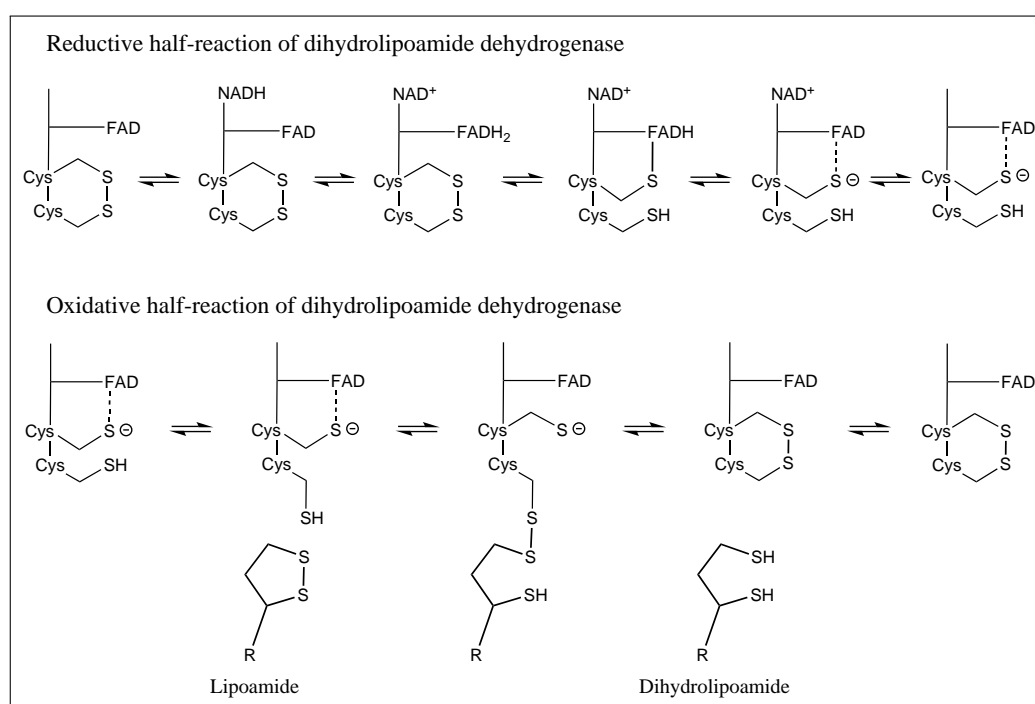
AND HOOPER, 1977; ZHOU *et al.*, 2001). A higher order of organization of the QncN/L heterodimers is therefore very likely.

PENG *et al.* (2012) could show that the QncN/L component catalyzes the ketol cleavage of ketose substrates from the pentose phosphate pathway (xylulose 5-phosphate, fructose 6-phosphate and sedoheptulose 7-phosphate) rather than the decarboxylation of pyruvate or hydroxypyruvate. Xylulose 5-phosphate was described as the best substrate for the QncN/L reaction. This reaction corresponds to the donor half reaction of transketolase, an enzyme from the pentose phosphate pathway. They proposed a catalytic mechanism in which the enzyme transfers a hydroxyacetyl unit resulting from the oxidative ketol cleavage of the ketose phosphate catalyzed by the QncN/L component to the thiol group of the phosphopantetheine moiety of the QncM component (scheme 3.2), which is homologous to the acyl carrier protein. The protein is suggested to supply the hydroxyacetyl unit, derived from the reaction of the QncN/L component into the nonribosomal peptide assembly line of the quinocarcin biosynthesis (HIRATSUKA *et al.*, 2013; PENG *et al.*, 2012). This hydroxyacetyl unit is the origin of the C5 and C6 atoms in the skeleton of quinocarcin (scheme 3.1).



Scheme 3.2: Proposed catalytic cycle of the QncN/L-QncM reaction. For explanation, see text. Adapted from PENG *et al.* (2012).

After the transfer of the hydroxyacetyl unit to the QncM molecule, the lipoyl moiety remains in its reduced form as dihydrolipoyl. The reoxidation of this group is necessary for the conversion of the next substrate molecule. The oxidation of the dihydrolipoyl group is assumed to be performed by the E3 component of PDHc (PENG *et al.*, 2012). The E3 component is a dihydrolipoamide dehydrogenase (EC 1.8.1.4) and catalyzes the reversible, NAD^+ -dependent oxidation of the dihydrolipoyl moiety resulting in the reoxidized lipoyl group and in generation of NADH. The active site of the enzyme contains a FAD molecule and a catalytic disulfide. The catalytic cycle of the E3 component can be subdivided in two half-reactions: oxidative and reductive half-reactions (ARGYROU *et al.*, 2002). The oxidative half-reaction consists of the catalytic steps leading to the oxidation of the dihydrolipoyl moiety, which results in the reduced E3 component (scheme 3.3). The reductive half-reaction includes the catalytic steps leading to the reduction of NAD^+ and the reoxidation of the enzyme.



Scheme 3.3: Proposed catalytic cycle of the E3 reaction. Adapted from ARGYROU *et al.* (2002).

3.1.3 Motivation

The QncN/L-M protein system is an interesting subject for kinetic and structural analysis. The proteins exhibit sequence similarity to enzymes from the central metabolism such as transketolase and pyruvate dehydrogenase complex. The QncN/L component combines the activities of transketolase and dihydrolipoyl transacetylase. The investigation of the catalytic cycle of this protein system can provide new information for a deeper understanding of the mode of action of these enzymes from the central metabolism.

The aim of the work presented here was to establish protocols for the expression and purification of the QncN/L and QncM components. Additionally, spectrophotometric kinetic methods for the analysis of the related enzymes transketolase and pyruvate dehydrogenase complex should be applied to the QncN/L-M protein system. Finally, crystallization conditions for the single components should be identified, providing the basis for the structural analysis of the system.

3.2 Results

3.2.1 Recombinant Expression and Purification of the QncN/L Component

In the present work, different DNA constructs were generated in order to establish a suitable expression and purification protocol for the QncN/L component yielding a reasonable amount of catalytic active protein.

The *SmeQncNML*-pET28a construct containing the native coding cassette from the *Streptomyces melanovinaceus* genome was tested for expression in different *E. coli* strains (section 1.6.2.3). The cultivation was performed in LB medium at 16 °C. Although the *SmeQncNML*-pET28a construct contains coding sequences for all three proteins (QncN, QncL and QncM) only the QncN protein was expressed in *E. coli* (DE3) BL21 StarTM and Rosetta 2 strains. However, after cell disruption the protein was in the insoluble fraction (figure 3.2.1).

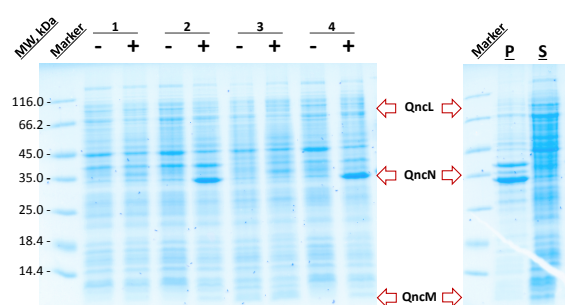


Figure 3.2.1: Expression of the QncN/L and QncM components from the *SmeQncNML*-pET28a construct (SDS-PAGE, 12 %). 1 – 4: different *E. coli* (DE3) strains (Rosetta, Rosetta 2, SoluBL21 and BL21 StarTM, respectively). -/+ : before and after induction with 200 μ M IPTG. P and S: pellet and supernatant fractions after cell disruption.

Another construct, which was tested for the expression, is the QncNL-pET-SUMO construct. In contrast to the *SmeQncNML*-pET28a construct, which contains DNA sequences isolated from the *Streptomyces melanovinaceus* genome, the coding sequences in the QncNL-pET-SUMO construct are codon optimized for the recombinant expression in *E. coli* strains. The expression of each component is controlled by the respective T7-promotor. His₆-tagged SUMO protein is fused to the QncN component (N-terminal). Two *E. coli* (DE3) strains (SoluBL21 and BL21 StarTM) were tested for the expression in three different cultivation media (LB, M9 minimal medium and ZYM5052 auto-induction medium) at 16 °C. In all cases, the expression of both proteins occurred properly but the proteins were in the insoluble fraction after cell disruption.

The published protocol for the recombinant expression and purification of the QncN/L component remains the best available protocol (PENG *et al.*, 2012). The proteins were recombinantly expressed in the BL21 StarTM *E. coli* (DE3) strain containing the QncNL-pCDFDuet-1 construct. This

construct includes codon optimized (*E. coli*) sequences for the QncN and QncL subunits. The sequence of the QncN protein contains an N-terminal His₆-tag. The protein was purified to homogeneity yielding ~0.25 mg protein per 1 g cell pellet.

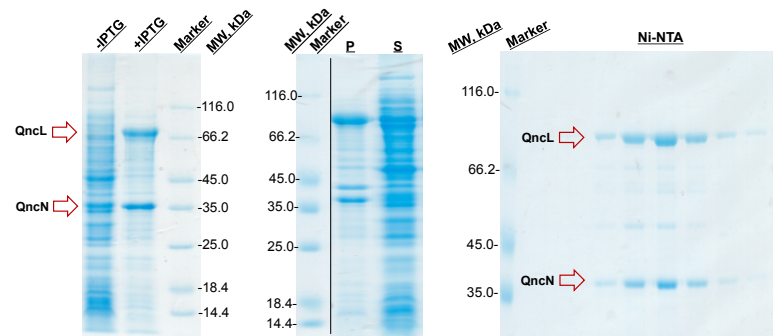


Figure 3.2.2: Expression and purification of the QncN/L component from the QncNL-pET-SUMO construct (SDS-PAGE, 12 %). -/+ IPTG: before and after induction with 50 μ M IPTG, respectively. P and S: pellet and supernatant fractions after cell disruption. NiNTA: fractions after Ni²⁺-NTA.

The lipoylation of the QncL subunit was verified by liquid chromatography mass spectrometry (data not shown). This post-translational modification is essential for the catalytic activity of the enzyme.

The activity of the protein for the substrate F6P was determined in presence of *SliE3* and holoQncM components as described in section 1.6.4.5. After ketol cleavage of the F6P and the transfer of a hydroxyacetyl unit to the phosphopantetheine-moiety of the holoQncM component the reduced lipoyl-moiety of the QncL subunit is reoxidized by the E3 component coupled to the conversion of NAD⁺ to NADH. The formation of NADH can be monitored spectrophotometrically at 340 nm (figure 3.2.3). The specific activity was determined to $A_{\text{spec}} = 34 \text{ mU/mg}$, which is comparable to the published activity (PENG *et al.*, 2012). After the storage of the protein on ice for one week, the activity of the enzyme dropped to ~20 %.

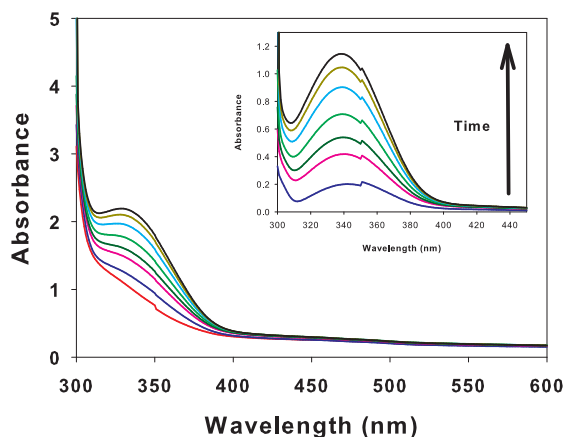


Figure 3.2.3: F6P-dependent reduction of NAD^+ in a spectrophotometric assay. The formation of NADH can be monitored at 340 nm. After ketol cleavage of the F6P and the transfer of a hydroxyacetyl unit to the phosphopantetheine-moiety of the holoQncM component the reduced lipoyl-moiety of the QncL subunit is reoxidized by the E3 component coupled to the conversion of NAD^+ to NADH. Inset: difference spectra using the start spectrum (red line) as baseline.

3.2.2 Recombinant Expression and Purification of the holoQncM Component

The implementation of the published expression and purification protocol for the holoQncM component results in very low protein yields (~ 0.25 mg per 1 g cell pellet). In order to improve the expression of the protein, the QncM-pET-SUMO construct was generated. This construct contains the codon optimized (*E. coli*) coding sequence for the QncM component fused to the His₆-tagged SUMO protein. The use of the QncM-pET-SUMO construct for the recombinant expression results in a significant improvement of the protein amount purified from 1 g cell pellet (~ 1.3 mg).

In order to find the best buffer conditions for the purification and storage of the protein, the ThermoFluor assay was applied (figure 3.2.4). The buffer conditions used for the storage of the protein are 100 mM imidazole (pH 7.4), 100 mM NaCl, 10 % (v/v) glycerol and 1 mM DTT. The flash frozen protein solution can be stored at -80°C for several months.

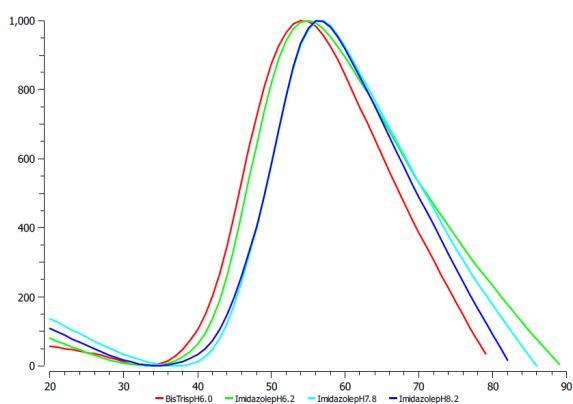


Figure 3.2.4: Normalized melting curves of the holoQncM protein in presence of SYPRO[®] Orange. The best four buffer conditions are represented: BisTris pH 6.0 (red), imidazole pH 6.2 (green), imidazole pH 7.8 (blue) and imidazole pH 8.2 (dark blue).

In order to recombinantly express the QncM SUMO-fusion protein in its physiological active holo-form, the Sfp-pQE60 plasmid (kindly provided by PROF. DR. M. A. MARAHIEL [Philipps-University,

Marburg]) was co-transferred into the QncM-pET-SUMO plasmid containing BL21 StarTM (DE3) *E. coli* strain. The Sfp-pQE60 plasmid contains the coding sequence for the phosphopantetheinyl transferase from *Bacillus subtilis* (*BsSfp*). *BsSfp* catalyzes the transfer of the phosphopantetheinyl moiety from CoA to the conserved Ser-residue of ACP homologs such as the QncM component (MARAHIEL *et al.*, 1997; MOFID *et al.*, 1999; PENG *et al.*, 2012; QUADRI *et al.*, 1998). The post-translational modification (phosphopantetheinylation of Ser³³) of the protein was verified by MALDI-TOF mass spectrometry (data not shown). The phosphopantetheinylation of the QncM component is necessary for its physiological function.

3.2.3 Crystal Structure of the holoQncM Component

After the automated crystallization screen (section 1.6.3) and subsequent additive screen (page 18) diffracting crystals of the holoQncM protein could be obtained. For the crystallization, 2 μ L of the protein solution (10 mg/mL holoQncM in 100 mM imidazole, 100 mM NaCl, 10 % (v/v) glycerol, 1 mM DTT, pH 7.4) were mixed at RT with 2 μ L of the reservoir solution (25 % (w/v) PEG-monomethyl ether 2000, 100 mM HEPES, pH 7.5) and 0.4 μ L of the additive solution (100 mM BaCl₂). This crystallization mix was equilibrated against 250 μ L of the reservoir solution according to the hanging-drop vapor diffusion approach. The crystals were grown for 7 – 10 days at 8 °C.

Single crystals were cryoprotected by transfer into 85 % (v/v) of the reservoir solution supplemented with 10 % (v/v) glycerol and 5 % (v/v) PEG400. The cryoprotection procedure was performed at 8 °C for ~30 s. The single crystals were flash frozen in liquid nitrogen and stored for several weeks.

The diffraction data were collected using synchrotron radiation (DESY, beamline P13, Hamburg, Germany) under cryogenic conditions (100 K). The data were processed as described in section 1.6.3.3. HoloQncM crystallizes in an orthorhombic space group P2₁2₁2₁. The initial phase determination was performed by DR. PIOTR NEUMANN (Department of Molecular Structural Biology, Institute for Microbiology and Genetics, Georg-August-University Göttingen) using the ARCIMBOLDO_LITE-software (SAMMITO *et al.*, 2015).

The resulting initial model containing twelve poly-alanine α -helices was completed manually using the Coot-software (EMSLEY *et al.*, 2010; EMSLEY AND COWTAN, 2004). The model was refined against the experimental data to 1.70 Å resolution (table A.4 in the appendix). The final model corresponds to the diffraction data with $R_{\text{work}} = 20.21\%$ and $R_{\text{free}} = 23.20\%$ (table A.8 in the appendix).

The crystallographic asymmetric unit contains three copies of the holoQncM molecule, which are arranged in a trimer. Each molecule consists of four α -helices connected by loops. In two of the three molecules, the residue Ser³³ is covalently modified by the phosphopantetheine moiety. Because only the phosphate moiety of the prosthetic group exhibits a proper electron density, only this part of the cofactor was modeled into the structure. The remaining parts (pantothenate and β -mercaptoethylamine) of the cofactor are assumed to be flexible. A flexible phosphopantetheine moiety of the holoQncM component corresponds well to its physiological function as carrier unit. The modified Ser³³ residues are oriented towards the three-fold symmetry axis of the trimer within the asymmetric unit.

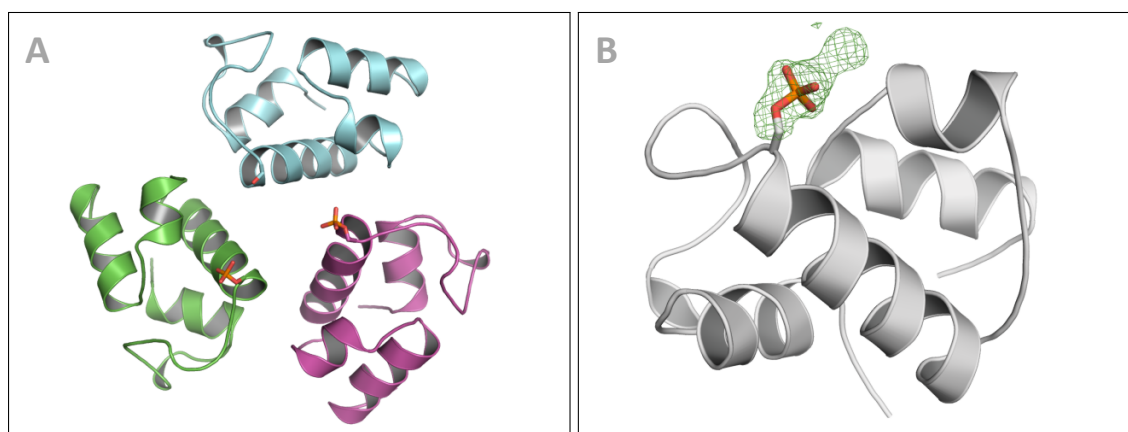


Figure 3.2.5: Crystal structure of the holoQncM protein. Polypeptide backbone is represented as secondary structure. **A:** Three copies of holoQncM in the asymmetric unit are represented as secondary structure. **B:** mF_o-DF_c simulated annealing omit map (green mesh, contour level 3.0σ). Only the phosphate group of the phosphopantetheine moiety covalently linked to Ser³³ was modeled (sticks).

Although the holoQncM component crystallizes as a trimer in the crystallographic asymmetric unit, this oligomerization state is assumed to be a crystallographic artifact. The SEC-MALS analysis of the oligomerization state of the holoQncM component in solution results in the detection of monomers and dimers but not of trimeric states.

3.2.4 Purification of the *SliE3* Component

The codon optimized (*E. coli*) sequence of *SliE3* was synthesized by GeneArtTM (Regensburg, Germany). The *SliE3* gene was supplied as an *NdeI/XhoI*-insert in pET28a vector (*SliE3*-pET28a). The coding sequence used in the present work starts with the sequence MHGGRDVANDAS. According to the actual sequence deposited in the UniProt-data bank (<http://www.uniprot.org>;

(UniProt Consortium, 2015)) the codon for the Val⁷ residue is annotated as start codon. This results in an offset (+6 aa) of the residue numbers of the sequence used in this work compared to the actual sequence in the data bank. In the present work, the residue numbering refers to the sequence used for the expression of *SliE3* component plus three amino acid residues remaining on the N-terminus after thrombin cleavage (section 1.6.2.9). The *SliE3* component was purified based on the protocol for the E3 homolog from *E. coli* (Tietzel, 2015). The purification results in 8 mg protein per 1 g of cell pellet.

In order to determine the concentration of the active sites containing FAD, the molar extinction coefficient of the enzyme bound cofactor was determined optically, using the intrinsic absorption signal of the cofactor at 458 nm (section 1.6.2.2). The molar extinction coefficient of the enzyme bound FAD was determined to $\epsilon_{458} = 11171 \text{ M}^{-1}\text{cm}^{-1}$ (figure 3.2.6). The comparison of the protein concentration determined using BRADFORD assay with the concentration of the enzyme bound FAD shows that ~70 % of the active sites are occupied by the cofactor. The presence of FAD in the active site of *SliE3* is necessary for its catalytic activity.

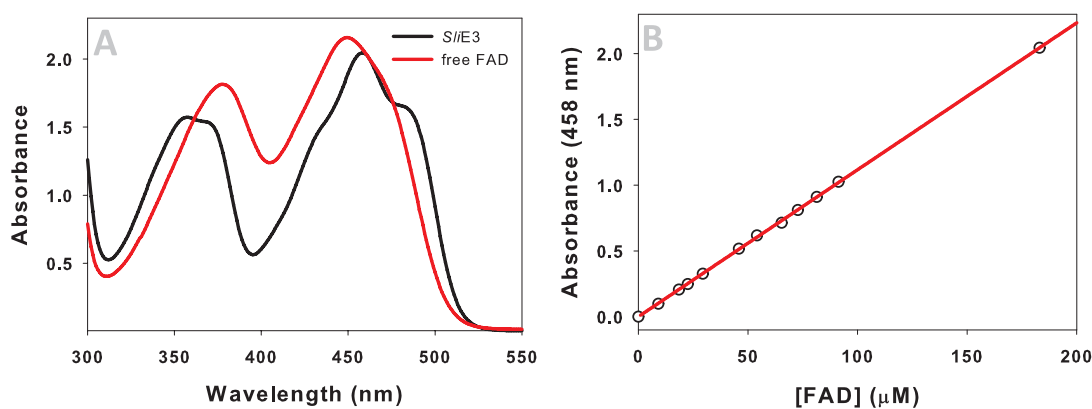


Figure 3.2.6: Molar extinction coefficient of the *SliE3* Bound FAD. **A:** Absorption spectra of the enzyme bound FAD (black line) and the free FAD after addition of 4.5 mM guanidinium chloride (red line). **B:** Absorbance of the *SliE3* containing solution (different concentrations) plotted versus the concentration of free FAD calculated from the absorbance after addition of 4.5 mM guanidinium chloride. The slope of the linear regression (red line) corresponds to the molar extinction coefficient of the enzyme bound FAD.

3.2.5 Steady-State Analysis of the *SliE3* Component

In the physiological context *SliE3* component uses NAD^+ to oxidize the dihydrolipoyl moiety (scheme 1.2 A in the methods). This reversible reaction results in the reoxidation of the lipoyl

moiety and in generation of reducing equivalents (NADH). The activity of the *SliE3* component was analyzed by measurement of the lipoamide reduction by the *SliE3* enzyme using NADH as reducing equivalent corresponding to the reverse physiological reaction (scheme 1.2 B in the methods). The NADH consumption was used to monitor the progress of the reaction as absorbance depletion at 340 nm (figure 3.2.7 A). The NAD^+ resulting from the reaction acts as an activator of the E3 component from *Mycobacterium tuberculosis* (ARGYROU AND BLANCHARD, 2001). This activation effect could be shown for the *SliE3* as well (figure 3.2.7 A). In order to avoid the perturbation of the initial phase of the reaction by the product activation effect of the concomitant NAD^+ formation, NAD^+ was added to the reaction mixture in a concentration resulting in constitutively activated E3 component according to ARGYROU AND BLANCHARD (2001).

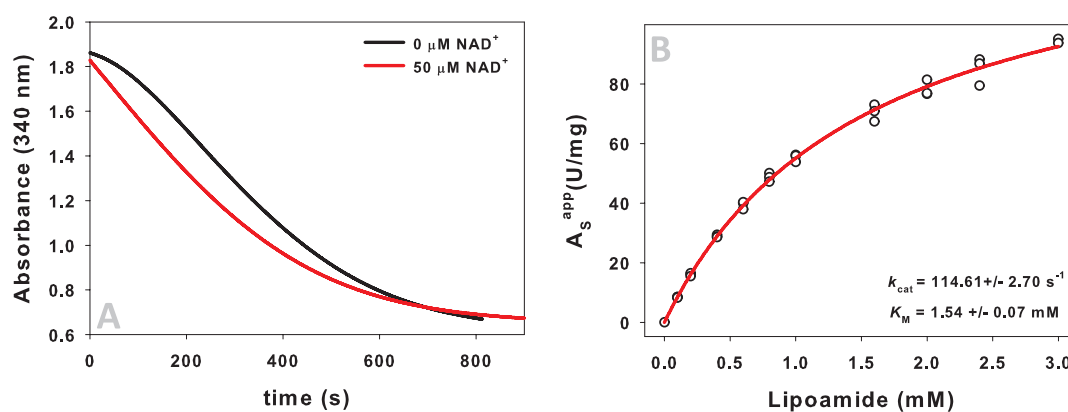


Figure 3.2.7: Steady-state analysis of *SliE3* in reaction with lipoamide and NADH. **A:** Representative progress curves in presence (red line) and absence (black line) of NAD^+ . Note the activation effect along with the NAD^+ formation during the first 150 s of the reaction (black line). **B:** MICHAELIS-MENTEN analysis of the reduction of lipoamide (0.1 – 3.0 mM) by *SliE3* (10 nM, 20 °C). The MICHAELIS-MENTEN fit (eq. 1.6.2, solid line) is indicated by red. Circles indicate the measured steady-state activity.

The turnover number was determined to $k_{\text{cat}} = 114.61 \pm 2.70 \text{ s}^{-1}$ (based on the concentration of the FAD containing active sites). The apparent MICHAELIS constant for substrate lipoamide is $K_{\text{M}}^{\text{app}} = 1.54 \pm 0.07 \text{ mM}$, resulting in the catalytic efficiency of $k_{\text{cat}}/K_{\text{M}}^{\text{app}} = 74.42 \text{ s}^{-1} \text{ mM}^{-1}$. Because of the low solubility of the substrate in water, the steady-state measurements could not be performed at lipoamide concentrations higher than 3 mM. Consequently, measurements at saturating concentrations of the substrate could not be performed (figure 3.2.7 B). The macroscopic kinetic constants resulting from the hyperbolic MICHAELIS-MENTEN fit were verified using the double reciprocal plot (LINEWEAVER AND BURK, 1934). The values calculated from the linear regression correspond well to the constants resulting from the hyperbolic fit (figure 3.2.8).

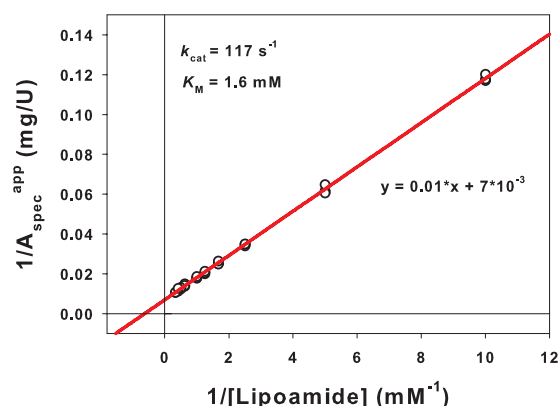


Figure 3.2.8: Double reciprocal plot for the lipamide conversion by *SliE3*.

3.2.6 Stopped-Flow Measurements of the *SliE3* Component

The catalytic cycle of the E3 component can be subdivided in two half-reactions: oxidative and reductive half-reactions (ARGYROU *et al.*, 2002). The oxidative half-reaction consists of the catalytic steps in up to the oxidation of the dihydrolipoyl moiety resulting in the reduced E3 component. The reductive half-reaction includes the catalytic steps corresponding to the reduction of NAD^+ and the reoxidation of the enzyme. Because all the catalytic steps are reversible, the enzyme can be reduced using NADH (reverse reductive half-reaction). As described by ARGYROU *et al.* (2002) the reverse reductive half-reaction can be subdivided in three phases: the formation of the NAD^+ - FADH_2 intermediate, the S^- -FAD charge transfer and the formation of the fully reduced enzyme (EH_4). The appearance of these phases corresponds to characteristic changes in the UV-Vis spectrum compared to that of the oxidized form of the E3 component (Eox).

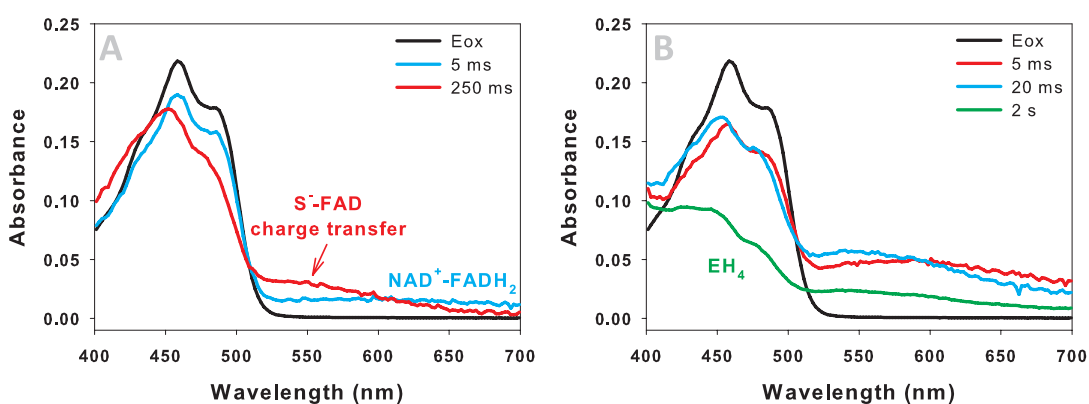


Figure 3.2.9: Stopped-flow measurements of the *SliE3* component. Eox: *SliE3* in its oxidized form (without the addition of NADH) **A:** 20 μM *SliE3* after mixing with 20 μM NADH. **B:** 20 μM *SliE3* after mixing with 200 μM NADH.

The formation of the NAD^+ -FADH₂ intermediate corresponds to a depletion in absorbance at 400 – 500 nm and an increase in absorbance at 550 – 700 nm. The S⁻-FAD charge transfer is characterized by the increase in absorbance at 500 – 550 nm (figure 3.2.9 A). The enzyme can be completely reduced (FAD and the disulfide are both reduced) using an excess of NADH. This EH₄ state of the enzyme is characterized by loss in absorbance at 400 – 500 nm (figure 3.2.9 B).

3.2.7 Crystal Structure of the *SliE3* Component

The crystallization conditions for the *SliE3* component were determined using the automated crystallization screen (section 1.6.3). For the crystallization, 2 μL of the protein solution (7 mg/mL *SliE3* in 50 mM $\text{KH}_2\text{PO}_4/\text{K}_2\text{HPO}_4$, 150 mM NaCl, pH 7.6) were mixed at RT with 1 μL of the reservoir solution (20 % (w/v) PEG3350, 200 mM NH_4Cl). This crystallization mix was equilibrated against 250 μL of the reservoir solution according to the hanging-drop vapor diffusion approach. The crystals were grown for 7 – 10 days at 8 °C.

Single crystals were cryoprotected by transfer into the cryoprotectant solution (22 % (w/v) PEG3350, 25 % (v/v) PEG200, 200 mM NH_4Cl , 100 mM $\text{KH}_2\text{PO}_4/\text{K}_2\text{HPO}_4$, 300 mM NaCl, pH 7.6). The cryoprotection procedure was performed at 8 °C for ~30 s. The single crystals were flash frozen in liquid nitrogen and stored for several weeks.

The diffraction data were collected using synchrotron radiation (DESY, beamline P13, Hamburg, Germany) under cryogenic conditions (100 K). The experimental data were processed as described in section 1.6.3.3. *SliE3* crystallizes in an orthorhombic space group $\text{P}2_12_12_1$. The initial phasing was performed using the molecular replacement approach (section 1.6.3.4).

The model was refined against the experimental data to 2.02 Å resolution (table A.4 in the appendix). The final model corresponds to the diffraction data with $R_{\text{work}} = 23.35\%$ and $R_{\text{free}} = 27.39\%$ (table A.8 in the appendix).

The crystallographic asymmetric unit contains one functional homodimer of *SliE3*. Each monomer consists of the FAD-binding domain (10 – 155 aa), the NAD^+ -binding domain (156 – 285 aa), the central domain (286 – 353 aa) and the interface domain (354 – 471 aa) (CHANDRASEKHAR *et al.*, 2013). Each monomer contains a FAD molecule in the active site. The first few N-terminal residues were not modeled, due to the lack in electron density (chain A: 1-13 aa, chain B: 1-12 aa). This part of the protein is assumed to be flexible.

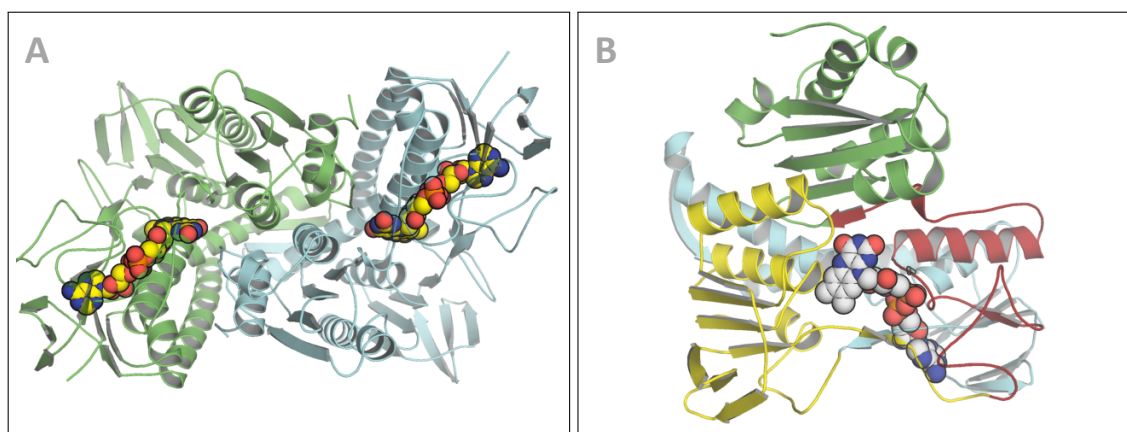


Figure 3.2.10: Crystal structure of the *SliE3* protein. Polypeptide backbone is represented as secondary structure. The FAD molecule is shown as space-filling model. **A:** The functional dimer in the asymmetric unit. The monomers are colored in green or cyan. Each monomer contains a FAD molecule (yellow) in the active site. **B:** The domain architecture of a *SliE3* monomer. FAD-binding domain: cyan, NAD⁺-binding domain: yellow, central domain: red, interface domain: green. Enzyme bound FAD molecule is colored in gray.

3.2.8 Sequence of the E3 Component from *Streptomyces Melanovinaceus*

As the sequence of the genome of *Streptomyces melanovinaceus* is not published and the coding sequence of the native E3 component is unknown, the homologous E3 protein from *Streptomyces lividans* was analyzed in the present work. *SliE3* component was described to catalyze the reoxidation of the dihydrolipoyl moiety of the QncL subunit (PENG *et al.*, 2012). In order to obtain information about the coding sequence of the native E3 component, the *Streptomyces melanovinaceus* strain was cultivated (section 1.6.1.11). The genomic DNA was isolated (section 1.6.1.12) and sequenced by DR. ANJA POEHLEIN (Georg-August University of Göttingen, Department of Genomic and Applied Microbiology). The draft sequence was automatically annotated by the Integrated Microbial Genomes Database (<https://img.jgi.doe.gov/>, MARKOWITZ *et al.* (2012)).

The sequence of the gene annotated as dihydrolipoyl dehydrogenase (E3 component, EC: 1.8.1.4) was used for the primer design to amplify the coding sequence from *Streptomyces melanovinaceus* using the PCR technique (figure 3.2.11). The amplified coding sequence for the E3 component from *Streptomyces melanovinaceus* (*SmeE3*) was cloned into the pJET1.2 vector (CloneJet PCR cloning Kit) using blunt-end cloning according to the manufacturer's manual (MBI Fermentas, Germany).

```

1   ATGCATGGAGGACGTGACGTGGCGAACGACGCCAGCACCGTTTTTCGACCTAGTGATCCTCGGCGGTGGTAGCGCGGTTACGCCCGGCC   90
91  CTGCGCGGAGCGCAGCTGGGCTGGACCTCGCTCTGATCGAGAAGGCAAGTTCGGCGGCACCTGCCTGCACAACCGTTGTATCCCCACG   180
181 AAGGCCCTGCTGCACGCCGGTGAATCGCCGACCAGGCGCGGAGTCCGAGCAGTTCGGTGTCAAGGCCACCTTCGAGGGGCATCGACATC   270
271 GACGCCGTCCACAAGTACAAGGACGACGTGATCTCGGGCTGTACAAGGTTCTGCAGGGTCTCATCGCCTCGCGCAAGGTCACTACATC   360
361 GAGGGTGAAGGACGGCTCTCTCCCCACCTCGGTGGATGTGAACGGCCAGCGGTCAGGGCCGCCACGTGCTGCTCGCGACCGGCTCC   450
451 GTGCCGAAGTCTGCTGCGGGCTGGAGATCGACGGCAACCGCATCATCTCGTGGACACCGGCTCAAGCTGGACCGGCTCCCGAAGTCC   540
541 GCGATCGTCTGGGCGGCGGCTCATCGGCGTCGAGTTCCGCTCGGCGTGGACGTCCTTCGGTACCGACGTGACGATCATCGAGGGCCCTG   630
631 AAGCACCTCGTCCCGTTCGAGGACGAGAACAGCTCGAAGCTTCTTGAAGCGCGCTCCGCAAGCGCGGCATCAAGTTCAACCTCGGTACG   720
721 TTCTTCCAGGGCCCGAGTACACGCAGGACGGGCTCCGTGTGACCTTCGCCGACGGCAAGACCTTCGAGGCCGAGGTGCTGCTGGTCGCC   810
811 ATCGGCGCGGCCCGGTCTCGAGGGCTGGGCTACGAGGAGGCGCGCTCGCATGGACCGCGGTTACGTCCTGGTTCGACGAGTACATG   900
901 CAGACCAACGTGGAGACCGTCTCGGCCGTGGGTGACCTGGTCCCGACGCTCCAGCTCGCGCACGTCCGGCTTCGCCGAGGGGCATCCTGGTG   990
991 GCGGAGCGGCTGGCCGTTCTGAAGACCGTTCGATCGACTACGACGGTGTCCGCGGGTGACGTAAGTCCACCCGAGGTTCGCTCCGTTG   1080
1081 GGCATACCCGAGGCCAAGGCCAAGGAGCTCTACGGCGCGGACAAGTCTCGCTCTGAAGTACAACCTCGCGGGCAACGGCAAGAGCAAG   1170
1171 ATCCTCAAGACCGCGGCGAGATCAAGCTCGTCCAGGTCAAGGACGGTCCGCTGGTGGCGGTCCACATGTCGGTGAACGATGGGCGAG   1260
1261 CAGGTGGCGAAGCCAGCTGATCTACAACCTGGGAGGCGTGGCCGCGGAGTTCGCGCAGCTCATCCACGCCACCCGACCCAGAACGAG   1350
1351 GCGATGGCGAGGCCACCTGGCCCTGGCCGGAAGCTCTGCACTCCCAGACTGA   1407

```

Figure 3.2.11: The coding sequence for the E3 component from *Streptomyces melanovinaceus*.

3.3 Discussion

Additionally to the studies on transaldolase from *Thermoplasma acidophilum*, the protein system containing the QncN/L, QncM from *Streptomyces melanovinaceus* and the E3 component from *Streptomyces lividans* was preliminarily characterized in the present work. The components of the system are similar to enzymes from central metabolism (transketolase, pyruvate dehydrogenase complex and acyl carrier protein) in terms of sequence and mechanism of action. Investigations on this protein group can provide new insights for deeper understanding of the mechanism of action of the enzymes involved in the sugar metabolism. Furthermore, these proteins are members of the nonribosomal peptide assembly line of quinocarcin biosynthesis. As a novel kind of antibiotics, quinocarcin and its synthesis is an interesting subject for investigations. Establishing protocols for working with the enzymes from nonribosomal peptide assembly lines *in vitro* could give new opportunities in synthesis strategies of pharmaceutical important compounds.

In the present work, the QncM and E3 components could be expressed and purified with sufficient yields. QncM is an acyl carrier protein (ACP) homolog and plays an important role in the synthesis of quinocarcin, supplying the hydroxyacetyl unit derived from ketose phosphate into the nonribosomal peptide assembly line. A crystallization protocol for the biological active phosphopantetheinylated holo-form of the protein was established. Surprisingly, the asymmetric unit of the determined structure contains a homotrimer of holoQncM. This trimer is assumed to be a crystallographic artifact. The size exclusion chromatography coupled multiangle light scattering experiment results in the detection of a major fraction of monomeric holoQncM and a minor fraction of holoQncM dimers. A homotrimer of holoQncM was not detected. The presence of dimers can be explained by the oxidized form of holoQncM. A dimerization under oxidizing conditions was reported for the ACP homologs from *Escherichia coli* (Rock *et al.*, 1981) and *Plasmodium*

falciiparum (GALLAGHER AND PRIGGE, 2010). The phosphopantetheinyl groups of the protein form a disulfide bond with each other under oxidizing conditions, resulting in dimer formation. In order to verify the suggestion that holoQncM forms disulfide linked dimers at oxidizing conditions, SEC-MALS experiment using DTT containing buffer should be performed.

The addition of 10 mM BaCl₂ to the crystallization mix significantly improved the crystal quality of holoQncM in terms of diffraction ability. The stabilizing effect of divalent cations on the protein fold was reported for ACP from *E. coli* (TENER AND MAYO, 1990) and for ACP from *Vibrio harveyi* (CHAN *et al.*, 2010). It is to assume that the addition of divalent cations (MgCl₂ or CaCl₂) to the purification and storage buffers could further improve the purification protocol for the holoQncM component.

The structure of holoQncM exhibits a Trp³¹-His³⁶ dyad located in the direct environment of the phosphopantetheinylated Ser³³ residue. These residues interact with each other by hydrogen bond (figure 3.3.12). This motive is conserved in some bacterial homologs of ACP but not in the protein from *E. coli* (RAMELOT *et al.*, 2011). The role of this structural motive is unclear. As this pair is located near the entrance of the hydrophobic pocket, which binds the acylated prosthetic group, the Trp-His dyad is suggested to be important for the recognition of the acyl chain covalently linked to the phosphopantethein moiety (CROSBY AND CRUMP, 2012).

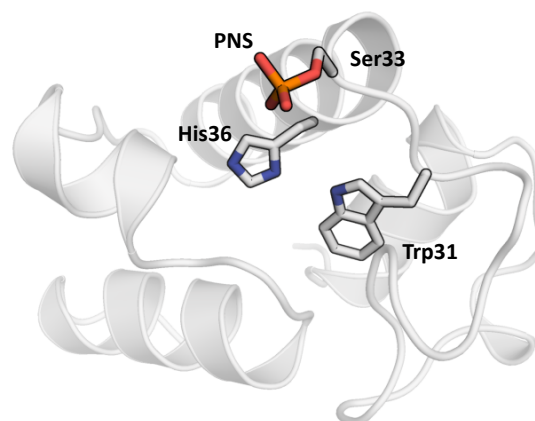


Figure 3.3.12: Trp³¹-His³⁶ dyad near the phosphopantetheinylated Ser³³ residue in holoQncM structure. The main chain is shown as secondary structure (gray), the residues Trp³¹, His³⁶, Ser³³ and the phosphate group of the phosphopantetheinyl moiety (PNS) as sticks.

Another protein, which was analyzed in the present work, is the E3 component. Due to the lack in sequence information about the original E3 component from *Streptomyces melanovinaceus*, the homologous protein from *Streptomyces lividans* (*SliE3*) was subjected for investigations. The *SliE3* component is reported to be able to recognize the dihydrolipoyl moiety of the QncL subunit and to catalyze its oxidation (PENG *et al.*, 2012). *SliE3* component arises as a good model for the investigations on the dihydrolipoyl dehydrogenase. The protein could be purified in its active

form with sufficient yields. The spectroscopic methods for the kinetic analysis as described by ARGYROU AND BLANCHARD (2001); ARGYROU *et al.* (2002) for the dihydrolipoyl dehydrogenase from *Mycobacterium tuberculosis* could be applied to the *SliE3* component. The protein efficiently catalyzes the reversible reduction of the lipoamide using NADH as reductant. Furthermore, the characteristic absorption bands for the formation of the reaction intermediates during the catalysis can be monitored using stopped-flow spectroscopy. Finally, the crystallization conditions and the crystal structure of the component were determined in this work. These methods give a good basis for the kinetical and structural analysis of the catalytic cycle of the dihydrolipoyl dehydrogenase.

The *Streptomyces melanovinaceus* strain could be cultivated and the genomic DNA was isolated. Using the information from the genome sequencing (Department of Genomic and Applied Microbiology), the coding sequence for the original dihydrolipoyl dehydrogenase from *Streptomyces melanovinaceus* could be identified. The sequences of the E3 component from *Streptomyces melanovinaceus* and *Streptomyces lividans* share 91.2 % identity and 97.0 % similarity (figure 3.3.13).

```

lividans:      1  MHGGRDVANDASTVFDLVLGGGSGGYAAALRGAQLGLDVALIEKNKLGGTCLHNGCIPKALLHAGEVADQ$RESEQ 78
melanovinaceus: 1  MHGGRDVANDASTVFDLVLGGGSGGYAAALRGAQLGLDVALIEKCKVGGTCLHNGCIPKALLHAGEIADQ$ARESEQ 78

lividans:      79  FGVKTSFEGVDMAGVHKYKDEVIAGLYKGLQGLVASRKITYIEGEGRLSSPTSVDVNGQRVQGRHVLLATGSVPKTLF 156
melanovinaceus: 79  FGVKATFEGIDIDAVHKYKDDVISGLYKGLQGLIASRKVTYIEGEGRLSSPTSVDVNGQRVQGRHVLLATGSVPKSLP 156

lividans:      157  GLEIDGNRIISSDHALLDRVPKSAIVLGGGVIGVEFASAWK$SFGSEVTVIEGLKHLVPVEDENSSKLLERAFRRKGI 234
melanovinaceus: 157  GLEIDGNRIISSDHALLDRVPKSAIVLGGGVIGVEFASAWT$SFGTDVTIIEGLKHLVPVEDENSSKLLERAFRRKGI 234

lividans:      235  KFNLGTFFFQ$AEYTDQGVKVTLADGKFEAEVLLVAIGRGPVSQGLGYEENGVA$DRGFVLVDEYMQTNVPTISAVGD 312
melanovinaceus: 235  KFNLGTFFFQ$AEYTDQGVKVTLADGKFEAEVLLVAIGRGPVSQGLGYEEAGVAMDRGYVLVDEYMQTNVETVSAVGD 312

lividans:      313  LVPTLQLAHVGF$AEGILVAERLAGLKTVPVDYDGVPRVTYCHPEVASVGLTEARAKEVYGADKVV$IKFPLGGNGKSR 390
melanovinaceus: 313  LVPTLQLAHVGF$AEGILVAERLAGLKTVPIDYDGVPRVTYCHPEVASVGLTEAKAKELYGADKVV$ALKYPLAGNGKSK 390

lividans:      391  ILKTAGEIKLVQVKDGAVVGVHVMVGD$RMGEQVGEAQLIYNWEALPAEVAQLIHAHPTQNEALGEAHLALAGKPLHMH$D 468
melanovinaceus: 391  ILKTAGEIKLVQVKDGAVVGVHVMVGD$RMGEQVGEAQLIYNWEALPAEVAQLIHAHPTQNEAMGEAHLALAGKPLHSH$D 468

```

Figure 3.3.13: Sequence alignment of the E3 components from *Streptomyces melanovinaceus* and *Streptomyces lividans*. The sequence for *St. lividans* was taken from UniProt-server (<http://www.uniprot.org>; 2012) The sequence alignment was performed using Clustal Omega server (<http://www.ebi.ac.uk/Tools/msa/clustalo/>; (GOUJON *et al.*, 2010; McWILLIAM *et al.*, 2013; SIEVERS *et al.*, 2011)). Red: fully conserved residues, blue: residues with similar properties, black: residues with weakly similar properties, gray: neutral.

The residue Ser²⁷ (numbering refers to the position of the residue in the amino acid sequence of the purified protein) is of particular interest. In the coding sequences for the dihydrolipoyl dehydrogenase from selected model organisms, the corresponding residue is a proline (alignment not shown). However, the Ser²⁷ residue is conserved in a number of *Streptomyces* species (alignment not shown). Interestingly, the analysis of the naturally occurring mutation in the dihydrolipoyl dehydrogenase gene from the lesser grain borer (*Rhyzopertha dominica*) and the rust-red flour beetle (*Tribolium castaneum*) showed that a mutation of the proline residue to the *Streptomyces*

specific serine results in insects, which are resistant against phosphine (CHEN *et al.*, 2015; KAUR *et al.*, 2015; SCHLIPALIUS *et al.*, 2012). Additionally, a number of other mutations in dihydrolipoyl dehydrogenase gene, which lowers the phosphine sensitivity of the insects, were reported. However, the mechanism of this resistance is not understood so far. In the structure of the *SliE3* component, the residue Ser²⁷ is located in the FAD-binding domain near the catalytic disulfide bond and would be able to influence the E3 reaction (figure 3.3.14).

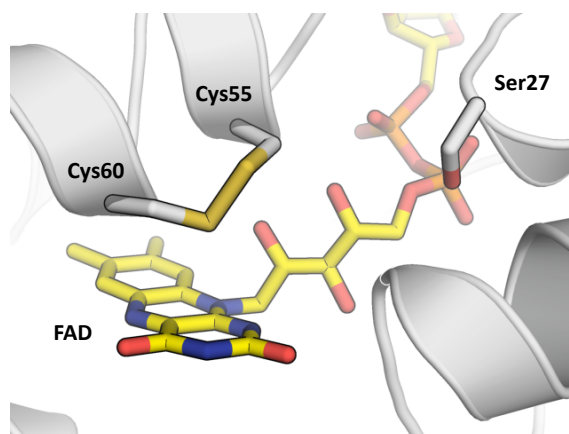


Figure 3.3.14: The active site of the *SliE3* component. The main chain is shown as secondary structure (gray), the residues Ser²⁷, Cys⁵⁵, Cys⁶⁰ and the FAD (yellow) as sticks.

The E3 component catalyzes the oxidation of the dihydrolipoyl moiety of the QncL subunit completing the catalytic cycle of the QncN/L-M protein system. The QncL and QncN subunits form together the QncN/L component, which provides the main catalytic functionality of the system. This component catalyzes the ketol cleavage of the ketose phosphate and the transfer of a hydroxyacetyl unit to the phosphopantetheine moiety of the holoQncM component. Unfortunately, the previously published expression and the purification protocol for the QncN/L component (PENG *et al.*, 2012) could not be optimized in the present work. The protein yields per 1 g cell pellet are low compared to the other components (E3 and QncM). The overall activity of the protein complex could be determined applying the continuous spectrophotometric assay, which is similar to the activity assay for the mechanistically related pyruvate dehydrogenase complex from *Escherichia coli* (NEMERIA *et al.*, 1998). In previous studies, this activity was determined using a discontinuous HPLC based assay, in which the formation of the hydroxyacetylated holoQncM was detected (PENG *et al.*, 2012). The activity assay used in the present work detects the reduction of NAD⁺, which is catalyzed by the E3 component along with the QncN/L reaction. The determined activity using this assay is consistent with the published activity.

Appendix

A Tables

Table A.1: Estimated properties of *TacTAL*_{wt} and variants. Molecular weights (MW), molar extinction coefficients (ϵ_{280nm}) and isoelectric points (pI) were calculated with ProtParam online-tool (<http://web.expasy.org/protparam/>) (GASTEIGER *et al.*, 2005).

Protein	MW (Da)	ϵ_{280nm} (M ⁻¹ cm ⁻¹)	pI
<i>TacTAL</i> _{wt}	24464.5	16960	6.44
<i>TacTAL</i> _{E60Q}	24463.5	16960	6.91
<i>TacTAL</i> _{K86Q}	24464.5	16960	6.10
<i>TacTAL</i> _{F132Y}	24480.5	18450	6.44
<i>TacTAL</i> _{E60Q/F132Y}	24479.5	18450	6.91
<i>TacTAL</i> _{N108A/S130A}	24405.5	16960	6.44
<i>TacTAL</i> _{T30C/D211C} (oxidized)	24452.6	17085	6.90
<i>TacTAL</i> _{T30C/D211C} (reduced)	24454.6	16960	6.90
<i>TacTAL</i> _{FSA-mimic}	24522.7	18450	6.91

Table A.2: Expected holoQncM fragments after tryptic cleavage. The fragments were calculated with PeptideCutter online-tool (http://web.expasy.org/peptide_cutter/) (GASTEIGER *et al.*, 2005). The modified serine residue and the mass of the resulting modified peptide are indicated by red.

Position (aa)	Peptide sequence	Peptide length (aa)	Mass (Da)
28	MTTVENLVADV LGLAPEDIDDDTGPATR	28	2929.203
35	GEWTS ^{red} SLR	7	847.926 ^{red} 1188.26
50	HVQIVVAIEATYGIR	15	1668.957
54	LTAR	4	459.546
57	EVR	3	402.451
60	SCR	3	364.42
63	SVR	3	360.414
66	GLK	3	316.401
72	QALSAK	6	616.715
76	GLNS	4	389.409

Table A.3: Data collection statistics. Data for the highest-resolution shell are shown in parentheses. The respective substrates were co-crystallized.

	<i>Tac</i>TAL_{wt}+F6P	<i>Tac</i>TAL_{wt}+A5P	<i>Tac</i>TAL_{wt}+M1P	<i>Tac</i>TAL_{K86Q}+F6P	<i>Tac</i>TAL_{E60Q}+F6P
space group	C222 ₁	C222 ₁	C222 ₁	C222 ₁	C222 ₁
cell dimensions:					
<i>a</i> , <i>b</i> , <i>c</i> (Å)	148.50, 172.10, 100.60	148.00, 171.50, 100.10	148.00, 171.40, 99.70	147.95, 170.90, 101.14	146.30, 171.80, 99.10
α , β , γ (deg)	90.00, 90.00, 90.00	90.00, 90.00, 90.00	90.00, 90.00, 90.00	90.00, 90.00, 90.00	90.00, 90.00, 90.00
resolution (Å)	50.00-1.51 (1.61-1.51)	50.00-1.82 (1.92-1.82)	50.00-1.85 (1.95-1.85)	50.00-1.75 (1.85-1.75)	50.00-1.65 (1.75-1.65)
<i>R</i> _{meas} (%)	5.1 (66.5)	4.4 (68.3)	3.6 (57.3)	9.4 (53.0)	3.8 (67.2)
<i>I</i> / σ <i>I</i>	12.11 (2.36)	16.53 (2.05)	27.98 (3.07)	8.81 (2.94)	19.60 (2.55)
CC _{1/2} (%)	99.8 (73.0)	99.9 (72.4)	100.0 (89.5)	99.6 (83.1)	99.9 (84.0)
completeness (%)	97.9 (99.7)	97.0 (95.6)	98.4 (98.2)	97.8 (98.6)	98.7 (99.3)
redundancy	3.3 (3.3)	3.4 (3.3)	4.8 (4.8)	4.3 (4.9)	3.6 (3.7)
wavelength (Å)	0.82661	0.82661	0.82656	0.82656	0.92012
<i>Tac</i>TAL_{E60Q}/F132Y+F6P					
space group	C222 ₁	C222 ₁	C222 ₁	C222 ₁	C222 ₁
cell dimensions:					
<i>a</i> , <i>b</i> , <i>c</i> (Å)	148.87, 172.07, 100.21	148.58, 172.87, 100.09	147.10, 171.20, 100.20	149.02, 172.48, 100.81	148.58, 170.97, 102.00
α , β , γ (deg)	90.00, 90.00, 90.00	90.00, 90.00, 90.00	90.00, 90.00, 90.00	90.00, 90.00, 90.00	90.00, 90.00, 90.00
resolution (Å)	50.00-1.80 (1.90-1.80)	100.0-1.90 (2.00-1.90)	50.00-1.63 (1.73-1.63)	50.00-2.05 (2.15-2.05)	50.00-2.25 (2.35-2.25)
<i>R</i> _{meas} (%)	4.5 (45.2)	6.7 (69.6)	4.5 (70.0)	7.5 (68.9)	7.7 (63.6)
<i>I</i> / σ <i>I</i>	23.26 (3.96)	14.77 (2.64)	15.30 (2.24)	14.42 (2.63)	15.86 (2.64)
CC _{1/2} (%)	99.9 (92.1)	99.8 (83.9)	99.9 (80.8)	99.9 (86.9)	99.9 (87.0)
completeness (%)	99.9 (99.9)	99.6 (99.7)	97.1 (98.1)	100.0 (100.0)	100.0 (100.0)
redundancy	5.6 (5.7)	5.4 (5.5)	3.6 (3.5)	6.7 (6.8)	6.6 (6.3)
wavelength (Å)	0.91000	0.85506	0.92012	0.85000	0.85000
<i>Tac</i>TAL_{N108A}/S130A+F6P					
space group	C222 ₁	C222 ₁	C222 ₁	C222 ₁	C222 ₁
cell dimensions:					
<i>a</i> , <i>b</i> , <i>c</i> (Å)	148.87, 172.07, 100.21	148.58, 172.87, 100.09	147.10, 171.20, 100.20	149.02, 172.48, 100.81	148.58, 170.97, 102.00
α , β , γ (deg)	90.00, 90.00, 90.00	90.00, 90.00, 90.00	90.00, 90.00, 90.00	90.00, 90.00, 90.00	90.00, 90.00, 90.00
resolution (Å)	50.00-1.80 (1.90-1.80)	100.0-1.90 (2.00-1.90)	50.00-1.63 (1.73-1.63)	50.00-2.05 (2.15-2.05)	50.00-2.25 (2.35-2.25)
<i>R</i> _{meas} (%)	4.5 (45.2)	6.7 (69.6)	4.5 (70.0)	7.5 (68.9)	7.7 (63.6)
<i>I</i> / σ <i>I</i>	23.26 (3.96)	14.77 (2.64)	15.30 (2.24)	14.42 (2.63)	15.86 (2.64)
CC _{1/2} (%)	99.9 (92.1)	99.8 (83.9)	99.9 (80.8)	99.9 (86.9)	99.9 (87.0)
completeness (%)	99.9 (99.9)	99.6 (99.7)	97.1 (98.1)	100.0 (100.0)	100.0 (100.0)
redundancy	5.6 (5.7)	5.4 (5.5)	3.6 (3.5)	6.7 (6.8)	6.6 (6.3)
wavelength (Å)	0.91000	0.85506	0.92012	0.85000	0.85000
<i>Tac</i>TAL_{T30C}/D211C+F6P					
space group	C222 ₁	C222 ₁	C222 ₁	C222 ₁	C222 ₁
cell dimensions:					
<i>a</i> , <i>b</i> , <i>c</i> (Å)	148.87, 172.07, 100.21	148.58, 172.87, 100.09	147.10, 171.20, 100.20	149.02, 172.48, 100.81	148.58, 170.97, 102.00
α , β , γ (deg)	90.00, 90.00, 90.00	90.00, 90.00, 90.00	90.00, 90.00, 90.00	90.00, 90.00, 90.00	90.00, 90.00, 90.00
resolution (Å)	50.00-1.80 (1.90-1.80)	100.0-1.90 (2.00-1.90)	50.00-1.63 (1.73-1.63)	50.00-2.05 (2.15-2.05)	50.00-2.25 (2.35-2.25)
<i>R</i> _{meas} (%)	4.5 (45.2)	6.7 (69.6)	4.5 (70.0)	7.5 (68.9)	7.7 (63.6)
<i>I</i> / σ <i>I</i>	23.26 (3.96)	14.77 (2.64)	15.30 (2.24)	14.42 (2.63)	15.86 (2.64)
CC _{1/2} (%)	99.9 (92.1)	99.8 (83.9)	99.9 (80.8)	99.9 (86.9)	99.9 (87.0)
completeness (%)	99.9 (99.9)	99.6 (99.7)	97.1 (98.1)	100.0 (100.0)	100.0 (100.0)
redundancy	5.6 (5.7)	5.4 (5.5)	3.6 (3.5)	6.7 (6.8)	6.6 (6.3)
wavelength (Å)	0.91000	0.85506	0.92012	0.85000	0.85000

Table A.4: Data collection statistics. Data for the highest-resolution shell are shown in parentheses. The respective substrates were co-crystallized or soaked (indicated by [*]).

	<i>TacTAL</i> _{TR30C/D211C} + F6P*	<i>TacTAL</i> _{TR30C/D211C} + DTT*	<i>TacTAL</i> _{TR30C/D211C} + F6P* + DTT*
space group	C222 ₁	C222 ₁	C222 ₁
cell dimensions:			
<i>a, b, c</i> (Å)	148.91, 172.35, 100.85	148.06, 171.72, 100.79	149.58, 172.71, 100.25
α, β, γ (deg)	90.00, 90.00, 90.00	90.00, 90.00, 90.00	90.00, 90.00, 90.00
resolution (Å)	50.00 – 2.50 (2.60 – 2.50)	50.00 – 2.15 (2.25 – 2.15)	50.00 – 2.10 (2.20 – 2.10)
R_{meas} (%)	13.8 (64.1)	8.9 (64.5)	11.5 (67.8)
$I/\sigma I$	9.64 (2.53)	12.66 (2.74)	10.23 (2.52)
$CC_{1/2}$ (%)	99.7 (86.4)	99.9 (89.1)	99.8 (84.4)
completeness (%)	99.9 (100.0)	99.9 (100.0)	99.9 (99.9)
redundancy	6.6 (6.8)	6.6 (6.7)	6.1 (6.3)
wavelength (Å)	0.85000	0.85000	0.85000
	<i>TacTAL</i>_{E60Q/RT132Y} + F6P (2)	holoQncM	SITE3
space group	C222 ₁	P2 ₁ 2 ₁ 2 ₁	P2 ₁ 2 ₁ 2 ₁
cell dimensions:			
<i>a, b, c</i> (Å)	147.86, 172.20, 99.07	44.95, 55.77, 89.62	84.24, 85.29, 151.80
α, β, γ (deg)	90.00, 90.00, 90.00	90.00, 90.00, 90.00	90.00, 90.00, 90.00
resolution (Å)	50.00 – 1.90 (2.00 – 1.90)	45.00 – 1.70 (1.80 – 1.70)	50.00 – 2.02 (2.12 – 2.02)
R_{meas} (%)	5.5 (75.7)	3.3 (57.7)	7.8 (78.2)
$I/\sigma I$	18.63 (2.50)	20.20 (2.56)	16.11 (2.09)
$CC_{1/2}$ (%)	99.9 (88.7)	99.9 (87.8)	99.9 (76.6)
completeness (%)	99.9 (100.0)	99.3 (99.5)	97.4 (98.1)
redundancy	5.7 (5.8)	4.1 (4.2)	4.1 (4.1)
wavelength (Å)	0.91000	0.918409	0.77318

Table A.5: Refinement statistics. The respective ligands were co-crystallized.

	<i>Tac</i> TAL _{wt} +F6P	<i>Tac</i> TAL _{wt} +A5P	<i>Tac</i> TAL _{wt} +MIP	<i>Tac</i> TAL _{K86Q} +F6P	<i>Tac</i> TAL _{E60Q} +F6P
resolution (Å)	32.29 – 1.51	47.41 – 1.82	47.41 – 1.85	47.38 – 1.75	46.96 – 1.65
no. of reflections	196105	110244	106240	125786	147165
test reflections	9807	5513	5314	6289	7356
$R_{\text{work}}, R_{\text{free}}$ (%)	15.98, 18.58	15.65, 18.16	18.39, 21.88	20.88, 25.04	16.23, 19.43
no. of atoms:					
protein	8751	8915	9478	8696	8694
ligands	123	107	111	122	123
waters	836	565	457	646	698
B factor (Å ²):					
protein	34.67	47.34	43.04	39.62	34.70
ligands	31.90	44.74	48.91	40.29	31.80
waters	42.97	48.97	44.37	44.36	41.68
rmsd:					
bond lengths (Å)	0.015	0.010	0.007	0.015	0.015
bond angles (Å)	1.535	1.208	1.077	1.573	1.556
B factor (Wilson plot, Å ²)	27.37	36.25	30.67	29.38	24.89
RAMACHANDRAN plot:					
outliers (%)	0.00	0.00	0.00	0.00	0.09
allowed (%)	1.06	0.79	0.57	2.51	1.16
favored (%)	98.94	99.21	99.43	97.49	98.75
ligands	F6P, GOL, ACT	A5P, GOL, ACT	MIP, GOL, ACT	F6P, GOL, ACT	F6P, GOL, ACT

Table A.6: Refinement statistics. The respective substrates were co-crystallized.

	<i>Tac</i> TAL _{E60Q/F132Y} +F6P	<i>Tac</i> TAL _{FSA-mimic} +F6P	<i>Tac</i> TAL _{N108A/S130A} +F6P	<i>Tac</i> TAL _{T30C/D211C} +F6P	<i>Tac</i> TAL _{T30C/D211C}
resolution (Å)	49.08 – 1.80	53.72 – 1.90	45.70 – 1.63	47.73 – 2.05	47.57 – 2.25
no. of reflections	118566	100842	152204	81407	61769
test reflections	5904	5042	7612	4072	3089
R_{work} , R_{free} (%)	16.22, 19.38	17.80, 20.99	16.56, 19.27	16.64, 20.62	16.84, 20.98
no. of atoms:					
protein	9037	9348	8865	8471	8413
ligands	72	113	123	127	42
waters	750	388	891	394	293
B factor (Å ²):					
protein	36.73	47.83	31.57	51.77	57.86
ligands	39.93	47.33	28.56	45.99	54.38
waters	43.48	46.09	40.43	49.13	51.43
rmsd:					
bond lengths (Å)	0.014	0.014	0.014	0.009	0.008
bond angles (Å)	1.363	1.375	1.487	1.083	1.007
B factor (Wilson plot, Å ²)	26.61	35.28	25.30	38.00	44.38
RAMACHANDRAN plot:					
outliers (%)	0.09	0.08	0.00	0.00	0.00
allowed (%)	1.99	1.85	1.23	1.93	2.12
favored (%)	97.93	98.07	98.77	98.07	97.88
ligands	DHA, ACT	GA3P, GOL, F6P, GOL, ACT	F6P, GOL, ACT	F6P, GOL, ACT	GOL, ACT

Table A.7: Refinement statistics. The F6P substrate and DTT were soaked.

	<i>Tac</i> TAL _{T30C/D211C} + F6P	<i>Tac</i> TAL _{T30C/D211C} + DTT	<i>Tac</i> TAL _{T30C/D211C} + F6P + DTT
resolution (Å)	47.70 – 2.50	47.43 – 2.15	47.90 – 2.10
no. of reflections	45147	69892	75697
test reflections	2258	3496	3785
R_{work} , R_{free} (%)	19.77, 23.40	17.98, 21.40	19.56, 23.02
no. of atoms:			
protein	8416	8386	8505
ligands	116	42	123
waters	151	348	444
B factor (Å ²):			
protein	55.97	54.18	48.24
ligands	60.33	50.71	49.83
waters	46.56	50.01	46.01
rmsd:			
bond lengths (Å)	0.007	0.004	0.005
bond angles (Å)	0.859	0.764	0.838
B factor (Wilson plot, Å ²)	43.84	39.76	35.32
RAMACHANDRAN plot:			
outliers (%)	0.09	0.00	0.00
allowed (%)	0.92	2.04	1.74
favored (%)	98.98	97.96	98.26
ligands	F6P, GOL, ACT	GOL, ACT	F6P, GOL, ACT

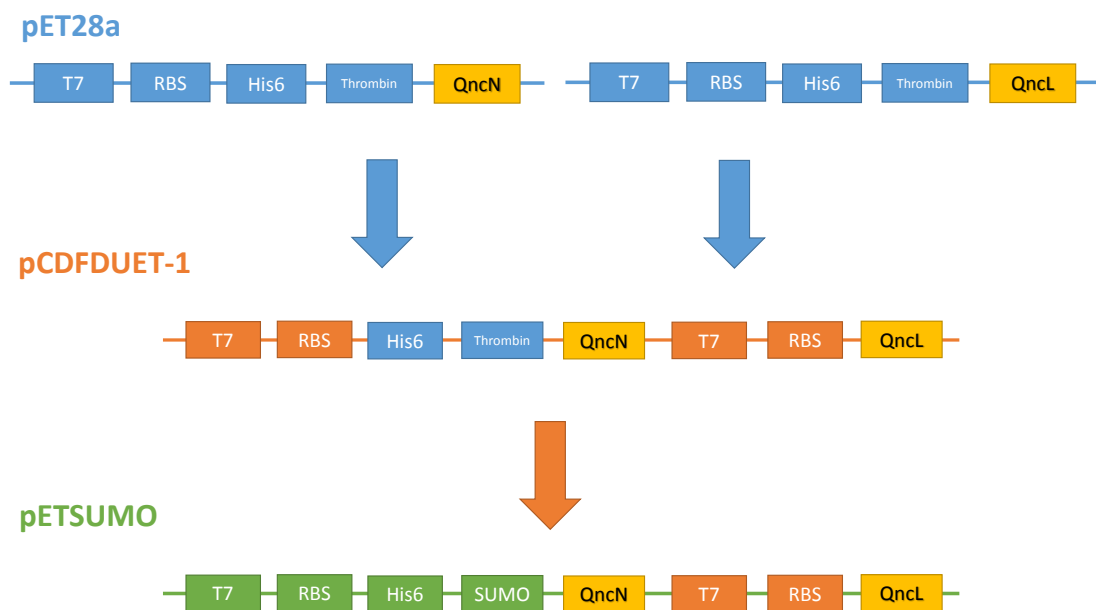
Table A.8: Refinement statistics. The F6P substrate was co-crystallized.

	<i>Tac</i> TAL _{E60Q} /F132Y + F6P (2)	holoQncM	SIE3
resolution (Å)	48.81 – 1.90	40.18 – 1.70	47.03 – 2.02
no. of reflections	99280	25295	70470
test reflections	4964	1265	3524
R_{work} , R_{free} (%)	18.23, 22.01	20.21, 23.20	23.35, 27.39
no. of atoms:			
protein	9067	1707	6779
ligands	83	10	106
waters	439	105	196
B factor (Å ²):			
protein	45.93	49.99	44.04
ligands	47.51	60.77	34.01
waters	48.50	45.57	40.23
rmsd:			
bond lengths (Å)	0.008	0.011	0.003
bond angles (Å)	1.030	1.182	0.720
B factor (Wilson plot, Å ²)	33.28	34.29	29.85
RAMACHANDRAN plot:			
outliers (%)	0.00	0.00	0.00
allowed (%)	2.17	1.36	2.99
favored (%)	97.83	98.64	97.01
ligands	F6P, GOL, ACT	PNS	FAD

Table A.9: Buffer conditions screened in the ThermoFluor assay. The pH-step was 0.4.

Substance	pH	Substance	pH
MES	4.6–7.4	Phosphate	5.8–8.6
BisTris	5.2–8.0	HEPES	6.0–8.8
Imidazole	5.4–8.2	Tris	6.6–9.4

B Schemes

**Scheme B.1:** Cloning strategy for generation of the QncNL-pET-SUMO construct.

C Figures

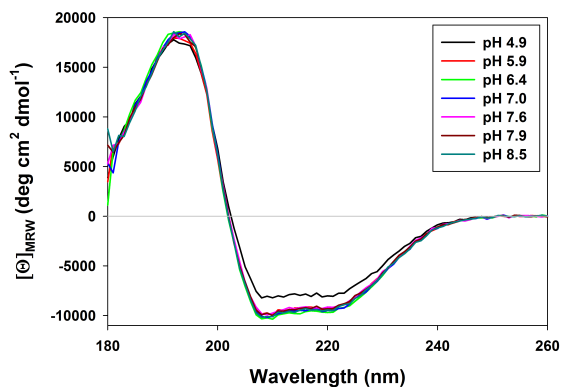


Figure C.1: Representative CD-spectra for the pH-titration of *TacTAL* (the data for *TacTAL*_{FSA-mimic} are shown). The far-UV-CD spectra were recorded at 30 °C in 10 mM KH₂PO₄/K₂HPO₄ (pH 4.9–8.5, section 1.6.4.3). CD spectra at different pH are indicated by respective color (see legend). Minor changes in secondary structure occur first at a pH below 5.9.

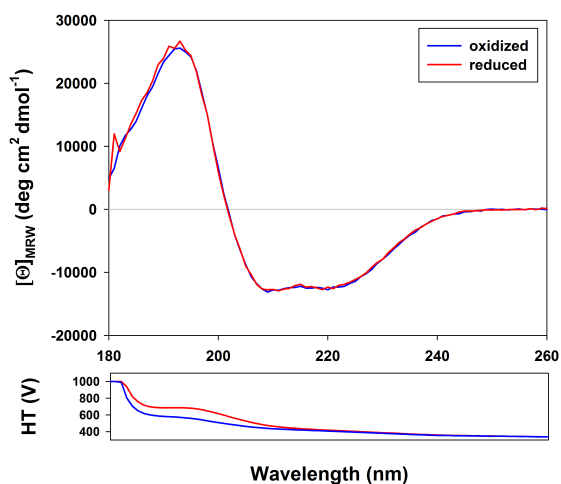


Figure C.2: Far-UV-CD spectra of *TacTAL*_{T30C/D211C} in presence and absence of DTT. The CD spectra were recorded under the same conditions as described in section 1.6.4.3 (pH 7.5, 0.125 mg/mL *TacTAL*, 30 °C). Blue solid line: absence of DTT (oxidized form); red solid line: presence of DTT (reduced form). The HT-plot (bottom) shows the high-voltage value of the detector at respective wavelength. No changes in secondary structure of the variant could be detected after incubation with 1 mM DTT.

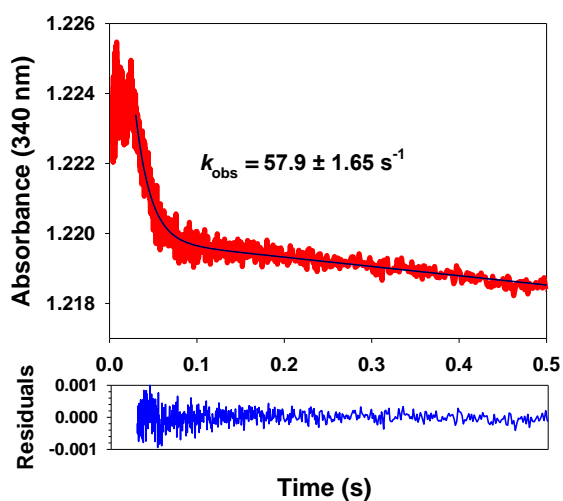


Figure C.3: Representative stopped-flow progress curve (cleavage of F6P into GA3P and DHA) for *TacTAL*_{FSA-mimic} recorded at 340 nm. The measurements were performed at 30 °C. The F6P concentration was 10 mM after mixing with enzyme (final concentration 0.22 mg/mL). The deviation of the applied fit (for details, see Materials and Methods) from the data is shown as residuals-plot. The progress curve consists of a lag-phase prior to an exponential burst phase followed by the linear aldolase steady-state phase. k_{obs} = observed rate constant of the burst phase.

Figure C.4: Representative stopped-flow progress curve for *TacTAL*_{E60Q} recorded at 340 nm. The measurements were performed at 30 °C. The F6P concentration was 10 mM after mixing with enzyme (final concentration 0.22 mg/mL). The deviation of the applied fit (for details, see Materials and Methods) from the data is shown as residuals-plot. The progress curve consists of an exponential burst phase following by the linear aldolase steady-state phase. k_{obs} = observed rate constant of the burst phase.

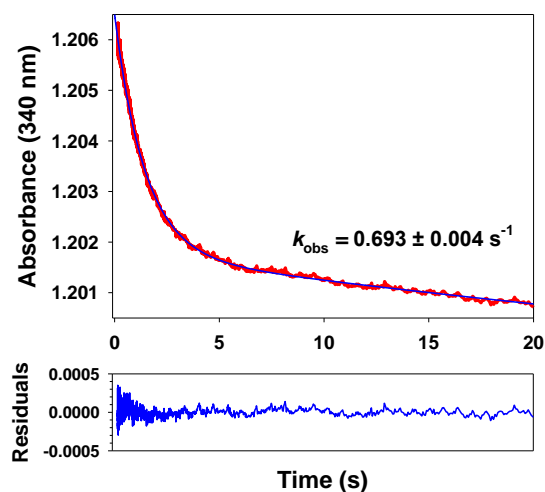


Figure C.5: Active site of *TacTAL*_{wt} co-crystallized with F6P. The selected active site residues (gray) and the F6P-SCHIFF base-intermediate (yellow) are represented as sticks. The ϵ -amino group of the reactive lysine (framed) is placed in hydrogen bond distance to the oxygen atom of the main chain carbonyl of Thr²⁷.

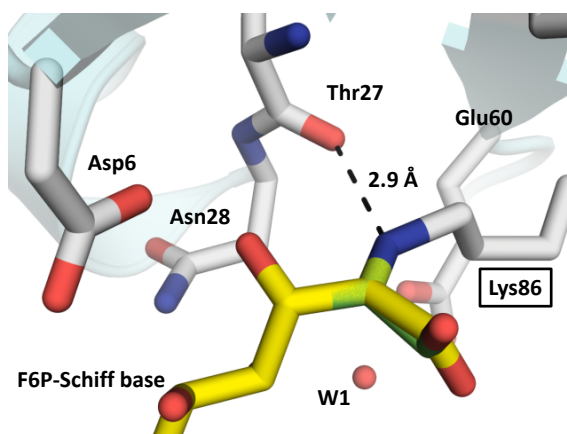
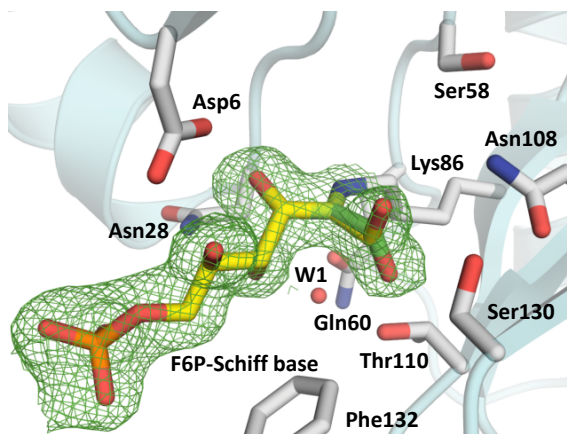


Figure C.6: *mF*_O-*DF*_C simulated annealing omit map of *TacTAL*_{E60Q} co-crystallized with F6P. The difference electron density map is shown as green mesh (contour level 3σ). The selected active site residues (gray) and the F6P-SCHIFF base-intermediate (yellow) are represented as sticks. The polypeptide backbone is shown as secondary structure (cyan).



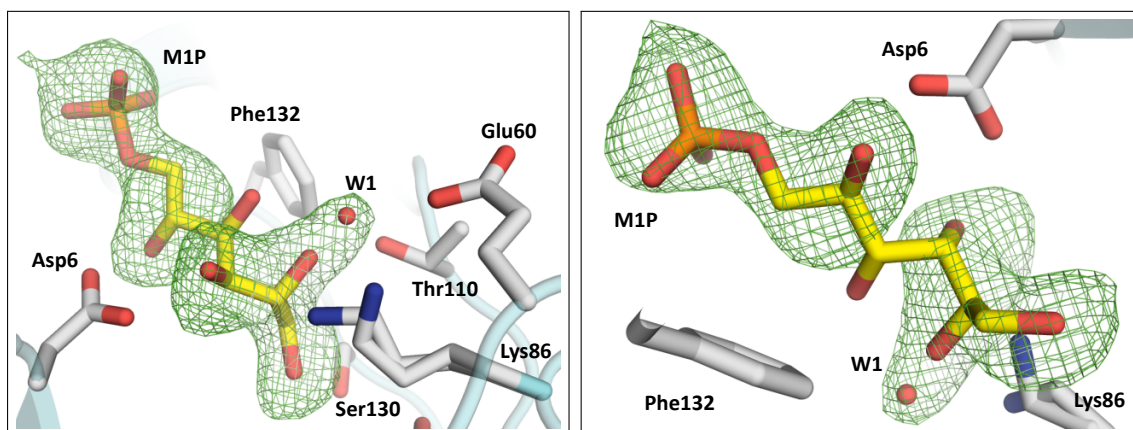


Figure C.7: mF_0 - DF_C simulated annealing omit map of *TacTAL*_{wt} co-crystallized with M1P. The difference electron density map is shown as green mesh (contour level 2.5σ). The selected active site residues (gray) and the non-covalently bound M1P (yellow) are represented as sticks. The polypeptide backbone is shown as secondary structure (cyan). The C3OH-group is not covered by the electron density.

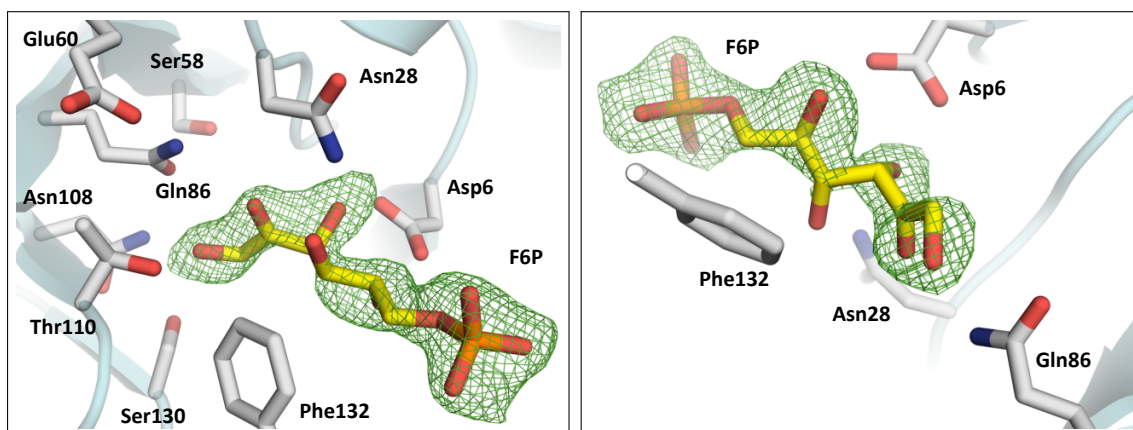


Figure C.8: mF_0 - DF_C simulated annealing omit map of *TacTAL*_{K86Q} co-crystallized with F6P. The difference electron density map is shown as green mesh (contour level 2.5σ). The selected active site residues (gray) and the non-covalently bound F6P (yellow) are represented as sticks. The polypeptide backbone is shown as secondary structure (cyan). The C4OH-group is not covered by the electron density.

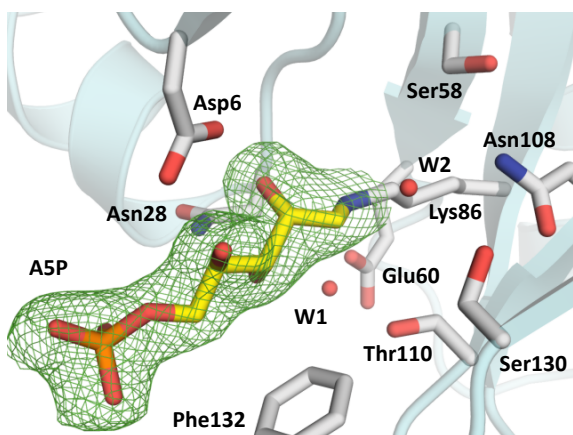


Figure C.9: mF_0 - DF_C simulated annealing omit map of *TacTAL*_{wt} co-crystallized with A5P. The difference electron density map is shown as green mesh (contour level 3σ). The selected active site residues (gray) and the A5P-Schiff base-intermediate (yellow) are represented as sticks. The polypeptide backbone is shown as secondary structure (cyan).

Figure C.10: mF_O - DF_C simulated annealing omit map of $TacTAL_{N108A/S130A}$ co-crystallized with F6P. The difference electron density map is shown as green mesh (contour level 3σ). The selected active site residues (gray) and the F6P-SCHIFF base-intermediate (yellow) are represented as sticks. The polypeptide backbone is shown as secondary structure (cyan).

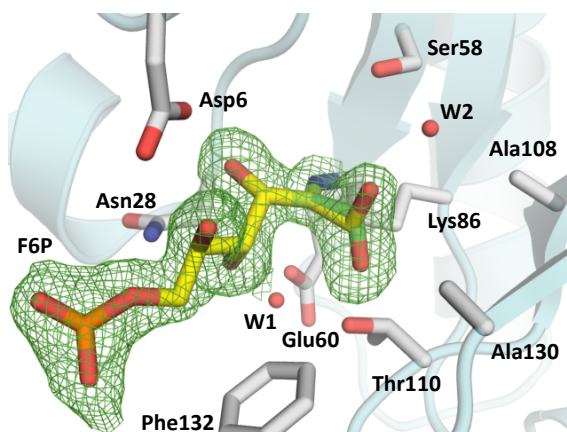


Figure C.11: Different conformations of the reactive lysine in the structures of $TacTAL_{wt}$ co-crystallized with F6P or A5P. The conformation of the reactive lysine (gray sticks) in the structure of the F6P-SCHIFF base-intermediate (yellow sticks) is U-shaped, while the reactive lysine (cyan sticks) in the structure of the A5P-SCHIFF base-intermediate (purple sticks) exists in its fully extend, all-*trans* conformation.

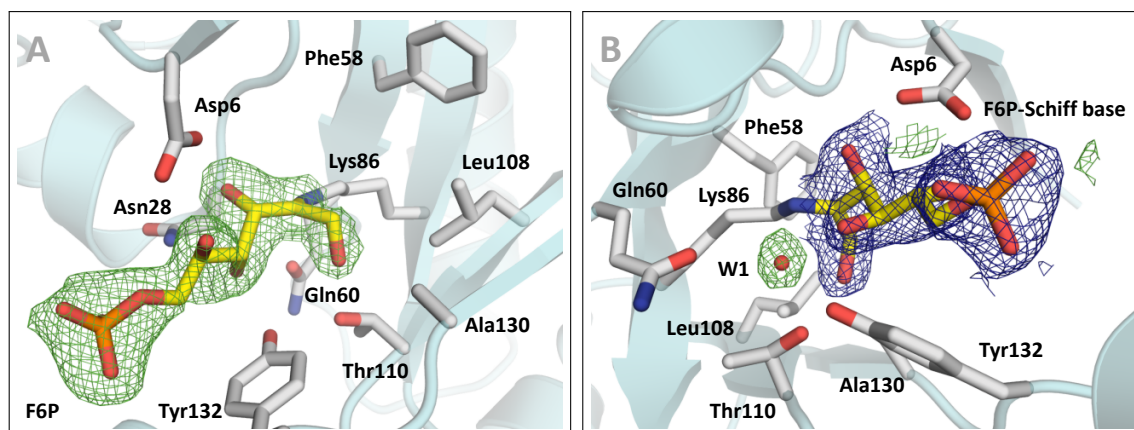
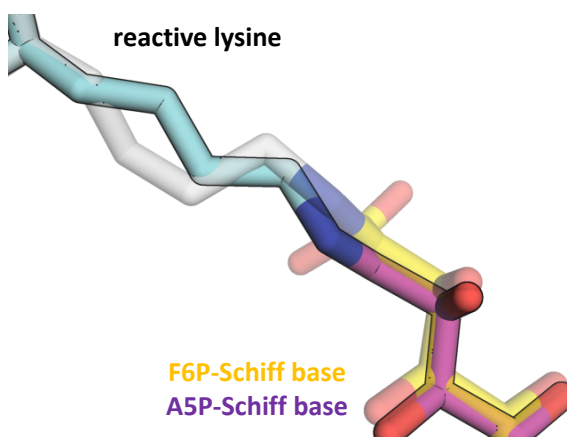


Figure C.12: Electron density maps for the $TacTAL_{FSA-mimic}$ variant co-crystallized with F6P. The selected active site residues (gray) and the F6P-SCHIFF base-intermediate (yellow) are represented as sticks. The polypeptide backbone is shown as secondary structure (cyan). **A:** mF_O - DF_C simulated annealing omit map. The difference electron density map is shown as green mesh (contour level 3σ). **B:** $2mF_O$ - DF_C electron density map (blue mesh, contour level 1σ) for the intermediate and mF_O - DF_C electron density map (green mesh, contour level 2.5σ) for the catalytic water molecule (W1, red sphere). Because of the weak electron density, the catalytic water molecule was not modeled.

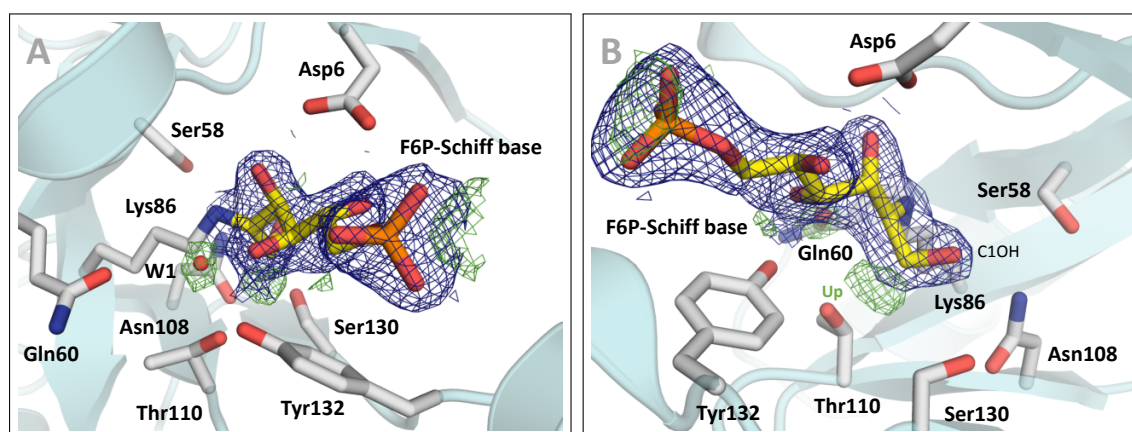


Figure C.13: Electron density maps for the *TacTAL*_{E60Q/F132Y} variant co-crystallized with F6P. The selected active site residues (gray) and the F6P-SCHIFF base-intermediate (yellow) are represented as sticks. The polypeptide backbone is shown as secondary structure (cyan). **A:** $2mF_o-DF_c$ electron density map (blue mesh, contour level 1σ) for the intermediate and mF_o-DF_c electron density map (green mesh, contour level 2.5σ) for the catalytic water molecule (W1, red sphere). Because of the weak electron density, the catalytic water molecule was not modeled. **B:** $2mF_o-DF_c$ electron density map (blue mesh, contour level 1σ) for the intermediate and mF_o-DF_c electron density map (green mesh, contour level 2.5σ). Additional positive electron density is present corresponding to the „up“ conformation of the intermediate. Because of the weak electron density, the „up“ conformation of the intermediate was not modeled.

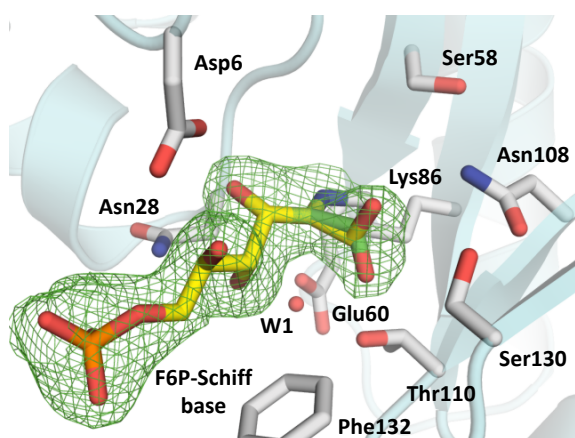


Figure C.14: mF_o-DF_c simulated annealing omit map of *TacTAL*_{T30C/D211C} co-crystallized with F6P. The difference electron density map is shown as green mesh (contour level 3σ). The selected active site residues (gray) and the F6P-SCHIFF base-intermediate (yellow) are represented as sticks. The polypeptide backbone is shown as secondary structure (cyan).

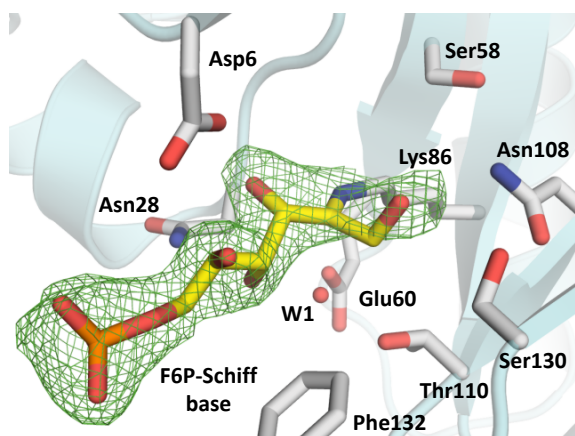
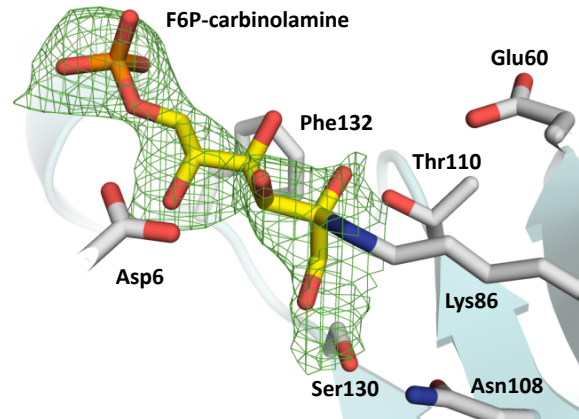


Figure C.15: mF_o-DF_c simulated annealing omit map of *TacTAL*_{T30C/D211C} soaked with F6P and DTT, simultaneously. The difference electron density map is shown as green mesh (contour level 3σ). The selected active site residues (gray) and the F6P-SCHIFF base-intermediate (yellow) are represented as sticks. The polypeptide backbone is shown as secondary structure (cyan).

Figure C.16: mF_0-DF_C simulated annealing omit map of $TacTAL_{T30C/D211C}$ soaked with F6P. The difference electron density map is shown as green mesh (contour level 2.5σ). The selected active site residues (gray) and the F6P-carbinolamine-intermediate (yellow) are represented as sticks. The polypeptide backbone is shown as secondary structure (cyan).



<i>A. thaliana</i>	156	KLVPGRVST	EV	DARLAYDTNGLIRK	VHDLRLRYNEIDVPHDRLLFKIPATWQGI	211	(THEOLOGIS <i>et al.</i> , 2000)	
<i>F. tularensis</i>	90	DVIEGKVS	SE	VDARVFN	SATTIDYAKRIIARYENSGIPKDRVLKIAATWEGIKA	145	(LARSSON <i>et al.</i> , 2005)	
<i>E. coli</i>	87	KLVPGRIST	EV	DARLSYDTEASTAKAKRLIKLYNDAGISNDRILIKLASTWQGI	142	(SPRENGER <i>et al.</i> , 1995)		
<i>C. thermophilum</i>	88	ELIPGKVS	TE	VDAAFSFD	TQKSVEKALHLIK----AGVSKDRVLKIASTWEGIKA	139	(AMLACHER <i>et al.</i> , 2011)	
<i>D. melanogaster</i>	97	KVVPGRVST	TE	DARLSFD	TKKSVEKALKLI	IALYKSLGVDKERILIKLASTWEGIKA	152	(ADAMS <i>et al.</i> , 2000)
<i>Homo sapiens</i>	97	KKIPGRVST	TE	DARLSFD	KDAMVARARRLIELYKEAGISKDRILIKLSS	TWEGIOA	152	(BANKI <i>et al.</i> , 1994)
<i>Mus musculus</i>	97	KKIPGRVST	TE	DARLSFD	KDAMVARARRLIELYKEAGVSKDRILIKLSS	TWEGIOA	152	(KUSUDA <i>et al.</i> , 1998)
<i>S. cerevisiae</i>	99	KIVPGRVST	TE	DARLSFD	TQATIEKARHLIKLFEQEGVSKERVLKIASTWEGIOA	154	(SCHAAFF <i>et al.</i> , 1990)	
<i>Zea mays</i>	160	DGADGYVSV	EV	SPRLAND	TQGTVEAAKWLHKVV-----NRPNVYIKIPATAECVPS	210	(ALEXANDROV <i>et al.</i> , 2009)	
<i>M. tuberculosis</i>	103	DGVDGRVST	EV	DPRLAHETE	KTIQQAIELWKIV-----DRPNLFKIPATKAGLPA	153	(COLE <i>et al.</i> , 1998)	
<i>St. coelicolor</i>	109	GGRDGRVST	EV	DPRLAHD	TAATVAEARQLSWLV-----DRPNVMKIPATKAGLPA	159	(BENTLEY <i>et al.</i> , 2002)	
<i>B. subtilis</i>	49	DVVKGSVSA	EV	IVSL---KAEEMIEEGKELAKI	-----APNITVKIPMTSDGLKA	94	(TRACH <i>et al.</i> , 1988)	
<i>T. acidophilum</i>	51	KIVDGPVSV	EV	VST---KYEGVVEEARKIHGL	-----GDNAVVKIPMTEDGLRA	96	(RUEPP <i>et al.</i> , 2000)	

Figure C.17: Sequence alignment of the transaldolases from different species. A Ser residue (yellow box) located at $n - 2$ position of the general acid-base catalyst Glu is conserved in transaldolase sequences of different origins (plants, mammals, insects, fungi, bacteria and archaea). The sequences were taken from UniProt-server (<http://www.uniprot.org>; (UNIProt CONSORTIUM, 2015)) The multiple sequence alignment was performed using Clustal Omega server (<http://www.ebi.ac.uk/Tools/msa/clustalo/>; (GOUJON *et al.*, 2010; McWILLIAM *et al.*, 2013; SIEVERS *et al.*, 2011)). Red: fully conserved residues, blue: residues with similar properties, black: residues with weakly similar properties, gray: neutral.

<i>L. monocytogenes</i>	46	ELTDKQVF	VQ	TVGF	TYEELI	LADARMLL	TMFGDKD	KIAIKIP	AHEAGTN	VIDT	96	(GUÉRARD-HÉLAINE <i>et al.</i> , 2015)				
<i>Ae. hydrophila</i>	50	LGPKARLF	FA	QVM	AKTETE	MVREAF	ALRELD	-R-DLV	IKIPV	CEEGLAA	IKT	96	(GUÉRARD-HÉLAINE <i>et al.</i> , 2015)			
<i>E. coli</i>	50	MGGQGRLF	FA	QVM	ATTAEC	GMVNDAL	KLR	SII-A-DIV	VKVPV	TAEGLAA	IKM	96	(SCHÜRMAN AND SPRENGER, 2001)			
<i>Sh. sonnei</i>	50	IGDEGILF	FA	Q	TMSR	DAQGMVE	EAKRL	RD	AI-P-GIV	VKIPV	TSEGLAA	IKI	96	(YANG <i>et al.</i> , 2005)		
<i>Ci. amalonaticus</i>	50	IGEHGVL	FA	Q	TMSR	DAQGMVE	EAKRL	NN	AV-P-GIV	VKIPV	TSEGLVA	IKQ	96	(AINALA <i>et al.</i> , 2013)		
<i>Sa. typhi</i>	50	IGEEGTL	FA	Q	TMSR	DAKGMVE	EAKRL	NN	AI-P-GIV	VKIPV	TAEGLAA	IKL	96	(PARKHILL <i>et al.</i> , 2001)		
<i>Cl. beijerinckii</i>	50	LPEGAQL	HA	Q	VVSL	TAEK	MVDE	AQHM	IEVLGK-DTY	IKIPV	TPEGIK	AMKL	96	(GUÉRARD-HÉLAINE <i>et al.</i> , 2015)		
<i>Str. pneumoniae</i>	51	IGSTPSI	HV	Q	VISQ	DFEG	ILKDA	HKIR	RQAGD-DIF	IKVPV	T	PAGLRA	ITKA	98	(GUÉRARD-HÉLAINE <i>et al.</i> , 2015)	
<i>Str. suis</i>	51	IGPNASL	HV	Q	VVAK	DYEG	ILDA	AKKIR	ELAPE-NIY	IKVPV	T	PAGLAA	MKT	98	(GUÉRARD-HÉLAINE <i>et al.</i> , 2015)	
<i>Str. agalactiae</i>	51	IGREASL	HV	Q	VVAK	DYQ	GLDD	AAKIR	QETDD-DIY	IKVPV	T	PDGLAA	IKT	98	(GUÉRARD-HÉLAINE <i>et al.</i> , 2015)	
<i>Str. pyogenes</i>	51	IGDKASL	HV	Q	VVIA	QDYEG	ILKDA	AAEIR	RQCGD-SVY	VKVPV	T	TEGLAA	IKT	98	(GUÉRARD-HÉLAINE <i>et al.</i> , 2015)	
<i>Str. gordonii</i>	51	IGEGPSI	HV	Q	VVAK	DYEG	ILKDA	AKKIR	R	CGD-AVY	IKVPV	T	PDGLAA	IKT	98	(GUÉRARD-HÉLAINE <i>et al.</i> , 2015)

Figure C.18: Sequence alignment of the FSA proteins from different prokaryotes. The residue in place of $TacTAL$'s Ser⁵⁸ is replaced by either phenylalanine or histidine in sequences of FSA (yellow box). The sequences were taken from UniProt-server (<http://www.uniprot.org>; (UNIProt CONSORTIUM, 2015)) The multiple sequence alignment was performed using Clustal Omega server (<http://www.ebi.ac.uk/Tools/msa/clustalo/>; (GOUJON *et al.*, 2010; McWILLIAM *et al.*, 2013; SIEVERS *et al.*, 2011)). Red: fully conserved residues, blue: residues with similar properties, black: residues with weakly similar properties, gray: neutral.

References

- Abel, M., Planas, A. and Christensen, U., (Jul 2001). Presteady-state kinetics of *Bacillus* 1,3-1,4- β -glucanase: binding and hydrolysis of a 4-methylumbelliferyl trisaccharide substrate. *Biochemical Journal*. 357(Pt 1), 195–202.
- Adams, M.D., Celniker, S.E., Holt, R.A., Evans, C.A., Gocayne, J.D., Amanatides, P.G., Scherer, S.E., Li, P.W., Hoskins, R.A., Galle, R.F., George, R.A., Lewis, S.E., Richards, S., Ashburner, M., Henderson, S.N., Sutton, G.G., Wortman, J.R., Yandell, M.D., Zhang, Q., Chen, L.X., Brandon, R.C., Rogers, Y.H., Blazej, R.G., Champe, M., Pfeiffer, B.D., Wan, K.H., Doyle, C., Baxter, E.G., Helt, G., Nelson, C.R., Gabor, G.L., Abril, J.F., Agbayani, A., An, H.J., Andrews-Pfannkoch, C., Baldwin, D., Ballew, R.M., Basu, A., Baxendale, J., Bayraktaroglu, L., Beasley, E.M., Beeson, K.Y., Benos, P.V., Berman, B.P., Bhandari, D., Bolshakov, S., Borkova, D., Botchan, M.R., Bouck, J., Brokstein, P., Brottier, P., Burtis, K.C., Busam, D.A., Butler, H., Cadieu, E., Center, A., Chandra, I., Cherry, J.M., Cawley, S., Dahlke, C., Davenport, L.B., Davies, P., de Pablos, B., Delcher, A., Deng, Z., Mays, A.D., Dew, I., Dietz, S.M., Dodson, K., Doup, L.E., Downes, M., Dugan-Rocha, S., Dunkov, B.C., Dunn, P., Durbin, K.J., Evangelista, C.C., Ferraz, C., Ferriera, S., Fleischmann, W., Fosler, C., Gabrielian, A.E., Garg, N.S., Gelbart, W.M., Glasser, K., Glodek, A., Gong, F., Gorrell, J.H., Gu, Z., Guan, P., Harris, M., Harris, N.L., Harvey, D., Heiman, T.J., Hernandez, J.R., Houck, J., Hostin, D., Houston, K.A., Howland, T.J., Wei, M.H., Ibegwam, C., Jalali, M., Kalush, F., Karpen, G.H., Ke, Z., Kennison, J.A., Ketchum, K.A., Kimmel, B.E., Kodira, C.D., Kraft, C., Kravitz, S., Kulp, D., Lai, Z., Lasko, P., Lei, Y., Levitsky, A.A., Li, J., Li, Z., Liang, Y., Lin, X., Liu, X., Mattei, B., McIntosh, T.C., McLeod, M.P., McPherson, D., Merkulov, G., Milshina, N.V., Mobarry, C., Morris, J., Moshrefi, A., Mount, S.M., Moy, M., Murphy, B., Murphy, L., Muzny, D.M., Nelson, D.L., Nelson, D.R., Nelson, K.A., Nixon, K., Nusskern, D.R., Pacleb, J.M., Palazzolo, M., Pittman, G.S., Pan, S., Pollard, J., Puri, V., Reese, M.G., Reinert, K., Remington, K., Saunders, R.D., Scheeler, F., Shen, H., Shue, B.C., Sidén-Kiamos, I., Simpson, M., Skupski, M.P., Smith, T., Spier, E., Spradling, A.C., Stapleton, M., Strong, R., Sun, E., Svirskas, R., Tector, C., Turner, R., Venter, E., Wang, A.H., Wang, X., Wang, Z.Y., Wassarman, D.A., Weinstock, G.M., Weissenbach, J., Williams, S.M., Woodage, T., Worley, K.C., Wu, D., Yang, S., Yao, Q.A., Ye, J., Yeh, R.F., Zaveri, J.S., Zhan, M., Zhang, G., Zhao, Q., Zheng, L., Zheng, X.H., Zhong, F.N., Zhong,

- W., Zhou, X., Zhu, S., Zhu, X., Smith, H.O., Gibbs, R.A., Myers, E.W., Rubin, G.M. and Venter, J.C., (Mar 2000). The genome sequence of *Drosophila melanogaster*. *Science*. 287 (5461), 2185–2195.
- Adams, P.D., Afonine, P.V., Bunkóczi, G., Chen, V.B., Davis, I.W., Echols, N., Headd, J.J., Hung, L.W., Kapral, G.J., Grosse-Kunstleve, R.W., McCoy, A.J., Moriarty, N.W., Oeffner, R., Read, R.J., Richardson, D.C., Richardson, J.S., Terwilliger, T.C. and Zwart, P.H., (Feb 2010). PHENIX: a comprehensive Python-based system for macromolecular structure solution. *Acta Crystallographica. Section D, Biological Crystallography*. 66(Pt 2), 213–221. doi: 10.1107/S0907444909052925. URL <http://dx.doi.org/10.1107/S0907444909052925>.
- Ainala, S.K., Ashok, S., Ko, Y. and Park, S., (Jun 2013). Glycerol assimilation and production of 1,3-propanediol by *Citrobacter amalonaticus* Y19. *Applied Microbiology and Biotechnology*. 97(11), 5001–5011. doi: 10.1007/s00253-013-4726-z. URL <http://dx.doi.org/10.1007/s00253-013-4726-z>.
- Alexandrov, N.N., Brover, V.V., Freidin, S., Troukhan, M.E., Tatarinova, T.V., Zhang, H., Swaller, T.J., Lu, Y.P., Bouck, J., Flavell, R.B. and Feldmann, K.A., (Jan 2009). Insights into corn genes derived from large-scale cDNA sequencing. *Plant Molecular Biology*. 69 (1-2), 179–194. doi: 10.1007/s11103-008-9415-4. URL <http://dx.doi.org/10.1007/s11103-008-9415-4>.
- Allen, F.H., Kennard, O., Watson, D.G., Brammer, L., Orpen, A.G. and Taylor, R., (Jan 1987). Tables of bond lengths determined by X-ray and neutron diffraction. Part 1. Bond lengths in organic compounds. *Journal of the Chemical Society, Perkin Transactions 2*. (12), S1–S19.
- Amlacher, S., Sarges, P., Flemming, D., van Noort, V., Kunze, R., Devos, D.P., Arumugam, M., Bork, P. and Hurt, E., (Jul 2011). Insight into structure and assembly of the nuclear pore complex by utilizing the genome of a eukaryotic thermophile. *Cell*. 146(2), 277–289. doi: 10.1016/j.cell.2011.06.039. URL <http://dx.doi.org/10.1016/j.cell.2011.06.039>.
- Aono, R., Sato, T., Imanaka, T. and Atomi, H., (May 2015). A pentose bisphosphate pathway for nucleoside degradation in Archaea. *Nature Chemical Biology*. 11(5), 355–360. doi: 10.1038/nchembio.1786. URL <http://dx.doi.org/10.1038/nchembio.1786>.

- Argyrou, A. and Blanchard, J.S.**, (Sep 2001). *Mycobacterium tuberculosis* lipoamide dehydrogenase is encoded by Rv0462 and not by the *lpdA* or *lpdB* genes. *Biochemistry*. 40(38), 11353–11363.
- Argyrou, A., Blanchard, J.S. and Palfey, B.A.**, (Dec 2002). The lipoamide dehydrogenase from *Mycobacterium tuberculosis* permits the direct observation of flavin intermediates in catalysis. *Biochemistry*. 41(49), 14580–14590.
- Banki, K., Halladay, D. and Perl, A.**, (Jan 1994). Cloning and expression of the human gene for transaldolase. a novel highly repetitive element constitutes an integral part of the coding sequence. *Journal of Biological Chemistry*. 269(4), 2847–2851.
- Belly, R.T. and Brock, T.D.**, (Dec 1972). Cellular stability of a thermophilic, acidophilic *mycoplasma*. *Journal of General Microbiology*. 73(3), 465–469. doi: 10.1099/00221287-73-3-465. URL <http://dx.doi.org/10.1099/00221287-73-3-465>.
- Bentley, S.D., Chater, K.F., Cerdeño Tarraga, A.M., Challis, G.L., Thomson, N.R., James, K.D., Harris, D.E., Quail, M.A., Kieser, H., Harper, D., Bateman, A., Brown, S., Chandra, G., Chen, C.W., Collins, M., Cronin, A., Fraser, A., Goble, A., Hidalgo, J., Hornsby, T., Howarth, S., Huang, C.H., Kieser, T., Larke, L., Murphy, L., Oliver, K., O’Neil, S., Rabinowitsch, E., Rajandream, M.A., Rutherford, K., Rutter, S., Seeger, K., Saunders, D., Sharp, S., Squares, R., Squares, S., Taylor, K., Warren, T., Wietzorrek, A., Woodward, J., Barrell, B.G., Parkhill, J. and Hopwood, D.A.**, (May 2002). Complete genome sequence of the model actinomycete *Streptomyces coelicolor* A3(2). *Nature*. 417(6885), 141–147. doi: 10.1038/417141a. URL <http://dx.doi.org/10.1038/417141a>.
- Bertani, G.**, (Sep 1951). Studies on lysogenesis. I. The mode of phage liberation by lysogenic *Escherichia coli*. *Journal of Bacteriology*. 62(3), 293–300.
- Bhattacharyya, R., Pal, D. and Chakrabarti, P.**, (Nov 2004). Disulfide bonds, their stereospecific environment and conservation in protein structures. *Protein Engineering, Design and Selection*. 17(11), 795–808. doi: 10.1093/protein/gzh093. URL <http://dx.doi.org/10.1093/protein/gzh093>.
- Bjelic, S., Kipnis, Y., Wang, L., Pianowski, Z., Vorobiev, S., Su, M., Seetharaman, J., Xiao, R., Kornhaber, G., Hunt, J.F., Tong, L., Hilvert, D. and Baker, D.**, (Jan 2014). Exploration of alternate catalytic mechanisms and optimization strategies for retroaldolase design. *Journal of*

- Molecular Biology. 426(1), 256–271. doi: 10.1016/j.jmb.2013.10.012. URL <http://dx.doi.org/10.1016/j.jmb.2013.10.012>.
- Boehr, D.D., McElheny, D., Dyson, H.J. and Wright, P.E.**, (Sep 2006). The dynamic energy landscape of dihydrofolate reductase catalysis. *Science*. 313(5793), 1638–1642. doi: 10.1126/science.1130258. URL <http://dx.doi.org/10.1126/science.1130258>. This study suggests that every functional intermediate of dihydrofolate reductase fluctuates into a higher energy conformation that is structurally similar to the next and/or previous complex in the catalytic cycle.
- Boehr, D.D., Nussinov, R. and Wright, P.E.**, (Nov 2009). The role of dynamic conformational ensembles in biomolecular recognition. *Nature Chemical Biology*. 5(11), 789–796. doi: 10.1038/nchembio.232. URL <http://dx.doi.org/10.1038/nchembio.232>.
- Bradford, M.M.**, (May 1976). A rapid and sensitive method for the quantitation of microgram quantities of protein utilizing the principle of protein-dye binding. *Analytical Biochemistry*. 72, 248–254.
- Brock, T.D.**, (Nov 1967). Life at high temperatures. evolutionary, ecological, and biochemical significance of organisms living in hot springs is discussed. *Science*. 158(3804), 1012–1019.
- Bunkóczi, G. and Read, R.J.**, (Apr 2011). Improvement of molecular-replacement models with Sculptor. *Acta Crystallographica. Section D, Biological Crystallography*. 67(Pt 4), 303–312. doi: 10.1107/S0907444910051218. URL <http://dx.doi.org/10.1107/S0907444910051218>.
- Bürgi, H., Dunitz, J. and Shefter, E.**, (Jul 1973). Geometrical reaction coordinates. II. Nucleophilic addition to a carbonyl group. *Journal of the American Chemical Society*. 95(15), 5065–5067.
- Bürgi, H., Dunitz, J., Lehn, J. and Wipff, G.**, (1974). Stereochemistry of reaction paths at carbonyl centres. *Tetrahedron*. 30(12), 1563–1572. doi: [http://dx.doi.org/10.1016/S0040-4020\(01\)90678-7](http://dx.doi.org/10.1016/S0040-4020(01)90678-7). URL <http://www.sciencedirect.com/science/article/pii/S0040402001906787>.
- Caillau, M. and Paul Quick, W.**, (Jul 2005). New insights into plant transaldolase. *Plant Journal*. 43(1), 1–16. doi: 10.1111/j.1365-313X.2005.02427.x. URL <http://dx.doi.org/10.1111/j.1365-313X.2005.02427.x>.

- Castillo, J.A., Guérard-Hélaine, C., Gutiérrez, M., Garrabou, X., Sancelme, M., Schürmann, M., Inoue, T., Hélaine, V., Charmantray, F., Gefflaut, T. *et al.*, (2010). A mutant D-fructose-6-phosphate aldolase (Ala129Ser) with improved affinity towards dihydroxyacetone for the synthesis of polyhydroxylated compounds. *Advanced Synthesis & Catalysis*. 352(6), 1039–1046.
- Cedervall, P., Aulabaugh, A., Geoghegan, K.F., McLellan, T.J. and Pandit, J., (Mar 2015). Engineered stabilization and structural analysis of the autoinhibited conformation of PDE4. *Proceedings of the National Academy of Sciences of the United States of America*. 112(12), E1414–E1422. doi: 10.1073/pnas.1419906112. URL <http://dx.doi.org/10.1073/pnas.1419906112>.
- Chan, D.I., Chu, B.C.H., Lau, C.K.Y., Hunter, H.N., Byers, D.M. and Vogel, H.J., (Oct 2010). NMR solution structure and biophysical characterization of *Vibrio harveyi* acyl carrier protein A75H: effects of divalent metal ions. *Journal of Biological Chemistry*. 285(40), 30558–30566. doi: 10.1074/jbc.M110.128298. URL <http://dx.doi.org/10.1074/jbc.M110.128298>.
- Chandrasekhar, K., Wang, J., Arjunan, P., Sax, M., Park, Y.H., Nemeria, N.S., Kumaran, S., Song, J., Jordan, F. and Furey, W., (May 2013). Insight to the interaction of the dihydro-lipoamide acetyltransferase (E2) core with the peripheral components in the *Escherichia coli* pyruvate dehydrogenase complex via multifaceted structural approaches. *Journal of Biological Chemistry*. 288(21), 15402–15417. doi: 10.1074/jbc.M113.466789. URL <http://dx.doi.org/10.1074/jbc.M113.466789>.
- Chen, V.B., Arendall, 3rd, W.B., Headd, J.J., Keedy, D.A., Immormino, R.M., Kapral, G.J., Murray, L.W., Richardson, J.S. and Richardson, D.C., (Jan 2010). MolProbity: all-atom structure validation for macromolecular crystallography. *Acta Crystallographica. Section D, Biological Crystallography*. 66(Pt 1), 12–21. doi: 10.1107/S0907444909042073. URL <http://dx.doi.org/10.1107/S0907444909042073>.
- Chen, Z., Schlipalius, D., Opit, G., Subramanyam, B. and Phillips, T.W., (2015). Diagnostic molecular markers for phosphine resistance in U.S. populations of *Tribolium castaneum* and *Rhyzopertha dominica*. *PLoS One*. 10(3), e0121343. doi: 10.1371/journal.pone.0121343. URL <http://dx.doi.org/10.1371/journal.pone.0121343>.
- Chiba, H., Oishi, S., Fujii, N. and Ohno, H., (Sep 2012). Total synthesis of (-)-quinocarcin by gold(i)-catalyzed regioselective hydroamination. *Angewandte Chemie. International Edition in*

- English. *51*(36), 9169–9172. doi: 10.1002/anie.201205106. URL <http://dx.doi.org/10.1002/anie.201205106>.
- Chiba, H., Sakai, Y., Ohara, A., Oishi, S., Fujii, N. and Ohno, H.**, (Jul 2013). Convergent synthesis of (-)-quinocarcin based on the combination of sonogashira coupling and gold(i)-catalyzed 6-endo-dig hydroamination. *Chemistry*. *19*(27), 8875–8883. doi: 10.1002/chem.201300687. URL <http://dx.doi.org/10.1002/chem.201300687>.
- Ciszak, E.M., Korotchkina, L.G., Dominiak, P.M., Sidhu, S. and Patel, M.S.**, (Jun 2003). Structural basis for flip-flop action of thiamin pyrophosphate-dependent enzymes revealed by human pyruvate dehydrogenase. *Journal of Biological Chemistry*. *278*(23), 21240–21246. doi: 10.1074/jbc.M300339200. URL <http://dx.doi.org/10.1074/jbc.M300339200>.
- Cole, S.T., Brosch, R., Parkhill, J., Garnier, T., Churcher, C., Harris, D., Gordon, S.V., Eiglmeier, K., Gas, S., Barry, 3rd, C., Tekaia, F., Badcock, K., Basham, D., Brown, D., Chillingworth, T., Connor, R., Davies, R., Devlin, K., Feltwell, T., Gentles, S., Hamlin, N., Holroyd, S., Hornsby, T., Jagels, K., Krogh, A., McLean, J., Moule, S., Murphy, L., Oliver, K., Osborne, J., Quail, M.A., Rajandream, M.A., Rogers, J., Rutter, S., Seeger, K., Skelton, J., Squares, R., Squares, S., Sulston, J.E., Taylor, K., Whitehead, S. and Barrell, B.G.**, (Jun 1998). Deciphering the biology of *Mycobacterium tuberculosis* from the complete genome sequence. *Nature*. *393*(6685), 537–544. doi: 10.1038/31159. URL <http://dx.doi.org/10.1038/31159>.
- Crosby, J. and Crump, M.P.**, (Oct 2012). The structural role of the carrier protein–active controller or passive carrier. *Natural Product Reports*. *29*(10), 1111–1137. doi: 10.1039/c2np20062g. URL <http://dx.doi.org/10.1039/c2np20062g>.
- Daniels, A.D., Campeotto, I., van der Kamp, M.W., Bolt, A.H., Trinh, C.H., Phillips, S.E.V., Pearson, A.R., Nelson, A., Mulholland, A.J. and Berry, A.**, (Apr 2014). Reaction mechanism of N-acetylneuraminic acid lyase revealed by a combination of crystallography, QM/MM simulation, and mutagenesis. *ACS Chemical Biology*. *9*(4), 1025–1032. doi: 10.1021/cb500067z. URL <http://dx.doi.org/10.1021/cb500067z>.
- Darland, G., Brock, T.D., Samsonoff, W. and Conti, S.F.**, (Dec 1970). A thermophilic, acidophilic mycoplasma isolated from a coal refuse pile. *Science*. *170*(3965), 1416–1418.

- de Beer, T.A.P., Berka, K., Thornton, J.M. and Laskowski, R.A.**, (Jan 2014). PDBsum additions. *Nucleic acids research*. 42, D292–D296. ISSN 1362-4962. doi: 10.1093/nar/gkt940.
- Di Tommaso, P., Moretti, S., Xenarios, I., Orobittg, M., Montanyola, A., Chang, J.M., Taly, J.F. and Notredame, C.**, (Jul 2011). T-Coffee: a web server for the multiple sequence alignment of protein and RNA sequences using structural information and homology extension. *Nucleic Acids Research*. 39(Web Server issue), W13–W17. doi: 10.1093/nar/gkr245. URL <http://dx.doi.org/10.1093/nar/gkr245>.
- Edelhoch, H.**, (Jul 1967). Spectroscopic determination of tryptophan and tyrosine in proteins. *Biochemistry*. 6(7), 1948–1954.
- Eisenmesser, E.Z., Millet, O., Labeikovsky, W., Korzhnev, D.M., Wolf-Watz, M., Bosco, D.A., Skalicky, J.J., Kay, L.E. and Kern, D.**, (Nov 2005). Intrinsic dynamics of an enzyme underlies catalysis. *Nature*. 438(7064), 117–121. doi: 10.1038/nature04105. URL <http://dx.doi.org/10.1038/nature04105>.
- Ellis, K.J. and Morrison, J.F.**, (1982). Buffers of constant ionic strength for studying pH-dependent processes. *Methods in Enzymology*. 87, 405–426.
- Emsley, P., Lohkamp, B., Scott, W.G. and Cowtan, K.**, (Apr 2010). Features and development of Coot. *Acta Crystallographica. Section D, Biological Crystallography*. 66(Pt 4), 486–501. doi: 10.1107/S0907444910007493. URL <http://dx.doi.org/10.1107/S0907444910007493>.
- Emsley, P. and Cowtan, K.**, (Dec 2004). Coot: model-building tools for molecular graphics. *Acta Crystallographica. Section D, Biological Crystallography*. 60(Pt 12 Pt 1), 2126–2132. doi: 10.1107/S0907444904019158. URL <http://dx.doi.org/10.1107/S0907444904019158>.
- Fan, J., Jiang, D., Zhao, Y., Liu, J. and Zhang, X.C.**, (May 2014). Crystal structure of lipid phosphatase *Escherichia coli* phosphatidylglycerophosphate phosphatase B. *Proceedings of the National Academy of Sciences of the United States of America*. 111(21), 7636–7640. doi: 10.1073/pnas.1403097111. URL <http://dx.doi.org/10.1073/pnas.1403097111>.
- Faure, M., Bourguignon, J., Neuburger, M., MacHerel, D., Sieker, L., Ober, R., Kahn, R., Cohen-Addad, C. and Douce, R.**, (May 2000). Interaction between the lipoamide-containing H-protein and the lipoamide dehydrogenase (L-protein) of the glycine decarboxylase multienzyme system 2. Crystal structures of H- and L-proteins. *European Journal of Biochemistry*. 267(10), 2890–2898.

- Fukuyama, T. and Nunes, J.J.**, (1988). Stereocontrolled total synthesis of (+-)-quinocarcin. *Journal of the American Chemical Society*. *110*(15), 5196–5198.
- Fullerton, S.W.B., Griffiths, J.S., Merkel, A.B., Cheriyan, M., Wymer, N.J., Hutchins, M.J., Fierke, C.A., Toone, E.J. and Naismith, J.H.**, (May 2006). Mechanism of the class I KDPG aldolase. *Bioorganic and Medicinal Chemistry*. *14*(9), 3002–3010. doi: 10.1016/j.bmc.2005.12.022. URL <http://dx.doi.org/10.1016/j.bmc.2005.12.022>.
- Gallagher, J.R. and Prigge, S.T.**, (Feb 2010). Plasmodium falciparum acyl carrier protein crystal structures in disulfide-linked and reduced states and their prevalence during blood stage growth. *Proteins*. *78*(3), 575–588. doi: 10.1002/prot.22582. URL <http://dx.doi.org/10.1002/prot.22582>.
- Garrabou, X., Castillo, J.A., Guérard-Hélaine, C., Parella, T., Joglar, J., Lemaire, M. and Clapés, P.**, (2009). Asymmetric self- and cross-aldol reactions of glycolaldehyde catalyzed by D-fructose-6-phosphate aldolase. *Angewandte Chemie. International Edition in English*. *48* (30), 5521–5525. doi: 10.1002/anie.200902065. URL <http://dx.doi.org/10.1002/anie.200902065>.
- Gasteiger, E., Hoogland, C., Gattiker, A., Duvaud, S., Wilkins, M., Appel, R. and Bairoch, A.**, (2005). „Protein Identification and Analysis Tools on the ExPASy Server“, in *The Proteomics Protocols Handbook*, pages 571–607. Humana Press.
- Gefflaut, T., Blonski, C., Perie, J. and Willson, M.**, (1995). Class i aldolases: substrate specificity, mechanism, inhibitors and structural aspects. *Progress in Biophysics and Molecular Biology*. *63* (3), 301–340.
- Giganti, D., Albasa-Jové, D., Urresti, S., Rodrigo-Unzueta, A., Martínez, M.A., Comino, N., Barilone, N., Bellinzoni, M., Chenal, A., Guerin, M.E. and Alzari, P.M.**, (Jan 2015). Secondary structure reshuffling modulates glycosyltransferase function at the membrane. *Nature Chemical Biology*. *11*(1), 16–18. doi: 10.1038/nchembio.1694. URL <http://dx.doi.org/10.1038/nchembio.1694>.
- Giger, L., Caner, S., Obexer, R., Kast, P., Baker, D., Ban, N. and Hilvert, D.**, (Aug 2013). Evolution of a designed retro-aldolase leads to complete active site remodeling. *Nature Chemical Biology*. *9*(8), 494–498. doi: 10.1038/nchembio.1276. URL <http://dx.doi.org/10.1038/nchembio.1276>.

- Gill, S.C. and von Hippel, P.H.**, (Nov 1989). Calculation of protein extinction coefficients from amino acid sequence data. *Analytical Biochemistry*. 182(2), 319–326.
- Gonçalves, S., Miller, S.P., Carrondo, M.A., Dean, A.M. and Matias, P.M.**, (Sep 2012). Induced fit and the catalytic mechanism of isocitrate dehydrogenase. *Biochemistry*. 51(36), 7098–7115. doi: 10.1021/bi300483w. URL <http://dx.doi.org/10.1021/bi300483w>.
- Goujon, M., McWilliam, H., Li, W., Valentin, F., Squizzato, S., Paern, J. and Lopez, R.**, (Jul 2010). A new bioinformatics analysis tools framework at EMBL-EBI. *Nucleic Acids Research*. 38(Web Server issue), W695–W699. doi: 10.1093/nar/gkq313. URL <http://dx.doi.org/10.1093/nar/gkq313>.
- Güclü, D., Szekrenyi, A., Garrabou, X., Kickstein, M., Junker, S., Clapés, P. and Fessner, W.D.**, (2016). Minimalist protein engineering of an aldolase provokes unprecedented substrate promiscuity. *ACS Catalysis*. 6(3), 1848–1852.
- Guérard-Hélaine, C., de Berardinis, V., Besnard-Gonnet, M., Darii, E., Debacker, M., Debarb, A., Fernandes, C., Hélaine, V., Mariage, A., Pellouin, V., Perret, A., Petit, J.L., Sancelme, M., Lemaire, M. and Salanoubat, M.**, (2015). Genome mining for innovative biocatalysts: new dihydroxyacetone aldolases for the chemists toolbox. *ChemCatChem*. 7(12), 1871–1879.
- Haid, E., Lehmann, P. and Ziegenhorn, J.**, (Jun 1975). Molar absorptivities of beta-NADH and beta-NAD at 260 nm. *Clinical Chemistry*. 21(7), 884–887.
- Hammes, G.G., Chang, Y.C. and Oas, T.G.**, (Aug 2009). Conformational selection or induced fit: a flux description of reaction mechanism. *Proceedings of the National Academy of Sciences of the United States of America*. 106(33), 13737–13741. doi: 10.1073/pnas.0907195106. URL <http://dx.doi.org/10.1073/pnas.0907195106>.
- Hammes, G.G., Benkovic, S.J. and Hammes-Schiffer, S.**, (Dec 2011). Flexibility, diversity, and cooperativity: pillars of enzyme catalysis. *Biochemistry*. 50(48), 10422–10430. doi: 10.1021/bi201486f. URL <http://dx.doi.org/10.1021/bi201486f>.
- Hammes-Schiffer, S. and Benkovic, S.J.**, (2006). Relating protein motion to catalysis. *Annual Review of Biochemistry*. 75, 519–541. doi: 10.1146/annurev.biochem.75.103004.142800. URL <http://dx.doi.org/10.1146/annurev.biochem.75.103004.142800>.

- Harris, T.K. and Turner, G.J.**, (Feb 2002). Structural basis of perturbed pKa values of catalytic groups in enzyme active sites. *IUBMB Life*. 53(2), 85–98. doi: 10.1080/15216540211468. URL <http://dx.doi.org/10.1080/15216540211468>.
- Hartley, B.S. and Kilby, B.A.**, (Mar 1952). The inhibition of chymotrypsin by diethyl *p*-nitrophenyl phosphate. *Biochemical Journal*. 50(5), 672–678.
- Hartley, B.S. and Kilby, B.A.**, (Feb 1954). The reaction of *p*-nitrophenyl esters with chymotrypsin and insulin. *Biochemical Journal*. 56(2), 288–297.
- Heinemann, U. and Hahn, M.**, (Sep 1995). Circular permutations of protein sequence: not so rare? *Trends in Biochemical Sciences*. 20(9), 349–350.
- Henzler-Wildman, K.A., Thai, V., Lei, M., Ott, M., Wolf-Watz, M., Fenn, T., Pozharski, E., Wilson, M.A., Petsko, G.A., Karplus, M., Hübner, C.G. and Kern, D.**, (Dec 2007). Intrinsic motions along an enzymatic reaction trajectory. *Nature*. 450(7171), 838–844. doi: 10.1038/nature06410. URL <http://dx.doi.org/10.1038/nature06410>.
- Hill, G.C., Wunz, T.P. and Remers, W.A.**, (Jul 1988). Computer simulation of the binding of quinocarcin to DNA. prediction of mode of action and absolute configuration. *Journal of Computer-Aided Molecular Design*. 2(2), 91–106.
- Hiratsuka, T., Koketsu, K., Minami, A., Kaneko, S., Yamazaki, C., Watanabe, K., Oguri, H. and Oikawa, H.**, (Dec 2013). Core assembly mechanism of quinocarcin/SF-1739: bimodular complex nonribosomal peptide synthetases for sequential mannich-type reactions. *Chemistry and Biology*. 20(12), 1523–1535. doi: 10.1016/j.chembiol.2013.10.011. URL <http://dx.doi.org/10.1016/j.chembiol.2013.10.011>.
- Hirayama, N. and Shirahata, K.**, (1983). X-Ray determination of the molecular structure of the novel antibiotic DC-52-d, 6-hydroxymethyl-3, 12-imino-7-methoxy-13-methyl-1, 2, 3, 4-tetrahydroazepino [1, 2-b] isoquinoline-1-carboxylic acid. *Journal of the Chemical Society, Perkin Transactions 2*. (9), 1705–1708.
- Holm, L. and Rosenström, P.**, (Jul 2010). Dali server: conservation mapping in 3D. *Nucleic Acids Research*. 38(Web Server issue), W545–W549. doi: 10.1093/nar/gkq366. URL <http://dx.doi.org/10.1093/nar/gkq366>.

- Hopkins, N. and Williams, Jr, C.**, (Sep 1995). Characterization of lipoamide dehydrogenase from *Escherichia coli* lacking the redox active disulfide: C44S and C49S. *Biochemistry*. 34(37), 11757–11765.
- Horecker, B.L. and Smyrniotis, P.Z.**, (Feb 1955). Purification and properties of yeast transaldolase. *Journal of Biological Chemistry*. 212(2), 811–825.
- Horecker, B. and Smyrniotis, P.**, (1953). Transaldolase: the formation of fructose-6-phosphate from sedoheptulose-7-phosphate. *Journal of the American Chemical Society*. 75(8), 2021–2022.
- Horecker, B., Tsolas, O. and Lai, C.**, (1972). „Aldolases“, in *The enzymes*, vol. 7, pages 213–258. Academic Press, New York.
- Hsung, J.C. and Haug, A.**, (May 1975). Intracellular pH of *Thermoplasma acidophila*. *Biochimica et Biophysica Acta*. 389(3), 477–482.
- Hutchinson, E.G. and Thornton, J.M.**, (1990). HERA—a program to draw schematic diagrams of protein secondary structures. *Proteins*. 8, 203–212. ISSN 0887-3585. doi: 10.1002/prot.340080303.
- Inoue, H., Nojima, H. and Okayama, H.**, (Nov 1990). High efficiency transformation of *Escherichia coli* with plasmids. *Gene*. 96(1), 23–28.
- Izard, T., Aevarsson, A., Allen, M.D., Westphal, A.H., Perham, R.N., de Kok, A. and Hol, W.G.**, (Feb 1999). Principles of quasi-equivalence and Euclidean geometry govern the assembly of cubic and dodecahedral cores of pyruvate dehydrogenase complexes. *Proceedings of the National Academy of Sciences of the United States of America*. 96(4), 1240–1245.
- Jia, J., Huang, W., Schörken, U., Sahm, H., Sprenger, G.A., Lindqvist, Y. and Schneider, G.**, (Jun 1996). Crystal structure of transaldolase B from *Escherichia coli* suggests a circular permutation of the alpha/beta barrel within the class I aldolase family. *Structure*. 4(6), 715–724.
- Jia, J., Schörken, U., Lindqvist, Y., Sprenger, G.A. and Schneider, G.**, (Jan 1997). Crystal structure of the reduced Schiff-base intermediate complex of transaldolase B from *Escherichia coli*: mechanistic implications for class I aldolases. *Protein Science*. 6(1), 119–124. doi: 10.1002/pro.5560060113. URL <http://dx.doi.org/10.1002/pro.5560060113>.

- Kabsch, W.**, (Feb 2010). XDS. *Acta Crystallographica. Section D, Biological Crystallography*. 66(Pt 2), 125–132. doi: 10.1107/S0907444909047337. URL <http://dx.doi.org/10.1107/S0907444909047337>.
- Kaur, R., Subbarayalu, M., Jagadeesan, R., Daghish, G.J., Nayak, M.K., Naik, H.R., Ramasamy, S., Subramanian, C., Ebert, P.R. and Schlipalius, D.I.**, (Sep 2015). Phosphine resistance in india is characterised by a dihydrolipoamide dehydrogenase variant that is otherwise unobserved in eukaryotes. *Heredity (Edinb)*. 115(3), 188–194. doi: 10.1038/hdy.2015.24. URL <http://dx.doi.org/10.1038/hdy.2015.24>.
- Keil-Dlouhá, V., Zylber, N., Imhoff, J.M., Tong, N.T. and Keil, B.**, (Sep 1971). Proteolytic activity of pseudotrypsin. *FEBS Letters*. 16(4), 291–295.
- Kelly, S.M., Jess, T.J. and Price, N.C.**, (Aug 2005). How to study proteins by circular dichroism. *Biochimica et Biophysica Acta*. 1751(2), 119–139. doi: 10.1016/j.bbapap.2005.06.005. URL <http://dx.doi.org/10.1016/j.bbapap.2005.06.005>.
- Kleywegt, G.J.**, (Jul 1996). Use of non-crystallographic symmetry in protein structure refinement. *Acta crystallographica. Section D, Biological crystallography*. 52, 842–857. ISSN 0907-4449. doi: 10.1107/S0907444995016477.
- Koch, C., Neumann, P., Valerius, O., Feussner, I. and Ficner, R.**, (2016). Crystal structure of alcohol oxidase from *Pichia pastoris*. *PLoS One*. 11(2), e0149846. doi: 10.1371/journal.pone.0149846. URL <http://dx.doi.org/10.1371/journal.pone.0149846>.
- Koziol, J.**, (1971). Fluorometric analyses of riboflavin and its coenzymes. *Methods in Enzymology*. 18, 253–285. ISSN 0076-6879. doi: 10.1016/s0076-6879(71)18089-5. URL [http://dx.doi.org/10.1016/S0076-6879\(71\)18089-5](http://dx.doi.org/10.1016/S0076-6879(71)18089-5).
- Kufareva, I., Gustavsson, M., Holden, L.G., Qin, L., Zheng, Y. and Handel, T.M.**, (2016). Disulfide trapping for modeling and structure determination of receptor: Chemokine complexes. *Methods in Enzymology*. 570, 389–420. doi: 10.1016/bs.mie.2015.12.001. URL <http://dx.doi.org/10.1016/bs.mie.2015.12.001>.
- Kusuda, J., Hirai, M., Toyoda, A., Tanuma, R., Nomura-Kitabayashi, A. and Hashimoto, K.**, (Mar 1998). Cloning and chromosomal localization of a paralog and a mouse homolog of the human transaldolase gene. *Gene*. 209(1-2), 13–21.

- Laemmli, U.K.**, (Aug 1970). Cleavage of structural proteins during the assembly of the head of bacteriophage T4. *Nature*. 227(5259), 680–685.
- Lafrance-Vanasse, J. and Sygusch, J.**, (Aug 2007). Carboxy-terminus recruitment induced by substrate binding in eukaryotic fructose bis-phosphate aldolases. *Biochemistry*. 46(33), 9533–9540. doi: 10.1021/bi700615r. URL <http://dx.doi.org/10.1021/bi700615r>.
- Langworthy, T.A.**, (Apr 1977). Long-chain diglycerol tetraethers from *Thermoplasma acidophilum*. *Biochimica et Biophysica Acta*. 487(1), 37–50.
- Langworthy, T.A., Smith, P.F. and Mayberry, W.R.**, (Dec 1972). Lipids of *Thermoplasma acidophilum*. *Journal of Bacteriology*. 112(3), 1193–1200.
- Larsson, P., Oyston, P.C.F., Chain, P., Chu, M.C., Duffield, M., Fuxelius, H.H., Garcia, E., Hälltorp, G., Johansson, D., Isherwood, K.E., Karp, P.D., Larsson, E., Liu, Y., Michell, S., Prior, J., Prior, R., Malfatti, S., Sjöstedt, A., Svensson, K., Thompson, N., Vergez, L., Wagg, J.K., Wren, B.W., Lindler, L.E., Andersson, S.G.E., Forsman, M. and Titball, R.W.**, (Feb 2005). The complete genome sequence of *Francisella tularensis*, the causative agent of tularemia. *Nature Genetics*. 37(2), 153–159. doi: 10.1038/ng1499. URL <http://dx.doi.org/10.1038/ng1499>.
- Laskowski, R.A.**, (Jan 2009). PDBsum new things. *Nucleic acids research*. 37, D355–D359. ISSN 1362-4962. doi: 10.1093/nar/gkn860.
- Lehwess-Litzmann, A.** Title: „Biochemische kinetische und strukturelle Untersuchungen der Transaldolase aus *Thermoplasma acidophilum*“. PhD thesis, Martin-Luther-Universität Halle-Wittenberg, July 2011.
- Lehwess-Litzmann, A., Neumann, P., Golbik, R., Parthier, C. and Tittmann, K.**, (May 2011a). Crystallization and preliminary X-ray diffraction analysis of transaldolase from *Thermoplasma acidophilum*. *Acta Crystallographica Section F: Structural Biology Communications*. 67 (Pt 5), 584–586. doi: 10.1107/S1744309111009274. URL <http://dx.doi.org/10.1107/S1744309111009274>.
- Lehwess-Litzmann, A., Neumann, P., Parthier, C., Lüdtke, S., Golbik, R., Ficner, R. and Tittmann, K.**, (Oct 2011b). Twisted schiff base intermediates and substrate locale revise transaldolase mechanism. *Nature Chemical Biology*. 7(10), 678–684. doi: 10.1038/nchembio.633. URL <http://dx.doi.org/10.1038/nchembio.633>.

- Lietzow, T.H.**, (2015). Untersuchungen an open/closed-konformationen des aktiven zentrums der transaldolase aus *Thermoplasma acidophilum*. Bachelor thesis, unpublished.
- Light, S.H. and Anderson, W.F.**, (Mar 2014). Arabinose 5-phosphate covalently inhibits transaldolase. *Journal of Structural and Functional Genomics*. 15(1), 41–44. doi: 10.1007/s10969-014-9174-1. URL <http://dx.doi.org/10.1007/s10969-014-9174-1>.
- Light, S.H., Minasov, G., Duban, M.E. and Anderson, W.F.**, (Feb 2014). Adherence to Bürgi-Dunitz stereochemical principles requires significant structural rearrangements in Schiff-base formation: insights from transaldolase complexes. *Acta Crystallographica. Section D, Biological Crystallography*. 70(Pt 2), 544–552. doi: 10.1107/S1399004713030666. URL <http://dx.doi.org/10.1107/S1399004713030666>.
- Lineweaver, H. and Burk, D.**, (1934). The determination of enzyme dissociation constants. *Journal of the American Chemical Society*. 56(3), 658–666.
- Marahiel, M.A., Stachelhaus, T. and Mootz, H.D.**, (Nov 1997). Modular peptide synthetases involved in nonribosomal peptide synthesis. *Chemical Reviews*. 97(7), 2651–2674.
- Markowitz, V.M., Chen, I.M.A., Palaniappan, K., Chu, K., Szeto, E., Grechkin, Y., Ratner, A., Jacob, B., Huang, J., Williams, P., Huntemann, M., Anderson, I., Mavromatis, K., Ivanova, N.N. and Kyrpides, N.C.**, (Jan 2012). IMG: the integrated microbial genomes database and comparative analysis system. *Nucleic Acids Research*. 40(Database issue), D115–D122. doi: 10.1093/nar/gkr1044. URL <http://dx.doi.org/10.1093/nar/gkr1044>.
- Mattevi, A., Obmolova, G., Schulze, E., Kalk, K.H., Westphal, A.H., de Kok, A. and Hol, W.G.**, (Mar 1992). Atomic structure of the cubic core of the pyruvate dehydrogenase multienzyme complex. *Science*. 255(5051), 1544–1550.
- Maurady, A., Zdanov, A., de Moissac, D., Beaudry, D. and Sygusch, J.**, (Mar 2002). A conserved glutamate residue exhibits multifunctional catalytic roles in D-fructose-1,6-bisphosphate aldolases. *Journal of Biological Chemistry*. 277(11), 9474–9483. doi: 10.1074/jbc.M107600200. URL <http://dx.doi.org/10.1074/jbc.M107600200>.
- McCoy, A.J., Grosse-Kunstleve, R.W., Adams, P.D., Winn, M.D., Storoni, L.C. and Read, R.J.**, (Aug 2007). Phaser crystallographic software. *Journal of Applied Crystallography*. 40 (Pt 4), 658–674. doi: 10.1107/S0021889807021206. URL <http://dx.doi.org/10.1107/S0021889807021206>.

- McWilliam, H., Li, W., Uludag, M., Squizzato, S., Park, Y.M., Buso, N., Cowley, A.P. and Lopez, R.**, (Jul 2013). Analysis tool web services from the EMBL-EBI. *Nucleic Acids Research*. 41(Web Server issue), W597–W600. doi: 10.1093/nar/gkt376. URL <http://dx.doi.org/10.1093/nar/gkt376>.
- Michaelis, L. and Menten, M.M.L.**, (1913). Die Kinetik der Invertinwirkung. *Biochem. z.* 49 (333-369), 352.
- Mofid, M.R., Marahiel, M.A., Ficner, R. and Reuter, K.**, (May 1999). Crystallization and preliminary crystallographic studies of Sfp: a phosphopantetheinyl transferase of modular peptide synthetases. *Acta Crystallographica. Section D, Biological Crystallography*. 55(Pt 5), 1098–1100.
- Morse, D.E. and Horecker, B.L.**, (1968). The mechanism of action of aldolases. *Advances in Enzymology and Related Areas of Molecular Biology*. 31, 125–181.
- Moscato, B., Swain, M. and Loria, J.P.**, (Jan 2016). Induced fit in the selection of correct versus incorrect nucleotides by DNA polymerase β . *Biochemistry*. 55(2), 382–395. doi: 10.1021/acs.biochem.5b01213. URL <http://dx.doi.org/10.1021/acs.biochem.5b01213>.
- Mullis, K., Faloona, F., Scharf, S., Saiki, R., Horn, G. and Erlich, H.**, (1986). Specific enzymatic amplification of DNA in vitro: the polymerase chain reaction. *Cold Spring Harbor symposia on quantitative biology*. 51 Pt 1, 263–273. ISSN 0091-7451.
- Nagano, N., Orengo, C.A. and Thornton, J.M.**, (Aug 2002). One fold with many functions: the evolutionary relationships between TIM barrel families based on their sequences, structures and functions. *Journal of Molecular Biology*. 321(5), 741–765.
- Nemeria, N., Volkov, A., Brown, A., Yi, J., Zipper, L., Guest, J.R. and Jordan, F.**, (Jan 1998). Systematic study of the six cysteines of the E1 subunit of the pyruvate dehydrogenase multienzyme complex from *Escherichia coli*: none is essential for activity. *Biochemistry*. 37(3), 911–922. doi: 10.1021/bi9722251. URL <http://dx.doi.org/10.1021/bi9722251>.
- Nikodinovic, J., Barrow, K.D. and Chuck, J.A.**, (Nov 2003). High yield preparation of genomic DNA from *Streptomyces*. *Biotechniques*. 35(5), 932–4, 936.
- Niu, C., Zhu, L., Xu, X. and Li, Q.**, (2016). Rational design of disulfide bonds increases thermostability of a mesophilic 1,3-1,4- β -glucanase from *Bacillus terquilensis*. *PLoS One*. 11

- (4), e0154036. doi: 10.1371/journal.pone.0154036. URL <http://dx.doi.org/10.1371/journal.pone.0154036>.
- Orita, I., Sato, T., Yurimoto, H., Kato, N., Atomi, H., Imanaka, T. and Sakai, Y.,** (Jul 2006). The ribulose monophosphate pathway substitutes for the missing pentose phosphate pathway in the archaeon *Thermococcus kodakaraensis*. *Journal of Bacteriology*. 188(13), 4698–4704. doi: 10.1128/JB.00492-06. URL <http://dx.doi.org/10.1128/JB.00492-06>.
- Pace, C.N., Vajdos, F., Fee, L., Grimsley, G. and Gray, T.,** (Nov 1995). How to measure and predict the molar absorption coefficient of a protein. *Protein Science*. 4(11), 2411–2423. doi: 10.1002/pro.5560041120. URL <http://dx.doi.org/10.1002/pro.5560041120>.
- Parkhill, J., Dougan, G., James, K.D., Thomson, N.R., Pickard, D., Wain, J., Churcher, C., Mungall, K.L., Bentley, S.D., Holden, M.T., Sebaihia, M., Baker, S., Basham, D., Brooks, K., Chillingworth, T., Connor, P., Cronin, A., Davis, P., Davies, R.M., Dowd, L., White, N., Farrar, J., Feltwell, T., Hamlin, N., Haque, A., Hien, T.T., Holroyd, S., Jagels, K., Krogh, A., Larsen, T.S., Leather, S., Moule, S., O’Gaora, P., Parry, C., Quail, M., Rutherford, K., Simmonds, M., Skelton, J., Stevens, K., Whitehead, S. and Barrell, B.G.,** (Oct 2001). Complete genome sequence of a multiple drug resistant *Salmonella enterica serovar Typhi* CT18. *Nature*. 413(6858), 848–852. doi: 10.1038/35101607. URL <http://dx.doi.org/10.1038/35101607>.
- Pellequer, J.L. and Chen, S.w.W.,** (Oct 2006). Multi-template approach to modeling engineered disulfide bonds. *Proteins*. 65(1), 192–202. doi: 10.1002/prot.21059. URL <http://dx.doi.org/10.1002/prot.21059>.
- Peng, C., Pu, J.Y., Song, L.Q., Jian, X.H., Tang, M.C. and Tang, G.L.,** (May 2012). Hijacking a hydroxyethyl unit from a central metabolic ketose into a nonribosomal peptide assembly line. *Proceedings of the National Academy of Sciences of the United States of America*. 109(22), 8540–8545. doi: 10.1073/pnas.1204232109. URL <http://dx.doi.org/10.1073/pnas.1204232109>.
- Perham, R.N. and Hooper, E.A.,** (Feb 1977). Polypeptide chain stoichiometry in the self-assembly of the pyruvate dehydrogenase multienzyme complex of *Escherichia coli*. *FEBS Letters*. 73(2), 137–140.

- Quadri, L.E., Weinreb, P.H., Lei, M., Nakano, M.M., Zuber, P. and Walsh, C.T.**, (Feb 1998). Characterization of Sfp, a *Bacillus subtilis* phosphopantetheinyl transferase for peptidyl carrier protein domains in peptide synthetases. *Biochemistry*. 37(6), 1585–1595. doi: 10.1021/bi9719861. URL <http://dx.doi.org/10.1021/bi9719861>.
- Ramelot, T.A., Smola, M.J., Lee, H.W., Ciccocanti, C., Hamilton, K., Acton, T.B., Xiao, R., Everett, J.K., Prestegard, J.H., Montelione, G.T. and Kennedy, M.A.**, (Mar 2011). Solution structure of 4'-phosphopantetheine - GmACP3 from *Geobacter metallireducens*: a specialized acyl carrier protein with atypical structural features and a putative role in lipopolysaccharide biosynthesis. *Biochemistry*. 50(9), 1442–1453. doi: 10.1021/bi101932s. URL <http://dx.doi.org/10.1021/bi101932s>.
- Reed, L.J., Koike, M., Levitch, M.E. and Leach, F.R.**, (May 1958). Studies on the nature and reactions of protein-bound lipoic acid. *Journal of Biological Chemistry*. 232(1), 143–158.
- Rice, R.H., Means, G.E. and Brown, W.D.**, (Jun 1977). Stabilization of bovine trypsin by reductive methylation. *Biochimica et Biophysica Acta*. 492(2), 316–321.
- Rock, C.O., Cronan, Jr, J. and Armitage, I.M.**, (Mar 1981). Molecular properties of acyl carrier protein derivatives. *Journal of Biological Chemistry*. 256(6), 2669–2674.
- Rose, I.A., O'Connell, E.L. and Mehler, A.H.**, (Apr 1965). Mechanism of the aldolase reaction. *Journal of Biological Chemistry*. 240, 1758–1765.
- Ruepp, A., Graml, W., Santos-Martinez, M.L., Koretke, K.K., Volker, C., Mewes, H.W., Frishman, D., Stocker, S., Lupas, A.N. and Baumeister, W.**, (Sep 2000). The genome sequence of the thermoacidophilic scavenger *Thermoplasma acidophilum*. *Nature*. 407(6803), 508–513. doi: 10.1038/35035069. URL <http://dx.doi.org/10.1038/35035069>.
- Samland, A.K. and Sprenger, G.A.**, (Jul 2009). Transaldolase: from biochemistry to human disease. *International Journal of Biochemistry and Cell Biology*. 41(7), 1482–1494. doi: 10.1016/j.biocel.2009.02.001. URL <http://dx.doi.org/10.1016/j.biocel.2009.02.001>.
- Samland, A.K., Baier, S., Schürmann, M., Inoue, T., Huf, S., Schneider, G., Sprenger, G.A. and Sandalova, T.**, (Mar 2012). Conservation of structure and mechanism within the transaldolase enzyme family. *FEBS Journal*. 279(5), 766–778. doi: 10.1111/j.1742-4658.2011.08467.x. URL <http://dx.doi.org/10.1111/j.1742-4658.2011.08467.x>.

- Sammito, M., Millán, C., Frieske, D., Rodríguez-Freire, E., Borges, R.J. and Usón, I.**, (Sep 2015). ARCIMBOLDO_LITE: single-workstation implementation and use. *Acta Crystallographica. Section D, Biological Crystallography.* 71(Pt 9), 1921–1930. doi: 10.1107/S1399004715010846. URL <http://dx.doi.org/10.1107/S1399004715010846>.
- Sautner, V.** Strukturelle und mechanistische Analyse der Transaldolase aus *Thermoplasma acidophilum*. Master's thesis, Martin-Luther-Universität Halle-Wittenberg, August 2012.
- Sautner, V., Friedrich, M.M., Lehweß-Litzmann, A. and Tittmann, K.**, (Jul 2015). Converting transaldolase into aldolase through swapping of the multifunctional acid-base catalyst: Common and divergent catalytic principles in F6P aldolase and transaldolase. *Biochemistry.* 54(29), 4475–4486. doi: 10.1021/acs.biochem.5b00283. URL <http://dx.doi.org/10.1021/acs.biochem.5b00283>.
- Schaaff, I., Hohmann, S. and Zimmermann, F.K.**, (Mar 1990). Molecular analysis of the structural gene for yeast transaldolase. *European Journal of Biochemistry.* 188(3), 597–603.
- Schlipalius, D.I., Valmas, N., Tuck, A.G., Jagadeesan, R., Ma, L., Kaur, R., Goldinger, A., Anderson, C., Kuang, J., Zuryn, S., Mau, Y.S., Cheng, Q., Collins, P.J., Nayak, M.K., Schirra, H.J., Hilliard, M.A. and Ebert, P.R.**, (Nov 2012). A core metabolic enzyme mediates resistance to phosphine gas. *Science.* 338(6108), 807–810. doi: 10.1126/science.1224951. URL <http://dx.doi.org/10.1126/science.1224951>.
- Schneider, S., Sandalova, T., Schneider, G., Sprenger, G.A. and Samland, A.K.**, (Oct 2008). Replacement of a phenylalanine by a tyrosine in the active site confers fructose-6-phosphate aldolase activity to the transaldolase of *Escherichia coli* and human origin. *Journal of Biological Chemistry.* 283(44), 30064–30072. doi: 10.1074/jbc.M803184200. URL <http://dx.doi.org/10.1074/jbc.M803184200>.
- Schörken, U., Thorell, S., Schürmann, M., Jia, J., Sprenger, G.A. and Schneider, G.**, (Apr 2001). Identification of catalytically important residues in the active site of *Escherichia coli* transaldolase. *European Journal of Biochemistry.* 268(8), 2408–2415.
- Schürmann, M. and Sprenger, G.A.**, (Apr 2001). Fructose-6-phosphate aldolase is a novel class I aldolase from *Escherichia coli* and is related to a novel group of bacterial transaldolases. *Journal of Biological Chemistry.* 276(14), 11055–11061. doi: 10.1074/jbc.M008061200. URL <http://dx.doi.org/10.1074/jbc.M008061200>.

- Schwans, J.P., Sunden, F., Gonzalez, A., Tsai, Y. and Herschlag, D.**, (Nov 2013). Uncovering the determinants of a highly perturbed tyrosine pka in the active site of ketosteroid isomerase. *Biochemistry*. 52(44), 7840–7855. doi: 10.1021/bi401083b. URL <http://dx.doi.org/10.1021/bi401083b>.
- Scott, J.D. and Williams, R.M.**, (May 2002). Chemistry and biology of the tetrahydroisoquinoline antitumor antibiotics. *Chemical Reviews*. 102(5), 1669–1730.
- Segerer, A., Langworthy, T.A. and Stetter, K.O.**, (1988). *Thermoplasma acidophilum* and *Thermoplasma volcanium* sp. nov. from solfatara fields. *Systematic and Applied Microbiology*. 10(2), 161–171.
- Shepherd, M.D., Kharel, M.K., Bosserman, M.A. and Rohr, J.**, (Aug 2010). Laboratory maintenance of *Streptomyces* species. *Current Protocols in Microbiology*. Chapter 10, Unit 10E.1. doi: 10.1002/9780471729259.mc10e01s18. URL <http://dx.doi.org/10.1002/9780471729259.mc10e01s18>.
- Shevchenko, A., Wilm, M., Vorm, O. and Mann, M.**, (Mar 1996). Mass spectrometric sequencing of proteins silver-stained polyacrylamide gels. *Analytical Chemistry*. 68(5), 850–858.
- Sievers, F., Wilm, A., Dineen, D., Gibson, T.J., Karplus, K., Li, W., Lopez, R., McWilliam, H., Remmert, M., Söding, J., Thompson, J.D. and Higgins, D.G.**, (2011). Fast, scalable generation of high-quality protein multiple sequence alignments using Clustal Omega. *Molecular Systems Biology*. 7, 539. doi: 10.1038/msb.2011.75. URL <http://dx.doi.org/10.1038/msb.2011.75>.
- Soderberg, T.**, (May 2005). Biosynthesis of ribose-5-phosphate and erythrose-4-phosphate in archaea: a phylogenetic analysis of archaeal genomes. *Archaea*. 1(5), 347–352.
- Sprenger, G.A., Schörken, U., Sprenger, G. and Sahm, H.**, (Oct 1995). Transaldolase B of *Escherichia coli* K-12: cloning of its gene, *talB*, and characterization of the enzyme from recombinant strains. *Journal of Bacteriology*. 177(20), 5930–5936.
- St-Jean, M. and Sygusch, J.**, (Oct 2007). Stereospecific proton transfer by a mobile catalyst in mammalian fructose-1,6-bisphosphate aldolase. *Journal of Biological Chemistry*. 282(42), 31028–31037. doi: 10.1074/jbc.M704968200. URL <http://dx.doi.org/10.1074/jbc.M704968200>.

- St-Jean, M., Lafrance-Vanasse, J., Liotard, B. and Sygusch, J.**, (Jul 2005). High resolution reaction intermediates of rabbit muscle fructose-1,6-bisphosphate aldolase: substrate cleavage and induced fit. *Journal of Biological Chemistry*. 280(29), 27262–27270. doi: 10.1074/jbc.M502413200. URL <http://dx.doi.org/10.1074/jbc.M502413200>.
- Stellmacher, L., Sandalova, T., Leptihn, S., Schneider, G., Sprenger, G.A. and Samland, A.K.**, (2015). Acid–base catalyst discriminates between a fructose 6-phosphate aldolase and a transaldolase. *ChemCatChem*. 7(19), 3140–3151.
- Stellmacher, L., Sandalova, T., Schneider, S., Schneider, G., Sprenger, G.A. and Samland, A.K.**, (Apr 2016). Novel mode of inhibition by D-tagatose 6-phosphate through a Heyns rearrangement in the active site of transaldolase B variants. *Acta Crystallographica. Section D, Biological Crystallography*. 72(Pt 4), 467–476. doi: 10.1107/S2059798316001170. URL <http://dx.doi.org/10.1107/S2059798316001170>.
- Studier, F.W.**, (May 2005). Protein production by auto-induction in high density shaking cultures. *Protein Expression and Purification*. 41(1), 207–234.
- Sun, S. and Toney, M.D.**, (Mar 1999). Evidence for a two-base mechanism involving tyrosine-265 from arginine-219 mutants of alanine racemase. *Biochemistry*. 38(13), 4058–4065. doi: 10.1021/bi982924t. URL <http://dx.doi.org/10.1021/bi982924t>.
- Szekrenyi, A., Soler, A., Garrabou, X., Guérard-Hélaine, C., Parella, T., Joglar, J., Lemaire, M., Bujons, J. and Clapés, P.**, (Sep 2014). Engineering the donor selectivity of D-fructose-6-phosphate aldolase for biocatalytic asymmetric cross-aldol additions of glycolaldehyde. *Chemistry*. 20(39), 12572–12583. doi: 10.1002/chem.201403281. URL <http://dx.doi.org/10.1002/chem.201403281>.
- Takahashi, K. and Tomita, F.**, (May 1983). DC-52, a novel antitumor antibiotic. 2. Isolation, physico-chemical characteristics and structure determination. *Journal of Antibiotics (Tokyo)*. 36(5), 468–470.
- Tener, D.M. and Mayo, K.H.**, (May 1990). Divalent cation binding to reduced and octanoyl acyl-carrier protein. *European Journal of Biochemistry*. 189(3), 559–565.
- Theologis, A., Ecker, J.R., Palm, C.J., Federspiel, N.A., Kaul, S., White, O., Alonso, J., Altafi, H., Araujo, R., Bowman, C.L., Brooks, S.Y., Buehler, E., Chan, A., Chao, Q., Chen, H.,**

- Cheuk, R.F., Chin, C.W., Chung, M.K., Conn, L., Conway, A.B., Conway, A.R., Creasy, T.H., Dewar, K., Dunn, P., Ertgu, P., Feldblyum, T.V., Feng, J., Fong, B., Fujii, C.Y., Gill, J.E., Goldsmith, A.D., Haas, B., Hansen, N.F., Hughes, B., Huizar, L., Hunter, J.L., Jenkins, J., Johnson-Hopson, C., Khan, S., Khaykin, E., Kim, C.J., Koo, H.L., Kremenetskaia, I., Kurtz, D.B., Kwan, A., Lam, B., Langin-Hooper, S., Lee, A., Lee, J.M., Lenz, C.A., Li, J.H., Li, Y., Lin, X., Liu, S.X., Liu, Z.A., Luros, J.S., Maiti, R., Marziali, A., Militscher, J., Miranda, M., Nguyen, M., Nierman, W.C., Osborne, B.I., Pai, G., Peterson, J., Pham, P.K., Rizzo, M., Rooney, T., Rowley, D., Sakano, H., Salzberg, S.L., Schwartz, J.R., Shinn, P., Southwick, A.M., Sun, H., Tallon, L.J., Tambunga, G., Toriumi, M.J., Town, C.D., Utterback, T., Van Aken, S., Vaysberg, M., Vysotskaia, V.S., Walker, M., Wu, D., Yu, G., Fraser, C.M., Venter, J.C. and Davis, R.W.,** (Dec 2000). Sequence and analysis of chromosome 1 of the plant *Arabidopsis thaliana*. *Nature*. 408(6814), 816–820. doi: 10.1038/35048500. URL <http://dx.doi.org/10.1038/35048500>.
- Thorell, S., Schürmann, M., Sprenger, G.A. and Schneider, G.,** (May 2002). Crystal structure of decameric fructose-6-phosphate aldolase from *Escherichia coli* reveals inter-subunit helix swapping as a structural basis for assembly differences in the transaldolase family. *Journal of Molecular Biology*. 319(1), 161–171. doi: 10.1016/S0022-2836(02)00258-9. URL [http://dx.doi.org/10.1016/S0022-2836\(02\)00258-9](http://dx.doi.org/10.1016/S0022-2836(02)00258-9).
- Tietzel, M.** Title: „Structure and Mechanism of the Flavoenzyme Lipoamide Dehydrogenase from *Escherichia coli*.“. PhD thesis, Georg-August-Universität Göttingen, September 2015.
- Tittmann, K.,** (Dec 2014). Sweet siblings with different faces: the mechanisms of FBP and F6P aldolase, transaldolase, transketolase and phosphoketolase revisited in light of recent structural data. *Bioorganic Chemistry*. 57, 263–280. doi: 10.1016/j.bioorg.2014.09.001. URL <http://dx.doi.org/10.1016/j.bioorg.2014.09.001>.
- Tomita, F., Takahashi, K. and Shimizu, K.,** (May 1983). DC-52, a novel antitumor antibiotic. 1. Taxonomy, fermentation and biological activity. *Journal of Antibiotics (Tokyo)*. 36(5), 463–467.
- Tomita, F., Takahashi, K. and Tamaoki, T.,** (Oct 1984). Quinocarcin, a novel antitumor antibiotic. 3. Mode of action. *Journal of Antibiotics (Tokyo)*. 37(10), 1268–1272.

- Trach, K., Chapman, J.W., Piggot, P., LeCoq, D. and Hoch, J.A.**, (Sep 1988). Complete sequence and transcriptional analysis of the *spo0F* region of the *Bacillus subtilis* chromosome. *Journal of Bacteriology*. *170*(9), 4194–4208.
- Tsolas, O. and Joris, L.**, (1975). Transaldolase. *Methods in Enzymology*. *42*, 290–297.
- UniProt Consortium**, (Jan 2015). UniProt: a hub for protein information. *Nucleic Acids Research*. *43*(Database issue), D204–D212. doi: 10.1093/nar/gku989. URL <http://dx.doi.org/10.1093/nar/gku989>.
- Venkataraman, R. and Racker, E.**, (Jul 1961). Mechanism of action of transaldolase. II. the substrate-enzyme intermediate. *Journal of Biological Chemistry*. *236*, 1883–1886.
- Vogt, A.D. and Di Cera, E.**, (Jul 2012). Conformational selection or induced fit? A critical appraisal of the kinetic mechanism. *Biochemistry*. *51*(30), 5894–5902. doi: 10.1021/bi3006913. URL <http://dx.doi.org/10.1021/bi3006913>.
- Vogt, A.D. and Di Cera, E.**, (Aug 2013). Conformational selection is a dominant mechanism of ligand binding. *Biochemistry*. *52*(34), 5723–5729. doi: 10.1021/bi400929b. URL <http://dx.doi.org/10.1021/bi400929b>.
- Vogt, A.D., Pozzi, N., Chen, Z. and Di Cera, E.**, (Feb 2014). Essential role of conformational selection in ligand binding. *Biophys Chem*. *186*, 13–21. doi: 10.1016/j.bpc.2013.09.003. URL <http://dx.doi.org/10.1016/j.bpc.2013.09.003>.
- Walsh, C.T.**, (Jan 2008). The chemical versatility of natural-product assembly lines. *Accounts of Chemical Research*. *41*(1), 4–10. doi: 10.1021/ar7000414. URL <http://dx.doi.org/10.1021/ar7000414>.
- Williams, J.F., Blackmore, P.F. and Clark, M.G.**, (Oct 1978). New reaction sequences for the non-oxidative pentose phosphate pathway. *Biochemical Journal*. *176*(1), 257–282.
- Williams, R.M., Glinka, T., Flanagan, M.E., Gallegos, R., Coffman, H. and Pei, D.**, (1992). Cannizzaro-based O₂-dependent cleavage of DNA by quinocarcin. *Journal of the American Chemical Society*. *114*(2), 733–740.
- Winn, M., Fyans, J.K., Zhuo, Y. and Micklefield, J.**, (Feb 2016). Recent advances in engineering nonribosomal peptide assembly lines. *Natural Product Reports*. *33*(2), 317–347. doi: 10.1039/c5np00099h. URL <http://dx.doi.org/10.1039/c5np00099h>.

- Woese, C.R. and Fox, G.E.**, (Nov 1977). Phylogenetic structure of the prokaryotic domain: the primary kingdoms. *Proceedings of the National Academy of Sciences of the United States of America*. *74*(11), 5088–5090.
- Wolf-Watz, M., Thai, V., Henzler-Wildman, K., Hadjipavlou, G., Eisenmesser, E.Z. and Kern, D.**, (Oct 2004). Linkage between dynamics and catalysis in a thermophilic-mesophilic enzyme pair. *Nature Structural and Molecular Biology*. *11*(10), 945–949. doi: 10.1038/nsmb821. URL <http://dx.doi.org/10.1038/nsmb821>.
- Wu, Y.C., Liron, M. and Zhu, J.**, (Jun 2008). Asymmetric total synthesis of (-)-quinocarcin. *Journal of the American Chemical Society*. *130*(22), 7148–7152. doi: 10.1021/ja800662q. URL <http://dx.doi.org/10.1021/ja800662q>.
- Yang, F., Yang, J., Zhang, X., Chen, L., Jiang, Y., Yan, Y., Tang, X., Wang, J., Xiong, Z., Dong, J., Xue, Y., Zhu, Y., Xu, X., Sun, L., Chen, S., Nie, H., Peng, J., Xu, J., Wang, Y., Yuan, Z., Wen, Y., Yao, Z., Shen, Y., Qiang, B., Hou, Y., Yu, J. and Jin, Q.**, (2005). Genome dynamics and diversity of *Shigella* species, the etiologic agents of bacillary dysentery. *Nucleic Acids Research*. *33*(19), 6445–6458. doi: 10.1093/nar/gki954. URL <http://dx.doi.org/10.1093/nar/gki954>.
- Zaremba, M. and Siksnys, V.**, (Sep 2015). An engineered SS bridge blocks the conformational change required for the nuclease activity of BfiI. *Biochemistry*. *54*(34), 5340–5347. doi: 10.1021/acs.biochem.5b00437. URL <http://dx.doi.org/10.1021/acs.biochem.5b00437>.
- Zhou, Z.H., McCarthy, D.B., O'Connor, C.M., Reed, L.J. and Stoops, J.K.**, (Dec 2001). The remarkable structural and functional organization of the eukaryotic pyruvate dehydrogenase complexes. *Proceedings of the National Academy of Sciences of the United States of America*. *98*(26), 14802–14807. doi: 10.1073/pnas.011597698. URL <http://dx.doi.org/10.1073/pnas.011597698>.
- Zhu, X., Tanaka, F., Lerner, R.A., Barbas, 3rd, C.F. and Wilson, I.A.**, (Dec 2009). Direct observation of an enamine intermediate in amine catalysis. *Journal of the American Chemical Society*. *131*(51), 18206–18207. doi: 10.1021/ja907271a. URL <http://dx.doi.org/10.1021/ja907271a>.

Curriculum Vitae

Viktor Sautner

Georg-August-University Göttingen
Department of Molecular Enzymology
Julia-Lermontowa-Weg 3
37077 Goettingen, Germany

Phone: +49 551 39177813
e-mail: vsautne@gwdg.de

Date of Birth: 24.10.1984
Place of Birth: Karaganda (Kazakhstan)
Nationality: German

Education

09/1991 – 06/2001	Secondary school, Karaganda (Kazakhstan)
09/2002 – 02/2003	Zentrale Deutsche Sprachprüfung, Herder-Institut, University Leipzig, interDaF e.V.. language course
08/2003 – 07/2006	Giebichenstein-Gymnasium „Thomas Müntzer“, Halle/Saale
08/2006	Matriculation, Martin-Luther-University Halle-Wittenberg, Biochemistry
2009 – 2010	Studying abroad (DAAD), Lomonosov Moscow State University, Faculty of Bioengineering and Bioinformatics
09/2012	Diploma examination, Martin-Luther-University Halle-Wittenberg Diploma Thesis: „Structural and Mechanistic Analysis of Transaldolase from <i>Thermoplasma Acidophilum</i> “, Georg-August-University Göttingen, department of bioanalytics
01/2013 – 06/2016	GGNB doctoral program Biomolecules: Structure – Function – Dynamics, Georg-August-University Göttingen, Department of Molecular Enzymology

Scientific Contribution

Publication	Sautner, V., Friedrich, M.M., Lehwess-Litzmann, A. and Tittmann, K., (Jul 2015). Converting transaldolase into aldolase through swapping of the multifunctional acid-base catalyst: Common and divergent catalytic principles in F6P aldolase and transaldolase. <i>Biochemistry</i> . 54(29), 4475 – 4486.
Poster	Converting Transaldolase into Aldolase through Swapping of the Multifunctional Acid-Base Catalyst